



HAL
open science

Membrane-protein interactions regulate excitability through potassium and chloride channels

Pablo Avalos-Prado

► **To cite this version:**

Pablo Avalos-Prado. Membrane-protein interactions regulate excitability through potassium and chloride channels. Molecular biology. Université Côte d'Azur, 2020. English. NNT : 2020COAZ6023 . tel-04637385

HAL Id: tel-04637385

<https://theses.hal.science/tel-04637385>

Submitted on 6 Jul 2024

HAL is a multi-disciplinary open access archive for the deposit and dissemination of scientific research documents, whether they are published or not. The documents may come from teaching and research institutions in France or abroad, or from public or private research centers.

L'archive ouverte pluridisciplinaire **HAL**, est destinée au dépôt et à la diffusion de documents scientifiques de niveau recherche, publiés ou non, émanant des établissements d'enseignement et de recherche français ou étrangers, des laboratoires publics ou privés.

THÈSE DE DOCTORAT

Des interactions membrane-protéine
régulent l'excitabilité à travers des canaux
potassiques et chlorure

Pablo ÁVALOS PRADO

Institut de Biologie Valrose, Nice

**Présentée en vue de l'obtention
du grade de docteur en** Sciences de la Vie et de la
Santé, Interactions Moléculaires et Cellulaires
d'Université Côte d'Azur

Dirigée par : Guillaume Sandoz

Soutenu le : 30 octobre 2020

Devant le jury, composé de :

Jacques Barhanin, PhD, LP2M
Michel Vivaudou, PhD, IBS
Félix Viana de la Iglesia, PhD, IN-UMH
Geoffrey Abbott, Pr, PhD, UC Irvine
Stephen Tucker, Pr, PhD, University of Oxford
Raphaël Rapetti-Mauss, PhD, IBV
Florian Lesage, PhD, IPMC
Guillaume Sandoz, PhD, IBV

DES INTERACTIONS MEMBRANE- PROTEINE REGULENT L'EXCITABILITE A TRAVERS DES CANAUX POTASSIQUES ET CHLORURE

Jury

Président du Jury

Dr Jacques Barhanin, LP2M

Rapporteurs

Dr Michel Vivaudou, IBS

Dr Félix Viana de la Iglesia, IN-UMH

Examineurs

Pr Geoffrey Abbott, UC Irvine

Pr Stephen Tucker, University of Oxford

Dr Florian Lesage, IPMC

Dr Raphaël Rapetti-Mauss, IBV

Superviseur

Dr Guillaume Sandoz, IBV

Les protéines n'agissent pas seules mais s'assemblent dynamiquement en complexes protéiques dans la cellule afin d'y assurer leur fonction. Les complexes protéiques « canaux ioniques » sont constitués de sous-unités α qui forment le pore du canal et de sous-unités auxiliaires (β) régulatrices associées. La détermination de l'identité moléculaire des différentes sous-unités composant ce complexe protéique est essentielle pour comprendre la fonction et la régulation des canaux ioniques. Au cours de ma thèse, j'ai commencé à aborder la spécificité des sous-unités auxiliaires vis-à-vis de la sous-unité α . Plus précisément, j'ai étudié la capacité de KCNE1, classiquement considérée comme une sous-unité β du canal KCNQ1 de la superfamille des canaux voltage-dépendants, à interagir avec TMEM16A, un canal Cl^- activé par le Ca^{2+} de la superfamille anoctamine. Nous avons trouvé que KCNE1 remplit les 4 caractéristiques pour être considérée comme une sous-unité auxiliaire régulatrice du canal TMEM16A. Ces résultats démontrent que KCNE1 est une sous-unité auxiliaire « double » qui sert à la fois de sous-unité β pour les deux canaux KCNQ1 et TMEM16A. Canaux qui appartiennent à deux superfamilles de protéines distinctes qui ne sont pas apparentées phylogénétiquement. Deuxièmement, j'ai étudié l'implication des complexes protéiques dans l'induction de l'effet analgésique induit par la mycolactone, une toxine sécrétée par *Mycobacterium ulcerans*. J'ai trouvé que le récepteur 2 de l'angiotensine II, par un couplage physique, peut augmenter l'activité du canal potassique TRAAK suite à la liaison de la mycolactone sur le récepteur. J'ai démontré que ce couplage fonctionnel est indépendant de la voie de signalisation canonique des protéines G. En conclusion, les résultats obtenus brisent la spécificité dogmatique des sous-unités auxiliaires concernant les complexes protéiques, remettent en question la classification des canaux ioniques et ouvrent les portes au développement de nouvelles molécules analgésiques.

Mots-clés: Canaux ioniques, Sous-unités ancillaires, Canalopathies, Complexe protéique,

Proteins do not act alone but they assemble dynamically into protein complexes within the cell. Ion channel complexes are made up of an α -pore-forming-subunit associated with specific auxiliary (β) subunits and regulatory proteins. Determination of the molecular identity of subunits composing a protein complex is essential to understand the function and regulation of ion channels. During my thesis, I addressed the specificity of auxiliary subunits regarding to the α -pore-forming-subunit. More specifically, I studied the ability of KCNE1, classically considered as a β -subunit of the cardiac KCNQ1 pore-forming subunit belonging to the voltage-dependent K_v channel superfamily, to regulate the anoctamin superfamily channel TMEM16A, a Ca^{2+} -activated Cl^- channel. I found that KCNE1 fulfils all criteria of a *bona fide* auxiliary subunit of TMEM16A chloride channels. KCNE1 serves then as a β -subunit for two different superfamilies of ion channels phylogenetically unrelated. In the second part of my thesis, I studied the involvement of protein complexes in analgesia induced by mycolactone, a toxin secreted by *Mycobacterium ulcerans*. I found that the angiotensin II receptor 2, by being directly coupled to the two-pore-domain potassium channel TRAAK, increases the channel activity upon mycolactone binding, independently of the canonical G protein signaling pathway. All in all, the obtained results break the dogmatic specificity of auxiliary subunits regarding protein complexes questioning ion channels classification and open the doors to the development of new analgesic molecules.

Key words: Ion channels, Ancillary subunits, Channelopathies, Protein complex, Pain perception.

Acknowledgments

First of all, I want to thank Dr Jacques Barhanin, Dr Michel Vivaudou, Dr Félix Viana, Dr Florian Lesage, Dr Raphaël Rapetti-Mauss, Dr Geoffrey Abbott and Dr Stephen Tucker. Thank you all for having accepted to evaluate my work and being willing to move to Nice in such hard times of pandemic. I feel much honored for having such an impressive jury.

I want to express my gratefulness to my team. In the first place, Dr Guillaume Sandoz, thank you for trusting me without reservation from the beginning, opening the doors of your laboratory and giving me the opportunity of developing a whole scientific project. I will always be very grateful to you for it. Thank you Brigitte for your priceless help and your human quality. You made everything easier in the lab and also helped with the search of a place where to live and with the French bureaucracy. I also want to thank my former team mates Thomas, Olena, and Lynda and our current PhD student Arnaud. Your company made brighter the darkness of the electrophysiology room. A big thank for everything you gave me. A special acknowledgment to Perrine and Stephanie for teaching me, for your support, your friendship and all the moments we spent together inside and outside the lab. I will never be grateful enough for everything you have meant to me during these years.

For the same reason I thank all my PhD students fellows, with special gratitude to Anthony, Pierre, Yannis, Torsten and my flat mate Hortense. In short, my friends, you are the most precious thing I will keep from this experience. I want to extend my gratitude to all the members of the IBV, including scientific platforms, animal facility, technicians and secretaries for their assistance. And also to our neighbors of the fourth floor and people of the laboratory of “Ion channels and cancer” for their advice, and especially to Raph for his useful help and all the good moments.

I also feel much grateful to all my teachers in the Universidad de Sevilla and the Universidad Pablo de Olavide. Here I cannot forget the wise lessons and the patience of Dr Beatriz Benitez, Dr José Maria Delgado and Dr Agnès Gruart.

Para acabar, mamá, papá, Luis: vosotros sois el ejemplo a seguir. Gracias por todo el amor que me brindáis cada día, aún en la distancia. Sois todo lo que más quiero en el mundo. Esta tesis está dedicada a vosotros.

*“El sueño va sobre el tiempo
flotando como un velero.
Nadie puede abrir semillas
en el corazón del sueño”*

Así que pasen cinco años, 1931. Federico García Lorca

Table of contents

Résumé.....	5
Abstract	7
Acknowledgments.....	9
Table of contents	12
List of abbreviations.....	15
List of figures, tables and equations.....	18
Foreword: Ion channels and bioelectricity	21
Project 1. KCNE1 is an ancillary subunit of TMEM16A	25
A. Introduction	26
1. Ancillary subunits: The KCNE family	26
2. Calcium-activated chloride channels: TMEM16A.....	36
3. Hypothesis: KCNE1 activates the TMEM16A channel	44
B. Results	45
1. KCNE1 shifts TMEM16A from a calcium-dependent to a voltage-dependent Cl- channel.....	45
2. TMEM16A activation by KCNE1 involves physical interaction.....	52
3. The KCNE1-TMEM16A complex is carried by PCT cells.....	55
4. The N-terminal pre-transmembrane domain of KCNE1 is key for TMEM16A regulation	57
5. KCNE1 polymorphisms within the TMEM16A interacting sequence suppress the Cl- current	59
6. Specificity of KCNE1-TMEM16A	61
C. Discussion.....	62
1. KCNE1 as a cross-regulator of two different superfamilies of ion channels	62
2. Activation by KCNE1 involves voltage-dependent gating	63
3. KCNE1 stably interacts with TMEM16A	64
4. The KCNE1-TMEM16A complex in native tissues.....	65
5. KCNE5 can also activate TMEM16A	68
D. Conclusion.....	69

Project 2. Pain silencing through AT2R-TRAAK direct coupling	71
A. Introduction	72
1. Buruli Ulcer: A painless necrotic skin disease	72
2. TRAAK channels	79
3. AT2R receptors.....	87
4. Hypothesis: Analgesia in Buruli ulcer involves direct and G-protein-independent coupling between TRAAK channels and AT2R receptors	92
B. Results	93
1. Mycolactone induces hypoexcitability and prevents activation of sensory neurons through TRAAK channels activation.....	93
2. Mycolactone induces long-lasting hyperpolarization but not internalization of AT2R	97
3. Mycolactone does not involve intracellular signaling messengers	99
4. <i>AT2R and TRAAK are coupled in membrane a micro-regulatory domain</i>	101
5. Mycolactone activation is specific for AT2R and TRAAK	103
C. Discussion.....	105
1. Mycolactone induces hyperpolarization through TRAAK homomers.....	105
2. Mycolactone effect is G-protein independent and long-lasting due to the lack of AT2R desensitization.....	107
D. Conclusion.....	108
Final conclusions.....	109
Materials and methods	111
A. Molecular biology and cell culture.....	111
B. Electrophysiology of project 1	112
C. Electrophysiology of project 2	113
D. SiMPull assays.....	114
E. Time-resolved FRET assays.....	115
F. BRET assays	115
G. Behavioral tests.....	115

H. Nerve-skin experiments	116
References	117
Annexes: Articles and reviews	133

List of abbreviations

A01	T16 (inhibitor)-A01
AngII	Angiotensin II
AT1R/AT2R	Angiotensin II Receptor 1/2
ASIC	Acid Sensing Ion Channel
BRET	Bioluminescence Resonance Energy Transfer
CaCC	Calcium-activated Chloride Channel
CFTR	Cystic Fibrosis Transmembrane conductance Regulator
CHO cells	Chinese Hamster Ovary
CLCA1	Chloride Channel Accessory 1
COS cells	CV-1 (simian) in Origin carrying the SV40 genetic material
CPT-cAMP	8-(4-Chlorophenylthio) adenosine 3', 5'- cyclic monophosphate
Cryo-EM	Cryo-Electron Microscopy
CV	Conducting Velocity
DALDA	H-2',6'-dimethyltyrosine [Dmt ¹]-d-Arg-Phe-Lys-NH ₂
DRG	Dorsal Root Ganglion
ECC	Electrocardiogram
E _{ion}	Reversal potential for an ion
ER	Endoplasmic Reticulum
ERG channel	Ether-à-go-go-Related Gene
FRET	Fluorescence Resonance Energy Transfer
GABA	γ-aminobutyric acid
GFP	Green Fluorescent Protein
GPCR	G-Protein Coupled Receptor
H."X"	Helix "X"
HEK cells	Human Embryonic Kidney cells
I _{Kr}	Rapidly activating potassium current
I _{Ks}	Slowly activating potassium current

IPMC	Institut de Pharmacologie Moléculaire et Cellulaire
IRIS	Institut de Recherche et d'Ingénierie de la Santé
I_{ti}	Transient inward current
I_{to}	Transient inward current
K_{2P}	Two-pore domain potassium channels
KCNE	Potassium voltage-gated channel subfamily E member
LMPG micelles	Lyso-myristoyl phosphatidylglycerol micelles
LQTS	Long QT Syndrome
<i>M. ulcerans</i>	Mycobacterium ulcerans
MOR	μ -opioid receptor
Myco	Mycolactone
NFA	Niflumic acid
NMR	Nuclear Magnetic Resonance
PCT cells	Proximal Convoluted Tubule cells
PEG	Polyethylene Glycol
PGE_2	Prostaglandin E ₂
PLA_2	Phospholipase A ₂
PMA	Phorbol 12-myristate 13-acetate
PKA	Protein Kinase A
PKC	Protein Kinase C
PTX	Pertussis Toxin
PUFA	Polyunsaturated fatty acids
RVD	Regulatory Volume Decrease
SiMPull	Single Molecule Pulldown
TALK	TWIK-related Alkaline pH-activated K ⁺ channels
TASK	TWIK-related Acid Sensitive K ⁺ channels
THIK	TWIK-related Halothane Inhibited K ⁺ channels
TIRF	Total Internal Reflection Fluorescence
TM	Transmembrane

TMEM16	Transmembrane protein 16
TRAAK	TWIK-related Arachidonic acid Activated K ⁺ channels
TREK	TWIK-related K ⁺ channels
TRESK	TWIK-related Spinal cord K ⁺ channels
TRP	Transient Receptor Potential ion channel
TWIK	Tandem of P-domains in a Weak Inward rectifying K ⁺ channel
VRAC	Volume-Regulated Anion Channel

Figures

Figure 1. The KCNE family	26
Figure 2. Influence of KCNE subunits on KCNQ1.	28
Figure 3. Structure of the KCNE1 protein.	29
Figure 4. Density-dependent stoichiometry model of the KCNE1-KCNQ1 complex.....	31
Figure 5. Ionic basis for cardiac action potential.	33
Figure 6. Impact of KCNE1 and KCNQ1 in cardiac action potential and LQTS.....	34
Figure 7. Ribbon representation of TMEM16A.....	40
Figure 8. Pore and calcium binding sites of TMEM16A.	41
Figure 9. Calcium and voltage-dependent gating of TMEM16A.	42
Figure 10. KCNE1 converts the CaCC TMEM16A into a voltage-dependent chloride channel.	46
Figure 11. KCNE1 co-expression does not activate SK4 channels.	47
Figure 12. KCNE1 does not activated other TMEM16 channels.	48
Figure 13. KCNE1 does not shift the intrinsic voltage-dependence of TMEM16A.....	49
Figure 14. TMEM16A-TM domain I637A and Q645A mutations are not sensitive to KCNE1 co-expression.....	50
Figure 15. Calcium sensitivity of TMEM16A-KCNE1 channel complex.....	51
Figure 16. Schematic of SiMPull technique.....	52
Figure 17. KCNE1 and TMEM16A interact in a 2 α :2 β complex.....	54
Figure 18. KCNE1-TMEM16A complex creates a voltage-dependent chloride current in proximal convoluted tubule (PCT) cells.	56
Figure 19. The pre-transmembrane domain (Nter13) of KCNE1 is sufficient for KCNE1- induced TMEM16A conversion.....	58
Figure 20. Nter13 peptide is sufficient to switch the functioning mode of TMEM16A.....	58
Figure 21. The KCNE1 S38G and R32H do not impair KCNQ1 regulation, but abolish TMEM16A regulation.....	60
Figure 22. TMEM16A is activated by KCNE5.....	61
Figure 23. Schematic representation of mycolactone A/B structure.....	74
Figure 24. Mycolactone triggers cell hyperpolarization via the TRAAK channel upon binding to the AT2R receptor.....	75
Figure 25. The two-pore-domain K ⁺ channels family.....	80
Figure 26. Structure of TRAAK.....	82
Figure 27. Model for TRAAK mechanosensitivity.....	83
Figure 28. H.VIII blocks the putative G-protein/ β -arrestin-binding site of AT2R.	89
Figure 29. Mycolactone induces hyperpolarization of DRG neurons through TRAAK channels.....	94
Figure 30. Mycolactone induces analgesia through TRAAK channels.	96
Figure 31. Mycolactone effect is sustained as it does not desensitize.	98

Figure 32. Activation by mycolactone is G-protein independent and does not involve soluble second messengers. 100

Figure 33. AT2R and TRAAK are physically coupled within a micro-regulatory membrane domain. 102

Figure 34. Activation by mycolactone is specific for AT2R and TRAAK. 104

Tables

Table 1. Table 1. Intracellular and extracellular ion distribution found in animal fluids. 22

Table 2. Relative permeability (P_x/P_{Cl}) of the TMEM16A-KCNE1 current to anions. 47

Equations

Equation 1. Nernst equation (I). 22

Equation 2. Nernst equation (II). 23

Equation 3. Goldman-Hodgkin-Katz equation. 23

Science, my boy, is made up of mistakes, but they are mistakes which it is useful to make, because they lead little by little to the truth.

Vingt mille lieues sous les mers, 1870. Jules Verne

Electrophysiology can be defined as the science concerned with the transport of ions in biological tissues (bioelectricity) and the recording techniques that allow the measurement of this transport. The passive flow of ions is conducted by ion channels, small pore-forming proteins that have evolved to selectively and rapidly conduct them by following an electrochemical gradient across the plasma membrane. Ion channels are present across all six kingdoms of life and are essential for movement, development and sensing stimuli.

The first studies regarding electrical signals in animal tissues were carried out in the late 18th century by Luigi Galvani. He observed that touching exposed crural nerves of dead frogs with a scalpel connected to a voltaic pile resulted in twitching of frog legs. He addressed this phenomenon to what he called “animal electricity”. Nowadays, we know that this “animal electricity” is the ion flux across cell membrane. Additional pioneer works dedicated to understand “animal electricity” were performed from that moment. Carlo Matteucci showed that, in rest, there was a difference of potential between the damaged and the intact surface of a severed muscle (*i.e.* the inside and the outside of a muscle fiber) and Hermann von Helmholtz developed a number of accurate instruments that allowed him to determine the propagation speed of an electrical signal along a nerve cell (10-100 m/s). Modern era of electrophysiology came with experiments on squid giant axon carried out by Alan Hodgkin and Andrew Huxley in the early 20th century. They succeed in describing the nerve action potential as a mathematical model involving Na⁺ and K⁺ conductances across the axon membrane. This work, together with the patch-clamp technique established by Erwin Neher and Bert Sakmann, constitutes the basis of modern electrophysiology and the role of ion channels. More recent techniques like optogenetics or cryo-EM represent nowadays a new source of information about how ion channels work.

To understand ion channels function it is necessary to know the plasma membrane properties and the ionic environment of the cell. All living cells are enveloped by a plasma membrane that protects the cytoplasm from the extracellular space. The plasma membrane is mainly constituted by phospholipids that arrange themselves spontaneously in amphipathic structures in watery environments as the extracellular space is, forming a consistent barrier for charged molecules. Another characteristic of the plasma membrane is its fluidity, which represents a dynamic substrate for other membrane components (mostly ion channels, pumps, receptors and cytoskeletal anchors). Concerning the intracellular and extracellular environment, there is an ion distribution which is fairly constant among a large range of cell types. An overview of ranges of concentration of the principal ions in both intracellular and extracellular space is represented in *Table 1*.

Table 1. Table 1. Intracellular and extracellular ion distribution found in animal fluids.

Ion	Intracellular range (mM)	Extracellular range (mM)
Na ⁺	5-20	130-160
K ⁺	130-160	4-8
Ca ²⁺	50-1000 nM	1-4
Mg ²⁺	10-20	1-5
Cl ⁻	1-60	100-140
HCO ₃ ⁻	1-3	20-30

Passive movement of ions obeys to an electrochemical gradient defined by the Nernst equation (*Equation 1*).

Equation 1. Nernst equation (I).

$$\Delta G = -RT \ln \frac{[ion]_o}{[ion]_i}$$

Where ΔG is the energy to be released by the diffusion movement, R is the universal gas constant ($8.31 \text{ J mol}^{-1} \text{ K}^{-1}$), T is the temperature in Kelvin and $[\text{ion}]_o$ and $[\text{ion}]_i$ are the extracellular and intracellular concentrations of the particular ion. Thereby, if the plasma membrane is, for instance, permeable to potassium ions, they will move from the cytoplasm to the extracellular space and the exit of positive charges will render the cell negatively charged, starting to attract the potassium ions back into the cell. Once the electrical force that this movement creates is equal in size but opposite to the diffusion energy and there is no net movement of the ion, the ion will have reached its equilibrium. The electrical equilibrium potential for a considered ion is defined by the following arrangement of the Nernst equation where E_{ion} is the equilibrium potential for the respective ion (*Equation 2*).

Equation 2. Nernst equation (II).

$$E_{\text{ion}} = \frac{RT}{zF} \ln \frac{[\text{ion}]_o}{[\text{ion}]_i}$$

Because the particles are charged and they are distributed differently between the intracellular and extracellular space, the flux across the membrane is determined by a concentration gradient and an electric field established by the ions. If we assumed that every type of ion has a different permeability (because of ion channels specificity) to diffuse through the membrane, the electric field in the membrane will be constant and ions will cross it independently from each other. In others words, it is possible to calculate the resting membrane potential in a cell, which is given by the Goldman-Hodgkin-Katz equation (*Equation 3*).

Equation 3. Goldman-Hodgkin-Katz equation.

$$E_m = \frac{RT}{F} \ln \frac{PNa^+[Na^+]_o + PK^+[K^+]_o + PCl^- [Cl^-]_i}{PNa^+[Na^+]_i + PK^+[K^+]_i + PCl^- [Cl^-]_o}$$

E_m corresponds to the membrane potential and P_x to the different permeabilities for every ion. With several permeant ions (mainly K^+ , Na^+ and Cl^-), E_{rev} is actually a weighted mean of all the Nernst potentials. As K^+ is generally the most permeable ion in cells, it is not surprising that E_{rev} in many cells is very close to E_{K^+} .

Since membrane potential is dictated by ion permeability, it is reasonable to wonder how the permeability of the membrane for different ions is established and controlled. Ion channels possess characteristics that make them very effective to regulate membrane permeability to small water-soluble particles. The first characteristic is an aqueous pore that connects intracellular and extracellular spaces. This pore, usually lined by mainly hydrophobic residues, dictates the selectivity and the speed for each class of ion traversing it. The mechanism of selective permeability is based on a combination of the size of the ion (in its hydrated form) and its charge. Secondly, they have a gating (opening and closing) mechanism that consists in a conformational change induced by specific stimuli. The main stimuli governing ion channels gating are changes in the membrane potential, intracellular covalent modifications (such as addition of phosphate groups) or extracellular ligands (like neurotransmitters) that bind directly to the channel and second messengers (Ca^{2+} , cAMP...). Additional modulatory factors can regulate gating like, protons, temperature or osmotic changes. Moreover, the biophysical and pharmacological properties of ion channels can be also modulated by subunits that bind to the pore-forming subunits. These auxiliary or ancillary subunits play a crucial role in current diversity in the organism and their importance will be developed in this work. To sum up, ion channels are the most fundamental elements in the membrane of excitable cells.

Science is based on experiment, on a willingness to challenge old dogma, on an openness to see the universe as it really is. Accordingly, science sometimes requires courage – at the very least the courage to question the conventional wisdom.

Broca's Brain, 1976. Carl Sagan

A. Introduction

1. Ancillary subunits: The KCNE family

Generalities of the KCNE family

An expanding view of cell biology is that proteins do not act alone, but they assemble dynamically into large complexes adopting new properties within the cell. Electrical signals are conducted primarily by α -subunits that form the pore by which ions transverse the plasma membrane from one compartment to the other. The high variety of ion currents is enhanced by ancillary (β) subunits which constitute an important source for diversity of electrical signals in cells. Although ancillary subunits cannot induce native currents *per se*, they are capable to associate with α -subunits constituting the pore and change the pharmacological and biophysical properties of ion channels, as well as their trafficking and assembly (Pongs and Schwarz, 2010; McCrossan and Abbott, 2004). KCNE proteins are a family of transmembrane proteins broadly known for associating with voltage-gated KCNQ (K_v7) K⁺ channels and acting as β -subunits. They constitute a family of five members, ranging between 14-20 KDa or 103-177 residues, with a short hydrophobic domain spanning the plasma membrane and the carboxy- and amino-terminal domain facing towards the intracellular and extracellular side, respectively (Pongs and Schwarz, 2010; McCrossan and Abbott, 2004; Takumi et al., 1988; Abbott et al., 1999; Piccini et al., 1999) (**Figure 1**).

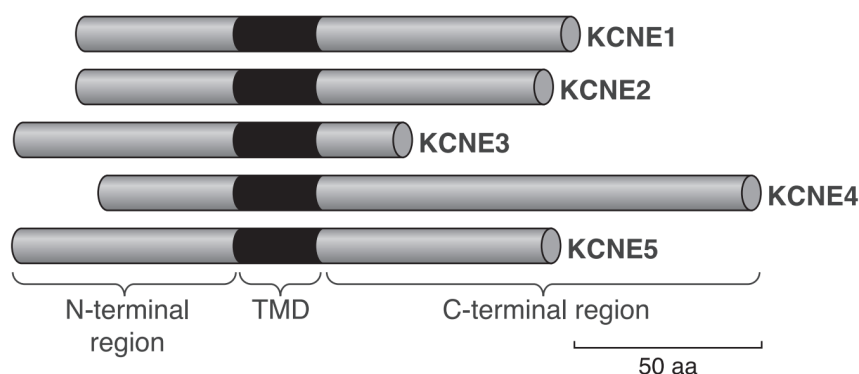


Figure 1. The KCNE family

The KCNE proteins share a common structure consisting of an extracellular N-terminus followed by a transmembrane segment and an intracellular C-terminal region. Extracted from Pongs and Schwarz, 2010.

The first cloned member of this family was KCNE1 (K⁺ voltage-gated Channel subfamily E regulatory subunit 1) from rat kidney (Takumi et al., 1988). As the injection of its RNA in *Xenopus* oocytes produces a slow activating K⁺ current, for some years KCNE1 was believed to be a K⁺ channel (Goldstein and Miller, 1991). Experiments with other heterologous models questioned this finding since expression of KCNE1 alone is not able to induce current in COS nor CHO cells. This question was later resolved by the discovery that endogenous KCNQ1 was needed to observe the KCNE1-induced K⁺ current (Sanguinetti et al., 1996; Barhanin et al., 1996). These experiments confirmed that KCNE1 is actually a β -subunit of these channels. KCNE1 changes the gating and the biophysical properties of KCNQ1, from a voltage-dependent rapidly activating and slowly deactivating to the slow activated and delayed-rectifier channel underlying the human ventricular slow K⁺ repolarizing current (I_{Ks}) (Wang and Goldstein, 1995; Barhanin et al., 1996; Sanguinetti et al., 1996). In addition, KCNE1 can also associate to the ether-à-go-go (hERG) channel, and the current carried by the complex underlies the human ventricular rapid K⁺ repolarizing current (I_{Kr}) (McDonald et al., 1997).

KCNE2, 3 and 4 were first screened for their functional partners by co-expressing them with different α -subunits in *Xenopus laevis* oocytes by the Goldstein lab, one decade after the discovery of KCNE1 (Abbott et al., 1999). All different KCNEs interact with KCNQ1, inducing different effects on its kinetics (Bendahhou et al., 2005) (**Figure 2**). KCNE2 has been reported to associate with KCNQ1 channels, converting them into leak channels that present instantaneous activation and fast deactivation (Tinel et al., 2000). Moreover, it has been suggested that KCNE2 can associate with KCNQ1 and KCNE1, forming a tripartite complex contributing to the I_{Ks} cardiac current (Jiang et al., 2009). Association of KCNE3 with KCNQ1 abolishes the voltage dependence of KCNQ1, converting it into a K⁺ leak channel whose current is solely dictated by the K⁺ driving force (Schroeder et al., 2000). KCNE4 and KCNE5 produce a similar effect on the gating of KCNQ1 channels by different means. Whereas KCNE4 inhibits the binding of the channel with its activator calmodulin (Ciampa et al., 2011; Angelo et al., 2002), KCNE5 shifts the voltage-dependence of KCNQ1 to +140 mV, rendering the channel non-functional at physiological potentials. KCNE5 also slows activation and accelerate deactivation of KCNQ1 (Angelo et al., 2002). Moreover, both KCNE4 and KCNE5 partially inhibit the KCNE1-KCNQ1 current and right-shift its voltage-dependent activation (Lundquist et al., 2005).

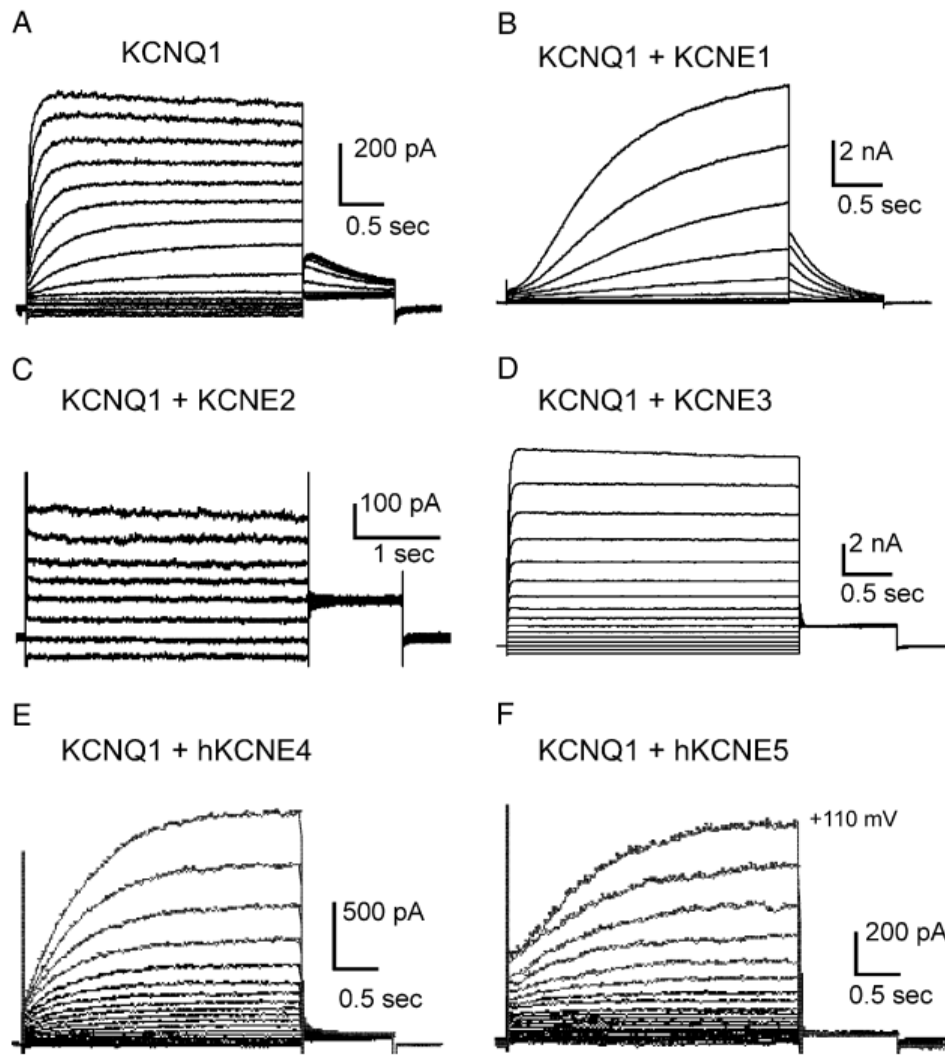


Figure 2. Influence of KCNE subunits on KCNQ1.

The distinct KCNE proteins regulate differently the gating of KCNQ1 channels. From Bendahhou et al., 2005.

The KCNE1 protein

Most of the available information of the KCNE1 structure comes from NMR and reconstitution studies in LMPG micelles and phospholipids vesicles (Kang et al., 2008; Coey et al., 2011; Zhang et al., 2017b). The human KCNE1 is a 129-residue single span protein consisting of a transmembrane α -helix (22 residues), which is flanked by two extra and intracellular domains (44 and 63 residues, respectively) bordered by flexible polar linkers (Kang et al., 2008; Coey et al., 2011; Zhang et al., 2017b) (**Figure 3**). The N-terminal domain is located in the extracellular side and it is glycosylated in three residues by post-translational modifications. Mutation of these residues do not alter KCNE1 function but strongly reduce cell expression and are implicated in cardiac arrhythmias (Chandrasekhar et al., 2011). NMR spectroscopy suggests that residues in the extracellular helix interact with phospholipids heads of the plasma membrane, increasing its fluidity (Zhang et al., 2017b). Moreover, half of this segment adopts a helical conformation. The transmembrane domain adopts a curved helical conformation induced by the backbone conformational balance between several glycines and a number of β -branched residues located in this segment (Kang et al., 2008). The C-terminal domain enters in the cytosol, where it interacts not only with KCNQ1 domains, but also with additional proteins like protein kinase C (PKC) and the T-cap sarcomeric component of cardiac muscle (Furukawa et al., 2001; Xu et al., 2009).

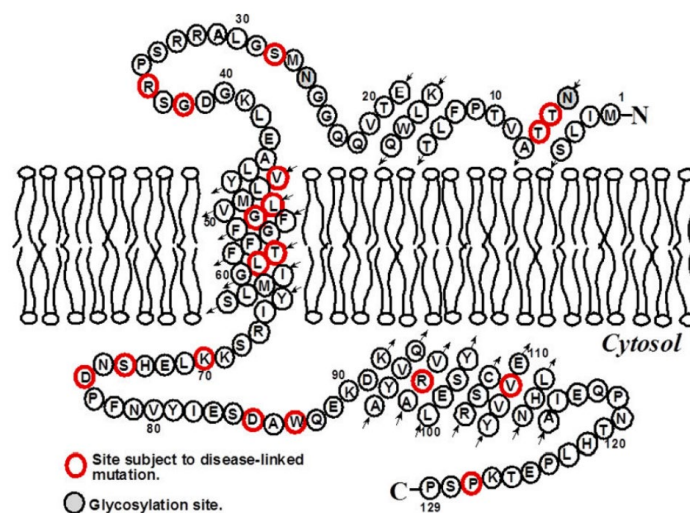


Figure 3. Structure of the KCNE1 protein.

KCNE1 is a single transmembrane protein consisting of an extracellular N-terminus, a transmembrane segment and an intracellular C-terminus. Extracted from Zhang et al., 2017.

As an ancillary subunit, KCNE1 is mainly known to control the gating properties of the KCNQ1 α pore subunit. It has been demonstrated that, although they do not contribute in the same way, all KCNE1 domains are involved in KCNQ1 regulation. Accordingly, a structural work has shown that the distal part of the KCNE1 transmembrane segment lies on the KCNQ1 S4-S5 linker (the link between the voltage sensor domain and the gate) (Kang et al., 2008). The proximal extracellular domain of KCNE1 also interacts with KCNQ1 in S1 and S6 modifying the pH and pharmacological sensitization instead (Kang et al., 2008; Chung et al., 2009; Xu et al., 2008). Nevertheless, major findings in KCNQ1 gating regulation have been shown in the KCNE1 C-terminal domain (Attali et al., 1993; Pongs and Schwarz, 2010). It is not clear how KCNE1 induces KCNQ1 slow activation. One possibility is that KCNE1 slows the upward movement of the KCNQ1 S4 voltage sensor domain upon membrane depolarization (Ruscic et al., 2013). Such low mobility could be also responsible of its altered inactivation (Gofman et al., 2012). Another study has suggested that the low activation of the KCNE1-KCNQ1 complex is due to the action of two phenylalanine residues of KCNE1 on the S4 voltage sensor domain and the S6 pore domain of KCNQ1, which collide during S4 movement, slowing the opening of KCNQ1 (Nakajo and Kubo, 2014).

In addition, KCNE1 seems to modify also KCNQ1 trafficking. One study has shown, by using truncated mutants, that deletion of the C-terminus of KCNE1 prevents co-assembly with KCNQ1 channels (Tapper and George, 2000). Another study has demonstrated, using a KCNE1 long-QT-syndrome (LQTS) related mutant, that KCNE1 is retained in the ER if KCNQ1 is not translated in the co-synthesis at the same time, suggesting that the KCNE1-KCNQ1 interaction occurs in early stages (Krumerman et al., 2004). Nevertheless, this is in contrast with another study that indicates that co-translation is not required for subunit co-assembly (Vanoye et al., 2010). KCNE1 also regulates the endocytic pathway of KCNQ1. Although KCNQ1 can be internalized by Rab5 and the ubiquitylating Nedd44 proteins independently from KCNE1 (Seeböhm et al., 2007; Jespersen et al., 2007), KCNE1 is involved in endocytosis mediated by clathrin proteins in cardiac myocytes. When KCNE1 is phosphorylated by PKC at its C-terminal domain (Ser102) the β -subunit becomes a chaperone of its associated KCNQ1 subunits, leading to clathrin-mediated and dynamin 2-dependent endocytosis of the complex. This is translated in a dramatic decrease of the KCNE1-KCNQ1 complex at the cell surface (Xu et al., 2008; Kanda et al., 2011).

Regarding to the stoichiometry of the complex KCNE1-KCNQ1, there is currently a broad debate about the number of subunits involved. Whereas some studies suggest that its stoichiometry is fixed to either $4\alpha:2\beta$ or $4\alpha:4\beta$ (Morin and Kobertz, 2008; Plant et al., 2014), single molecule co-localization method in living cell and photo-crosslinking experiments indicate that KCNE1-KCNQ1 can vary from $4\alpha:1\beta$, $4\alpha:2\beta$ to $4\alpha:4\beta$ (Nakajo et al., 2010; Murray et al., 2016) (*Figure 4*).

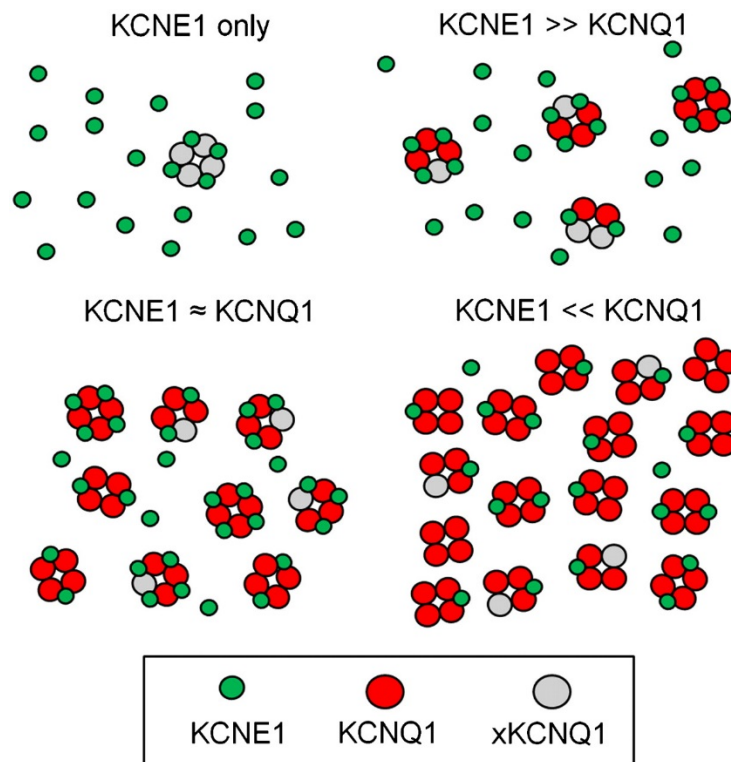


Figure 4. Density-dependent stoichiometry model of the KCNE1-KCNQ1 complex.

*Model of density-dependent stoichiometry of the KCNQ1-KCNE1 complex. Stoichiometry of the KCNQ1-KCNE1 complex depends on how many free KCNE1 subunits (green circles) are available for the exogenous KCNQ1 channels (red circles). Endogenous KCNQ1 subunits in *Xenopus oocytes* (xKCNQ1) are depicted as grey circles. Extracted from Nakajo et al., 2010.*

Physiological role of KCNE1

KCNE1 is broadly known for its contribution to ventricular repolarization in cardiac action potentials when it associates to KCNQ1 (Sanguinetti et al., 1996; Barhanin et al., 1996). The propagation of the cardiac action potential is dependent of a battery of ion channels acting in fine concert with ancillary subunits (**Figure 5**). The cardiac action potential is initiated by a localized membrane depolarization that activates voltage-gated Na⁺ channels, allowing rapid and transient Na⁺ currents. This phenomenon represents the classical upstroke in the electrocardiogram (ECC) known as phase 0. This depolarization is followed by a rapid transient repolarization (phase 1) mediated fast-gating K_v4.3 channels (Dixon et al., 1996; George, 2013). During phases 0 and 1, Na⁺ channels rapidly inactivate and L-type Ca²⁺ channels activate, contributing to a long depolarizing plateau (phase 2). This inactivation is in balance with inward currents carried by L-type Ca²⁺ channels, residual Na⁺ currents, and emerging outward currents carried by K⁺ channels (Qin et al., 1999; George, 2013). Activation of rapid and slow activating K⁺ currents mediated by hERG-KCNE1 and KCNQ1-KCNE1, respectively, in tune with the Ca²⁺ and voltage-dependent inactivation of Ca²⁺ channels, tips the balance in favor of the outward current. These events promote phase 3 (repolarization) of the action potential (Sanguinetti et al., 1996; Sanguinetti et al., 1995; Barhanin et al., 1996)

As said above, KCNE1 has been reported to associate *in vitro* with the hERG channel and the complex is believed to participate in the I_{Kr} component of the repolarizing phase (McDonald et al., 1997) and with KCNQ1 to constitute the I_{Ks} component (Sanguinetti et al., 1996; Barhanin et al., 1996). I_{Ks} appears to be more important during physical effort or similar contexts when β-adrenergic stimulation is produced. In fact, sympathetic nervous system increases I_{Ks} density and accelerates repolarization to compensate for higher heart rates by inducing a reserve of nearly-open closed channels (Knollmann et al., 2007). This phenomenon is due to phosphorylation by protein kinase A (PKA) of residue Ser27 of KCNQ1, which is facilitated by KCNE1 and the kinase-anchoring protein Yotiao (Kurokawa et al., 2009). Interestingly, the response of the complex to PKA stimulation seems to be dependent of KCNE1-KCNQ1 stoichiometry (Thompson et al., 2018). However, stimulation of α-1 adrenergic receptors activates PKC, which phosphorylates KCNE1 in residue S102 promoting clathrin-mediated and dynamin 2-dependent endocytosis of the KCNE1-KCNQ1. Thus, the I_{Ks} component duration is shortened (Kanda et al., 2011; Xu et al., 2009).

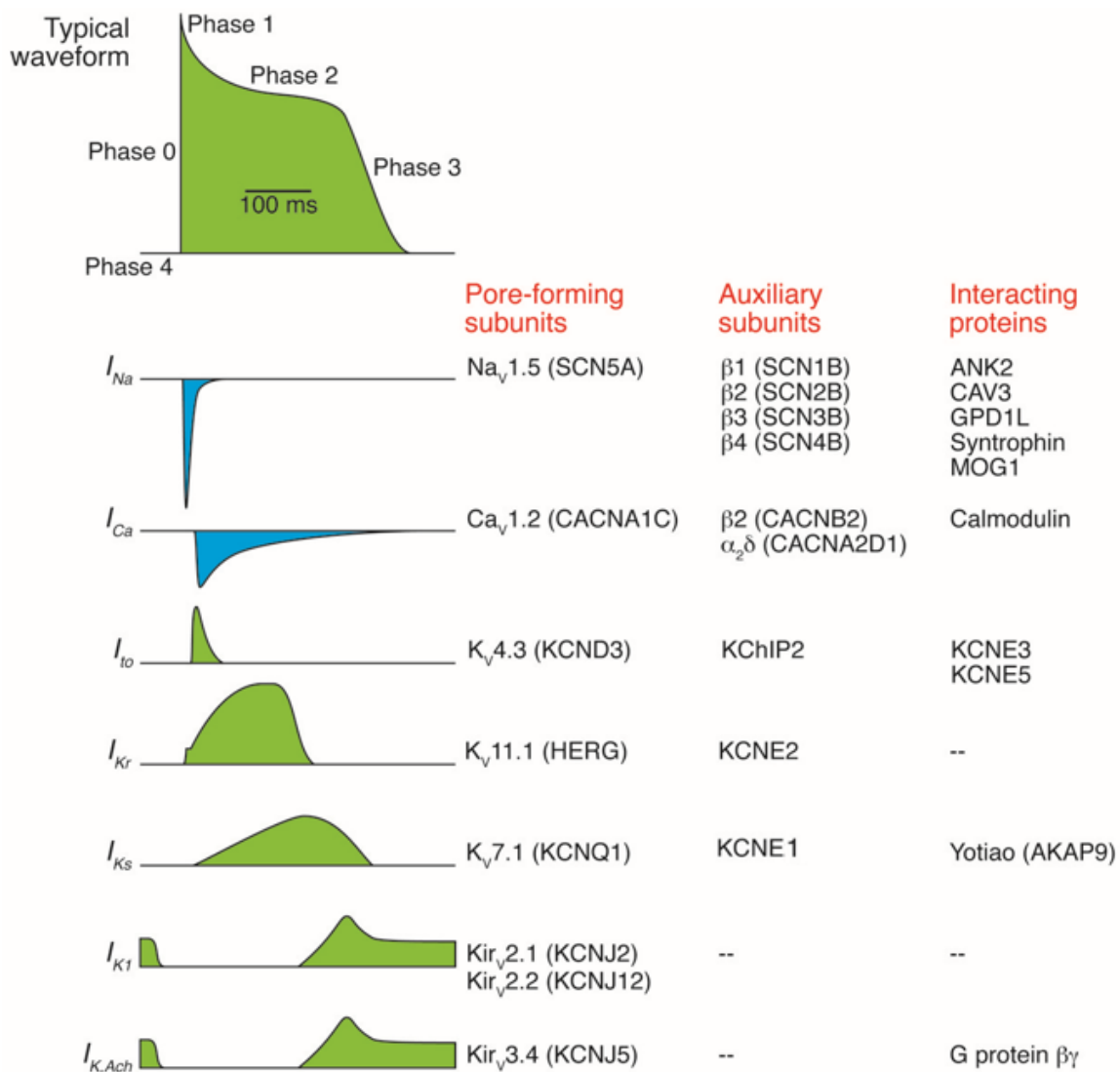


Figure 5. Ionic basis for cardiac action potential.

A battery of different ion channels and ancillary subunits controls the cardiac action potential. Extracted from George, 2013.

The physiological importance of KCNE1 on the cardiac action potential is reflected on the high number of cardiac arrhythmias related with dysfunction of this protein, notably LQTS (Crump and Abbott, 2014). LQTS is characterized by a prolonged QT interval in the ECC, due to delayed repolarization of the cardiac action potential (**Figure 6**) (Crump and Abbott, 2014). It may be autosomal dominant (Romano-Ward syndrome) or autosomal recessive (Jervell and Lange-Nielsen syndrome) (George, 2013). LQTS caused by *kcne1* mutations is categorized as LQTS-5 and as LQTS-1 when it is due to *kcnql* mutations (Barhanin et al., 1996; Bianchi et al., 1999).

Interestingly, both S38G (present in ~20 % of studied populations) and R32H KCNE1 polymorphisms, which cause predisposition to LQTS (Fatini et al., 2010), have no or negligible effects on the I_{K_s} cardiac current (Westenskow et al., 2004; Yao et al., 2018). This may indicate another function for KCNE1. Surprisingly, *kcne1*^{-/-} mice show a similar QT interval compared to wild type mice, although their QT-RR (*i.e.* the distance between two successive R waves) adaptation in ECC is exacerbated, leading to a prolonged QT interval during bradycardia (Drici et al., 1998).

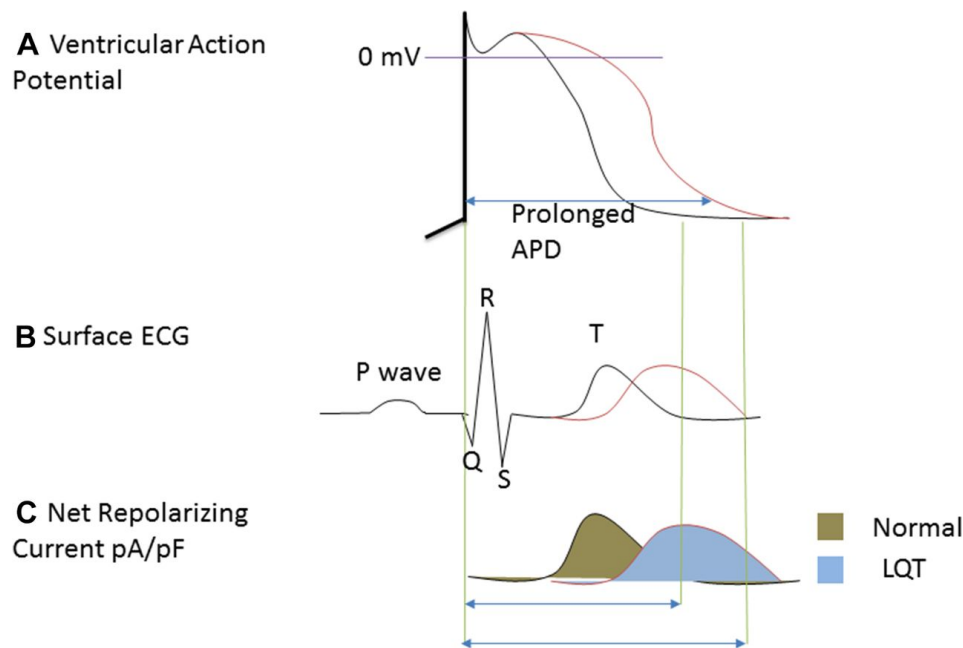


Figure 6. Impact of KCNE1 and KCNQ1 in cardiac action potential and LQTS.

The LQTS is caused by an aberrant prolongation of the QT interval. Modified from Ezeani and Elom, 2017).

Concerning to the function of KCNE1 *in vivo* outside the heart, most of the available information come from studies performed on *kcne1*^{-/-} mice. In the inner ear, it has been proposed that KCNE1-KCNQ1 provides a conduit for K⁺ secretion that recycles K⁺ in endolymph of vestibular dark cells (Warth et al., 2002; Vetter et al., 1996; Abbott, 2016). As a result, mice lacking of the *kcne1* present Shaker-Waltzer behavior and bilateral deafness (Vetter et al., 1996). *Kcne1*^{-/-} mice are also hypokalemic and exhibit increased hematocrit, suggesting impaired renal electrolyte and enhanced water loss (Vallon et al., 2001). It has been also shown that these mice present irregularly distributed pancreatic secretory granules and their pancreatic acinar basolateral membrane lacks of KCNQ1 (Warth et al., 2002). They also exhibit fecal salt loss, suggesting a potential role in intestine (Arrighi et al., 2001).

KCNE1 as a dual ancillary subunit of potassium and chloride channels

Another intriguing feature of KCNE1 is its ability to induce not only K⁺, but also Cl⁻ currents when its RNA is injected in *Xenopus* oocytes (Attali et al., 1993). Moreover, chimeric KCNE1 showed that, while the C-terminus seems to be crucial for the induction of K⁺ currents (KCNQ1), the N-terminal part induces Cl⁻ currents (mutants S68T, ΔTr80 and Δ11-38) (Attali et al., 1993) suggesting that KCNE1 is a dual activator of endogenous silent K⁺ and Cl⁻ channels in *Xenopus* oocytes (Attali et al., 1993; Ben-Efraim et al., 1996).

Moreover, *in vivo* experiments performed with proximal convoluted tubule (PCT) cells from kidney have shown that KCNE1 is needed to induce a Cl⁻ current that is lost in *kcne1*^{-/-} cells (Barrière et al., 2003). A similar Ca²⁺-activated Cl⁻ current has been described in the same cell line, although its identity remains elusive up to date (Rubera et al., 1998). All in all, KCNE1 seems to regulate not only K_v channels, but also Cl⁻ channels.

2. Calcium-activated chloride channels: TMEM16A

TMEM16 proteins: ion channels and scramblases

Ca²⁺-activated Cl⁻ channels (CaCCs) play a major role in cell physiology, including transduction of signals, regulation of cardiac and neuronal excitability, epithelial secretion and muscle contraction, among others (Pedemonte and Galiotta, 2014). TMEM16A, the main CaCC, was first cloned by three independent laboratories which used different approaches. The first one identified the channel from pools of cDNA from *Xenopus laevis* injected in Axolotl salamander oocytes, which, contrarily to those from *Xenopus*, do not express endogenous TMEM16A (Schroeder et al., 2008). The second one found it by bio-informatics analysis (Yang et al., 2008) and the third one discovered it by using gene expression microarrays (Caputo et al., 2008). As this protein was thought to be made of eight transmembrane domains (Katoh, 2004), it was initially proposed to call it anoctamin 1 (anion and octa). However, also the alternative terminology, TMEM16A (Transmembrane protein 16) is currently used in parallel.

Ten members of the TMEM16 superfamily have been found in mammals (Pedemonte and Galiotta, 2014; Falzone et al., 2018), which can be classified according to their function and homology. TMEM16A and B are considered as full CaCCs (Yang et al., 2008; Schroeder et al., 2008; Caputo et al., 2008), whereas TMEM16C, D, G and J operate as scramblases translocating lipids rapidly and bidirectionally in order to maintain plasma membrane asymmetry (Gyobu et al., 2017). Only the F form possess dual channel-scramblase activity (Gyobu et al., 2016; Yu et al., 2015; Suzuki et al., 2013). TMEM16H and K need to be studied in more detail in order to determine their real function.

Most of the structural and functional analyses of the ion channel and scramblase activity of anoctamins are based on cryo-EM assays and homology modeling of the fungal homolog scramblase nhTMEM16 from *Nectria hematococca* and the CaCC mouse homolog mTMEM16A (Brunner et al., 2016; Bethel and Grabe, 2016; Paulino et al., 2017a; Dang et al., 2017; Paulino et al., 2017b). TMEM16 channels and scramblases share an overall similar structure: they are both homodimers, consisting of ten transmembrane domains and one pore per subunit with an extensive intracellular domain that adopts a ferredoxin-like fold. Each subunit harbors two Ca²⁺ binding sites and presents a hydrophilic cavity exposed to the membrane which is surrounded by five helices (TM3-7). In the scramblase homolog

nhTMEM16 the cavity is wide at its intracellular end and narrows towards the extracellular end. In the CaCC homolog mTMEM16A the narrowing of the cleft at the extracellular end is more pronounced (Brunner et al., 2016; Bethel and Grabe, 2016; Paulino et al., 2017a; Dang et al., 2017). Some studies suggest that such cavity may serve as a common hub to both scramblase and ion channel activity by Ca^{2+} regulation. As a matter of a fact, mutations in residues within this cavity alter conduction for both lipids and ions in nhTMEM16 and mTMEM16A, respectively (Jiang et al., 2017; Lee et al., 2018).

Although anoctamins form a widespread protein superfamily, with homologs found in all eukaryotic phyla (Milenkovic et al., 2010), the fact that no homologs of TMEM16 have been found in prokaryotic organisms suggests that these proteins appeared relatively late in evolution. Moreover, TMEM16 proteins across different phyla behave differently. Ist2, a yeast TMEM16 homologue from *Saccharomyces cerevisiae*, is involved in salt tolerance and acts as a tether connecting the ER and plasma membrane (Kim et al., 2005; Wolf et al., 2014). The fungus homolog nhTMEM16 acts as a Ca^{2+} -activated phospholipid scramblase but does not present an evident ionic channel activity (Paulino et al. 2017). Another ancestral fungus homolog, afTMEM16 (from *Aspergillus fumigatus*), shows a Ca^{2+} -dependent dual-function, as an ion channel and a scramblase (Malvezzi et al., 2013; Pelz et al., 2018) similarly to TMEM16F (Suzuki et al., 2013; Yu et al., 2015).

The voltage-dependent and calcium-activated TMEM16A channel

As a CaCC, TMEM16A presents three main hallmarks: outward rectification of the steady-state current-voltage relationship due to activation and deactivation at positive and negative membrane potentials, respectively; permeability to anions; and activation by cytosolic Ca^{2+} with (Yang et al., 2008; Schroeder et al., 2008; Caputo et al., 2008).

TMEM16A activation involves the binding of up to two Ca^{2+} ions located in a coordinated binding site near to the pore of the channel and the movement of a flexible transmembrane helix (TM6), inducing conformational changes within the channel that allow it to enter either into an open outward-rectifying state or an ohmic state, depending of the number of bound Ca^{2+} ions and the conformation of this helix priming the channel to voltage-dependent changes (Paulino et al., 2017a; Dang et al., 2017; Peters et al., 2018; Paulino et al., 2017b). Concerning its permeability, TMEM16A follows an Eisenman type I sequence anion selectivity ($\text{SCN} > \text{I} > \text{NO}_3 > \text{Br} > \text{Cl} > \text{F} > \text{gluconate}$), in which anions with lower hydration energy have higher permeability compared to anions with higher dehydration energy (Peters et al., 2018; Schroeder et al., 2008; Yang et al., 2008).

TMEM16A can be regulated by other stimuli. Cholesterol depletion and decrease of intracellular pH have been reported to reduce CaCC amplitude in smooth muscle cells expressing endogenous CaCC and in transfected HEK cells (Sones et al., 2010; Chun et al., 2015). Heat is another activator of TMEM16A present in dorsal root ganglia (DRG) neurons (Cho et al., 2012). It is believed that TMEM16A could act also as a mechanosensitive channel in arterial smooth muscle cells since they are activated by swelling induced by hypoosmolarity, independently from the VRAC channel LRRC8 (Bulley et al., 2012). A recent study showed that PIP_2 binds also to TMEM16A facilitating its opening (Le et al., 2019).

Another characteristic of TMEM16A arises from alternative splicing. There are multiple isoforms generated by skipping/inclusion of alternative exons which are distributed among the different tissues and have different biophysical properties (Ferrera et al., 2009; Sondo et al., 2014). There exist, at least, four alternative segments: a (116 amino acids), b (22 amino acids), c (4 amino acids) and d (26 amino acids) (Ferrera et al., 2009). For instance, the ac isoform (lacking of segments b and d) is more sensitive to Ca^{2+} than the isoform abd (lacking of segment c) (Ferrera et al., 2009).

Selective compounds against TMEM16A may be useful tools for studying this channel. The lack of selective compounds has historically slowed-down the research on CaCCs. Niflumic acid, which was considered as specific blocker of CaCC, has been demonstrated to act on other channels by emptying intracellular Ca^{2+} stores (Poronnik et al., 1992; Cruickshank et al., 2003; Balderas et al., 2012). Since its discovery, many inhibitors have been designed in order to block TMEM16A, including $\text{CaCC}_{\text{inh}}\text{-A01}$, $\text{T16A}_{\text{inh}}\text{-A01}$ and MONNA, although they are not promising due to their low specificity (De La Fuente et al., 2008; Namkung et al., 2011; Peters et al., 2015). So far, Ani9 has been determined as the most specific (with negligible effects on TMEM16B) and potent blocker ($\text{IC}_{50} > 0.11 \mu\text{M}$) of TMEM16A, without affecting Ca^{2+} intracellular signaling nor CFTR Cl^- channel activity (Seo et al., 2016). Fewer advances have been made for TMEM16A activators. A screening of small molecules in FRT cells transfected with TMEM16A in 2011 revealed the existence of two compounds which seem to fully activate the channel without inducing intracellular Ca^{2+} mobilization. However, they are also activators of TMEM16B (De La Fuente et al., 2008; Namkung et al., 2011; Peters et al., 2015). Some herbal compounds used in traditional medicine such as ginsenoside (Guo et al., 2020) and resveratrol (Chai et al., 2017) have been also found to activate TMEM16A, although their specificity remains unclear.

Concerning its distribution, TMEM16A is mainly an epithelial channel (Pedemonte and Galiotta, 2014). Particular importance is given to this channel in airways epithelia, where it mediates mucus secretion and fluidity in goblet cells (Huang et al., 2012). Interestingly, TMEM16A acts on airways epithelial cells in tune with Cl^- CFTR channels, and dysfunction of both of them are related with cystic fibrosis (Benedetto et al., 2017).

Structure of TMEM16A

Major advances concerning the TMEM16 structure have been made in the last years by cryo-EM, which allows a near atomic resolution by capturing multiple dynamic states. TMEM16A is a homodimer consisting in an intracellular C-terminus and N-terminus and a TM domain of ten α -helices. The interface between both subunits is the outer part of both α -10, which are in similar location to nhTMEM16's but extend further towards the outside (Paulino et al., 2017a; Dang et al., 2017; Peters et al., 2018; Brunner et al., 2014; Paulino et al., 2017b).

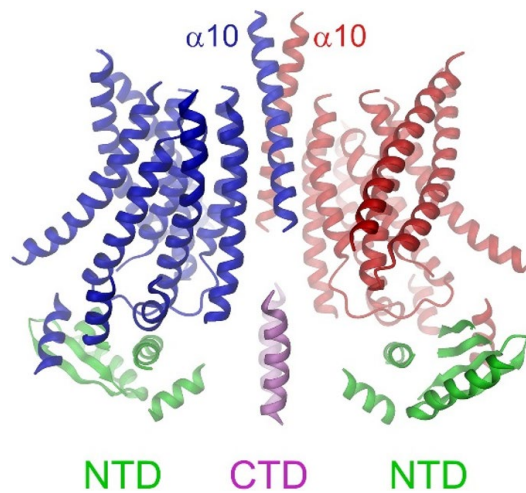


Figure 7. Ribbon representation of TMEM16A.

Ribbon representation of the TMEM16A dimer. The transmembrane domains of individual subunits are colored in blue and red, respectively, N-terminal domains (NTD) in green and the C-terminal domains (CTD) in violet. Extracted from Paulino et al., 2017.

Each subunit of the dimer is harboring one anion pore, which works independently from the other under the same mechanism (Brunner et al., 2014; Jeng et al., 2016; Lim et al., 2016; Paulino et al., 2017a). The ion conduction pore is lined by residues located on TM3-7 (Paulino et al., 2017a). TM4 and 5 form, together with TM3, 5 and 7, the narrow neck of an aqueous pore that spans the extracellular two thirds of the plasma membrane. Towards the cytosolic side, the detachment between TM4 and 6 results in a wide intracellular vestibule of the pore that is exposed to both the cytoplasm and the lipidic bilayer. As a result, the ion-conducting pore adopts an hourglass as shown in **Figure 8** (Paulino et al., 2017a; Paulino et al., 2017b).

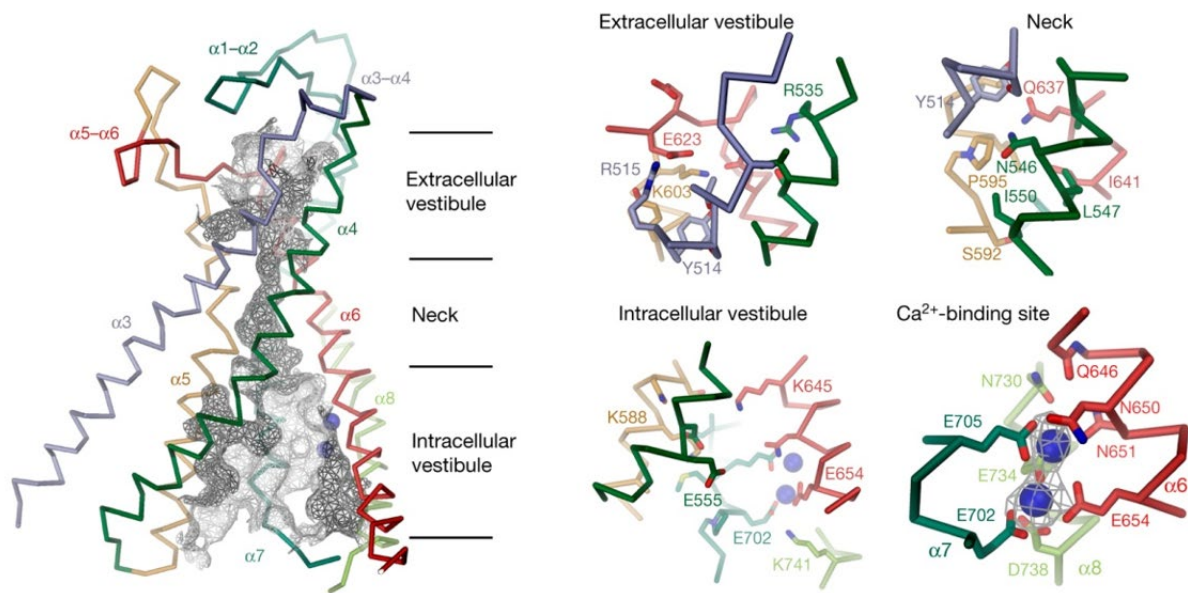


Figure 8. Pore and calcium binding sites of TMEM16A.

Grey mesh, pore surface. Sections of the pore: the extracellular vestibule, the neck and the intracellular vestibule. Structure of the Ca^{2+} -binding site with cryo-EM density of the two Ca^{2+} ions superimposed as mesh. Protein is shown in unique colors; sticks, sidechains of selected residues; blue spheres, Ca^{2+} ions. Extracted from Paulino et al., 2017.

Some residues involved in the pore are essential for anion conductance and channel gating. Peters and co-workers demonstrated that mutations in four basic residues located in the outer mouth change anion selectivity, suggesting that the presence of the positively charged side chains of these residues might preferentially promote flux of Cl^- ions (Peters et al., 2015). Additionally, another work has recently found more residues within the segments constituting the pore which seem to be also important for anion selectivity (Dang et al., 2017).

Voltage – dependence and calcium activation of TMEM16A

A hallmark of CaCCs is their voltage-dependence and outward rectification at low Ca^{2+} concentrations and ohmic and leaky kinetics at high concentrations, suggesting the existence of multiple open states (Kuruma and Hartzell, 2000; Perez-Cornejo et al., 2004). Initially it was believed that activation by Ca^{2+} came from the association between TMEM16A and calmodulin (Tian et al., 2011). However, this is not actually true since the channel binds directly up to two Ca^{2+} ions (Yu et al., 2014; Dang et al., 2017; Paulino et al., 2017a; Tien et al., 2014).

Peters and co-workers have recently demonstrated by electrophysiology and cryo-EM the crucial role of the sixth transmembrane segment of TMEM16A in gating (Peters et al., 2018). It was previously shown that this segment is highly flexible due in part to a helical distortion in Gly640 and its poorly ordered structure (Dang et al., 2017; Paulino et al., 2017a). The model for the Ca^{2+} and voltage-dependent gating mode of TMEM16A is depicted in **Figure 9**: In the absence of cytosolic Ca^{2+} , TMEM16A is closed but is able to bind Ca^{2+} ions. As concentration of internal Ca^{2+} increases (~ 400 nM), a single Ca^{2+} ion binds to the channel and Cl^- anions enter the outer pore. The pore enters then into an outward-rectifying conducting state and primers the channel to undergo a fast voltage-dependent conformational change involving TM6. Association of the second Ca^{2+} ion results in stabilization of the fully activated conformation of TM6, resulting in the ohmic anion conductance open state of the pore (Peters et al., 2018). The finding that mutations residues located in the first intracellular loop of the channel reduce Ca^{2+} activation indicate that TMEM16A may have multiple Ca^{2+} binding sites or a binding site involving disparate regions on the channel (Xiao and Cui, 2014).

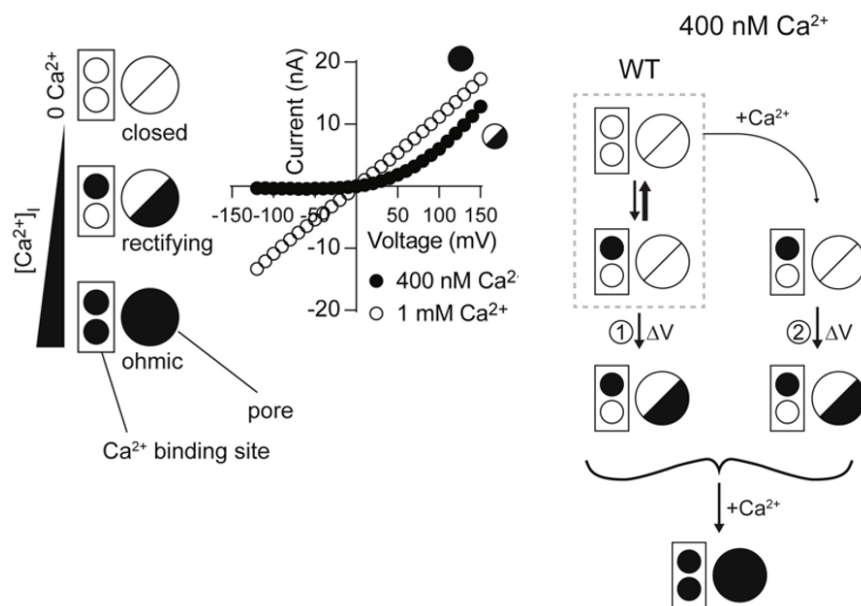


Figure 9. Calcium and voltage-dependent gating of TMEM16A.

A simplified model of TMEM16A gating. Two circles within the box represent the two Ca^{2+} -binding sites, with filled circles indicating occupancy by Ca^{2+} . The larger circle represents the pore, with a line indicating a closed pore, half-filled circle for the outward-rectifying open state and fully filled circle for the ohmic open state. At right, a sample steady-state I-V distinguishing the two open states for channels with single or double Ca^{2+} occupancy. Modified from Peters et al., 2018.

A series of works developed by Xiao and co-workers suggest that both voltage and Ca^{2+} dependent gating might be physically coupled to the first intracellular loop of TMEM16A. In their research they demonstrated that deletion of the residues $_{444}\text{EEEEEEAVKD}_{453}$ in that region results in loss of both Ca^{2+} -sensitivity and voltage-dependence. Interestingly, the mutant channel $_{444}\text{EEEEEE}_{449}/\text{AAAAA}$ conserves the same Ca^{2+} affinity as the wild type channel but loses voltage-dependent activation, while the $\Delta_{449}\text{EAVK}_{452}$, which corresponds to the *abd* alternative splicing form, is activated more readily by depolarization compared to the wild type form and strongly decreased Ca^{2+} affinity. However, since this loop is located in the intracellular part and not in the voltage-field of the membrane, it is unlikely to directly sense the voltage (Xiao and Cui, 2014; Xiao et al., 2011).

Another feature of TMEM16A's gating is that it can be modified by external anions (Xiao and Cui, 2014; Xiao et al., 2011; Peters et al., 2018). Substitution of external Cl^- by I^- increases the interaction of the anion in the outer pore to stabilize TM6 in its voltage-dependent-inducing conformation, therefore favoring the subsequent voltage-dependent changes at less depolarizing voltages (Xiao and Cui, 2014; Xiao et al., 2011; Peters et al., 2018). Furthermore, replacement by NO_3^- or SCN^- greatly reduces voltage-dependent gating of the channel, shifting the activation at negative potentials (Xiao and Cui, 2014; Xiao et al., 2011; Peters et al., 2018).

All these data suggest that gating of TMEM16A consists in a synergistic complex model involving intracellular Ca^{2+} mobilization, changes in membrane potential, conformational transitions and electrostatic interactions between conducting anions and the channel pore. Although these recent findings of structures implicated in the gating have demonstrated the complexity of the gating mechanism and more research is needed to fully understand it.

3. Hypothesis: KCNE1 activates the TMEM16A channel

As described previously in this chapter, injection of RNA of KCNE1 induces activation of endogenous silent K^+ and Cl^- channels in *Xenopus laevis* oocytes (Attali et al., 1993). Moreover, it has been also shown that PCT cells from *kcne1*^{-/-} mice do not exhibit an osmosensitive Cl^- current responsible of the efflux of Cl^- in the regulatory volume decrease (RVD) phenomenon in renal cells (Barrière et al., 2003). Another study has reported the existence of a CaCC in the same cell line, which may compensate lack of the Cl^- CFTR conductance in cystic fibrosis (Rubera et al., 1998). Additionally, mutations in the extracellular segment of KCNE1 have been found to be polymorphisms related with cardiac arrhythmias with negligible impact on the I_{Ks} current (Westenskow et al., 2004; Yao et al., 2018).

The strong presence of TMEM16A in both *Xenopus* oocytes (Schroeder et al., 2008) and in the apical membrane of PCT cells (Faria et al., 2014), where it co-localizes with KCNE1 (Vallon et al., 2001), suggests that KCNE1 is not only an ancillary subunit of K_v channels, but also of TMEM16A Cl^- channels. Since these channels are belonging to the voltage-gated and the anoctamin superfamilies, respectively, this work aims to decipher whether cross-modulation between different protein subfamilies is possible by a shared β -subunit and its potential impact in physiopathology.

B. Results

1. KCNE1 shifts TMEM16A from a calcium-dependent to a voltage-dependent Cl⁻ channel

To test the ability of KCNE1 to regulate TMEM16A, HEK293T cells were used as heterologous model, since they do not express neither TMEM16A nor KCNE1 endogenously. Whereas transfection of HEK293T cells with either TMEM16A or KCNE1 alone produced no significant current, co-expression of both proteins induced a voltage-dependent current, whose density was of 18.1 ± 2.8 pA/pF at +100 mV (**Figure 10A, B**). The reversal potential was -4.8 ± 1.3 mV, which is similar to the expected reversal Cl⁻ potential in the experimental conditions used. This Cl⁻ current was inhibited by niflumic acid (NFA), T16Ainh-A01 (Davis et al., 2013) and also by Ani9, the most specific TMEM16A inhibitor (Seo et al., 2016) (**Figure 10C, D**). Furthermore, as expected, the TMEM16A-KCNE1 current presented higher permeability for large anions with lower hydration energy, as it has been shown before for TMEM16A alone in the presence of calcium (**Table 2**) (Yang et al., 2008; Caputo et al., 2008; Schroeder et al., 2008). In addition, the channel does not become cation permeable, since replacement of the external solution by a 15 mM NaCl solution supplemented with D-mannitol allowed determination of a P_{Na}/P_{Cl} of ~ 0.1 (data not shown). This value is consistent with the calculated prediction through the Goldman-Hodgkin-Katz equation for the used conditions (**Equation 3**) and similar to the reported value (Yang et al., 2008; Peters et al., 2018). This suggests that KCNE1 switches TMEM16A from a Ca²⁺-dependent to a voltage-dependent Cl⁻ channel.

To preclude the possibility that KCNE1 activates endogenous Ca²⁺ channels, similar experiments were conducted in the presence of the fast Ca²⁺ chelator BAPTA (**Figure 10E, F**). As shown in **Figure 10F**, BAPTA did not affect the voltage-dependent current evoked by the TMEM16A-KCNE1 complex. To totally rule out a potential modulation of endogenous Ca²⁺ channels by KCNE1 leading to TMEM16A activation, we co-expressed KCNE1 with the Ca²⁺-activated SK4 channel, which has a similar Ca²⁺ sensitivity as TMEM16A (Cao and Houamed, 1999). As shown in **Figure 11**, KCNE1 overexpression did not induce any increase of the SK4 current in absence of Ca²⁺. Altogether, these results exclude an implication of an intracellular Ca²⁺ rise in KCNE1-induced voltage-dependent activation of TMEM16A.

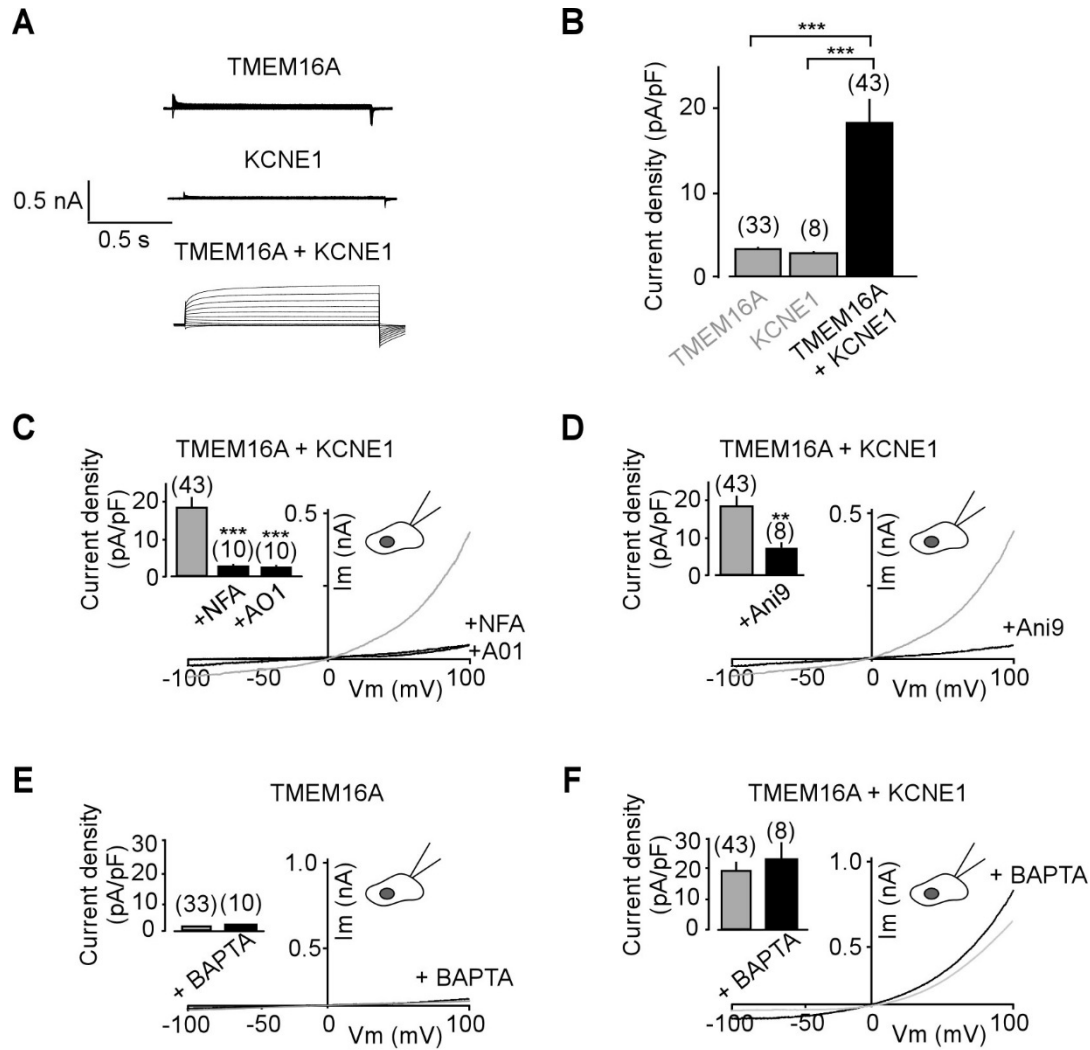


Figure 10. KCNE1 converts the CaCC TMEM16A into a voltage-dependent chloride channel.

(A) Representative traces showing the effect of expression of either KCNE1 or TMEM16A or both TMEM16A and KCNE1 in HEK293T cells. Traces were generated using pulses between -100 and +100 mV at 20 mV intervals from a holding potential of -80 mV. (B) Summary of current densities obtained at +100 mV (C-D) Representative traces of HEK293T cells co-expressing TMEM16A and KCNE1 after incubation with NFA (100 μ M), A01 (10 μ M) (C) or Ani9 (300 nM) (D). (E-F) Representative traces of TMEM16A alone (E) or co-expressed with KCNE1 (F) in the presence of 1 mM of BAPTA. Currents were elicited by voltage-ramps (from -100 to +100 mV, 1s duration). Insets show current densities obtained at +100 mV. Man-Whitney test (** $p < 0.01$, *** $p < 0.001$). Mean \pm SEM.

Table 2. Relative permeability (P_x/P_{Cl}) of the TMEM16A-KCNE1 current to anions.

Salt	E_{rev}	Relative permeability	n
NaCl (140 mM)	-5.4 ± 1.4	1	11
NaI (140 mM)	-15 ± 2.8	1.5	6
NaNO ₃ (140 mM)	-23.2 ± 1.4	2	5

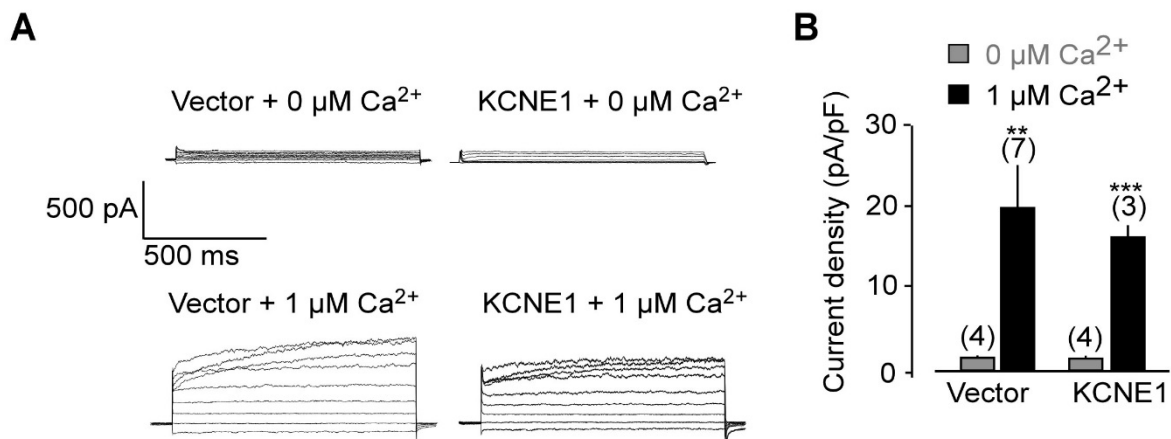


Figure 11. KCNE1 co-expression does not activate SK4 channels.

(A) Representative current traces obtained from HEK293T cells transfected with SK4 and either an empty vector or KCNE1 in the presence or absence of 1 μM cytosolic Ca^{2+} . Traces were generated using pulses between -100 and +100 mV from a holding potential at -80 mV. (B) Summary of current densities obtained at +100 mV. Mann-Whitney test (** $p < 0.01$, *** $p < 0.001$). Mean \pm SEM.

Modulation of additional TMEM16 members by KCNE1 was also investigated. As it shares ~57 % of protein homology with TMEM16A and also exhibits Ca²⁺-sensitivity and voltage-dependence (Milenkovic et al., 2010), potential regulation of TMEM16B by KCNE1 was examined. Additionally, the effect of KCNE1 on TMEM16F was also tested. TMEM16F is a scramblase that shares low homology with TMEM16A but it also acts as an anionic channel activated by Ca²⁺ (Milenkovic et al., 2010). None of the two challenged channels presented an apparent activation when they were co-expressed with KCNE1 in HEK293T cells (**Figure 12**), indicating that KCNE1 specifically activates TMEM16A.

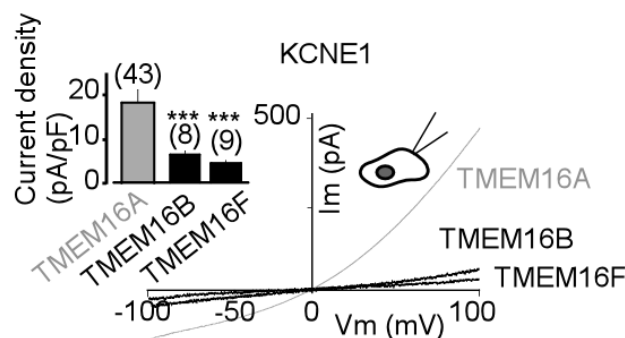


Figure 12. KCNE1 does not activated other TMEM16 channels.

Representative traces obtained from HEK cells co-expressing KCNE1 with TMEM16A, TMEM16B and TMEM16F. Bar graphs at left indicate current densities. Currents were elicited by voltage-ramps (from -100 to +100 mV, 1s duration). Current densities are depicted in bar graph a left. Mann-Whitney test (***) $p > 0.001$. Mean \pm SEM.

TMEM16A does not have any obvious classical voltage-sensor domains, but several cytoplasmic and transmembrane domains have been shown to be implicated in its regulation, notably the first intracellular loop (Xiao et al., 2011) and the sixth transmembrane domain ((Peters et al., 2018). To determine which domain could be involved in the KCNE1-induced voltage-gating of the channel, KCNE1 effect was first tested on the mutation 444EEEE₄₄₇/444AAAA₄₄₇, which is known to abolish the intrinsic TMEM16A voltage-dependence (Xiao et al., 2011). The mutation 444EEEE₄₄₇/444AAAA₄₄₇ did not prevent channel regulation by KCNE1, ruling out the hypothesis that KCNE1 modifies the TMEM16A gating by acting on the 444EEEE₄₄₇ sequence underlying the intrinsic voltage-dependence of the channel (**Figure 13**).

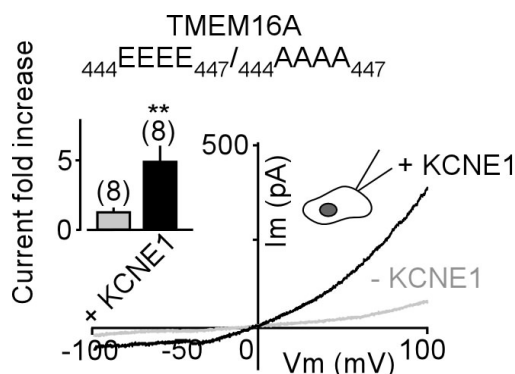


Figure 13. KCNE1 does not shift the intrinsic voltage-dependence of TMEM16A.

Representative current traces showing the effect of expression of either TMEM16A_{444EEEE447/444AAAA447} alone or with KCNE1 in HEK293T cells. Currents were elicited by voltage-ramps (from -100 to +100 mV, 1s duration), insets show a summary of current density fold increase induced by KCNE1 co-expression obtained at +100 mV. Mann-Whitney test (** $p < 0.01$). Mean \pm SEM.

Implication of TMEM16A TM6 domain was then tested using two TMEM16A mutants bearing the TM6 mutations I637A and Q645A, which enable the channel to be activated in the absence of Ca^{2+} (Peters et al., 2018). As expected, these two mutants produced current in the absence of elevated Ca^{2+} , but no additional effect was observed upon co-expression of KCNE1 (**Figure 14A-C**). The absence of an additive effect strongly supports the idea that KCNE1 modulates channel gating by acting on the TM6 conformation. This conformation mimics a single Ca^{2+} occupancy state as has been already demonstrated for both mutations (Peters et al., 2018). Supporting this, the conductance vs V_m curve observed for TMEM16A + KCNE1 overlapped with the curve obtained with TMEM16A alone at moderate Ca^{2+} concentrations (0.5 μM) (**Figure 14D**).

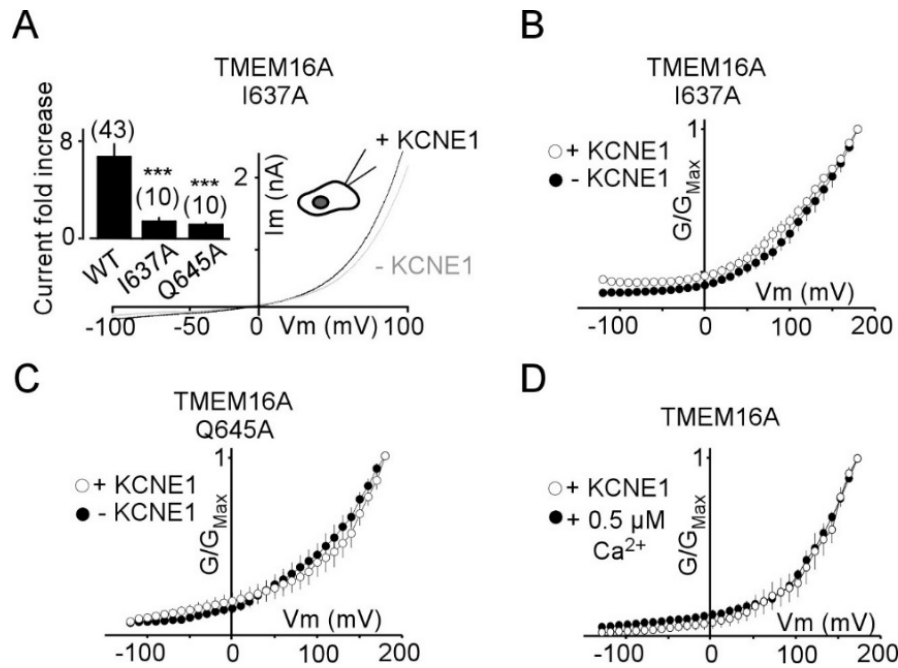


Figure 14. TMEM16A-TM domain I637A and Q645A mutations are not sensitive to KCNE1 co-expression.

(A) Representative current traces showing the effect of expression of either TMEM16A I637A alone or with KCNE1 in HEK293T cells. Currents were elicited by voltage-ramps (from -100 to +100 mV, 1s duration), insets show a summary of current density fold increase induced by KCNE1 co-expression with the wild type and mutants forms of TMEM16A at +100 mV. (B-C) KCNE1 does not modify the voltage sensitivity of the TMEM16A-TM6 I637A and Q645A mutants. G/G_{Max} vs V_m curves for I637A (B) and Q645A (C) mutants expressed alone or co-expressed with KCNE1 in whole-cell patch clamp. (D) TMEM16A activation at a moderate Ca²⁺ concentration, as seen with single Ca²⁺ occupancy. G/G_{Max} vs V_m curves for TMEM16A alone in the presence of 0.5 μM Ca²⁺ and TMEM16A co-expressed with KCNE1. Mann-Whitney test (*** p < 0.001). Mean ± SEM.

Beside their ability to enable channel activation in the absence of Ca²⁺, the TM6 I637A and Q645A mutations are still modulated by Ca²⁺ (Peters et al., 2018). Therefore, the Ca²⁺ sensitivity of TMEM16A-KCNE1 current was challenged. Similarly to both mutants, TMEM16A-KCNE1 was Ca²⁺-activated, reinforcing the idea that KCNE1 modulates channel gating by acting on the TM6 conformation (Figure 15A-C). Interestingly, no differences were observed between cells expressing TMEM16A with or without KCNE1 at saturating concentrations of Ca²⁺ (Figure 15D). This discarded the hypothesis of a potential increase of the number of channels at the surface, since this would have been translated in a higher current density in the presence of KCNE1.

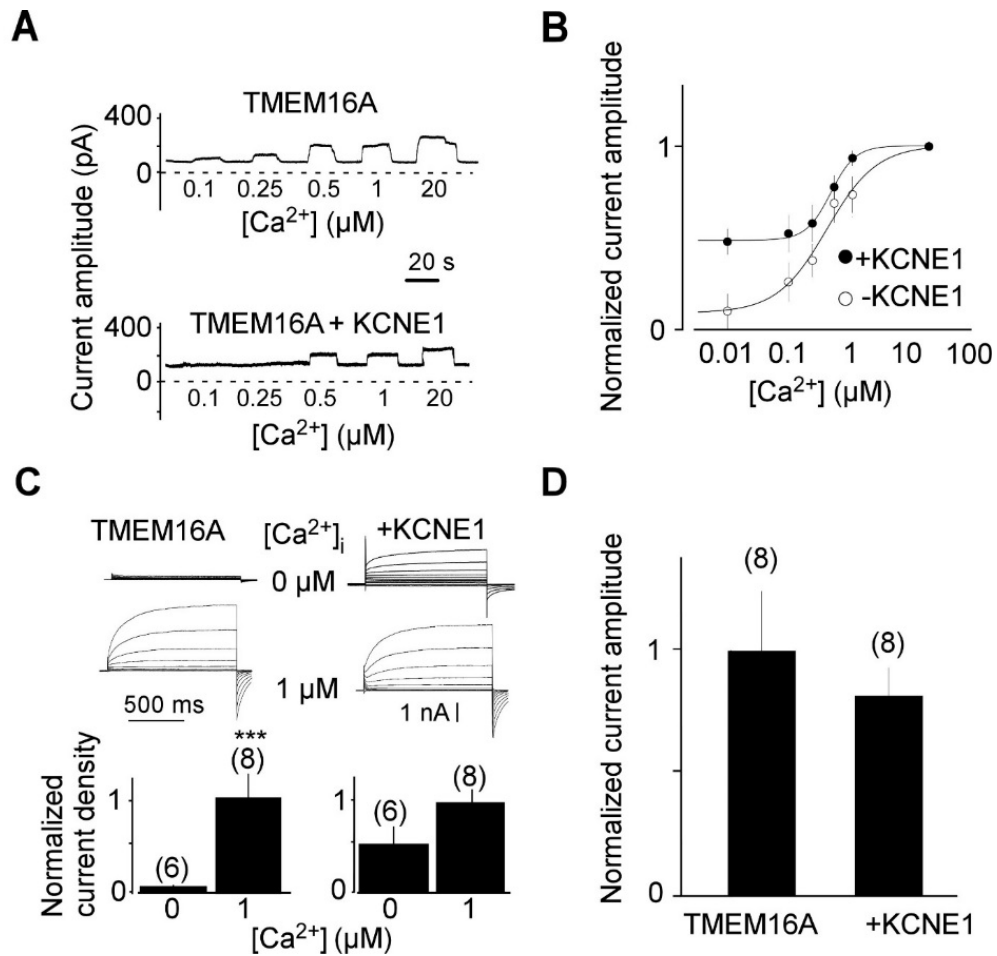


Figure 15. Calcium sensitivity of TMEM16A-KCNE1 channel complex.

(A) Representative recordings of TMEM16A-CaCC in inside-out patch configuration in response to various intracellular calcium concentrations. (B) Calcium concentration–response of TMEM16A channel. (C) Whole-cell current traces showing TMEM16A and TMEM16A + KCNE1 currents in the presence or absence of 1 μM Ca²⁺_i. Bar graph represents the relative current densities of TMEM16A and TMEM16A with KCNE1 at the two different Ca²⁺ concentrations. (D) Bar graph representing normalized current densities of TMEM16A and TMEM16A + KCNE1 at a saturating Ca²⁺ concentration (10 μM). Mann-Whitney test (***) $p < 0.001$. Mean ± SEM.

2. TMEM16A activation by KCNE1 involves physical interaction

Once determined that KCNE1 activates TMEM16A by modifying its gating, a physical association between both proteins was suggested, like KCNE1 does with KCNQ1 to form a protein complex. This hypothesis was tested by using the Single Molecule Pulldown (SiMPull) method developed by Jain and co-workers to see individual immobilized protein complexes (Jain et al., 2011). To perform this technique, HEK cells are transfected with DNA of the two proteins forming the complex: a “bait” protein which is labelled with a HA-tag and a “prey” protein fused to a GFP label. After 24 h of expression, cells are lysed and then pulled down on slides previously coated with polyethylene glycol (PEG) and neutravidin, which allows biotin binding. Then the slides are conjugated with a biotinylated antibody anti-HA which immobilizes the protein expressing the HA-tag. If there is a physical interaction between the bait and the prey protein, this is observed by the GFP signal coming from the prey protein upon excitation with a laser of a total internal reflection fluorescence (TIRF) microscope (**Figure 16**). This technique not only allows to see if two proteins are physically coupled, but also enables to determine the number of subunits implicated in the complex. This is possible by counting the number of photobleaching steps corresponding to every GFP-subunit of the prey protein after TIRF excitation.

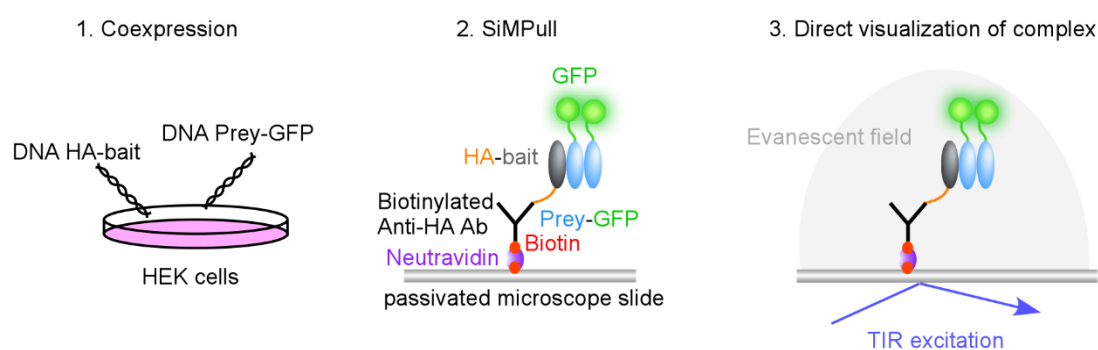


Figure 16. Schematic of SiMPull technique.

Firstly, HEK cells are co-transfected with DNA of the protein of interest fused to a HA-tag and of the potential partner fused to a GFP-label. Secondly, the cellular lysate is pulled down in microscope slides coated with PEG, neutravidin and conjugated with a biotinylated anti-HA antibody. Finally, the samples are looked under TIRF microscopy, whose excitation allows to see the GFP signal coming from the protein partner.

Co-transfection of KCNE1 and TMEM16A, one of them fused with a HA affinity tag and the other with a GFP label (**Figure 17A, E**), led to the visualization of many fluorescent spots for both conditions (**Figure 17B, F**). This demonstrated the physical interaction between KCNE1 and TMEM16A. By observing bleaching steps for immobilized HA-KCNE1-TMEM16A-GFP complexes, it was possible to count the number of TMEM16A-GFP subunits within the complex. The majority of fluorescence intensity trajectories showed two-step bleaching (~70 %) with the remaining spots bleaching in one step (~20 %) or occasionally three or more steps (~10 %) (**Figure 17C, D**). This distribution agrees well with the binomial distribution predicted for a strict dimer based on an estimated GFP maturation probability of ~75% (Ulbrich and Isacoff, 2007). Analysis of the SiMPull experiments with HA-TMEM16A-KCNE1-GFP showed that most complexes presented two bleaching steps (~65%) and some remaining spots bleaching in one (~25 %) and three steps (~10 %) (**Figure 17G, H**). This distribution corresponds to the presence of two KCNE1-GFP subunits. Therefore, two KCNE1 subunits assemble with a dimeric TMEM16A channel (Takumi et al., 1988; Dang et al., 2017), following a $2\alpha:2\beta$ stoichiometry. Importantly, when HA-KCNE1 or HA-TMEM16A were not co-expressed, no proteins fused to GFP were pulled-down (**Figure 17I-L**), confirming the specificity of the HA-antibody used in the SiMPull experiments.

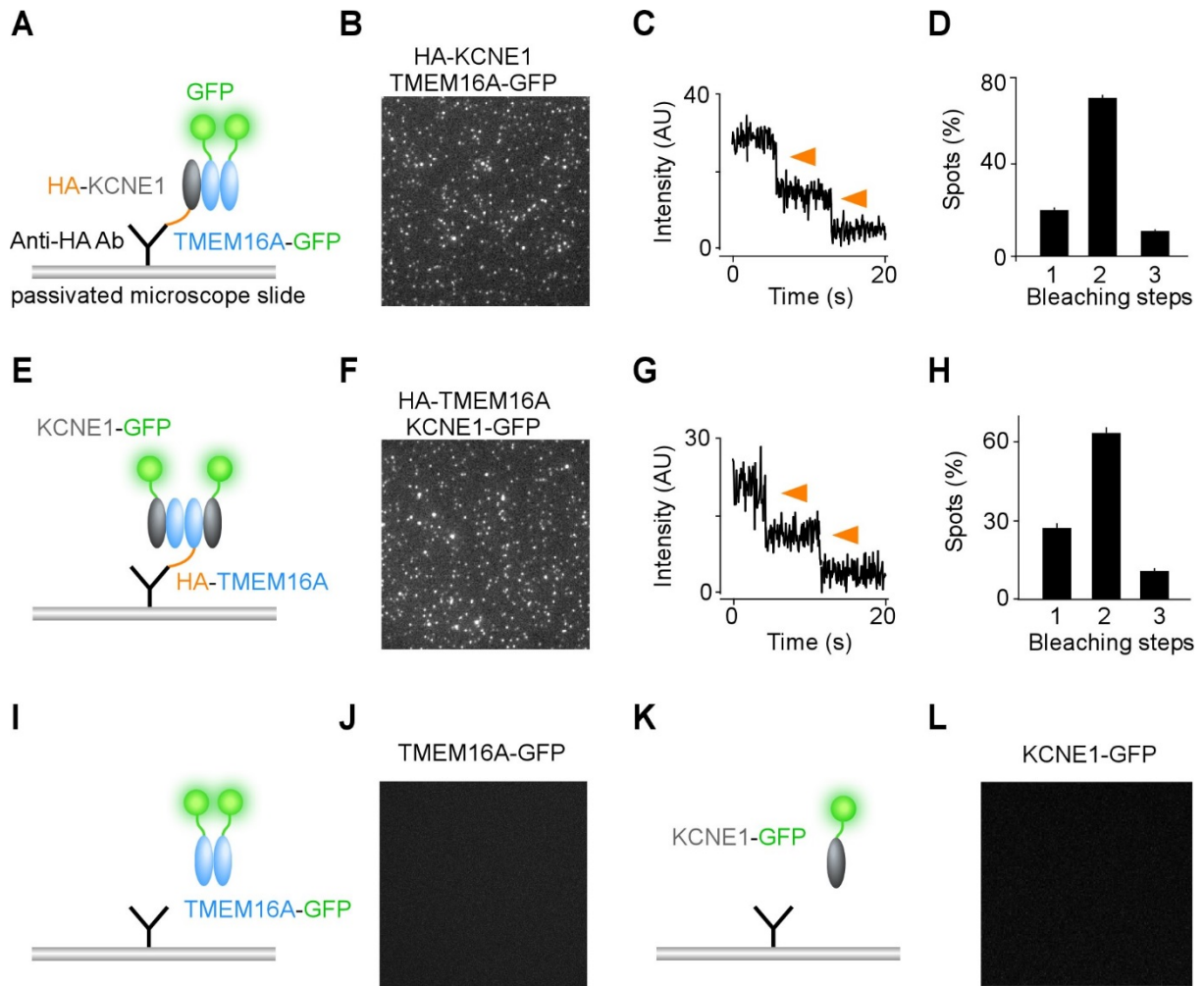


Figure 17. KCNE1 and TMEM16A interact in a 2 α :2 β complex.

(A) HEK293T cells co-expressing TMEM16A-GFP and an HA-tagged KCNE1 were lysed and then immobilized on a PEG-passivated coverslip conjugated to a biotinylated anti-HA antibody. (B) Representative TIRF image of single molecules showing the pull-down of TMEM16A-GFP by HA-KCNE1. (C) Representative trace showing two photobleaching steps (red arrows) of TMEM16A-GFP (AU, for Arbitrary Units). (D) Summary of photobleaching step distribution for TMEM16A-GFP. (E-H) same as (A-D) for the SiMPull of KCNE1-GFP by HA-TMEM16A. (I) TMEM16A-GFP pull-down in the absence of the HA-tagged partner. (J) Absence of protein spots after TIRF excitation (K-L) same as (I-J) for the KCNE1-GFP pull-down.

3. The KCNE1-TMEM16A complex is carried by PCT cells

To be considered as a *bona fide* auxiliary subunit, the protein must interact with α -subunits in a native environment. To confirm that KCNE1 is an auxiliary subunit of TMEM16A in native tissue and to eliminate possible artifacts due to heterologous overexpression we used PCT cells obtained from wild type and *kcne1* KO mice (Barrière et al., 2003). PCT cells are considered as a relevant model, as they naturally co-express both TMEM16A and KCNE1 (Faria et al., 2014; Vallon et al., 2001) and do not necessitate any genetic manipulation to record TMEM16A channel carried currents. Moreover, while no modification of the K^+ current was found in PCT cells from *kcne1*^{-/-} KO compared to wild type, a DIDS (4,4'-Diisothiocyanostilbene-2,2'-disulfonic acid)-sensitive Cl^- conductance was impaired (Barrière et al., 2003). The current, whose reversal potential was similar to the expected Cl^- reversal potential, was lost in *kcne1*^{-/-} PCT cells (18.07 ± 1.21 pA/pF vs 5.37 ± 0.56 pA/pF for PCT wild type and KO mice, respectively, $P < 0.001$) (**Figure 18A**). This current was inhibited by NFA (4.51 ± 0.28 pA/pF), T16Ainh-A01 (5.52 ± 0.72 pA/pF) and Ani9 (2.88 ± 0.38 pA/pF) (**Figure 18B-D**). Moreover, knock-down of TMEM16A by a previously validated siRNA transfection (Sala-Rabanal et al., 2017) in wild type PCT cells significantly reduced the Cl^- current amplitude (4.23 ± 0.48 pA/pF) (**Figure 18E**). This demonstrates the involvement of TMEM16A subunits in the channel complex responsible for the herein studied Cl^- current. A rescue experiment by KCNE1 transfection in *kcne1*^{-/-} cells fully restored the voltage-dependent Cl^- current (21.59 ± 1.38 pA/pF) (**Figure 18F**), showing that the absence of Cl^- current in these cells was only due to the genetic invalidation of *kcne1* and not due to any modification that might have occurred during the culture process.

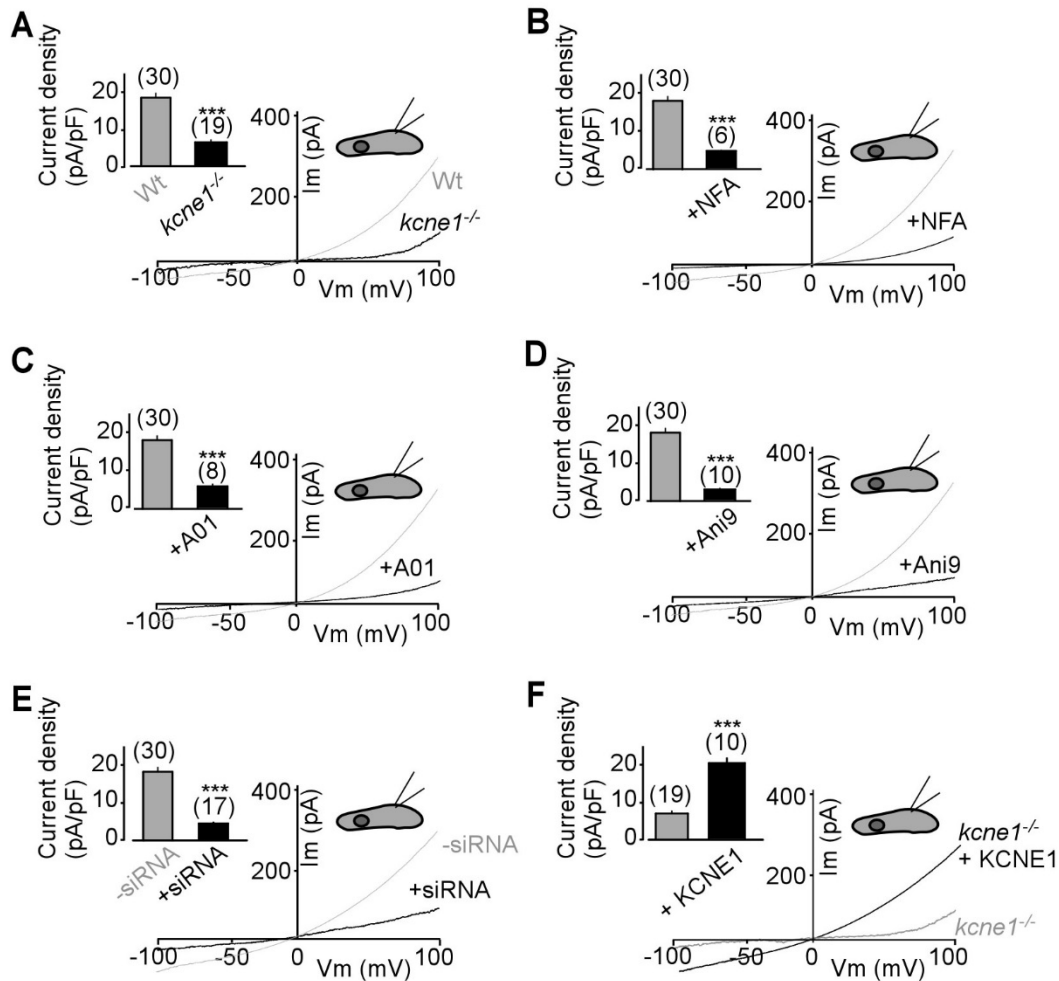


Figure 18. KCNE1-TMEM16A complex creates a voltage-dependent chloride current in proximal convoluted tubule (PCT) cells.

(A) Representative traces obtained from wild type and *kcne1*^{-/-} PCT cells. (B-D) Representative traces from wild type cells after incubation with NFA (100 μ M, B), A01 (10 μ M, C), Ani9 (5 μ M, D). (E) Trace obtained after transfection with siRNA against TMEM16A. (F) Trace obtained from a *kcne1*^{-/-} PCT cell after transfection with KCNE1 cDNA. Currents were generated by voltage-ramps (from -100 to +100 mV, 1s duration). Insets show current densities. Mann-Whitney test (***) $p < 0.001$. Mean \pm SEM.

4. The N-terminal pre-transmembrane domain of KCNE1 is key for TMEM16A regulation

KCNE1 is a single transmembrane protein with an extracellular N-terminal part and a C-terminal domain within the cytosol (Takumi et al., 1988). To determine the interacting site with TMEM16A, a series of truncated KCNE1 forms were produced (**Figure 19A**) and tested for their ability to regulate TMEM16A. Truncation of the KCNE1 C-terminal domain did not abolish the KCNE1-mediated TMEM16A regulation (25.04 ± 4.9 pA/pF, $P > 0.15$) (**Figure 19B**). By contrast, deletion of the full N-terminal domain suppressed the ability of KCNE1 to regulate TMEM16A (6.56 ± 0.89 pA/pF, $P < 0.001$) (**Figure 19B**). No effect was observed for the partial N-terminal truncations, neither for $\Delta Nt16$ (25.43 ± 4.46 pA/pF) nor for $\Delta Nt30$ (25.23 ± 6.62 pA/pF) (**Figure 19C**), demonstrating that the sequence of 13 residues (from L30 to L42) preceding the transmembrane domain is essential for TMEM16A activation. This result is in line with the previous observation, that a partial deletion of KCNE1, including eight of the thirteen amino acids of this sequence (KCNE1 Δ_{11-38}), abolished the KCNE1-induced chloride current in *Xenopus* oocytes (Attali et al., 1993). To check if this small domain is sufficient to recapitulate the properties of the entire KCNE1 on the TMEM16A current, we used a corresponding synthetic peptide (Nter13), bearing the L30-L42 sequence. In HEK293T cells only expressing TMEM16A, application of 100 μ M Nter13 elicited an Ani9 sensitive current (15.48 ± 3.25 pA/pF) (**Figure 19D**). Again, the reversal potential was similar to the current observed when KCNE1 is co-expressed, whereas no effect was observed by application of a scrambled peptide (**Figure 19D, Figure 20A, B**). A concentration-response experiment with Nter13 demonstrated an EC₅₀ of $\sim 110 \mu$ M (**Figure 20C**).

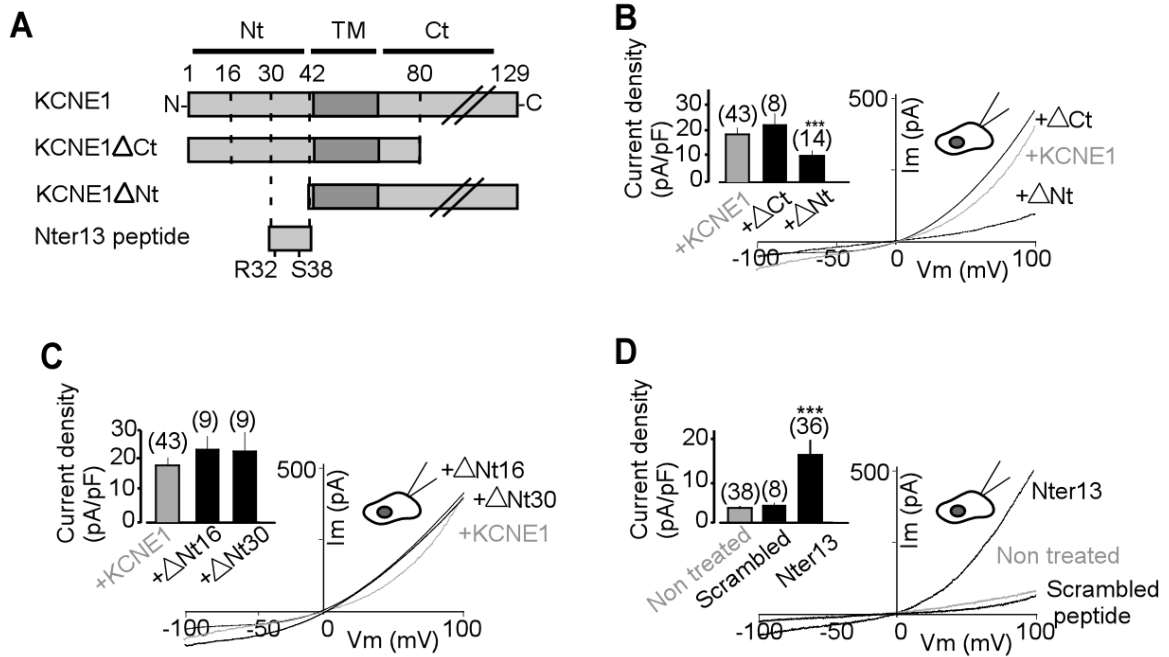


Figure 19. The pre-transmembrane domain (Nter13) of KCNE1 is sufficient for KCNE1-induced TMEM16A conversion

(A) Cartoon depicting KCNE1 truncated forms used to determine the domains implicated in TMEM16A interaction. (B-C) Representative traces obtained from HEK293T cells co-expressing TMEM16A and KCNE1ΔCt, KCNE1ΔNt (B), KCNE1ΔNt16, or KCNE1ΔNt30 (C). (D) Representative traces showing the effect of the Nter13 and a scrambled peptide on HEK293T cells expressing TMEM16A alone. Currents were elicited by voltage-ramps (from -100 to +100 mV, 1s duration). Insets show the summary of current densities obtained for the different conditions at +100 mV. Mann-Whitney test (***) $p < 0.001$. Mean \pm SEM.

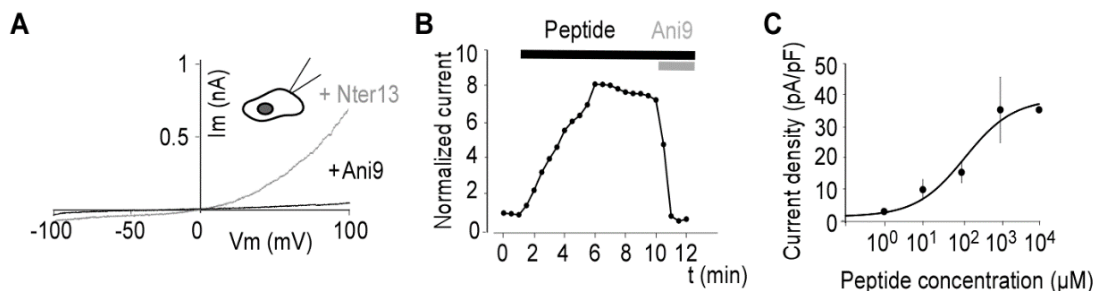


Figure 20. Nter13 peptide is sufficient to switch the functioning mode of TMEM16A.

(A) Representative traces showing the effect of Nter13 peptide application (100 μ M) and its reversion by Ani9 (5 μ M) on a HEK293T cell expressing TMEM16A alone. (B) Effect of Nter13 peptide on TMEM16A current over time followed by inhibition through co-application of Ani9 in HEK293T cells. (C) Concentration-response curve representing the current density observed for different peptide concentrations in HEK293T cells expressing TMEM16A.

5. KCNE1 polymorphisms within the TMEM16A interacting sequence suppress the Cl⁻ current

Previous research have shown that polymorphisms involving different forms of KCNE1 are related with cardiac arrhythmias, and notably LQTS (Moss and Kass, 2005; Crump and Abbott, 2014). LQTS is frequently associated with abnormalities in slow ventricular repolarization because of dysfunctions of the complex KCNE1-KCNQ1 (Crump and Abbott, 2014). Nevertheless, some of these variants, such as R32H and S38G have not or very little impact on KCNQ1 regulation (Westenskow et al., 2004; Yao et al., 2018). Interestingly, these residues are located within the 13-residues extracellular domain of KCNE1 regulating TMEM16A activation. Therefore, we performed whole-cell recordings in HEK293T cells co-expressing either KCNQ1 or TMEM16A with the KCNE1 mutants R32H and S38G. The T7I mutant form was used as a control, since its punctual mutation does not affect the regulating domain. As expected, none of the KCNE1 mutants modify the KCNE1-KCNQ1 K⁺ current (**Figure 21A, B**). However, whereas mutation T7I did not alter the KCNE1-dependent regulation of TMEM16A (24.69 ± 1.57 pA/pF, $P > 0.4$), both mutations R32H and S38G abolished the ability of KCNE1 to modulate the TMEM16A current (5.69 ± 1.18 pA/pF and 6.96 ± 0.78 pA/pF for R32H and S38G, respectively) (**Figure 21C, D**), suggesting a potential implication of the KCNE1-TMEM16A complex in human cardiac diseases.

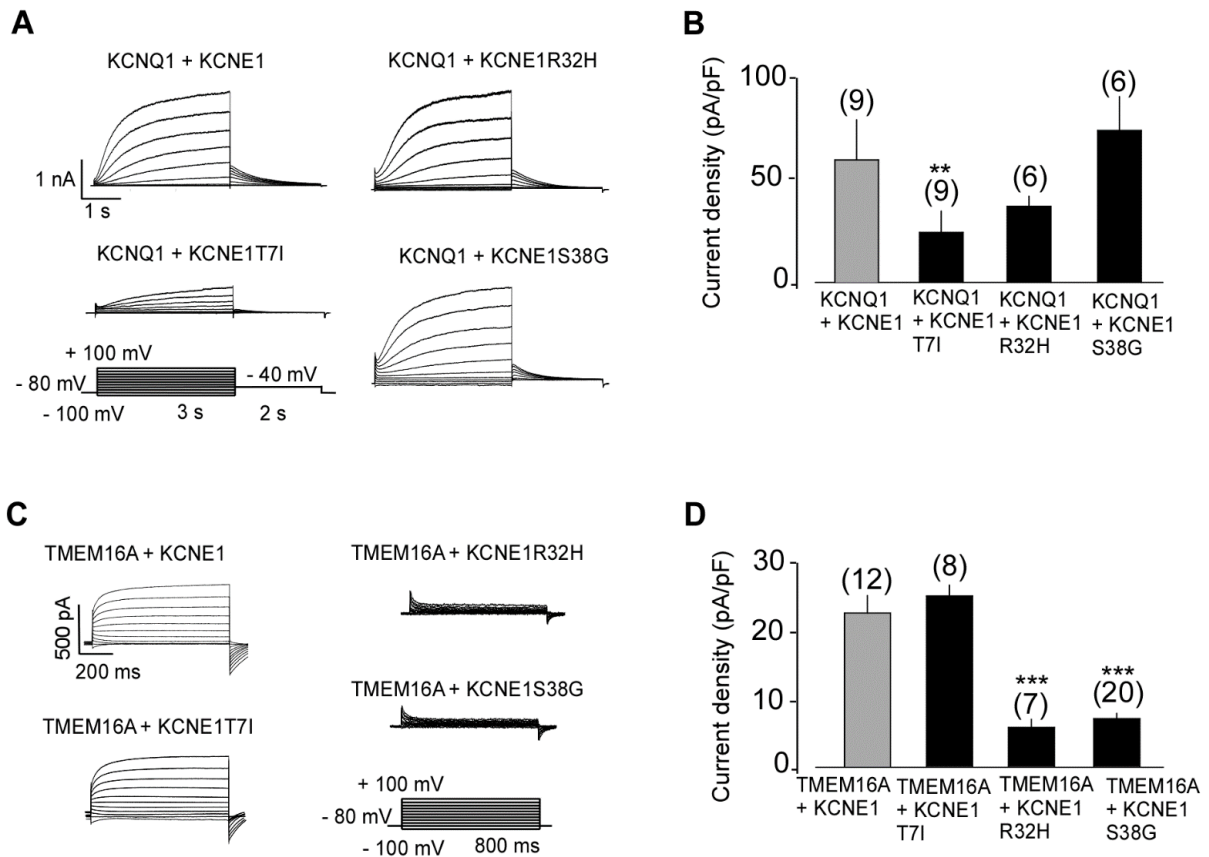


Figure 21. The KCNE1 S38G and R32H do not impair KCNQ1 regulation, but abolish TMEM16A regulation.

(A) Current traces of whole-cell patch-clamp recordings from cells transfected with wild type KCNQ1 alone and co-transfected with KCNE1 or KCNE1 T7I or KCNE1 R32H or KCNE1 S38G. (B) Summary of current densities obtained for the different conditions at +40 mV. (C-D) Same as (A-B), with cells co-expressing KCNE1 and TMEM16A. Current densities were calculated at +100 mV. Mann-Whitney test (** $p < 0.01$, *** $p < 0.001$). Mean \pm SEM.

6. Specificity of KCNE1-TMEM16A

As the K^+ channel KCNQ1 is regulated by the five members that conform the KCNE family (Bendahhou et al., 2005), it was reasonable to wonder if TMEM16A could be also modulated by more of them. Whole-cell recordings of HEK293T cells expressing TMEM16A showed that only KCNE5, which shares low protein homology with KCNE1, was able to activate the channel, increasing its current amplitude and changing its kinetics similarly as KCNE1 does (21.11 ± 3.90 pA/pF, 14.44 ± 2.75 pA/pF for KCNE1 and KCNE5, respectively). (**Figure 22A, B**). Thus, TMEM16A is not only activated by KCNE1, but also by KCNE5.

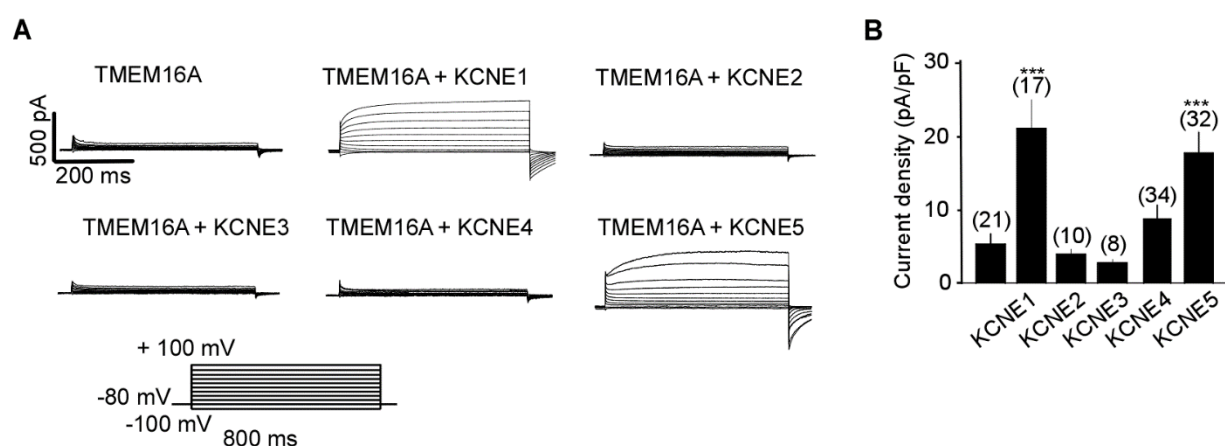


Figure 22. TMEM16A is activated by KCNE5.

(A) Representative traces recorded from HEK293T cells co-transfected with TMEM16A and the different members of the KCNE family. The protocol used to generate the IV curves is depicted below the traces. (B) Summary of the obtained current densities at +100 mV compared to TMEM16A alone. Mann-Whitney test (***) $p < 0.001$. Mean \pm SEM.

C. Discussion

1. KCNE1 as a cross-regulator of two different superfamilies of ion channels

Most of ion channels are assembled as complexes of a pore forming α -subunit, associated with auxiliary (β) subunits. This study demonstrates that KCNE1, which is classically considered a β -subunit of the cardiac KCNQ1 pore-forming subunit belonging to the voltage-dependent K_v channel superfamily, serves also as an auxiliary subunit of the anoctamin superfamily channel TMEM16A, a Ca^{2+} -activated Cl^- channel (CaCC). By interacting stably with TMEM16A following a $2\alpha:2\beta$ subunit stoichiometry, KCNE1 induces a voltage-dependent current in the absence of intracellular elevation of calcium. KCNE1 polymorphisms within the TMEM16A-interacting domain abolish its ability to regulate TMEM16A, suggesting a possible implication of this voltage-dependent chloride current in human diseases. This work demonstrates that KCNE1 not only modulates the K^+ channel KCNQ1, but also regulates the Cl^- channel TMEM16A, in line with prior observations suggesting KCNE1 as a dual activator of silent K^+ and Cl^- channels expressed in *Xenopus* oocytes (Ben-Efraim et al., 1996; Attali et al., 1993). Furthermore, KCNE1 has been shown to regulate other KCNQ members and the trafficking of several voltage-gated K^+ channels (Strutz-Seebohm et al., 2006; Roura-Ferrer et al., 2009; Kanda et al., 2011).

Previous β -subunits have been demonstrated to be able to modulate different ion channel families which originated from the same superfamily. $Nav\beta_1$, which acts as an ancillary subunit of voltage-gated Na^+ channels controlling their cell expression in the surface and current amplitude (Brackenbury and Isom, 2011), is also a molecular chaperone of $K_v4.2$ channels that stabilizes their presence in the surface of cortical pyramidal neurons, (Marionneau et al., 2012). Moreover, it also associates with some K_v1 channels and $K_v7.3$ channels, modulating neuronal excitability in the cortex and regulating the M current in the brain (Nguyen et al., 2012). Nevertheless, such regulation only involves channels belonging to the same superfamily of voltage-gated channels, which share a common ancestor (Moran et al., 2015). The results of the present manuscript show that KCNE1 cross-modulates two different superfamilies of proteins which are not phylogenetically related: voltage-gated and anoctamin superfamilies.

2. Activation by KCNE1 involves voltage-dependent gating

The data obtained in the present manuscript gives important information about how KCNE1 increases the current amplitude of cells expressing TMEM16A. The fact that at saturating Ca^{2+} concentrations the TMEM16A current was not modified by the presence of KCNE1 demonstrates that KCNE1 does not increase the number of channels at the surface. Finally, current upregulation by the Nter13 peptide in HEK293T cells expressing the channel alone was fast (a few seconds), indicating that this activation is not related with protein synthesis, but rather with association with an existing pool of TMEM16A. Taken together, the mechanism by which KCNE1 promotes TMEM16A current amplitude seems not to be related with an increase of TMEM16A at the cell surface.

KCNE1 did not modify the current density of cells expressing SK4 nor TMEM16B, which are activated by similar concentrations of Ca^{2+} as TMEM16A (Schroeder et al., 2008; Yang et al., 2008; Caputo et al., 2008; Cao and Houamed, 1999). Moreover, the concentration-response curve for Ca^{2+} followed a similar slope in conditions with or without KCNE1, except for values when there was no intracellular Ca^{2+} , ruling out a potential impact for Ca^{2+} sensitivity. Also, experiments with the Ca^{2+} chelator BAPTA ruled out the possibility of an eventual implication of activation following a local intracellular Ca^{2+} release.

Another mechanism for TMEM16A is proposed in this work involving the TMEM16A-TM6. Recently, the TMEM16A-TM6 segment was reported to play a crucial role in voltage and calcium sensing (Peters et al., 2018). The TM6 has been shown to be flexible and to adopt several stable conformations that would condition the channel activity mode. Its key function was demonstrated by showing that two mutations (I637A and Q645A) within the TM6 enable channel activation by membrane depolarization in the absence of calcium, similarly to KCNE1 co-expression. The absence of an additive effect of KCNE1 when co-expressed with the two TM6 mutants supports the idea of a shared mechanism. KCNE1 may modulate channel activity by modifying the TM6 conformation placing the channel in a voltage-dependent mode, enabling the channel to be activated independently of an elevation of intracellular Ca^{2+} .

3. KCNE1 stably interacts with TMEM16A

In order to see if activation by KCNE1 is direct, the SiMPull technique was used. This method, contrarily to Western Blot or co-immunoprecipitation assays not only allows to identify physical association between two proteins, but also enables elucidation of the number of subunits implicated in the protein complex (Jain et al., 2011). SiMPull assays revealed a remarkable number of spots, each one representing a single protein complex, when both proteins were pulled-down together, indicating physical interaction of TMEM16A and KCNE1. It also revealed, by counting the number of photobleaching steps in every spot, the presence of two TMEM16A subunits for two KCNE1 subunits (2 α :2 β stoichiometry).

After having determined that KCNE1 and TMEM16A stably interact within a complex, the next step was to find the domains implicated in this association. Whole-cell experiments demonstrated that the extracellular part of KCNE1, and more specifically, the first 13 residues before the transmembrane segment, are necessary and sufficient to activate TMEM16A. Strikingly, deletion of the 80 last intracellular amino-acid part does not alter the Cl⁻ channel, contrarily to the effect on KCNQ1 (Nakajo and Kubo, 2014). The importance of the extracellular domain was already pinpointed by Attali and co-workers when they showed that mutant forms of KCNE1 partially or completely lacking of the extracellular part were unable to activate Cl⁻ currents in *Xenopus* oocytes (Attali et al., 1993). Importantly, the partial mutants which involved some of the 13 extracellular residues of KCNE1 are highlighted in this manuscript. The experiments of the present work performed with the N13ter peptide on HEK293T cells expressing TMEM16A at the surface validate that the proximal part of the N-terminal domain is sufficient and necessary to activate TMEM16A in the absence of Ca²⁺.

Similarly, the CLCA1 activator of TMEM16A also associates with the channel via its extracellular domain (Sala-Rabanal et al., 2017; Sala-Rabanal et al., 2015). This subunit is secreted paracrinally and interacts with the last extracellular loop of TMEM16A through an extracellular Von Willebrand Factor (Sala-Rabanal et al., 2017; Sala-Rabanal et al., 2015). Nevertheless, CLCA1 acts differently to KCNE1: it increases TMEM16A current density by stabilizing the channel at the cell surface. KCNE1 is not the only ancillary subunit which regulates the α -pore forming subunit by an extracellular mechanism. The Ca²⁺ channel ancillary subunit Cav α 2 δ , which modifies many of the Cav α properties, acts extracellularly (Dolphin, 2016).

KCNE1-TMEM16A in kidney

TMEM16A is commonly found in studies carried out in epithelial cells (Pedemonte and Galletta, 2014). The mechanism of Cl⁻ secretion is usually the result of the coordinated activity of different channels and transporter localized in the basolateral and apical membranes of epithelial cells (Vallon et al., 2001; Faria et al., 2014). Notably, TMEM16A has been shown to be very important for Ca²⁺-dependent Cl⁻ transport in epithelium of airways and salivary and pancreatic glands (Pedemonte and Galletta, 2014).

In kidney, Cl⁻ channels participate in renal tubular transport to maintain fluid, electrolyte and acid-base balance. In PCT cells, where the largest fraction of Na⁺ is filtered along with water and HCO₃⁻, H⁺ is secreted via apical Na⁺/H⁺ transporters and vacuolar H⁺-ATPases. TMEM16A provides Cl⁻ to promote the electrogenic activity of these ATPases, counterbalancing the charge movement. A study performed with *ano1*^{-/-} mice demonstrated that TMEM16A is strongly expressed in apical and subapical compartments of PCT cells with some presence in glomerular podocytes and the collecting duct (Faria et al., 2014). *Ano1*^{-/-} mice from this study presented dehydration due to enhanced water loss.

KCNE1 is also prominent in the apical membrane of epithelial PCT cells (Vallon et al., 2001; Barrière et al., 2003). In addition, these mice also exhibit some similarities with *ano1*^{-/-} mice such as an increased hematocrit and dehydration (Vallon et al., 2001; Faria et al., 2014). The phenotype shared by both KO mice and co-localization of TMEM16A and KCNE1 at the apical membrane of PCT cells suggest that both proteins contribute together to water and Cl⁻ balance and cell volume regulation. Indeed, the data obtained using *kcne1*^{-/-} PCT cells confirmed that this protein is involved to the generation of a voltage-dependent Cl⁻ current. Concerning the identity of the Cl⁻ channel, the strong inhibition mediated by Ani9 and the specific siRNA against TMEM16A in wild type PCT cells revealed this one as the channel of interest.

These results are in line with previous research performed on PCT cells. The work of Rubera and co-workers found two different Cl⁻ conductances in PCT cells (Rubera et al., 1998). The first one was a volume-sensitive Cl⁻ conductance activated under hypotonic shock that could regulate RVD, a phenomenon mediated by water and KCl efflux following an increase of cell volume (Tauc et al., 1990). This swelling-activated Cl⁻ current has been reported to be lost in PCT cells from *kcne1*^{-/-} mice (Barrière et al., 2003). Therefore, it is possible that TMEM16A participates in RVD in PCT cells through KCNE1 when there is no high intracellular Ca²⁺ in proximal tubule of kidneys. The second Cl⁻ conductance found in PCT cells was a CaCC whose identity was not elucidated in that study, but it was proposed to compensate the lack of CFTR Cl⁻ current in cystic fibrosis (Rubera et al., 1998). Such compensation has been recently proved to be carried by TMEM16A channels (Benedetto et al., 2017).

KCNE1-TMEM16A in heart

In cardiac myocytes, intracellular and extracellular Cl⁻ concentrations are estimated to be ~10-20 mM and ~145 mM, respectively, setting the equilibrium potential for this ion between -65 and -40 mV (Duan, 2009). This value is more positive than the resting membrane potential of cardiac myocytes and can be either negative or positive to the actual membrane potential during the cardiac action potential. Thus, cardiac Cl⁻ channels exhibit the unique ability to generate both outward and inward currents and cause both depolarization and repolarization, depending of the action potential phase (Duan, 2009).

The knowledge concerning TMEM16A in heart is currently small. When intracellular Ca²⁺ is increased above the physiological resting level during early action potentials, TMEM16A, as a CaCC, seems to carry a significant amount of transient outward current I_{to} (Duan, 2009). However, its function as a voltage-dependent Cl⁻ channel independent of Ca²⁺ is not known and needs to be addressed. The time course of the decline of intracellular Ca²⁺ transient will determine the extent to which the CaCC contributes to early repolarization during phase 1 (Duan, 2009). Association of TMEM16A with KCNE1 makes to think that, in spite of its CaCC nature, the channel contribution in the cardiac action potential is more linked to changes in the membrane potential rather than to Ca²⁺ influx which may be important in the early phase of the action potential during the sodium channel opening (Hartzell et al., 2005).

Mutations in either KCNQ1 or KCNE1 are linked to cardiac arrhythmias like LQTS (Moss and Kass, 2005; Crump and Abbott, 2014). LQTS is a cardiovascular disorder translated into a prolonged QT interval. The most common form of LQTS is the Romano-Ward syndrome, a heterogenous and autosomal dominant disease related to delayed ventricular repolarization due to mutations in ventricular ion channels and auxiliary subunits (Moss and Kass, 2005; Crump and Abbott, 2014). The other form is the Jervell Lange-Nielsen syndrome, which is also characterized by bilateral deafness. There are different LQTS, classified according to the mutated gene causing abnormal QT. For instance, LQTS-1 and LQTS-5 correspond to LQTS caused by mutations in *kcnq1* and *kcne1*, respectively (Moss and Kass, 2005; Crump and Abbott, 2014).

Among all the KCNE1 variants producing LQTS-5, the location of two point mutations at the extracellular segment made them matter of interest for this work. The first one, KCNE1 S38G, was one of the first discovered LQTS-5 mutants (Lai et al., 2002). Most of the population possesses one S and one G allele of the gene, 38GG is the next most common and SS the least (Moss and Kass, 2005; Crump and Abbott, 2014). S38G genotype reportedly influences predisposition to LQTS. Several studies performed in different Chinese populations also correlate S38G polymorphism with atrial fibrillation (Lai et al., 2002; Li et al., 2014). The second one, KCNE1 R32H, is less common. Two different studies performed in populations of North America, Europe and Sweden have reported this variant with Jervell Lange-Nielsen syndrome (Splawski et al., 2000; Stattin et al., 2012).

The present work found that co-expression of TMEM16A with either S38G or R32H abolished the Cl⁻ current elicited by KCNE1 wild type and that the same two variants generated the same current as the wild type form when they were co-expressed with KCNQ1. Therefore it might be that the aberrant long QT interval generated by KCNE1 S38G and R32H may be due to an abnormal ventricular repolarization caused by an impairment of the TMEM16A-KCNE1 complex in heart. An exhaustive screening of ion channels interacting with KCNE1 and its variants and the use of selective compounds targeting TMEM16A would help to determine the importance of the KCNE1-TMEM16A in the cardiac action potential.

5. KCNE5 can also activate TMEM16A

One of the main features of ancillary subunits, including KCNE members, is that they show promiscuous partnering with different ion channels of the same family. For instance, KCNE1 is able to act as an ancillary subunit of K⁺ hERG and KCNQ1 channels, regulating both rapid and slow ventricular repolarization (Crump and Abbott, 2014). TMEM16B and TMEM16F were chosen in this study due to their ability to conduct Cl⁻. Neither TMEM16B nor TMEM16F showed an increase of their current density when they were co-expressed with KCNE1. Nevertheless, in spite of such absence of effect on their channel activity, this work did not solve if a potential modification in the scramblase activity was produced by KCNE1. Notably, a computational study found that insertion of 35 aminoacids from TMEM16F to TMEM16A between its TM4-TM5 domain confers to the latter scramblase activity (Gyobu et al., 2017). If TMEM16 scramblase activity was also shown to be regulated by KCNE1, this would mean that the role of KCNE1 as an ancillary subunit is more ancient than it was believed up to now.

Finally, this work demonstrated that KCNE5 is also an activator of TMEM16A channels. KCNE5 is mainly known to inhibit KCNQ1 by inducing a shift of the voltage-dependence by +140 mV, rendering the channel nonfunctional at physiological potentials (Angelo et al., 2002). The similar effect of KCNE1 and KCNE5 on TMEM16A despite their low protein homology may be overcome by different mechanisms. This is, for instance, the case of KCNE4 and KCNE5 inhibition of KCNQ1 channels. Whereas, KCNE5 shifts KCNQ1 voltage-dependence, KCNE4 avoids the binding between the channel and calmodulin (Ciampa et al., 2011). This regulation opens the door to the existence of trimeric complexes involving KCNEs and TMEM16A, as it has been already demonstrated with KCNQ1-KCNE1-KCNE2 in heart (Jiang et al., 2009).

D. Conclusion

This work demonstrates that KCNE1, a well-known auxiliary subunit of voltage-dependent K⁺ channels, meets the four needed conditions to be considered as an auxiliary subunit of the TMEM16A channels from the anoctamin anion channel superfamily (Adelman, 1995; Gurnett and Campbell, 1996; Trimmer, 1998; Arikath and Campbell, 2003; Cannon, 2007): first, KCNE1 does not show any ion channel activity by itself, second, KCNE1 and TMEM16A interact directly and stably with a fixed stoichiometry (2 α :2 β), third, KCNE1 modifies drastically the TMEM16A function enabling the channel to work in the absence of elevated cytosolic calcium, and fourth, KCNE1 regulates TMEM16A in native tissue. Therefore, KCNE1 fulfills all the criteria of a *bona fide* auxiliary subunit of two distinct classes of ion channel superfamilies which are not phylogenetically related: voltage-gated cation channels and anoctamin superfamilies. Finally, the TMEM16A-KCNE1 association should be considered when analyzing outcomes of clinically relevant KCNE1 mutations, as emphasized by the finding that two known cardiac arrhythmia related KCNE1 variants, including S38G, lost their ability to regulate TMEM16A.

Rather than propose a new theory or unearth a new fact, often the most important contribution a scientist can make is to discover a new way of seeing old theories or facts.

The Selfish Gene, 1976. Richard Dawkins

A. Introduction

1. Buruli Ulcer: A painless necrotic skin disease

Etiology of Buruli Ulcer

Buruli ulcer was discovered in the late 19th century by Sir Albert Cook, a missionary doctor appointed in Uganda and described for the first time in Australia by Mac Cullum and co-workers in 1948 (MacCULLUM, 1948). Buruli ulcer is one of the skin-related neglected tropical diseases and it is nowadays considered as the third most common disease caused by mycobacteria after tuberculosis and leprosy (Huang and Johnson, 2014).

The first descriptions of Buruli ulcer clinical features and disease progression come from observations made by Clancey and co-workers in the 60's in Uganda. The first symptoms are small painless indurated nodules, which initially look like small insect bites. A few weeks after the nodules start growing in depth and diameter, generating edematous plaques with ill-defined borders. Later on, the necrotic plaque sloughs off, generating a painless ulcer with irregular borders. The ulcer grows during some weeks or months, necrotizing the underlying skin and subcutaneous tissue border, leading to undermined borders. Eventually, in some cases ulcers can be very deep, exposing tendons and bones and leading to osteomyelitis and infections by other bacteria (CLANCEY et al., 1961).

Currently there are 33 countries around the globe reporting cases of this disease. Most of these countries belong to rural areas of tropical zones, with a special high incidence in West Africa, the main endemic focus. Among the affected countries, Ivory Coast, Ghana and Benin are the top three endemic countries, accounting for ~73 % of the total of Buruli ulcer cases reported globally. Children aged under 15 years old are the most affected group of patients by the infection, constituting the ~48 % of cases in Africa. There are also some other countries outside the tropical climate zone presenting cases of Buruli ulcer such as Japan and Australia (Yotsu et al., 2018; Yotsu et al., 2015).

Little knowledge is available about its mechanism of transmission. The etiological agent of Buruli ulcer is *Mycobacterium ulcerans* (*M. ulcerans*), whose toxin; mycolactone, a polyketide derived macrolide, causes extensive deep and painless ulceration (George et al., 1999). As most of cases have been reported in areas close to stagnant waters, the most probable is that the disease is transmitted from ponds and lakes. In line with this hypothesis, DNA of *M. ulcerans* has been found in aquatic invertebrates, small animals living in swamps, and directly from environmental water sources (Portaels et al., 2008). Nevertheless, the high variability of potential vectors across different areas hinders the elucidation of the transmission mode of *M. ulcerans*. Another possibility suggests that transmission to humans is mediated through small injuries like scratches or insect bites rather than through a specific vector or the respiratory tract (Yotsu et al., 2018; Yotsu et al., 2015; Sarfo et al., 2016).

Currently, there are four main diagnosis tests to confirm the presence of *M. ulcerans* and a Buruli ulcer infection: microscopic detection of acid-fast bacilli in smears from swabs of patients, cell cultures, real-time PCR using the IS2404 gene present in *M. ulcerans*' genome and histopathology analysis of ulcers in pre-ulcerative forms (CLANCEY et al., 1961; Ross et al., 1997; Sakyi et al., 2016; Guarner, 2018). Nowadays, the World Health Organization recommends a 12-week therapy with a combination of oral streptomycin, rifampicin and clarithromycin to treat Buruli ulcer (Asiedu et al., 2012). However, antibiotic invasiveness and side-effects like nephrotoxicity and hearing impairment make necessary to find new cures (Scherr et al., 2018). There is no specific recommendation to prevent Buruli ulcer. The main risk factors include fishing, swimming or walking by stagnant waters or artificial lakes. Daily prophylaxes such as wearing long sleeves and trousers or the use of mosquito repellents have been shown to prevent the disease (CLANCEY et al., 1961; Ross et al., 1997; Sakyi et al., 2016; Guarner, 2018).

Most of the cytotoxic effects caused by *M. ulcerans* are produced through mycolactone, the toxin released by the bacterium, which is key for bacterial virulence and host colonization (George et al., 1999). Mycolactone is synthesized by giant polyketide synthetases coded by the 174 kb megaplasmid pMUM001, which has three genes (*mlsA1*, *mlsA2* and *mlsB*). Mycolactone consists of a 12-membered lactone core and two highly-unsaturated large-polyketide side-chains (Northern and Southern chains), responsible of the virulence effect (**Figure 23**) (Guenin-Macé et al., 2015). Two isoforms differing in their unsaturated fatty acid side chain called mycolactone A and B have been isolated and characterized from *M. ulcerans* (George et al., 1999).

Mycolactone A/B

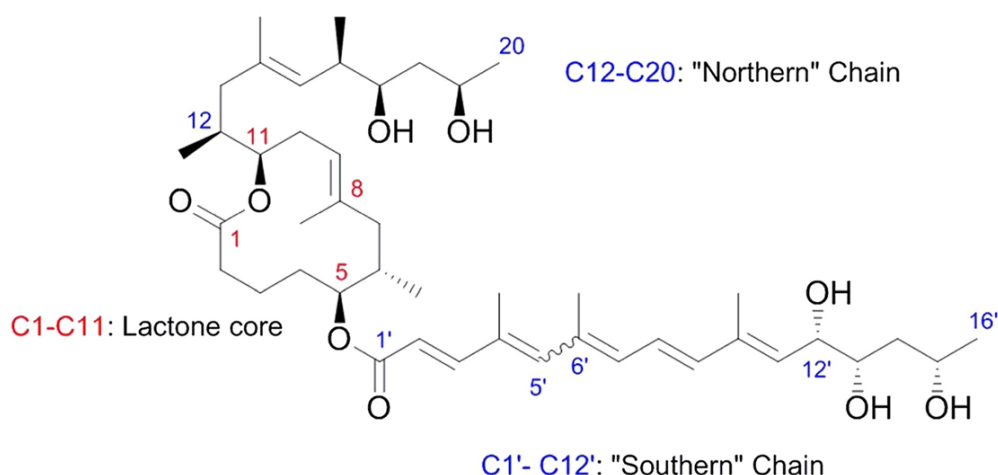


Figure 23. Schematic representation of mycolactone A/B structure

Mycolactone structure consists of a lactone core linked to a northern and a southern chain. Extracted from Sarfo et al., 2016

The biological function of mycolactone has been a subject of study since its identification (George et al., 1999). *In vivo* and *in vitro* application of purified lipid extracts from *M. ulcerans* and chemically synthesized mycolactone A/B show a painless and chronic skin ulceration which is associated with extensive necrosis alongside a minimal inflammatory response (CLANCEY et al., 1961; Ross et al., 1997; Sakyi et al., 2016; Guarner, 2018). Tissue necrosis, immunosuppression and painlessness in Buruli ulcer can be explained by the molecular targets of mycolactone. Targeting of scaffolding proteins controlling actin dynamics in anchorage-dependent like Wiskott-Aldrick Syndrome proteins cells leads to anoikis, cell death by detachment from the surrounding extracellular matrix, which explains tissue necrosis (Guenin-Macé et al., 2013). Immunosuppression is caused by prevention of co-translational translocation of cytokines via the Sec-61 translocon (Hall et al., 2014). Finally, the absence of pain is due to mycolactone binding to the angiotensin II type 2 receptor (AT2R) in sensory neurons, leading to cell hyperpolarization and pain suppression by silencing neuronal activity (Marion et al., 2014).

The analgesic mechanism, depicted in **Figure 24**, suggests that mycolactone binds to AT2R in a concentration-response dependent manner. Upon binding to AT2R and subsequent activation, mycolactone triggers a signaling pathway in which $G\alpha_i$ proteins lead to phospholipase 2 (PLA₂) activation. Following activation of PLA₂ and homologs, arachidonic acid is released from the plasma membrane phospholipids and converted into prostaglandins (notably to PGE₂) by the action of cyclooxygenase-1. The signaling pathway ends with activation of TRAAK, a two-pore-domain K⁺ (K_{2P}) channel by PGE₂ and subsequent hyperpolarization. The same work reported that *at2r*^{-/-} mice do not exhibit unaltered pain sensitivity in the tail-flick test after mycolactone inoculation into the footpads, thus revealing AT2R as a key agent in mycolactone-mediated hypoesthesia *in vivo* (Marion et al., 2014). In line with this, another work, has shown that mycolactone produces cell hyperpolarization in DRG neurons at non-cytotoxic concentrations via AT2R, constituting a good silencer of sensory neurons (Marion et al., 2014; Song et al., 2017).

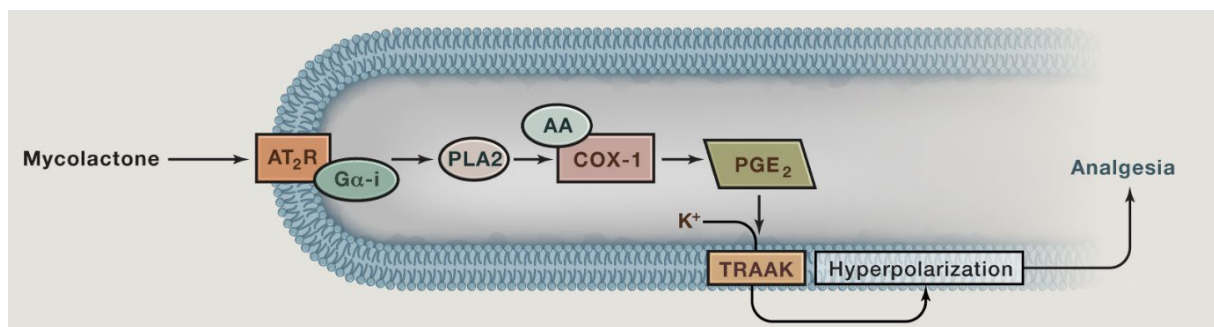


Figure 24. Mycolactone triggers cell hyperpolarization via the TRAAK channel upon binding to the AT2R receptor.

Mycolactone activates TRAAK channels through a molecular cascade involving G-protein signaling a production of prostaglandins. Extracted from Danser and Anand, 2014.

Supporting the hypothesis that AT2R could be a target in order to treat pain, previous studies have reported AT2R antagonist efficacy in rodent neuropathic pain models (Smith et al., 2013) and the AT2R antagonist EMA401 as a potential drug for treating post-herpetic neuralgia (McCarthy et al., 2012).

Nevertheless, another study using DRG neurons from human and rat describes a potent toxicity of mycolactone, suggesting that analgesia is caused by nerve destruction instead, similarly to leprosy (Anand et al., 2013). Furthermore, AT2R function in pain perception is controversial. Whereas some works do not identify the receptor in healthy adult humans outside of the brain (Ichiki, 2013) others indicate that it co-localizes with substance P and calcitonin gene-related peptide containing DRG neurons, thus suggesting a role in nociception (Patil et al., 2010). Besides, recent elucidation of the AT2R structure by crystallization indicates that the receptor does not produce its function via G-proteins (Zhang et al., 2017a), which contradicts the model suggested by Marion and co-workers (Marion et al., 2014). All these data pinpoint the necessity to revisit this model involving AT2R in mycolactone pain inhibition. As mycolactone targets several proteins in the cell it would not be surprising that analgesia is caused by a multi-factorial process involving more than one mechanism (Guenin-Macé et al., 2013).

Absence of pain in Buruli ulcer

Much research has been carried out in order to understand how neurons and nociceptors are altered by mycolactone. A pioneer study showed that inoculation of *M. ulcerans* in mouse footpads did not produce neither dermal ulcers nor nerve damage in early stages (33 days). However, in middle stages after the inoculation first dermal ulcers appeared and although peripheral nerves were well preserved, the perineurium of some nerve bundles showed the presence of acid-fast bacilli. At this stage animals showed decreased sensitivity in the sensory test of footpads with von Frey filaments. In late stages (50-70 days) animals most of nerve bundles were well preserved, but many of them showed massive intraendoneurial invasion that indicated loss of function. Moreover, myelin-forming Schwann cells showed deep degeneration (Goto et al., 2006).

A similar study by En and co-workers, in which mice footpads were directly injected with mycolactone, revealed a shift from normal response to hyposensitivity from day 28 to 42 after inoculation. The authors also observed peripheral nerve destruction and Schwann cells apoptosis some days later (En et al., 2008). The same group has reported cultured Schwann cells detachment in Petri dishes after mycolactone addition (En et al., 2017). Moreover, it has been recently shown that low concentrations of mycolactone induce apoptosis of cultured DRG neurons and Schwann cells from neonatal mice 48 h after mycolactone exposure. The same study reported that low concentrations of mycolactone prevent release of pro-inflammatory factors from DRG neurons and Schwann cells, indicating that analgesia could be linked to a suppression of the inflammatory response (Isaac et al., 2017).

Another work supporting that painlessness in Buruli ulcer is due to nerve degeneration has reported dramatic loss and degeneration of cultured DRG neurons and other nervous cells from rats and humans (Anand et al., 2016). This study also reported clustering of mitochondria in cell body of neurons and accumulation of mycolactone, suggesting impairment in axonal transport. The same work indicated that mycolactone reversibly prevents capsaicin response of TRPV1 channels, which are implicated in noxious stimuli (Anand et al., 2016).

Together, these works seem to indicate that absence of pain induced by mycolactone is related with nerve destruction and degeneration of myelin and interfering neuronal communication through Schwann cells apoptosis (Goto et al., 2006; En et al., 2008; Anand et al., 2016; En et al., 2017; Isaac et al., 2017). However, there are several observations, which strongly contradict this theory. For instance, when mycolactone was injected in footpads of mice, animals showed reduced pain perception wherea morphological changes in neurons and myelin that were only observed some days later (En et al., 2008). Also, although the studies described above converged on Schwann cells degeneration, it is not clear if they regenerate producing new myelin and consequently normal neuronal transmission (Goto et al., 2006; En et al., 2008; Anand et al., 2016; En et al., 2017; Isaac et al., 2017). Furthermore, Marion and co-workers also reported AT2R-dependent loss of pain in the tail-flick test but not nerve degeneration in sciatic nerves of mice injected with the toxin (Marion et al., 2014). They also reported that murine hippocampal neurons are resistant to a cytotoxic effect of mycolactone after 30 min of incubation (Marion et al., 2014). As a conclusion, they reported mycolactone-induced hyperpolarization through AT2R as an etiological cause of painlessness (Marion et al., 2014). In line with this hypothesis, a recent study performed with cultured murine DRG neurons showed that hyperpolarization was not observed in neurons from *at2r^{-/-}* cells and there is no DRG neuron degeneration at high concentrations (70 μ M) of the toxin, even 72 h after incubation (Song et al., 2017). Since one hypothesis contradicts the other, additional research is needed in order to elucidate the actual mechanism by which mycolactone induces analgesia.

2. TRAAK channels

TRAAK channels in the context of K_{2P} potassium channels

K^+ channels represent the largest and most diverse family of ion channels. Its diversity arises from alternative splicing, heteromeric assembly of pore-forming subunits, association with ancillary subunits and post-transcriptional modifications (Coetzee et al., 1999). They are expressed in virtually all mammalian cells, allowing the passive flux of K^+ across the plasma membrane through a conserved selectivity filter. They play a major role in K^+ homeostasis driving to hyperpolarization of the plasma membrane voltage (Baker et al., 1987). Hence, they regulate cell volume and excitability and control key physiological processes such as muscle contraction, neuronal communication and hormone secretion (Coetzee et al., 1999).

There exist three major families of K^+ channels according to their membrane topology. The first family is constituted by the Shaker channels, which are opened by either membrane depolarization (voltage-gating) or intracellular Ca^{2+} (Ca^{2+} -sensitivity). These channels are typically composed by four α -subunits, each one having between six and seven transmembrane domains and one P-loop. Their main role is to accelerate repolarization of the membrane and their voltage sensor is located in domain 4 (Coetzee et al., 1999). The second is the inward-rectifying K^+ channel family. They are also tetrameric channels and each subunit consists of two transmembrane domains and one P-loop. Their two main characteristics are their high conductivity at negative membrane potentials below E_{K^+} and an inward rectification due to Mg^{2+} or polyamine blockade of the channel at depolarized potentials (Coetzee et al., 1999). The third group includes the K_{2P} family, which corresponds to dimers with four transmembrane domains and two P-loops per subunit (Lesage et al., 1996; Ketchum et al., 1995). They set the resting membrane potential below the firing threshold in excitable cells (Baker et al., 1987). This family of 15 members is divided into 6 subfamilies, according to their homology and regulation mode (**Figure 25**): TWIK (Tandem of pore domains in a Weak Inward rectifying K^+ channels), TREK (TWIK-Related K^+ channels), TASK (TWIK-related Acid Sensitive K^+ channels), TALK (TWIK-related Alkaline pH-activated K^+ channels), THIK (TWIK-related Halothane Inhibited K^+ channels), TRESK (TWIK-related Spinal cord K^+ channels). The diversity of this group increases as some of them have the ability to form heteromers with others (Blin et al., 2016; Blin et al., 2014; Royal et al., 2019b; Levitz et al., 2016; Royal et al., 2019a).

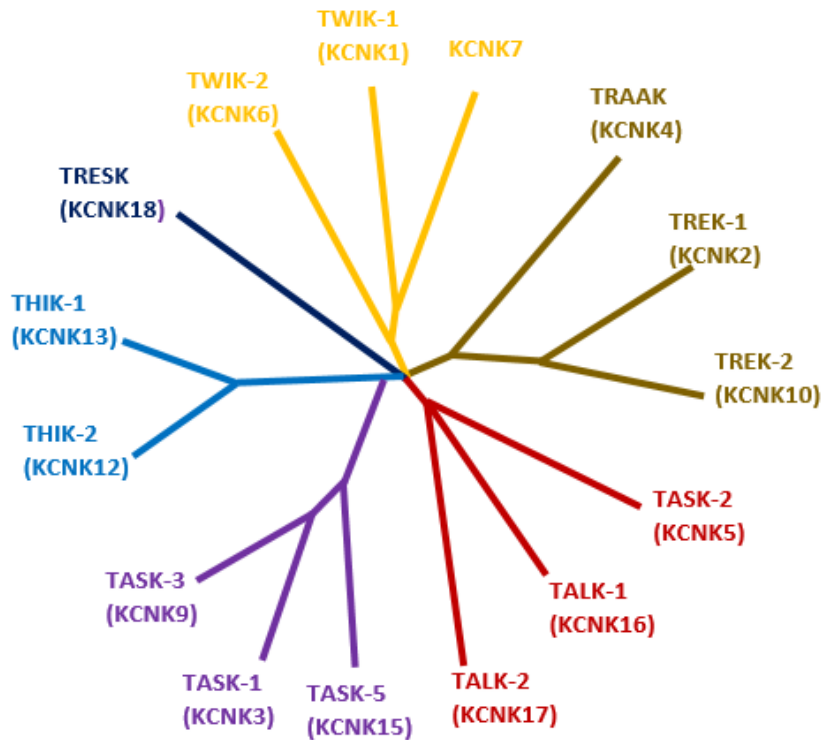


Figure 25. The two-pore-domain K^+ channels family.

The TREK subfamily is composed by three members that share more than 50% of homology between them: TREK1 (K2P.1), TREK2 (K2P10.1) and TRAAK (TWIK-Related Arachidonic Acid sensitive K^+ channels) (K2P4.1). The members of this K_{2P} subfamily are considered as polymodal regulated channels since they can be regulated by diverse stimuli, including changes in temperature and pH, membrane stretch and fatty acids, among others (Lesage and Lazdunski, 2000; Noël et al., 2011). Besides, they are not sensitive to typical blockers of K^+ channels such as 4-aminopyridine, quinidine or Cs^+ , but they are blocked by high concentration of Ba^{2+} and tetraethyl ammonium. They can be activated by some drugs like riluzole, used to protect motoneurons from degeneration in amyotrophic lateral sclerosis (Fink et al., 1998) and ML-67 (Bagriantsev et al., 2013).

Within this subfamily, TRAAK was the first arachidonic acid background K^+ channel to be cloned and characterized in neurons. The TRAAK channel was first cloned from mouse brain cDNA by Fink and co-workers (Fink et al., 1998). Compared to its partners TREK1 and TREK2, TRAAK generates smaller currents at physiological K^+ gradients (Fink et al., 1998; Lesage and Lazdunski, 2000; Maingret et al., 1999).

Concerning its distribution, TRAAK has been typically assumed to be restricted to the nervous system. It is highly expressed in the peripheral nervous system in DRG neurons and in the trigeminal ganglia neurons, where it senses mechanical stimuli and cold and heat perception (Medhurst et al., 2001; Kang et al., 2005; Noël et al., 2009). TRAAK channels have also been found in vagal afferent neurons of the nodose ganglia, where they are believed to modulate some processes of the autonomous system, such as gastrointestinal regulation of cardiac reflex (Zhao et al., 2010). Unlike other K_{2P} channels, TRAAK expression has not been found in glial cells (Medhurst et al., 2001; Kang et al., 2005; Noël et al., 2009).

Structure and gating of TRAAK channels

Crystallization of human TRAAK has allowed to determine important aspects related to its structure and function (Brohawn et al., 2012). TRAAK shares the same architecture of all K_{2P} channels: It is composed by two subunits, each one conformed by two concatenated pore domains on a single protein chain monomer. The crystal structure of the TRAAK channel revealed, that is composed by an outer helix, a pore helix, a selectivity filter and an inner helix, with the transmembrane region spanning the membrane (Brohawn et al., 2012) (**Figure 26**). The C-termini of both subunits, the inner helices and the linker between the two pore domains are located in the cytosol (Brohawn et al., 2012). On the extracellular side of the transmembrane region there is a ~ 35 Å helical cap structure extending above the membrane (Brohawn et al., 2012). The overall two-fold symmetric channel converges to an essentially four-fold symmetric pore helix and selectivity filter (Brohawn et al., 2012). Such convergence seems to be the result of strong evolutionary pressure to highly selective K^+ ion conduction through the channel when it is compared to the prokaryotic KcsA K^+ channel (Zhou et al., 2001). Regarding to its selectivity filter, the ones of pore domains 1 and 2 are formed by the sequences TVGYGNY and TIGFGDV, respectively (Maingret et al., 1999).

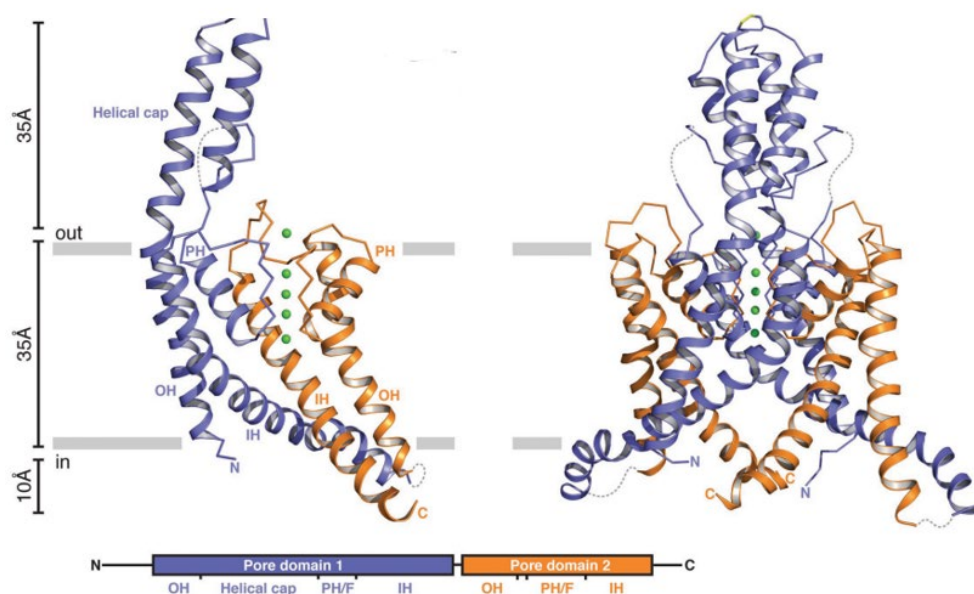


Figure 26. Structure of TRAAK.

TRAAK is a homodimer conformed by two concatenated pore-domains on a single protein monomer chain. Extracted from Brohawn et al., 2012.

Elucidation of TRAAK structure has allowed to understand the gating underlying its mechano-sensitivity. The orientation of inner helices generates a ~ 5 Å wide lateral opening similar to the one observed in the KcsA prokaryotic K^+ channel (Zhou et al., 2001). The fourth transmembrane segment of one of the TRAAK subunit (TM4A) is bent halfway through the membrane, packing hydrophobic residues on its extracellular-facing side against cytosolic facing-side of the second transmembrane segment of the other subunit (TM2B). This forms a barrier that seals the channel cavity from lipids like arachidonic acid or PIP_2 from the membrane. However, the fourth transmembrane domain of the other subunit (TM4B) is not kinked, creating an intramembrane opening between both subunits that expose TRAAK cavity to the inner leaflet of the lipid bilayer. The model, summarized in **Figure 27**, indicates that membrane tension pulls TRAAK into a wider and flatter state that is conductive because it seals holes to the membrane to prevent lipid block of ion conduction (Brohawn et al., 2012; Brohawn et al., 2014).

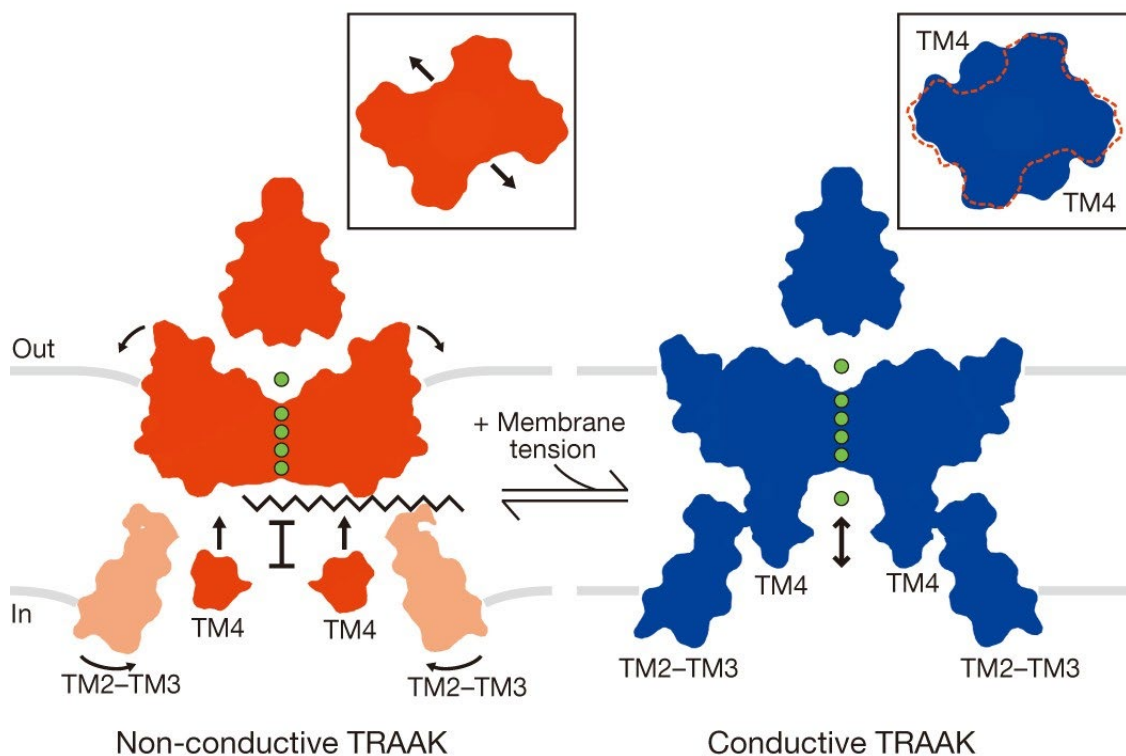


Figure 27. Model for TRAAK mechanosensitivity.

In the nonconductive conformation (red), a lipid acyl chain accesses the central cavity through intramembrane openings above TM4 to sterically block ion (green) conduction. In the conductive conformation (blue), conformational changes in TM4 seal the intramembrane openings to prevent lipid access and permit ion conduction through the channel. Extracted from Brohawn et al., 2014.

One of the main modulators of the TRAAK/TREK subfamily is temperature. Transfection of COS cells with TRAAK has shown that heat enhances progressively the TRAAK current (7-20 fold) from 17 °C to 40 °C, and decreases its activity above 42 °C, meaning that they are fully activated at physiological temperatures. Experiments with DRG neurons from wild type and KO animals, have shown that, together with TREK1, TRAAK channels modify the temperature threshold of heat nociceptors by silencing excitability produced by TRP channels (Medhurst et al., 2001; Kang et al., 2005; Noël et al., 2009).

Activation by poly-unsaturated fatty acids (PUFA), and notably by arachidonic acid, is one of the principal features of TRAAK channels. This activation is reversible and seems to be independent from the arachidonic acid metabolism since it is observed in the presence of cyclooxygenase and lipoxygenase inhibitors. Activation by PUFA depends on extent of saturation of the lipid (saturated fatty acids do not open TRAAK channels) and the length of the carbonyl chain. The threshold PUFA concentration to open TRAAK channels is ~100 nM and its effect does not saturate even at high concentration such as 100 µM (Fink et al., 1998). Lysophospholipids can also open TRAAK channels at low concentrations. The channel activation depends on the polar head group (like choline) and the length of the carbonyl chain and is independent of the saturation status of the lipid (Maingret et al., 1999). TRAAK activation by lipids has been suggested to be related to its mechanosensitivity (Brohawn et al., 2012; Brohawn et al., 2014). TRAAK channels can be also regulated by changes in pH (Sandoz et al., 2009; Levitz et al., 2016). TRAAK is activated by intracellular alkalization and is inhibited by extracellular acidification, but in less degree than TREK1 (Sandoz et al., 2009; Levitz et al., 2016). Interestingly, when TREK1 and TRAAK heteromerize, the resulting tandem presents intermediate inhibition by extracellular acidic pH (Levitz et al., 2016). Such heterodimers also present an intermediate current amplitude between TREK1 and TRAAK (Levitz et al., 2016; Blin et al., 2016). In addition, transposition of the TRAAK C-terminus by TREK-1's confers acid sensitivity to TRAAK (Maingret et al., 1999).

TRAAK channels and nociception

Sensory neurons residing in dorsal root and trigeminal ganglia detect changes in temperature, mechanical forces and chemical stimuli through their long axons that innervate peripheral tissues. This neuronal system is engaged with pain perception or nociception: whereas immediate pain is detected by rapid A δ -fibers, unmyelinated and slowly conducting C-fibers sense poor localized and slow pain. Dysfunction in these fibers can lead to pain-related troubles like allodynia (pain response to innocuous stimuli) or hyperalgesia (exaggerated pain response) (Basbaum et al., 2009).

Thermoception is mainly transduced by the non-specific cationic TRP channels (TRPV1-4 sense heat and TRPA1 and TRPM8 sense cold), ASIC channels and epithelial sodium channels. These channels induce depolarization of thermoreceptors, leading to more frequent afferent discharge (Enyedi and Czirják, 2010; Waxman and Zamponi, 2014). On the other hand, K⁺ channels, and specially K_{2P} channels, underlie the background K⁺ current that sets the resting potential in neurons, controlling membrane repolarization (Baker et al., 1987). As they are mainly expressed in small DRG neurons (Dang et al., 2005, Noël et al., 2009) and are activated by changes in temperature and membrane stretch (Lolicato et al., 2014; Brohawn et al., 2012; Brohawn et al., 2014), they are believed to be also major transducers of mechanical and thermal stimuli, but not of osmotic sensing associated with inflammation (Noël et al., 2009).

Indeed, *traak*^{-/-} and *trek1*^{-/-} mice are hypersensitive to mechanical stimulation in the von Frey assays, corresponding to allodynia, probably due to a lack of neuronal inhibition (Noël et al., 2009). Presumably, together with mechanosensitive excitatory cationic channels, they determine the mechanical threshold of nociceptors. For thermal perception, Noël and co-workers have suggested that, as they are opened at 37 °C, they must be important regulators for maintenance of internal physiological temperature. Moreover, genetic deletion of either TREK1 or TRAAK strongly increases the number of DRG neurons activated by capsaicin and heat between 30 and 50 °C, suggesting that heat perception depends on the balance of inhibitory TREK1 and TRAAK and excitatory channels (Dang et al., 2005; Noël et al., 2009).

The same works have shown that, in DRG neurons, TRAAK and TREK1 act as silencers of heat nociceptors (Noël et al., 2009). Therefore, the temperature threshold of heat nociceptors will be dictated by the respective proportion of TRAAK/TREK1 channels and excitatory cationic channels and by their respective temperature dependence (Noël et al., 2009). Additionally, in heat-sensitive C-fibers expressing the heat sensor TRPV-1, which is activated at high temperatures, deletion of TRAAK decreases the threshold activation up to 5 °C and increases their firing properties. Behavioral tests with mice also indicate that TRAAK and TREK1 channels are essential hubs that define firing properties and threshold of fibers associated with noxious heat perception (Noël et al., 2009).

Additionally, TRAAK gradually closes with linear temperature dependence below 30 °C (Noël et al., 2009). Genetic deletion of both TREK1 and TRAAK (and not separately) increases the number of DRG neurons that respond to cold temperatures (between 30 and 12 °C) and menthol, which indicates with the previous data that the two channels contribute together to cold perception (Noël et al., 2009). Also, additional experiments with C-fibers and behavioral tests with mice have shown that both channels have a great importance in unpleasant cold perception and that, in neuropathic conditions, deletion of TREK1 and TRAAK leads to a very marked hyperalgesia (Noël et al., 2009). Such observations characterize TRAAK (together with TREK1) channels as main sensors of cold stimuli, acting in fine tune with other channels such as the cold and menthol-activated TRPM8 channel, the pungent irritant-activated TRP1 channel and the I_h channel HCN (Enyedi and Czirjak, 2010; Waxman and Zamponi, 2014).

Taken together, these data suggest that TRAAK and TREK1 produce a local temperature-dependent control in sensory nerve terminals of the skin, regulating at the same time temperature sensitivity of TRP channels. This control overlies changes in membrane potential that dictate threshold activation of TRP channels and therefore fine perception of cold and warm (Noël et al., 2009).

3. AT2R receptors

Main characteristics of the angiotensin II type receptor 2

G-proteins coupled receptors (GPCRs), which are encoded by more than 800 genes in the human genome, represent one of the main hubs of signaling transduction (Fredriksson et al., 2003). Once they bind their ligands, a series of conformational rearrangements happen favoring the coupling and stabilization of G-proteins and other molecular effectors (Venkatakrisnan et al., 2013). Non-sensory GPCRs can be classified in four subfamilies according to their pharmacological properties: Class A rhodopsin-like, Class B secretin-like, Class C metabotropic glutamate/pheromone, and frizzled receptors (Fredriksson et al., 2003).

Within the class A rhodopsin-like subfamily, AT2R constitutes one of the most studied GPCRs (Porrello et al., 2009). Although most of physiological effects of AngII are typically associated with blood-pressure decrease in the renin-angiotensin system, AT2R actually plays a minor role on it, by counteracting the effect of its homolog AT1R (de Gasparo et al., 2000).

The exact function of AT2R is not clear. It has been reported that its activation induces an anti-proliferative effect, which opposes the AT1R in cardiac fibrosis promotion and myocardial hypertrophy (Suzuki et al., 1993; van Kesteren et al., 1997). In behavioral experiments, *at2r*^{-/-} mice show altered exploring and behavior (de Gasparo et al., 2000). As the receptor is particularly highly expressed in embryonic and neonatal tissues, this may also indicate a potential role of AT2R in early development and cell differentiation (Suzuki et al., 1993). Concerning its distribution, AT2R expression is widespread and complex: in several tissues it disappears after birth and sometimes it can be up-regulated after tissues injury. Its presence seems also to be specific of tissue and species, complicating the elucidation of its contribution on physiology (de Gasparo et al., 2000; Porrello et al., 2009; Karnik et al., 2015).

Unconventional structure of AT2R and G-protein signaling

Generally, GPCRs consist of three domains: an extracellular region divided in the N-terminus and three extracellular loops, the transmembrane region which consists in seven transmembrane segments, and the intracellular region that is composed by three intracellular loops and the C-terminus (Venkatakrishnan et al., 2013).

The extracellular part modulates ligands access by occluding or allowing accessibility to the ligand binding pocket and contributes to structural stability through disulfide bridges between the extracellular loops and the transmembrane segments (Venkatakrishnan et al., 2013). The transmembrane region is considered as a structural bridge between the ligand pocket and the G-protein-coupling domain and is the main element for membrane insertion. The bundle of transmembrane domains usually follows a tertiary inter-contact pattern which is well conserved among the different GPCRs (Fredriksson et al., 2003). Small rearrangements in these connections due to ligand binding induce conformational changes in the whole receptor by which signals are transduced to the intracellular part (Venkatakrishnan et al., 2013). The intracellular region binds the molecular effectors of the signaling pathway. Among them, G-proteins, β -arrestins and kinases are the principal molecules involved (Venkatakrishnan et al., 2013). In class A GPCRs there is an amphipathic helix (H.VIII) that seems to participate in G-protein binding (Venkatakrishnan et al., 2013; Zhang et al., 2015; Zhang et al., 2017a).

Recently, the AT2R structure was resolved by crystallization by Zhang and co-workers (Zhang et al., 2017a) (**Figure 28**). As other class A rhodopsin-like GPCR, its structure includes an extracellular N-terminus, which theoretically serves as a ligand-binding site, a seven transmembrane bundle and an intracellular amphipathic H.VIII (Zhang et al., 2017a). Concerning the transmembrane region, AT2R possesses some typical domains of other rhodopsin-like GPCRs (Venkatakrishnan et al., 2013; Zhang et al., 2015; Zhang et al., 2017a). Among these domains there is a β -hairpin conformation of the extracellular loop 2 and two pairs of disulfide bridges linking the N-terminus with the extracellular loop 3 and H.II with the extracellular loop 2 (Zhang et al., 2017a). Another criteria to classify AT2R within the class A GPCR family is the existence of an intracellular cleft between H.VI and H.VII, presumably involved in the recruitment of G-proteins and β -arrestins (Venkatakrishnan et al., 2016).

Nevertheless, its H.VIII remarkably differs from those typical from class A GPCRs. While in most of cases, including AT1R, this structure lies parallel to the plasma membrane and points outside the transmembrane region regardless the action state of the receptor (Zhang et al., 2015), AT2R's adopts a very different conformation in the active state. This H.VIII interacts with intracellular endings of H.III, V and VI and forms a strong complementary interface with the intracellular cavity of the transmembrane bundle, which is stabilized by hydrophobic interactions (Zhang et al., 2017a). These interactions are sterically unable to bind G-proteins and β -arrestins, which is of extreme importance regarding the theoretical lack of downstream G-protein signaling (Porrello et al., 2009, Karnik et al., 2015).

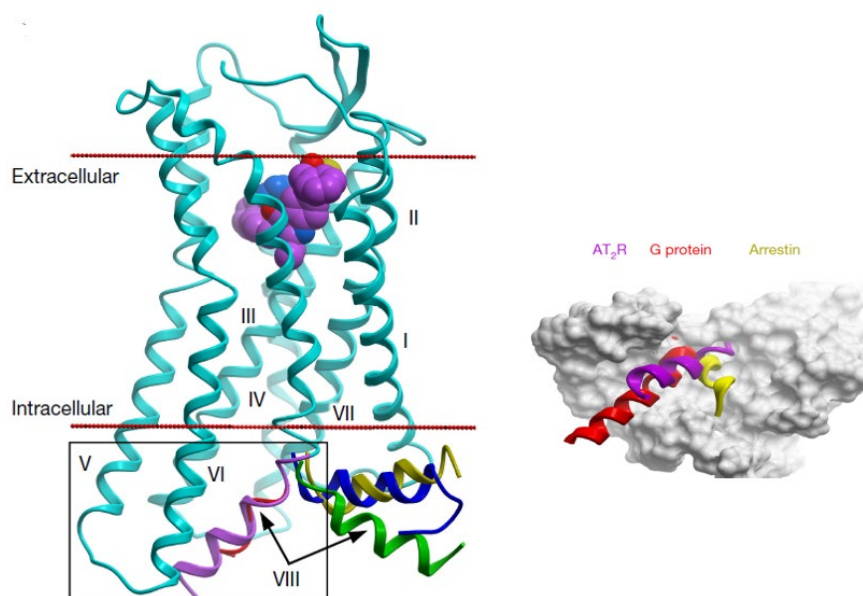


Figure 28. H.VIII blocks the putative G-protein/ β -arrestin-binding site of AT2R.

AT2R H.VIII is depicted in purple, whereas H.VIII from other GPCRs are in different colors. Modified from Zhang et al., 2017.

AT2R G-protein coupling has been historically questioned. First observations regarding to its activity showed that its activation does not modify intracellular Ca^{2+} levels nor cAMP, indicating lack of G_s or G_i -dependent signaling (de Gasparo et al., 2000). Also stimulation by AngII does not induce AT2R internalization, which does not match with class A GPCR way of action (Dudley et al., 1991). Furthermore, it does not alter GMPC levels, phosphotyrosine phosphatase activity nor arachidonic acid release (Mukoyama et al., 1995). Taken together with the recently crystallized structure, these observations suggest that there is no coupling between AT2R and G-proteins in spite of showing classic features of class A GPCRs.

However, several studies have reported that AT2R can bind G_i proteins, linking downstream signaling pathways (Zhang and Pratt, 1996; Hayashida et al., 1996). One of them suggests that the intracellular third loop allows coupling of $G\alpha_i$ (Hayashida et al., 1996). Additional works propose that this coupling is linked to induction of apoptotic responses in neuronal cell lines, reduction of IP_3 in *Xenopus* oocytes, inhibition of tubule Na^+ -ATPase and increase of nitric oxide synthase expression (Porrello et al., 2009, Karnik et al., 2015). On the other hand, it has been shown that pertussis toxin (PTX) does not avoid activation of SHP-1 by AT2R, which disagrees with AT2R- $G\alpha_i$ coupling (Feng et al., 2002). Interestingly, AT2R seems to interact with other non-G-proteins like the promyelocytic zinc finger protein (PLZF), the ErbB3 EGF receptor (Porrello et al., 2009, Karnik et al., 2015). Whether AT2R exerts its physiological effects through G-proteins or not is a challenging question that needs more experiments to be resolved (Porrello et al., 2009, Karnik et al., 2015).

Implication of AT2R in pain perception

Pioneer works have detected AngII expression in human trigeminal ganglia (Patil et al., 2010) and DRG neurons (Chakrabarty et al., 2008). Furthermore, the hormone co-localizes with calcitonin gene-related peptide and substance P in DRG neurons, which suggests a potential role for AT2R in pain perception (Patil et al., 2010). AT2R protein expression has been also shown in human and rat DRG small and medium neurons, where it co-localizes with the capsaicin-sensitive TRPV1 channel. The same work shows that the AT2R inhibitor EMA401 has an inhibitory effect on neurite outgrowth and capsaicin responses by reducing cAMP levels in DRG neurons. Thus, it has been suggested that when AngII is increased in physiological conditions, AT2R leads to sensitization of TRPV1 channels in DRG neurons and subsequent pain (Anand et al., 2013). AT2R implication in pain also agrees with a double-blinded phase II clinical trial, where pain relief associated with post-therapeutic neuralgia was observed after 4 weeks of administration of the same antagonist (Smith et al., 2016).

4. Hypothesis: Analgesia in Buruli ulcer involves direct and G-protein-independent coupling between TRAAK channels and AT2R receptors

Currently, two different theories try to explain the absence of pain induced by mycolactone in Buruli ulcer. The first one postulates that the absence of pain is due to nerve degeneration of sensory neurons (Goto et al., 2006). Nevertheless, nerve destruction is only observed in late stages of the disease, whereas painlessness occurs in early stages (Goto et al., 2006; En et al., 2008). Moreover, the cytotoxic effect of mycolactone on nociceptive DRG neurons is questioned (Anand et al., 2016; Song et al., 2017). The second theory links analgesia to a signaling pathway triggered by the toxin. In this model, mycolactone would bind to AT2R expressed in nociceptors, activating a molecular cascade involving G-proteins, cyclooxygenase components and the release of arachidonic acid. As a consequence, the opening of TRAAK channels in sensory neurons would induce analgesia (Marion et al., 2014). However, the finding that AT2R does not seem to induce its function through G-proteins (Zhang et al., 2017) weakens this model. Since experiments with *at2r^{-/-}* null mice have shown that this receptor plays a key role in neuronal hyperpolarization (Marion et al., 2014; Song et al., 2017), the present work suggests an alternative mechanism, which does not implicate G-protein participation.

1. Mycolactone induces hypoexcitability and prevents activation of sensory neurons through TRAAK channels activation

To investigate the mycolactone effect in neuronal excitability of sensory neurons, small and medium-sized DRG neurons (<25µm) were perfused with the toxin. As shown in **Figure 29A, B**, mycolactone perfusion (10 µM) almost fully abolished the ability of neurons to generate action potentials, even at high current injection (>300 pA). To see if the effect of the toxin reverses over the time, as observed for morphine (Williams et al., 2013), we perfused DRG neurons from wild type animals with mycolactone until they reached a hyperpolarizing plateau phase (-68.38 ± 3.03 mV) and then washed them out. The wash-out did not reverse the hyperpolarizing effect of the drug after 5 min, indicating irreversibility (**Figure 29C, D**).

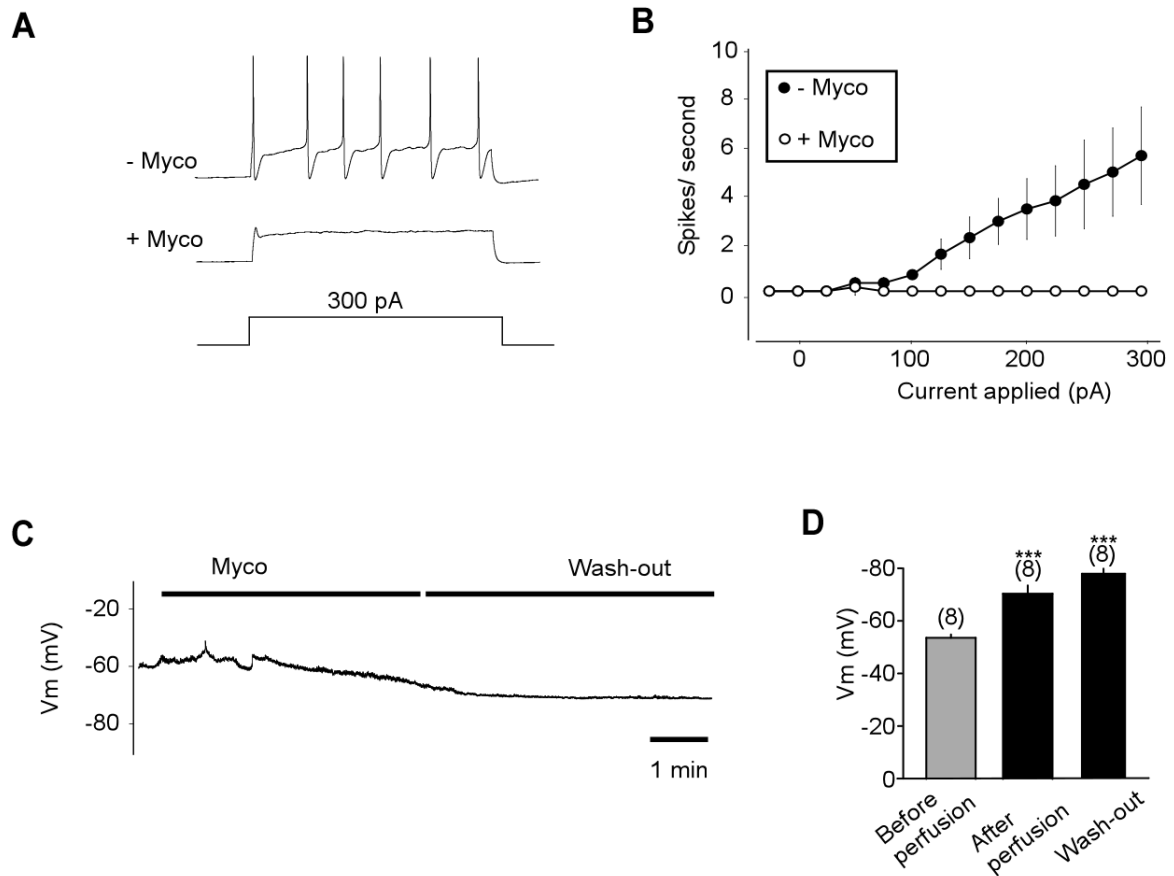


Figure 29. Mycolactone induces hyperpolarization of DRG neurons through TRAAK channels.

(A) Representative traces of action potentials (spikes) generated by incremental depolarizing current injections in small-diameter DRG neurons before and after application of mycolactone (10 μ M) ($n=6$). (B) Input-output plots of spike-frequency in response to 1-s depolarizing current injection in DRG neurons from wild type mice. (C) Membrane potential recording of a wild type DRG neuron perfused with mycolactone. (D) Δ membrane potential of DRG neurons after 3 min of perfusion. Mann-Whitney test ($***p < 0.001$). Mean \pm SEM.

Then, the effect of mycolactone application on the resting membrane potential (RMP) was studied. Whereas application of the vehicle solution (DMSO 0.2 %) had no effect on the RMP ($\Delta V_m -0.6 \pm 1.05$ mV), perfusion of mycolactone decreased it by more than 10 mV ($\Delta V_m 12.38 \pm 1.35$ mV) (Figure 30A, B). To demonstrate the role of TRAAK in the mycolactone-induced DRG neuron hyperpolarization, we used neurons from *traak*^{-/-} mice. TRAAK invalidation suppressed the ability of mycolactone to modify the RMP of the neurons ($\Delta V_m -1.76 \pm 0.64$ mV) (Figure 30A, B). Therefore, mycolactone induces hyperpolarization of DRG neurons through activation of TRAAK channels.

TRAAK is a mechanosensitive and temperature sensitive channel (Noël et al., 2009; Brohawn et al., 2014). To address the effect of mycolactone and TRAAK implication in peripheral nociceptors, C-fibers heat sensors were tested using the isolated skin-saphenous nerve preparation (Reeh, 1986). This experiment was performed in partnership with Dr Jacques Noël from the Institute of Molecular and Cellular Pharmacology (IPMC) in Sophia Antipolis. Single action potentials from slowly conducting velocity (CV <1.2 m/s) C-fibers were recorded and their receptive fields in the skin were probed for their modal sensitivity (Kress et al., 1992). The **Figure 30C** shows individual response from the same C-fiber to noxious heat before and after 10 min mycolactone incubation. Whereas in the absence of mycolactone the fiber was producing 53 spikes for a ramp from 30 to 50 °C, it produces only 3 spikes after the incubation with the toxin. We next conduct similar experiments on single fibers obtained from *traak*^{-/-} animals. **Figure 30C** shows the response to heat before and after 10 min mycolactone incubation. As expected and reported earlier, the *traak*^{-/-} C-fibers presented a basal activity at rest (66 spikes during the 2 min of recording) and as expected, mycolactone failed to suppress the noxious response as observed for wild type fibers (79 spikes). These results demonstrate that in an intact system, *ex vivo*, mycolactone reduces C-fibers activity through TRAAK channels activation in response to noxious thermal stimuli.

To fully demonstrate that TRAAK is needed to observe mycolactone-induced analgesia *in vivo*, the Hargreaves plantar pain test was performed with wild type and *traak*^{-/-} mice by the group of Dr Laurent Marsollier from Institut de Recherche et d'Ingénierie de la Santé (IRIS). This test consists of measuring the time which is needed to induce paw retraction (latency) induced by a thermal pain stimulus (Hargreaves et al., 1988). As shown in **Figure 30D**, 24h after mycolactone intracutaneous injection a ~7 s increase of the latency for the paw retraction was observed in wild type animals. To validate that the reduction of thermal sensitivity is linked to mycolactone-induced TRAAK activation, a similar experiment was conducted with *traak*^{-/-} mice. As expected, genetic invalidation of TRAAK suppresses the ability of mycolactone to induce analgesia (~12 s and ~14 s for mice injected with mycolactone and vehicle solution, respectively, **Figure 30D**). Altogether, the *ex vivo* and *in vivo* results demonstrate that TRAAK channels are necessary for thermal perception induced by mycolactone.

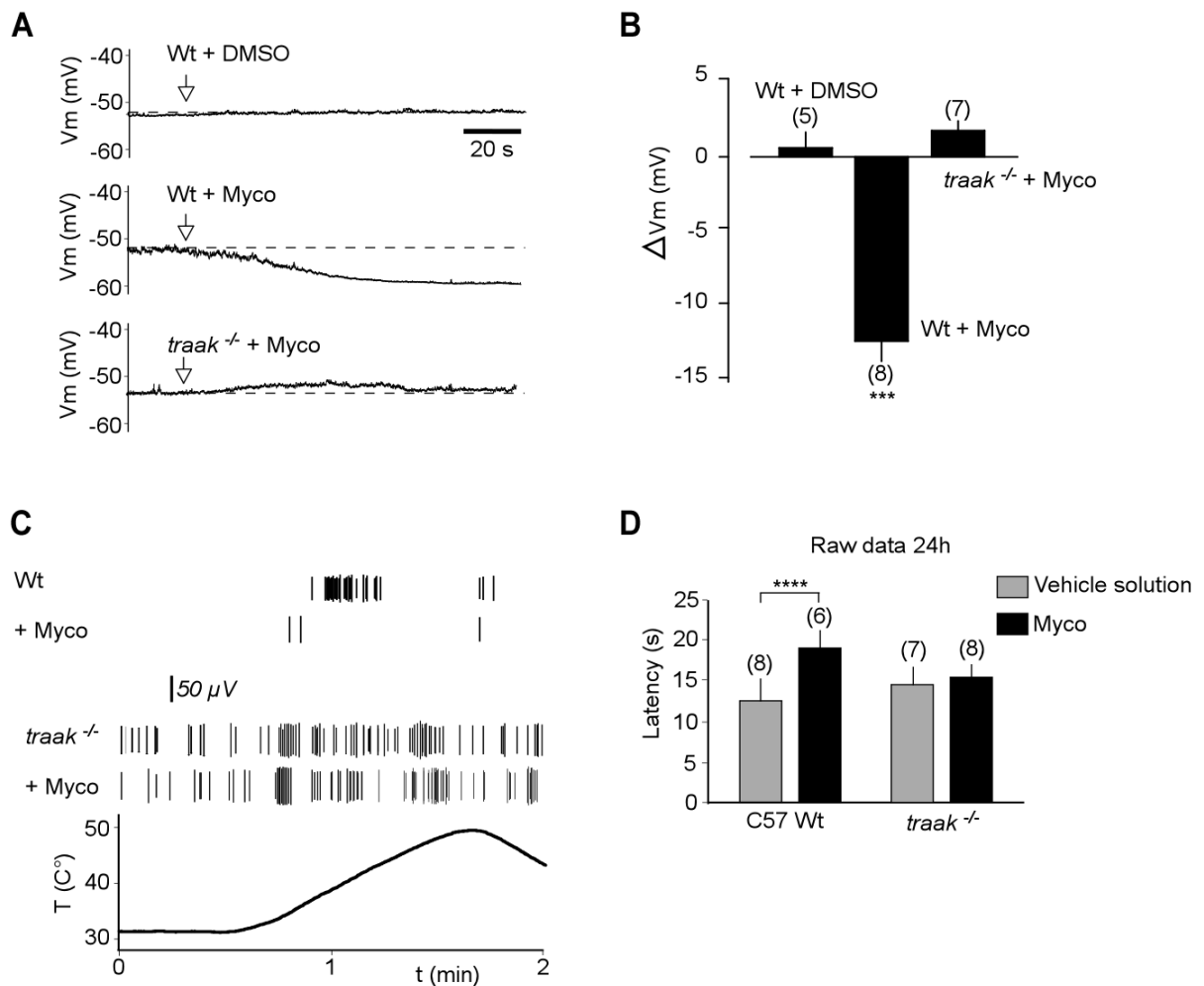


Figure 30. Mycolactone induces analgesia through TRAAK channels.

(A) Membrane potential recording of wild type and *traak*^{-/-} DRG neurons perfused with mycolactone (10 μM) or a vehicle solution (0.2 % DMSO). (B) Δ Membrane potential of DRG neurons after 3 min of perfusion. Mann-Whitney test (****p* < 0.001). Mean ± SEM. (C) C-fibers response to temperature from wild type and *traak*^{-/-} mice before and after incubation with mycolactone (10 μM). (D) Bar graphs representing the time latency of retraction of paw retraction of wild type and *traak*^{-/-} mice inoculated with mycolactone (3.75 μg) and a vehicle solution. Mean ± SEM. C-fibers experiments were performed in partnership with Dr Jacques Noël from IPMC in Valbonne, France. Behavioral experiments were performed by the group of Dr Laurent Marsollier from IRIS in Angers, France.

2. Mycolactone induces long-lasting hyperpolarization but not internalization of AT2R

Mycolactone induces a long-lasting hyperpolarization and no desensitization

In order to study the signaling pathway linking AT2R to TRAAK and its reversion without implication of other channels and receptors, we reproduced the experiments in a heterologous model: HEK293T transfected cells. First, as expected, mycolactone incubation (30 min) induced a strong TRAAK current increase (fold increase ~6). To test the reversion in this model, we incubated the cells for 4 h in the washing solution after 30 min exposure to mycolactone. As shown in **Figure 31A**, the current increase persisted along this period this long period (fold increase ~3.5). We next addressed the desensitization of the signaling pathway by incubating the cells with mycolactone for a longer period of time. This long-lasting incubation (90 min) did not modify the mycolactone effect. In fact, the TRAAK current remained stronger (fold increase ~6) than the one measured in non-incubated cells and similar to the one observed in cells incubated for 30 min (**Figure 31B**). These results suggest that the AT2R-TRAAK pathway does not desensitize. Thus, the mycolactone effect does not desensitize and does not reverse after several hours explaining its long lasting effect *in vivo* as it was observed previously (Babonneau et al., 2019).

AT2R does not internalize following mycolactone application.

Desensitization of protein complexes is due to the binding of β -arrestins to the signaling proteins, notably GPCRs, inducing their internalization (Smith and Rajagopal, 2016). Previous works have reported that AT2R does not internalize following binding to AngII (Turu et al., 2006; Hein et al., 1997; Mukoyama et al., 1995). The internalization of AT2R induced by mycolactone was challenged by time-resolved FRET assays by the ARPEGE platform in Montpellier. Briefly, in this test, the receptor of interest carries a SNAP-tag and is labelled with terbium cryptate (donor). Addition of free acceptor in a μ M range leads to efficient energy transfer. Upon internalization of the receptor by exposure to an agonist, energy transfer is reduced and lifetime of the donor is increased (**Figure 31C**). HEK293T transfected cells with either SNAP-AT1R or SNAP-AT2R were challenged with their natural ligand, AngII, as control, and with mycolactone. AT1R, whose crystal structure reveals a binding pocket for β -

arrestin binding, (Zhang et al., 2015) was internalized in the presence of AngII, but not of mycolactone (**Figure 31D**). For AT2R, the ratio of emission of terbium cryptate (620 nm) to the acceptor (520 nm) revealed that receptor is not internalized upon addition of any of the ligands (**Figure 31E**). Therefore, AT2R does not internalize upon mycolactone binding, explaining the non-sensitization of the mycolactone effect. Interestingly, AT2R is not internalized by AngII incubation, which is well fitting with previous reports demonstrating its inability to bind β -arrestins (Turu et al., 2006; Hein et al., 1997; Mukoyama et al., 1995).

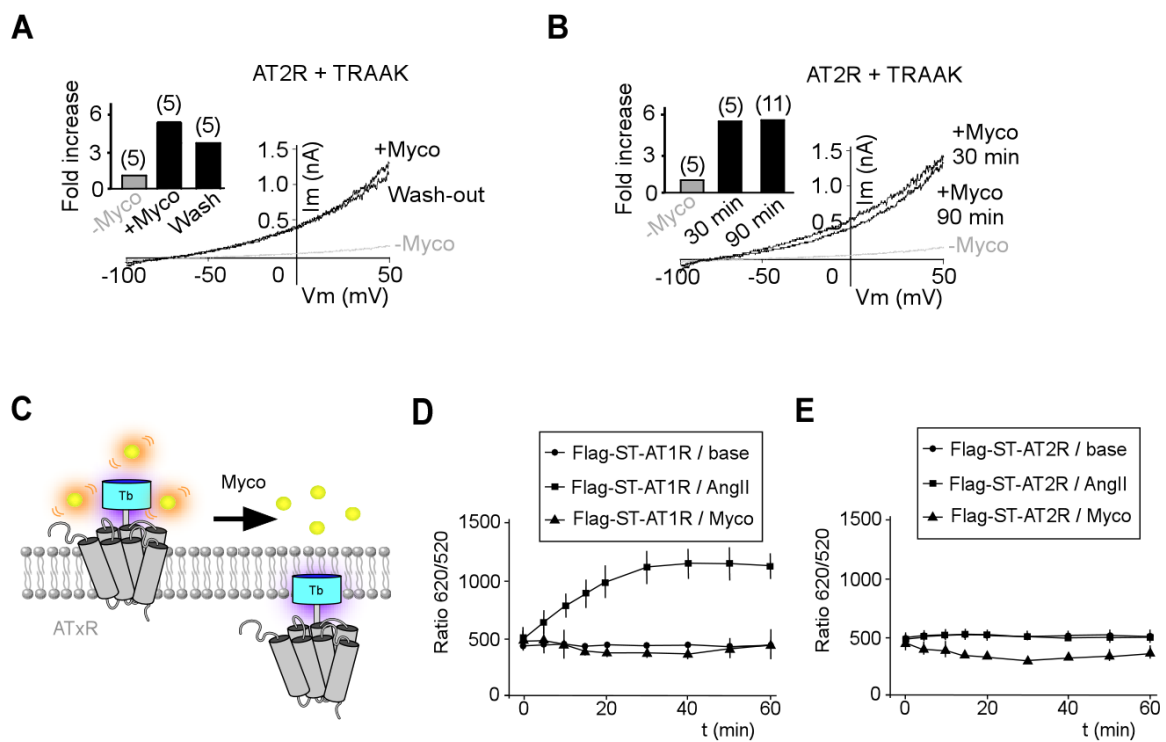


Figure 31. Mycolactone effect is sustained as it does not desensitize.

(A) Effect of short incubation (30 min) with mycolactone (10 μ M) and 4 h after washing-out. Currents were elicited by voltage-ramps (from -100 to +100 mV, 1s duration). Insets show current densities obtained at 0 mV. Man-Whitney test (**p < 0.01, ***p < 0.001). Mean \pm SEM. (B) Effect of short (30 min) and long (90 min) incubation with mycolactone (10 μ M). (C) Scheme of the principle of the time-resolved FRET assay. (D) Ratio 620/520 of SNAP-AT1R upon ligand addition (AngII, 10 μ M; mycolactone, 2 μ M). (E) Same as F, for SNAP-AT2R. Time-resolved FRET experiments were performed by the ARPEGE platform in Montpellier, France.

3. Mycolactone does not involve intracellular signaling messengers

Mycolactone-induced TRAAK activation does not involve G-proteins.

The crystal structure of AT2R exhibits an intracellular sterical blockage of the H.VIII on the G-protein recruitment domain of the receptor (Zhang et al., 2017a), which agrees with previous studies reporting a lack of G-protein signaling of AT2R (Dudley et al., 1991; Hayashida et al., 1996; de Gasparo et al., 2000). We therefore tested the role of G-protein in the AT2R-TRAAK signaling pathway activation by mycolactone. Firstly, HEK293T cells co-expressing AT2R and TRAAK were incubated 24 h with pertussis toxin (PTX) from *Bordetella pertussis*. PTX prevents coupling of $G\alpha_{i2,3}$ proteins in AT2R and thus, constitutes a good model for challenging G_i -proteins role in this signaling pathway (Kang et al., 1994; Sumners and Gelband, 1998). Cells treated with mycolactone and PTX exhibited an increased current density similar to the one observed in the absence of PTX (4.38 ± 0.68 pA/pF, 11.70 ± 1.49 pA/pF for non-treated and treated cells, respectively, $P < 0.081$), indicating that $G\alpha_{i2,3}$ proteins are not implicated (**Figure 32A**).

Secondly, BRET assays were performed in collaboration with the ARPEGE platform in Montpellier. Briefly, the different $G\alpha_{i/o}$ subunits were fused to *Renilla luciferase 8* (Rluc8, donor) and the $G\gamma$ subunit to Venus, a yellow fluorescent protein (acceptor). Activation of GPCRs promotes dissociation of the $G\alpha\beta\gamma$ complex, resulting in the BRET signal decay which is calculated by the ratio of emission of Venus (535 nm) to Rluc8 (480 nm) (**Figure 32B**). As positive control, HEK293T cells expressing the μ -opioid receptor (MOR) were treated with its agonist, the peptide DALDA. As expected, DALDA application induced a robust decrease of the BRET signal for a large set of G_i and G_o proteins, demonstrating the opioid receptor activation and validating the test. For the AT2R condition, no changes in the BRET signal were observed for any of the challenged G-proteins when cells expressed AT2R and were exposed to mycolactone (**Figure 32C**). This rules out the participation of G-proteins for TRAAK activation following mycolactone binding to AT2R.

Mycolactone does not involve intracellular signaling messengers.

Having found that G_i-proteins are not involved, participation of second soluble messengers was challenged. To test their potential involvement, we performed inside-out patches to isolate membrane proteins from cytosolic soluble messengers (**Figure 32D**). Whereas cells only expressing TRAAK were insensitive to mycolactone (**Figure 32E**; 22.39 ± 4.41 vs 28 ± 5.51 pA for cells non-exposed and exposed to mycolactone, respectively, $P < 0.45$), a strong current increase of the recorded current was observed in cells co-expressing TRAAK and AT2R (**Figure 32F**; 25.78 ± 4.24 vs 238.71 ± 89.07 pA for cells non-exposed and exposed to mycolactone, respectively, $P < 0.05$). This demonstrates that activation of the signaling pathway by mycolactone does not require intracellular soluble second messengers.

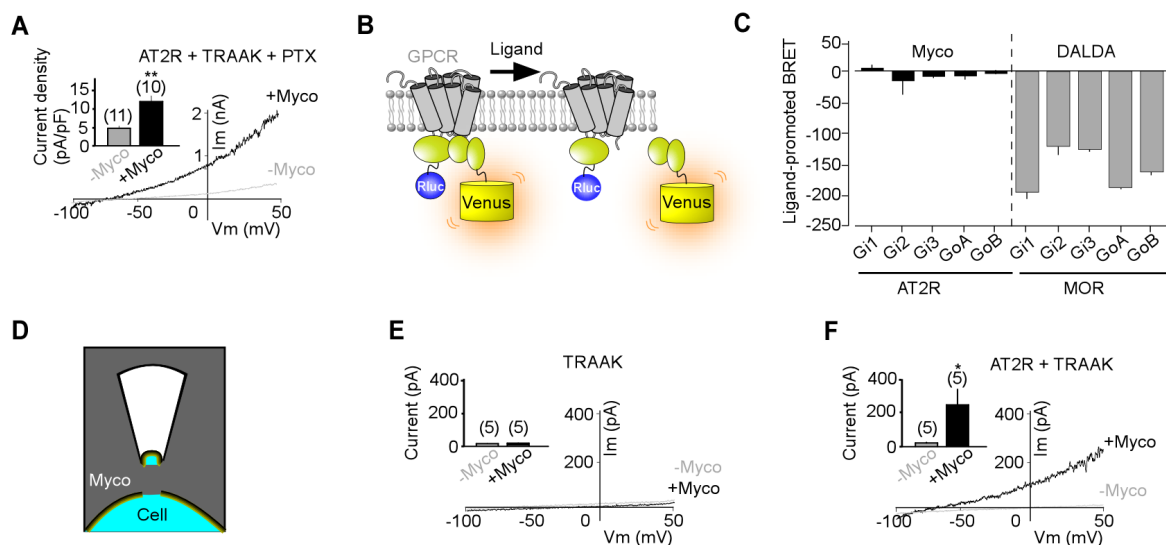


Figure 32. Activation by mycolactone is G-protein independent and does not involve soluble second messengers.

(A) Effect of mycolactone ($10 \mu\text{M}$) on HEK293T cells co-expressing AT2R and TRAAK and incubated with PTX ($0.5 \mu\text{g/mL}$). Currents were elicited by voltage-ramps (from -100 to $+100$ mV, 1 s duration). Insets show current densities obtained at 0 mV. Student's *t*-test (** $p < 0.01$). Mean \pm SEM. (B) Scheme of the BRET assay principle. (C) Ratio 535/480 of BRET signal for AT2R and MOR upon treatment with their respective ligands (mycolactone, $2 \mu\text{M}$; DALDA, 1 nM). (D) Principle of inside-out configuration of patch-clamp. (E) Representative inside-out recordings of HEK293T cells expressing TRAAK. (F) Representative inside-out recordings of HEK293T cells co-expressing TRAAK and AT2R. Currents were elicited by voltage-ramps (from -100 to $+100$ mV, 1 s duration). Insets show current densities obtained at 0 mV. Student's *t*-test (* $p < 0.05$). Mean \pm SEM. BRET experiments were performed by the ARPEGE platform in Montpellier, France.

4. *AT2R and TRAAK are coupled in membrane a micro-regulatory domain*

AT2R and TRAAK are in membrane a micro-regulatory domain.

Having found that TRAAK activation by mycolactone binding to AT2R does not require soluble messengers, we wondered if both proteins may be associated within the same micro-regulatory domain to be functionally coupled. To address this question, we used the cell-attached configuration of patch-clamp in cells co-expressing the two proteins. This configuration allows recording of channels solely confined inside the membrane patch. An increase of the current amplitude was only observed when mycolactone was inside the recording pipette (6.84 ± 1.09 pA vs 51.12 ± 7.31 pA, in the absence and in the presence of mycolactone, respectively, $P < 0.001$) but not when it was in the bath solution (6.84 ± 1.09 pA vs 7.70 ± 1.56 pA, in the absence and in the presence of mycolactone, respectively, $P > 0.66$) (**Figure 33A, B**). This demonstrates that only the channels which are in the vicinity of AT2R are activated upon mycolactone binding, suggesting that the signaling pathway is spatially restricted and that AT2R and TRAAK must be included within a common micro-regulatory domain.

AT2R and TRAAK are physically coupled

Then, the possible interaction between the two partners was studied. To demonstrate the physical coupling, we used the SiMPull assays previously described. Briefly, an AT2R construct carrying an N-terminal HA-tag and a TRAAK channel containing a C-terminal GFP were generated and transfected on HEK293T cells. 24 h after the transfection, the cells co-expressing both proteins were lysed and single complexes HA-AT2R-TRAAK-GFP were pulled down on glass coverslips using an anti-HA antibody and imaged with TIRF microscopy (**Figure 33C**). Visualization of GFP fluorescent spots, each one representing a single protein complex, confirmed the existence of TRAAK-AT2R complexes (**Figure 33D**). Negative control with TRAAK-GFP in the absence of a HA-tagged protein validates the specificity of the HA-antibody (**Figure 33E, F**).

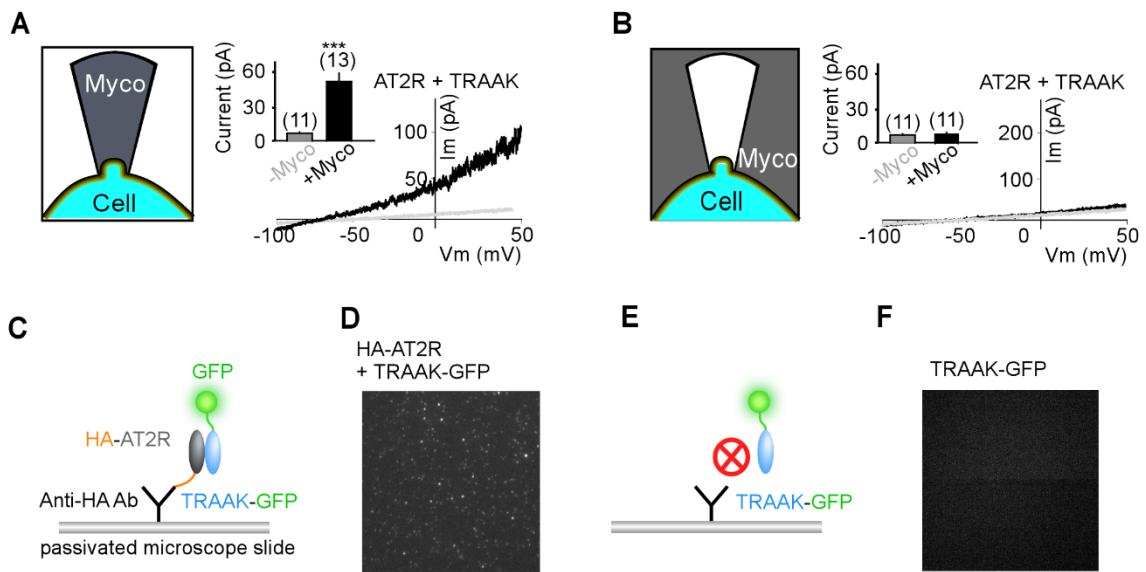


Figure 33. AT2R and TRAAK are physically coupled within a micro-regulatory membrane domain.

(A) Cell-attached recordings of HEK293T cells co-expressing AT2R and TRAAK with mycolactone ($10 \mu\text{M}$) in the pipette solution. (B) Cell-attached recordings of HEK293T cells co-expressing AT2R and TRAAK with mycolactone ($10 \mu\text{M}$) in the bath solution. (C) Schematic of SiMPull of TRAAK-GFP. HEK293T cells expressing TRAAK-GFP and an HA-tagged AT2R were lysed and then immobilized on a PEG-passivated coverslips conjugated to a biotinylated anti-HA antibody. (D) Representative TIRF image of single molecules complexes showing the pull-down of TRAAK-GFP by HA-AT2R. (E) SiMPull assay with TRAAK-GFP in the absence of HA-AT2R. (F) Absence of single molecule fluorescence, confirming the specificity of the anti-HA antibody.

5. Mycolactone activation is specific for AT2R and TRAAK

Once a direct functional and physical coupling between the channel and the receptor was found, the specificity of this unprecedented pathway was determined. In HEK293T cells, the effect of mycolactone was first compared on cells co-expressing TRAAK with either AT2R or AT1R. The two angiotensin receptors are known to counterbalance the effect of AngII, which is possibly due their very different regulation modes regarding to G-protein signaling (de Gasparo et al., 2000; Zhang et al., 2017a; Zhang et al., 2015). Whole-cell recordings showed that cells co-transfected with AT2R and TRAAK, exhibited a strong current increase when they were incubated with mycolactone (4.76 ± 0.42 pA/pF vs 21.75 ± 2.77 pA/pF for non-incubated and incubated, respectively, $P < 0.001$) (**Figure 34A**), whereas no increase of the current was observed in cells co-expressing AT1R and TRAAK (4.40 ± 0.52 pA/pF, 4.48 ± 0.66 pA/pF for non-incubated and incubated cells, respectively, $P = 0.13$) (**Figure 34B**), indicating specificity for AT2R.

Next, we tested cells co-expressing AT2R with TREK1, which belongs to the same K_{2P} subfamily as TRAAK and is also regulated by G-proteins (Noël et al., 2011). No current differences were observed between incubated and non-incubated cells (56.07 ± 8.86 pA/pF, 58.78 ± 5.94 pA/pF for non-incubated and incubated cells, respectively, $P = 0.8$) (**Figure 34C**). TRAAK and TREK1 can form heterodimers with intermediate properties from the original homodimers (Blin et al., 2016; Levitz et al., 2016). These heterodimers are particularly important for action potential propagation in Ranvier nodes (Kanda et al., 2019). For this reason, we also tested TRAAK-TREK1 but observed again no differences (94.71 ± 13.36 pA/pF, 97.99 ± 10.42 pA/pF before and after incubation, respectively, $P = 0.51$) (**Figure 34D**). These results discard the participation of heterodimers in the mycolactone-induced hyperpolarization of DRG neurons and suggest AT2R-TRAAK as a highly specific system.

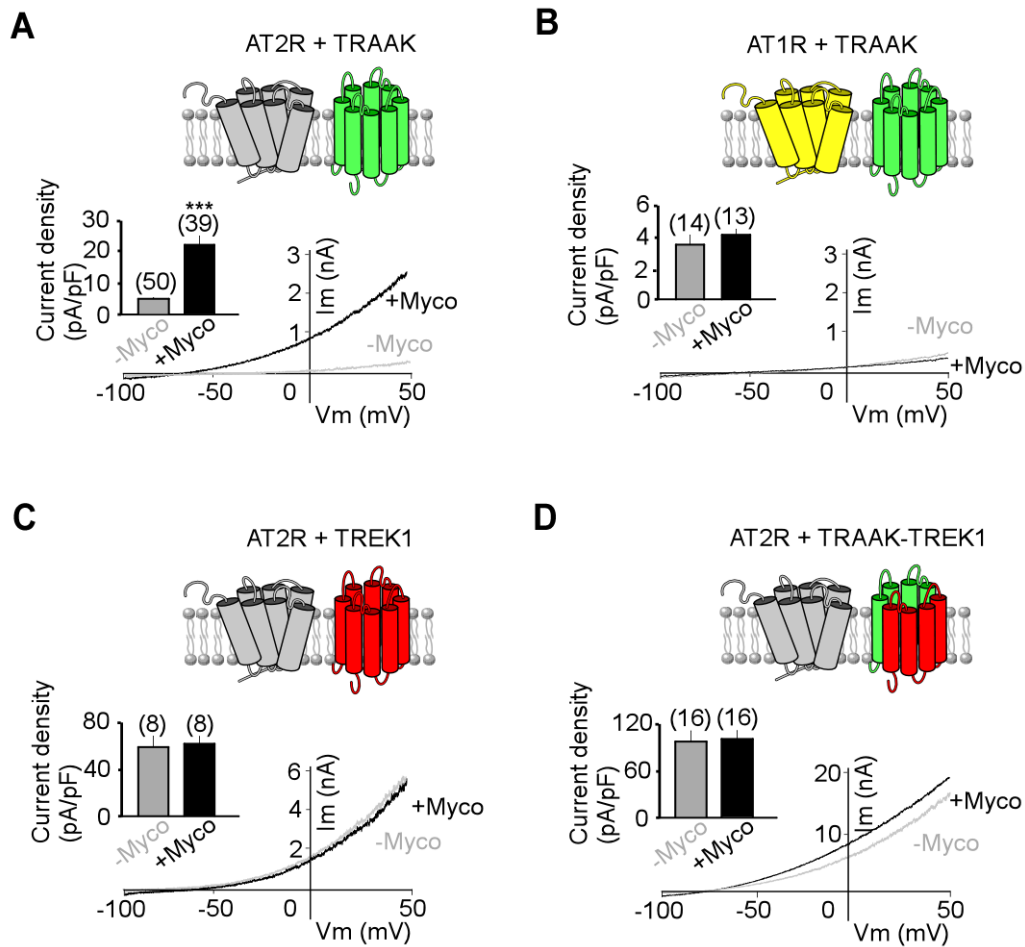


Figure 34. Activation by mycolactone is specific for AT2R and TRAAK.

(A-B) Representative traces obtained from HEK293T cells co-expressing TRAAK with either AT2R (A) or AT1R (B) before and after incubation with mycolactone (10 μ M). (C-D) Representative traces obtained from HEK293T cells co-expressing AT2R with either TREK1 (C) or TRAAK-TREK1 (D) before and after incubation with mycolactone. Currents were generated by voltage-ramps (from -100 to +100 mV, 1s duration). Insets show current densities obtained at 0 mV. Mean \pm SEM.

C. Discussion

1. Mycolactone induces hyperpolarization through TRAAK homomers

Buruli ulcer is a skin-related neglected tropical disease for which more than 2000 cases are reported every year, mainly affecting children under the age of 15 (Yotsu et al., 2018; Yotsu et al., 2015). This disease is characterized by a lack of inflammatory response upon tissue necrosis and pain suppression of the wound at early stages of the infection (Yotsu et al., 2018; Guenin-Macé et al., 2013; Hall et al., 2014; Marion et al., 2014). The mechanisms underlying analgesia in Buruli ulcer are matter of debate (Goto et al., 2006; En et al., 2008; Marion et al., 2014; Anand et al., 2016; En et al., 2017; Isaac et al., 2017; Song et al., 2017). The two different theories suggest either degeneration of sensory neurons (Goto et al., 2006) or their hyperpolarization induced by mycolactone (Marion et al., 2014). However, both theories are questioned, since nerve degeneration is only observed at late stages of the disease (Goto et al., 2006) when there is already painlessness, and AT2R seems not to bind G-proteins (Zhang et al., 2017), but one theory does not exclude the other one.

The present work addressed with heterologous models and *ex vivo* and *in vivo* experiments the molecular mechanism underlying the analgesia in Buruli ulcer, without addressing the problem of nerve degeneration that may occur on a longer time scale. Our study reports that binding of the disease causative toxin mycolactone to AT2R triggers the opening of TRAAK channels, resulting in hyperpolarization of sensory neurons as the origin of the analgesic effect. In line with this mechanism, *at2r*^{-/-} null mice have been reported to be insensitive to the analgesic mycolactone effects (Marion et al., 2014), and *at2r*^{-/-} DRG neurons do not hyperpolarize upon toxin incubation (Song et al., 2017). Nevertheless, sensory neurons and notably, DRG neurons, express a large set of distinct ion channels and receptors (Waxman and Zamponi, 2014; Noël et al., 2009), making it necessary to determine in what extent ion channels contribute to mycolactone-mediated hypoalgesia. This projects revisits the analgesia in Buruli ulcer and demonstrate an unprecedented highly coupling between TRAAK and AT2R which is not controlled by an exogenous ligand.

Using *traak*^{-/-} animals, we confirmed the pivotal role of TRAAK channels in sensory neuron silencing and analgesia produced by mycolactone. In fact, we have demonstrated that TRAAK is needed to induce hyperpolarization of DRG sensory neurons, silencing of C-fibers and analgesia in behaving mice. More specifically, by using a heterologous model, our results ruled out the participation of other K_{2P} channels, such as TREK1, which is G_i, G_s and G_q sensitive, and demonstrated a high specificity. In fact TRAAK-TREK1 heterodimers (Levitz et al., 2016), which are implicated in rapid axonal conduction of action potentials in Ranvier nodes are not sensitive to mycolactone (Kanda et al., 2019).

2. Mycolactone effect is G-protein independent and long-lasting due to the lack of AT2R desensitization

In agreement to Zhang and collaborators, our results demonstrate that AT2R does not act through G-protein signaling. In HEK293T cells, we found that the channel and receptor are directly coupled in a microregulatory domain and that there is no need of additional messengers to observe TRAAK activation. Such coupling was previously reported for TRPV1 and GABA_B receptors (Hanack et al., 2015). The originality of the AT2R-TRAAK coupling resides in the fact that it is not activated by the natural “endogenous” known receptor ligand (AngII) but by mycolactone which makes of the toxin an AT2R biased agonist. This result, together with prior examples, demonstrates that coupling between a channel and a receptor may be a frequent phenomenon in cell biology and suggests that an unknown endogenous ligand may exist, which would activate the TRAAK-AT2R pathway.

One important finding is also the long-lasting effect observed in the heterologous system, DRG neurons and *in vivo*, since the analgesic effects were observed 24 h after mycolactone injection (Babonneau et al., 2019). To determine how AT2R and TRAAK are coupled, we have reconstituted the system in HEK293T cells and used a series of electrophysiological and optical experiments. We found that the lack of sensitization is due to the non-internalization of AT2R. This non-internalization fits the model proposed recently by Zhang and *et al.*, in which β -arrestins cannot bind AT2R preventing the receptor from internalization following its ligand binding (Zhang et al., 2017a).

D. Conclusion

The discovery of a new analgesic mechanism linking AT2R and TRAAK may represent a new clinical strategy for pain management. Current pain treatment often requires continuous and increasing doses of opioids that frequently lead to adverse effects for individuals, including overdose and death (Ventafriidda et al., 1985; Rivat and Ballantyne, 2016). New non-toxic compounds based in the mycolactone's ability to specifically target the AT2R-TRAAK complex in nociceptors could overcome the tolerance problem, because of its long-lasting effect and non-desensitization of its target.

In summary, the present work shows two important findings concerning the analgesic effect of mycolactone and its mechanism of action. Firstly, TRAAK homodimer is required for suppression of pain induced by mycolactone, which alters notably temperature information by specifically decreasing excitability of small sensory neurons involved in pain perception. This painlessness is constant over the time notably by the lack of internalization of AT2R, who does not desensitize. This may represent a new promising way for the development of less addictive and more specific than opioids. Secondly, we have shown the specific crosstalk between TRAAK and AT2R, which obeys to a direct coupling between both proteins. Altogether, our results demonstrate a physical and functional coupling between a K_{2P} channel and an angiotensin receptor and its antalgic relevance in the nervous system.

The importance of membrane proteins is reflected on the wide range of functions that they mediate. These functions include transport of ions across the membrane that are transduced into a form usable for cell excitability or transmission of environmental signals to the interior of cells. The ability to conduct ions from one side to another of the membrane makes ion channels the main hubs for cell excitability.

This work shows two examples that demonstrate, that ion channels do not act alone, but work in fine tune with accessory proteins that change dramatically their function, causing a great impact on cell physiology. On one hand, the interaction between TMEM16A and its ancillary subunit KCNE1 turns this classical CaCC into a voltage-dependent Cl⁻ channel, questioning the historical ancillary subunit classification. On the other hand, the direct coupling between TRAAK and AT2R demonstrates that TRAAK and ion conduction is used to directly transmit an external signal to the interior of the cell while opening the doors for the development of new analgesics.

A. Molecular biology and cell culture

mTMEM16A (isoform a), hKCNE1 cDNA, mTRAAK, mTREK1, hAT2R and hAT1R were subcloned in pIRES2eGFP, pXOOM, pcDNA3.1, pCDNA3.1-GFP and pCMV-HA vectors. Truncations and mutations on clones were generated by standard PCR. For SiMPull experiments, HA-tags were fused to the N-terminus of sequences, whereas GFP-tags were fused to the C-terminus. AT2R and AT1R were fused to a SNAP-tag at their N-termini.

HEK293T and PCT cells were transiently co-transfected using Lipofectamine 2000 or the calcium phosphate method with a total amount of 1 and 3.5 μ g of DNA, respectively, and seeded on 18 mm diameter coverslips. HEK293T cells were maintained in DMEM with 5% FBS on poly-L-lysine-coated glass coverslips in 24 well plates. PCT cells from adult wild type and *kcne1*^{-/-} mice (129 SV/J) were micro-dissected as described previously (Vallon et al., 2001) and maintained in F12 supplemented medium on collagen-coated glass coverslips in 24 well plates. Lumbar DRG neurons were obtained from adult mice (C57BL/6), dissociated with 0.1 % collagenase, maintained in Neurobasal supplemented medium and plated on poly-D-lysine/laminine-coated glass coverslips in 24 well plates.

B. Electrophysiology of project 1

HEK293T and PCT cell electrophysiology was performed 24 – 48 h after transfection. For whole-cell patch-clamp experiments, cells were recorded in a bath solution containing (in mM) 150 NaCl, 5 KCl, 2 CaCl₂ and 10 HEPES, pH 7.4. The bath solution was supplemented with 0.05% BSA when the peptide N13ter was added. Glass pipettes (2-5 M Ω) were filled with (in mM) 5 NaCl, 135 CsCl, 2 MgCl₂, 5 EGTA, 10 HEPES, pH 7.3. For recordings of cells expressing SK4 the solutions were the same as in *Electrophysiology in Project 2* (see below). For anion permeability experiments, cells were recorded with a pipette solution containing (in mM) 144 CsCl and 10 HEPES. Bath solution (in mM) 140 Na_x, 2 MgCl₂ and 10 HEPES.

For an intracellular solution containing 10 μ M of free Ca²⁺, the intracellular solution was adjusted with 2 mM of MgCl₂ and 4.96 mM of CaCl₂. Total calcium concentration was calculated with Maxchelator (maxchelator.stanford.edu) for a temperature of 20°C. For inside-out recordings the extracellular (pipette) solution contained (in mM) 140 NaCl, 10 HEPES and 0.1 EGTA. The intracellular (bath) solution had the same composition as the pipette solutions for recordings in absence of Ca²⁺. A saturating Ca²⁺ solution (~20 μ M Ca²⁺) was made by adding 0.12 mM of CaCl₂ to the bath solution. Non-saturating solutions included (in mM) 1 EGTA and 0.59, 0.79, 0.89, 0.94 of CaCl₂ to obtain 0.1 μ M, 0.25 μ M, 0.5 μ M and 1 μ M free-Ca²⁺ solutions, respectively. The pH of inside-out solutions was adjusted to 7.4 with NaOH.

HEK293T and PCT cells were recorded at room temperature in voltage-clamp mode using an Axopatch 200A (Molecular Devices) amplifier. Signals were filtered at 10 kHz and digitalized at 20 kHz. Whole-cell currents were elicited by voltage-ramps (from -100 to +100 mV, 1 s) and I-V stimulation pulses (from -100 to +100 mV in 20 mV increments, 1 s each pulse), holding the cells at -80 mV. For inside-out recording the voltage was continuously clamped at +80 and -80 mV. Current densities were measured at +100 mV.

C. Electrophysiology of project 2

HEK293T cell electrophysiology was performed 24–72 h after transfection. For whole-cell patch-clamp experiments, cells were recorded in a bath solution containing (in mM) 145 NaCl, 4 KCl, 1 MgCl₂, 2 CaCl₂ and 10 HEPES. Glass pipettes (2–5 M Ω) were filled with (in mM) 140 KCl, 10 HEPES, 5 EGTA and 3 MgCl₂ (pH 7.4). For inside-out and cell-attached recordings, the bath solution corresponded to the pipette solution and viceversa. Currents were elicited by voltage-ramps (from -100 to +100 mV, 1 s) and I-V stimulation pulses (from -100 to +100 mV in 20 mV increments, 1 s each pulse), holding the cells at -80 mV. Current densities were measured at +100 mV.

Recordings of small and medium size DRG neurons were performed 24–72h after extraction. For whole-cell and current clamp recordings, cells were recorded in a bath solution containing (in mM): 140 NaCl, 5 KCl, 1 MgCl₂, 2 CaCl₂, 10 HEPES and 10 glucose. The pipette solution contained (in mM) 145 KCl, 2 MgCl₂, 1 CaCl₂, 10 EGTA and 5 HEPES (pH 7.3). The resting membrane potential was monitored using a current-clamp gap-free protocol and APs were induced using an incremental pulse protocol (from -25 to 300 pA in 25 pA increments, 1 s each pulse). All cell recordings, data acquisition and analysis of electrophysiology experiments of both projects were performed using pClamp software (Molecular Devices).

D. SiMPull assays

The SiMPull protocol was performed according to Jain and co-workers (Jain et al., 2012). Firstly, to construct the flow chambers, the slides and coverslips are thawed in the dark at room temperature for 10 min. A piece of double-sided tape was sandwiched between the slide and the coverslip, excluding a 5 mm channel where the inlet/outlet holes are located. The tape has to stick to both surfaces. The edges are sealed with epoxy glue and allowed to dry for 10 min. The volume of the flow channel is about 20 μ L.

Secondly, cells were previously co-transfected with an HA-tagged bait protein and a GFP-fused prey protein (applying the widely used eGFP A206K mutant which greatly reduces homo-dimerization events) (Zacharias et al., 2002). Cells were harvested from the coverslip using 500 μ L of PBS without Ca^{2+} during 35 min. Then, they were centrifuged for 2 min at 11000 rpm at 4°C and lysed in a buffer containing (in mM): 150 NaCl, 10 Tris pH 7.5, 1 EDTA, protease inhibitor cocktail (Thermo Scientific) and 1.5 % IGEPAL (Sigma). After 30-60 minute incubation at 4 °C, the lysate was centrifuged for 20 min at 16000 rpm and the supernatant was collected and kept at 4°C.

Lysates were collected and pulled-down on coverslips passivated with PEG (99 %) and biotin-PEG (1 %) and treated with neutravidin (1.4 mg/mL, Pierce) and a biotinylated anti-HA antibody (15 nM, abcam, #ab26228). Several washes with T50 buffer (in mM: 50 NaCl, 10 Tris, 20 EDTA; 0.1 mg/mL BSA, pH 7.5) were performed to avoid unspecific protein binding.

Finally, single molecule complexes were imaged using a 488 nm Argon laser in total internal reflection fluorescence microscopy with a 100x objective (Olympus). 13 x 13 μm^2 movies of 250 frames were acquired at frame rates of 10–30 Hz and analyzed using Fiji software (NIH). Multiple independent experiments were performed for each condition and only the spots which were fully bleached at the end of the illumination were considered. Representative data sets are presented to quantitatively compare the different conditions (minimum 15 movies per condition, at least 50 analyzed traces per movie).

E. Time-resolved FRET assays

HEK293T cells expressing SNAP-receptors were labeled with 100 nM of benzylguanine-terbium cryptate (BG-Tb) for 1 h at 37 °C in DMEM supplemented with 10 % FBS. After four washing steps with PBS, the fluorescence signal from BG-Tb was measured on an INFINITE F500 plate reader with an excitation at 337 nm and an emission at 620 nm.

F. BRET assays

24 h after transfection with receptors, HEK293T cells were washed twice with PBS and the reagents were added. For the basal condition, 5 μ M of coelenterazine H was added in the wells containing the cells, and for the test condition each ligand (DALDA 1 nM, mycolactone 2 μ M) was co-incubated with coelenterazine H. BRET between Rluc8 and Venus was measured after the addition of the Rluc8 substrate coelenterazine H (5 μ M). BRET readings were collected using a Mithras 2 plate reader. The BRET signal was then calculated by the ratio of emission of Venus (535 nm) to Rluc8 (480 nm).

G. Behavioral tests

Mycolactone (3.75 μ g), that does not induce tissular damages or inflammatory response, was injected subcutaneously into the right footpad of seven-week-old female mice (Charles River Laboratories, Saint-Germain-Nuelles, France). Pain receptivity was assessed by the Hargreaves method (Hargreaves et al., 1988), with a plantar test instrument (Ugo Basile, Gemonio, Italy). All animals were acclimatized to the apparatus for 15 min on at least three consecutive days before the experiment and for 10 min before each test. The response to an infrared stimulus focused on the right footpad was measured. The intensity of the stimulus was set at 35 % and a cut-off time of 30 s was applied to prevent the lesioning of mouse tissues by the stimulus. The time from the start of the stimulus to paw retraction (latency) was recorded automatically. The flicking/licking of the paw was confirmed by visual observation. Results were expressed as the ratio of the latencies of the response to a heat stimulus between mycolactone-treated groups and vehicle-treated groups 24 h after injection.

H. Nerve-skin experiments

Single C-fiber recording technique from the isolated skin-saphenous nerve preparation were used as described previously (Reeh, 1986; Noël et al., 2009). After euthanasia with CO₂, the hindpaw skin of 12 - 16 week-old male mouse was dissected with the saphenous nerve. The skin was pinned in a recording chamber superfused with warm (~30°C) synthetic interstitial fluid (SIF), in mM : 120 NaCl, 3.48 KCl, 5 NaHCO₃, 1.67 NaH₂PO₄, 2 CaCl₂, 0.69 MgSO₄, 9.64 Na-gluconate, 5.5 glucose, 7.6 sucrose, and 10 HEPES, pH adjusted to 7.4 with NaOH, saturated with O₂/CO₂—95%/5%. The receptive field of a C-fiber was searched by mechanical probing of the skin and further characterized for mechanosensitivity with calibrated von Frey filaments and conduction velocity with electrical stimulation. C-fibers were characterized with a conduction velocity below 1.3 m/s. C-fibers' receptive fields were isolated with a thick walled elrin ring inside which solutions were applied (internal volume of 400 µl) through local perfusion pipes of a CL-100 bipolar temperature controller (Warner instrument). Recordings with isolated DAM80 extracellular differential amplifier (WPI) were band-pass filtered between 60 Hz and 2 kHz and sampled at 10 kHz on computer with pClamp 10 software (Axon Instrument). Analysis of action-potentials was done off-line with Spike2 software (Cambridge Electronic Design). Spikes were detected with threshold crossing, set at twice the RMS noise, and single spike template analysis of Spike2 software. Each spike was visualized individually and false positive deleted. Data analysis was done with GraphPad Prism 4 for Wilcoxon signed rank test.

References

- Abbott GW (2016) KCNE1 and KCNE3: The yin and yang of voltage-gated K(+) channel regulation. *Gene* 576(1 Pt 1): 1-13.
- Abbott GW, Sesti F, Splawski I, et al. (1999) MiRP1 forms IKr potassium channels with HERG and is associated with cardiac arrhythmia. *Cell* 97(2): 175-187.
- Adelman JP (1995) Proteins that interact with the pore-forming subunits of voltage-gated ion channels. *Curr Opin Neurobiol* 5(3): 286-295.
- Anand U, Facer P, Yiangou Y, et al. (2013) Angiotensin II type 2 receptor (AT2 R) localization and antagonist-mediated inhibition of capsaicin responses and neurite outgrowth in human and rat sensory neurons. *Eur J Pain* 17(7): 1012-1026.
- Anand U, Sinisi M, Fox M, et al. (2016) Mycolactone-mediated neurite degeneration and functional effects in cultured human and rat DRG neurons: Mechanisms underlying hypoalgesia in Buruli ulcer. *Mol Pain* 12.
- Angelo K, Jespersen T, Grunnet M, et al. (2002) KCNE5 induces time- and voltage-dependent modulation of the KCNQ1 current. *Biophys J* 83(4): 1997-2006.
- Arikkath J and Campbell KP (2003) Auxiliary subunits: essential components of the voltage-gated calcium channel complex. *Curr Opin Neurobiol* 13(3): 298-307.
- Arrighi I, Bloch-Faure M, Grahammer F, et al. (2001) Altered potassium balance and aldosterone secretion in a mouse model of human congenital long QT syndrome. *Proc Natl Acad Sci U S A* 98(15): 8792-8797.
- Attali B, Guillemare E, Lesage F, et al. (1993) The protein IsK is a dual activator of K⁺ and Cl⁻ channels. *Nature* 365(6449): 850-852.
- Babonneau J, Bréard D, Reynaert ML, et al. (2019) Mycolactone as Analgesic: Subcutaneous Bioavailability Parameters. *Front Pharmacol* 10: 378.
- Bagriantsev SN, Ang KH, Gallardo-Godoy A, et al. (2013) A high-throughput functional screen identifies small molecule regulators of temperature- and mechano-sensitive K2P channels. *ACS Chem Biol* 8(8): 1841-1851.
- Baker M, Bostock H, Grafe P, et al. (1987) Function and distribution of three types of rectifying channel in rat spinal root myelinated axons. *J Physiol* 383: 45-67.
- Balderas E, Ateaga-Tlecuil R, Rivera M, et al. (2012) Niflumic acid blocks native and recombinant T-type channels. *J Cell Physiol* 227(6): 2542-2555.
- Barhanin J, Lesage F, Guillemare E, et al. (1996) K(V)LQT1 and IsK (minK) proteins associate to form the I(Ks) cardiac potassium current. *Nature* 384(6604): 78-80.
- Barrière H, Rubera I, Belfodil R, et al. (2003) Swelling-activated chloride and potassium conductance in primary cultures of mouse proximal tubules. Implication of KCNE1 protein. *J Membr Biol* 193(3): 153-170.

- Basbaum AI, Bautista DM, Scherrer G, et al. (2009) Cellular and molecular mechanisms of pain. *Cell* 139(2): 267-284.
- Ben-Efraim I, Shai Y and Attali B (1996) Cytoplasmic and extracellular IsK peptides activate endogenous K⁺ and Cl⁻ channels in *Xenopus* oocytes. Evidence for regulatory function. *J Biol Chem* 271(15): 8768-8771.
- Bendahhou S, Marionneau C, Haurogne K, et al. (2005) In vitro molecular interactions and distribution of KCNE family with KCNQ1 in the human heart. *Cardiovasc Res* 67(3): 529-538.
- Benedetto R, Ousingsawat J, Wanitchakool P, et al. (2017) Epithelial Chloride Transport by CFTR Requires TMEM16A. *Sci Rep* 7(1): 12397.
- Bethel NP and Grabe M (2016) Atomistic insight into lipid translocation by a TMEM16 scramblase. *Proc Natl Acad Sci U S A* 113(49): 14049-14054.
- Bianchi L, Shen Z, Dennis AT, et al. (1999) Cellular dysfunction of LQT5-minK mutants: abnormalities of IKs, IKr and trafficking in long QT syndrome. *Hum Mol Genet* 8(8): 1499-1507.
- Blin S, Ben Soussia I, Kim EJ, et al. (2016) Mixing and matching TREK/TRAAK subunits generate heterodimeric K₂P channels with unique properties. *Proc Natl Acad Sci U S A* 113(15): 4200-4205.
- Blin S, Chatelain FC, Feliciangeli S, et al. (2014) Tandem pore domain halothane-inhibited K⁺ channel subunits THIK1 and THIK2 assemble and form active channels. *J Biol Chem* 289(41): 28202-28212.
- Brackenbury WJ and Isom LL (2011) Na Channel β Subunits: Overachievers of the Ion Channel Family. *Front Pharmacol* 2: 53.
- Brohawn SG, Campbell EB and MacKinnon R (2014) Physical mechanism for gating and mechanosensitivity of the human TRAAK K⁺ channel. *Nature* 516(7529): 126-130.
- Brohawn SG, del Marmol J and MacKinnon R (2012) Crystal structure of the human K₂P TRAAK, a lipid- and mechano-sensitive K⁺ ion channel. *Science* 335(6067): 436-441.
- Brunner JD, Lim NK, Schenck S, et al. (2014) X-ray structure of a calcium-activated TMEM16 lipid scramblase. *Nature* 516(7530): 207-212.
- Brunner JD, Schenck S and Dutzler R (2016) Structural basis for phospholipid scrambling in the TMEM16 family. *Curr Opin Struct Biol* 39: 61-70.
- Bulley S, Neeb ZP, Burris SK, et al. (2012) TMEM16A/ANO1 channels contribute to the myogenic response in cerebral arteries. *Circ Res* 111(8): 1027-1036.
- Cannon SC (2007) Physiologic principles underlying ion channelopathies. *Neurotherapeutics* 4(2): 174-183.
- Cao YJ and Houamed KM (1999) Activation of recombinant human SK4 channels by metal cations. *FEBS Lett* 446(1): 137-141.

- Caputo A, Caci E, Ferrera L, et al. (2008) TMEM16A, a membrane protein associated with calcium-dependent chloride channel activity. *Science* 322(5901): 590-594.
- Chai R, Chen Y, Yuan H, et al. (2017) Identification of Resveratrol, an Herbal Compound, as an Activator of the Calcium-Activated Chloride Channel, TMEM16A. *J Membr Biol* 250(5): 483-492.
- Chakrabarty A, Blacklock A, Svojanovsky S, et al. (2008) Estrogen elicits dorsal root ganglion axon sprouting via a renin-angiotensin system. *Endocrinology* 149(7): 3452-3460.
- Chandrasekhar KD, Lvov A, Terrenoire C, et al. (2011) O-glycosylation of the cardiac I(Ks) complex. *J Physiol* 589(Pt 15): 3721-3730.
- Cho H, Yang YD, Lee J, et al. (2012) The calcium-activated chloride channel anoctamin 1 acts as a heat sensor in nociceptive neurons. *Nat Neurosci* 15(7): 1015-1021.
- Chun H, Cho H, Choi J, et al. (2015) Protons inhibit anoctamin 1 by competing with calcium. *Cell Calcium* 58(5): 431-441.
- Chung DY, Chan PJ, Bankston JR, et al. (2009) Location of KCNE1 relative to KCNQ1 in the I(KS) potassium channel by disulfide cross-linking of substituted cysteines. *Proc Natl Acad Sci U S A* 106(3): 743-748.
- Ciampa EJ, Welch RC, Vanoye CG, et al. (2011) KCNE4 juxtamembrane region is required for interaction with calmodulin and for functional suppression of KCNQ1. *J Biol Chem* 286(6): 4141-4149.
- CLANCEY JK, DODGE OG, LUNN HF, et al. (1961) Mycobacterial skin ulcers in Uganda. *Lancet* 2(7209): 951-954.
- Coetzee WA, Amarillo Y, Chiu J, et al. (1999) Molecular diversity of K⁺ channels. *Ann N Y Acad Sci* 868: 233-285.
- Coey AT, Sahu ID, Gunasekera TS, et al. (2011) Reconstitution of KCNE1 into lipid bilayers: comparing the structural, dynamic, and activity differences in micelle and vesicle environments. *Biochemistry* 50(50): 10851-10859.
- Cruikshank SF, Baxter LM and Drummond RM (2003) The Cl⁻ channel blocker niflumic acid releases Ca²⁺ from an intracellular store in rat pulmonary artery smooth muscle cells. *Br J Pharmacol* 140(8): 1442-1450.
- Crump SM and Abbott GW (2014) Arrhythmogenic KCNE gene variants: current knowledge and future challenges. *Front Genet* 5: 3.
- Dang S, Feng S, Tien J, et al. (2017) Cryo-EM structures of the TMEM16A calcium-activated chloride channel. *Nature* 552(7685): 426-429.
- Davis AJ, Shi J, Pritchard HA, et al. (2013) Potent vasorelaxant activity of the TMEM16A inhibitor T16A(inh)-A01. *Br J Pharmacol* 168(3): 773-784.
- de Gasparo M, Catt KJ, Inagami T, et al. (2000) International union of pharmacology. XXIII. The angiotensin II receptors. *Pharmacol Rev* 52(3): 415-472.

- De La Fuente R, Namkung W, Mills A, et al. (2008) Small-molecule screen identifies inhibitors of a human intestinal calcium-activated chloride channel. *Mol Pharmacol* 73(3): 758-768.
- Dixon JE, Shi W, Wang HS, et al. (1996) Role of the Kv4.3 K⁺ channel in ventricular muscle. A molecular correlate for the transient outward current. *Circ Res* 79(4): 659-668.
- Dolphin AC (2016) Voltage-gated calcium channels and their auxiliary subunits: physiology and pathophysiology and pharmacology. *J Physiol* 594(19): 5369-5390.
- Drici MD, Arrighi I, Chouabe C, et al. (1998) Involvement of Isk-associated K⁺ channel in heart rate control of repolarization in a murine engineered model of Jervell and Lange-Nielsen syndrome. *Circ Res* 83(1): 95-102.
- Duan D (2009) Phenomics of cardiac chloride channels: the systematic study of chloride channel function in the heart. *J Physiol* 587(Pt 10): 2163-2177.
- Dudley DT, Hubbell SE and Summerfelt RM (1991) Characterization of angiotensin II (AT₂) binding sites in R3T3 cells. *Mol Pharmacol* 40(3): 360-367.
- En J, Goto M, Nakanaga K, et al. (2008) Mycolactone is responsible for the painlessness of Mycobacterium ulcerans infection (buruli ulcer) in a murine study. *Infect Immun* 76(5): 2002-2007.
- En J, Kitamoto S, Kawashima A, et al. (2017) Mycolactone cytotoxicity in Schwann cells could explain nerve damage in Buruli ulcer. *PLoS Negl Trop Dis* 11(8): e0005834.
- Enyedi P and Czirják G (2010) Molecular background of leak K⁺ currents: two-pore domain potassium channels. *Physiol Rev* 90(2): 559-605.
- Falzone ME, Malvezzi M, Lee BC, et al. (2018) Known structures and unknown mechanisms of TMEM16 scramblases and channels. *J Gen Physiol* 150(7): 933-947.
- Faria D, Rock JR, Romao AM, et al. (2014) The calcium-activated chloride channel Anoctamin 1 contributes to the regulation of renal function. *Kidney Int* 85(6): 1369-1381.
- Fatini C, Sticchi E, Marcucci R, et al. (2010) S38G single-nucleotide polymorphism at the KCNE1 locus is associated with heart failure. *Heart Rhythm* 7(3): 363-367.
- Ferrera L, Caputo A, Ubbi I, et al. (2009) Regulation of TMEM16A chloride channel properties by alternative splicing. *J Biol Chem* 284(48): 33360-33368.
- Fink M, Lesage F, Duprat F, et al. (1998) A neuronal two P domain K⁺ channel stimulated by arachidonic acid and polyunsaturated fatty acids. *EMBO J* 17(12): 3297-3308.
- Fredriksson R, Lagerström MC, Lundin LG, et al. (2003) The G-protein-coupled receptors in the human genome form five main families. Phylogenetic analysis, paralogon groups, and fingerprints. *Mol Pharmacol* 63(6): 1256-1272.
- Furukawa T, Ono Y, Tsuchiya H, et al. (2001) Specific interaction of the potassium channel beta-subunit minK with the sarcomeric protein T-cap suggests a T-tubule-myofibril linking system. *J Mol Biol* 313(4): 775-784.

- George AL (2013) Molecular and genetic basis of sudden cardiac death. *J Clin Invest* 123(1): 75-83.
- George KM, Chatterjee D, Gunawardana G, et al. (1999) Mycolactone: a polyketide toxin from *Mycobacterium ulcerans* required for virulence. *Science* 283(5403): 854-857.
- Gofman Y, Shats S, Attali B, et al. (2012) How does KCNE1 regulate the Kv7.1 potassium channel? Model-structure, mutations, and dynamics of the Kv7.1-KCNE1 complex. *Structure* 20(8): 1343-1352.
- Goldstein SA and Miller C (1991) Site-specific mutations in a minimal voltage-dependent K⁺ channel alter ion selectivity and open-channel block. *Neuron* 7(3): 403-408.
- Goto M, Nakanaga K, Aung T, et al. (2006) Nerve damage in *Mycobacterium ulcerans*-infected mice: probable cause of painlessness in buruli ulcer. *Am J Pathol* 168(3): 805-811.
- Guarner J (2018) Buruli Ulcer: Review of a Neglected Skin Mycobacterial Disease. *J Clin Microbiol* 56(4).
- Guenin-Macé L, Baron L, Chany AC, et al. (2015) Shaping mycolactone for therapeutic use against inflammatory disorders. *Sci Transl Med* 7(289): 289ra285.
- Guenin-Macé L, Veyron-Churlet R, Thoulouze MI, et al. (2013) Mycolactone activation of Wiskott-Aldrich syndrome proteins underpins Buruli ulcer formation. *J Clin Invest* 123(4): 1501-1512.
- Guo S, Chen YF, Shi S, et al. (2020) The Molecular Mechanism of Ginsenoside Analogs Activating TMEM16A. *Biophys J* 118(1): 262-272.
- Gurnett CA and Campbell KP (1996) Transmembrane auxiliary subunits of voltage-dependent ion channels. *J Biol Chem* 271(45): 27975-27978.
- Gyobu S, Ishihara K, Suzuki J, et al. (2017) Characterization of the scrambling domain of the TMEM16 family. *Proc Natl Acad Sci U S A* 114(24): 6274-6279.
- Gyobu S, Miyata H, Ikawa M, et al. (2016) A Role of TMEM16E Carrying a Scrambling Domain in Sperm Motility. *Mol Cell Biol* 36(4): 645-659.
- Hall BS, Hill K, McKenna M, et al. (2014) The pathogenic mechanism of the *Mycobacterium ulcerans* virulence factor, mycolactone, depends on blockade of protein translocation into the ER. *PLoS Pathog* 10(4): e1004061.
- Hanack C, Moroni M, Lima WC, et al. (2015) GABA blocks pathological but not acute TRPV1 pain signals. *Cell* 160(4): 759-770.
- Hargreaves K, Dubner R, Brown F, et al. (1988) A new and sensitive method for measuring thermal nociception in cutaneous hyperalgesia. *Pain* 32(1): 77-88.
- Hartzell C, Putzier I and Arreola J (2005) Calcium-activated chloride channels. *Annu Rev Physiol* 67: 719-758.

- Hayashida W, Horiuchi M and Dzau VJ (1996) Intracellular third loop domain of angiotensin II type-2 receptor. Role in mediating signal transduction and cellular function. *J Biol Chem* 271(36): 21985-21992.
- Hein L, Meinel L, Pratt RE, et al. (1997) Intracellular trafficking of angiotensin II and its AT1 and AT2 receptors: evidence for selective sorting of receptor and ligand. *Mol Endocrinol* 11(9): 1266-1277.
- Huang F, Zhang H, Wu M, et al. (2012) Calcium-activated chloride channel TMEM16A modulates mucin secretion and airway smooth muscle contraction. *Proc Natl Acad Sci USA* 109(40): 16354-16359.
- Huang GK and Johnson PD (2014) Epidemiology and management of Buruli ulcer. *Expert Rev Anti Infect Ther* 12(7): 855-865.
- Ichiki T (2013) Regulation of angiotensin II receptor expression. *Curr Pharm Des* 19(17): 3013-3021.
- Isaac C, Mauborgne A, Grimaldi A, et al. (2017) Mycolactone displays anti-inflammatory effects on the nervous system. *PLoS Negl Trop Dis* 11(11): e0006058.
- Jain A, Liu R, Ramani B, et al. (2011) Probing cellular protein complexes using single-molecule pull-down. *Nature* 473(7348): 484-488.
- Jain A, Liu R, Xiang YK, et al. (2012) Single-molecule pull-down for studying protein interactions. *Nat Protoc* 7(3): 445-452.
- Jeng G, Aggarwal M, Yu WP, et al. (2016) Independent activation of distinct pores in dimeric TMEM16A channels. *J Gen Physiol* 148(5): 393-404.
- Jespersen T, Membrez M, Nicolas CS, et al. (2007) The KCNQ1 potassium channel is down-regulated by ubiquitylating enzymes of the Nedd4/Nedd4-like family. *Cardiovasc Res* 74(1): 64-74.
- Jiang M, Xu X, Wang Y, et al. (2009) Dynamic partnership between KCNQ1 and KCNE1 and influence on cardiac IKs current amplitude by KCNE2. *J Biol Chem* 284(24): 16452-16462.
- Jiang T, Yu K, Hartzell HC, et al. (2017) Lipids and ions traverse the membrane by the same physical pathway in the nhTMEM16 scramblase. *Elife* 6.
- Kanda H, Ling J, Tonomura S, et al. (2019) TREK-1 and TRAAK Are Principal K. *Neuron* 104(5): 960-971.e967.
- Kanda VA, Purtell K and Abbott GW (2011) Protein kinase C downregulates I(Ks) by stimulating KCNQ1-KCNE1 potassium channel endocytosis. *Heart Rhythm* 8(10): 1641-1647.
- Kang C, Tian C, Sönnichsen FD, et al. (2008) Structure of KCNE1 and implications for how it modulates the KCNQ1 potassium channel. *Biochemistry* 47(31): 7999-8006.

- Kang D, Choe C and Kim D (2005) Thermosensitivity of the two-pore domain K⁺ channels TREK-2 and TRAAK. *J Physiol* 564(Pt 1): 103-116.
- Kang J, Posner P and Summers C (1994) Angiotensin II type 2 receptor stimulation of neuronal K⁺ currents involves an inhibitory GTP binding protein. *Am J Physiol* 267(5 Pt 1): C1389-1397.
- Katoh M (2004) Identification and characterization of TMEM16E and TMEM16F genes in silico. *Int J Oncol* 24(5): 1345-1349.
- Ketchum KA, Joiner WJ, Sellers AJ, et al. (1995) A new family of outwardly rectifying potassium channel proteins with two pore domains in tandem. *Nature* 376(6542): 690-695.
- Kim Y, Chattopadhyay S, Locke S, et al. (2005) Interaction among Btn1p, Btn2p, and Ist2p reveals potential interplay among the vacuole, amino acid levels, and ion homeostasis in the yeast *Saccharomyces cerevisiae*. *Eukaryot Cell* 4(2): 281-288.
- Knollmann BC, Sirenko S, Rong Q, et al. (2007) Kcnq1 contributes to an adrenergic-sensitive steady-state K⁺ current in mouse heart. *Biochem Biophys Res Commun* 360(1): 212-218.
- Kress M, Koltzenburg M, Reeh PW, et al. (1992) Responsiveness and functional attributes of electrically localized terminals of cutaneous C-fibers in vivo and in vitro. *J Neurophysiol* 68(2): 581-595.
- Krumerman A, Gao X, Bian JS, et al. (2004) An LQT mutant minK alters KvLQT1 trafficking. *Am J Physiol Cell Physiol* 286(6): C1453-1463.
- Kurokawa J, Bankston JR, Kaihara A, et al. (2009) KCNE variants reveal a critical role of the beta subunit carboxyl terminus in PKA-dependent regulation of the IKs potassium channel. *Channels (Austin)* 3(1): 16-24.
- Kuruma A and Hartzell HC (2000) Bimodal control of a Ca²⁺-activated Cl⁻ channel by different Ca²⁺ signals. *J Gen Physiol* 115(1): 59-80.
- Lai LP, Su MJ, Yeh HM, et al. (2002) Association of the human minK gene 38G allele with atrial fibrillation: evidence of possible genetic control on the pathogenesis of atrial fibrillation. *Am Heart J* 144(3): 485-490.
- Le SC, Jia Z, Chen J, et al. (2019) Molecular basis of PIP. *Nat Commun* 10(1): 3769.
- Lee BC, Khelashvili G, Falzone M, et al. (2018) Gating mechanism of the extracellular entry to the lipid pathway in a TMEM16 scramblase. *Nat Commun* 9(1): 3251.
- Lesage F, Guillemare E, Fink M, et al. (1996) TWIK-1, a ubiquitous human weakly inward rectifying K⁺ channel with a novel structure. *EMBO J* 15(5): 1004-1011.
- Lesage F and Lazdunski M (2000) Molecular and functional properties of two-pore-domain potassium channels. *Am J Physiol Renal Physiol* 279(5): F793-801.

- Levitz J, Royal P, Comoglio Y, et al. (2016) Heterodimerization within the TREK channel subfamily produces a diverse family of highly regulated potassium channels. *Proc Natl Acad Sci U S A* 113(15): 4194-4199.
- Li YY, Wang LS and Lu XZ (2014) Mink S38G gene polymorphism and atrial fibrillation in the Chinese population: a meta-analysis of 1871 participants. *ScientificWorldJournal* 2014: 768681.
- Lim NK, Lam AK and Dutzler R (2016) Independent activation of ion conduction pores in the double-barreled calcium-activated chloride channel TMEM16A. *J Gen Physiol* 148(5): 375-392.
- Lundquist AL, Manderfield LJ, Vanoye CG, et al. (2005) Expression of multiple KCNE genes in human heart may enable variable modulation of I(Ks). *J Mol Cell Cardiol* 38(2): 277-287.
- MacCULLUM P (1948) A new mycobacterial infection in man; clinical aspects. *J Pathol Bacteriol* 60(1): 93-102.
- Maingret F, Fosset M, Lesage F, et al. (1999) TRAAK is a mammalian neuronal mechano-gated K⁺ channel. *J Biol Chem* 274(3): 1381-1387.
- Malvezzi M, Chalal M, Janjusevic R, et al. (2013) Ca²⁺-dependent phospholipid scrambling by a reconstituted TMEM16 ion channel. *Nat Commun* 4: 2367.
- Marion E, Song OR, Christophe T, et al. (2014) Mycobacterial toxin induces analgesia in buruli ulcer by targeting the angiotensin pathways. *Cell* 157(7): 1565-1576.
- Marionneau C, Carrasquillo Y, Norris AJ, et al. (2012) The sodium channel accessory subunit Navβ1 regulates neuronal excitability through modulation of repolarizing voltage-gated K⁺ channels. *J Neurosci* 32(17): 5716-5727.
- McCarthy CA, Vinh A, Broughton BR, et al. (2012) Angiotensin II type 2 receptor stimulation initiated after stroke causes neuroprotection in conscious rats. *Hypertension* 60(6): 1531-1537.
- McCrossan ZA and Abbott GW (2004) The MinK-related peptides. *Neuropharmacology* 47(6): 787-821.
- McDonald TV, Yu Z, Ming Z, et al. (1997) A minK-HERG complex regulates the cardiac potassium current I(Kr). *Nature* 388(6639): 289-292.
- Medhurst AD, Rennie G, Chapman CG, et al. (2001) Distribution analysis of human two pore domain potassium channels in tissues of the central nervous system and periphery. *Brain Res Mol Brain Res* 86(1-2): 101-114.
- Milenkovic VM, Brockmann M, Stöhr H, et al. (2010) Evolution and functional divergence of the anoctamin family of membrane proteins. *BMC Evol Biol* 10: 319.
- Moran Y, Barzilai MG, Liebeskind BJ, et al. (2015) Evolution of voltage-gated ion channels at the emergence of Metazoa. *J Exp Biol* 218(Pt 4): 515-525.

- Morin TJ and Kobertz WR (2008) Counting membrane-embedded KCNE beta-subunits in functioning K⁺ channel complexes. *Proc Natl Acad Sci U S A* 105(5): 1478-1482.
- Moss AJ and Kass RS (2005) Long QT syndrome: from channels to cardiac arrhythmias. *J Clin Invest* 115(8): 2018-2024.
- Mukoyama M, Horiuchi M, Nakajima M, et al. (1995) Characterization of a rat type 2 angiotensin II receptor stably expressed in 293 cells. *Mol Cell Endocrinol* 112(1): 61-68.
- Murray CI, Westhoff M, Eldstrom J, et al. (2016) Unnatural amino acid photo-crosslinking of the IKs channel complex demonstrates a KCNE1:KCNQ1 stoichiometry of up to 4:4. *Elife* 5.
- Nakajo K and Kubo Y (2014) Steric hindrance between S4 and S5 of the KCNQ1/KCNE1 channel hampers pore opening. *Nat Commun* 5: 4100.
- Nakajo K, Ulbrich MH, Kubo Y, et al. (2010) Stoichiometry of the KCNQ1 - KCNE1 ion channel complex. *Proc Natl Acad Sci U S A* 107(44): 18862-18867.
- Namkung W, Phuan PW and Verkman AS (2011) TMEM16A inhibitors reveal TMEM16A as a minor component of calcium-activated chloride channel conductance in airway and intestinal epithelial cells. *J Biol Chem* 286(3): 2365-2374.
- Nguyen HM, Miyazaki H, Hoshi N, et al. (2012) Modulation of voltage-gated K⁺ channels by the sodium channel β 1 subunit. *Proc Natl Acad Sci U S A* 109(45): 18577-18582.
- Noël J, Sandoz G and Lesage F (2011) Molecular regulations governing TREK and TRAAK channel functions. *Channels (Austin)* 5(5): 402-409.
- Noël J, Zimmermann K, Busserolles J, et al. (2009) The mechano-activated K⁺ channels TRAAK and TREK-1 control both warm and cold perception. *EMBO J* 28(9): 1308-1318.
- Patil J, Schwab A, Nussberger J, et al. (2010) Intraneuronal angiotensinergic system in rat and human dorsal root ganglia. *Regul Pept* 162(1-3): 90-98.
- Paul M, Poyan Mehr A and Kreutz R (2006) Physiology of local renin-angiotensin systems. *Physiol Rev* 86(3): 747-803.
- Paulino C, Kalienkova V, Lam AKM, et al. (2017a) Activation mechanism of the calcium-activated chloride channel TMEM16A revealed by cryo-EM. *Nature* 552(7685): 421-425.
- Paulino C, Neldner Y, Lam AK, et al. (2017b) Structural basis for anion conduction in the calcium-activated chloride channel TMEM16A. *Elife* 6.
- Pedemonte N and Galiotta LJ (2014) Structure and function of TMEM16 proteins (anoctamins). *Physiol Rev* 94(2): 419-459.
- Pelz T, Drose DR, Fleck D, et al. (2018) An ancestral TMEM16 homolog from Dictyostelium discoideum forms a scramblase. *PLoS One* 13(2): e0191219.

- Perez-Cornejo P, De Santiago JA and Arreola J (2004) Permeant anions control gating of calcium-dependent chloride channels. *J Membr Biol* 198(3): 125-133.
- Peters CJ, Gilchrist JM, Tien J, et al. (2018) The Sixth Transmembrane Segment Is a Major Gating Component of the TMEM16A Calcium-Activated Chloride Channel. *Neuron* 97(5): 1063-1077.e1064.
- Peters CJ, Yu H, Tien J, et al. (2015) Four basic residues critical for the ion selectivity and pore blocker sensitivity of TMEM16A calcium-activated chloride channels. *Proc Natl Acad Sci U S A* 112(11): 3547-3552.
- Piccini M, Vitelli F, Seri M, et al. (1999) KCNE1-like gene is deleted in AMME contiguous gene syndrome: identification and characterization of the human and mouse homologs. *Genomics* 60(3): 251-257.
- Plant LD, Xiong D, Dai H, et al. (2014) Individual IKs channels at the surface of mammalian cells contain two KCNE1 accessory subunits. *Proc Natl Acad Sci U S A* 111(14): E1438-1446.
- Pongs O and Schwarz JR (2010) Ancillary subunits associated with voltage-dependent K⁺ channels. *Physiol Rev* 90(2): 755-796.
- Poronnik P, Ward MC and Cook DI (1992) Intracellular Ca²⁺ release by flufenamic acid and other blockers of the non-selective cation channel. *FEBS Lett* 296(3): 245-248.
- Porrello ER, Delbridge LM and Thomas WG (2009) The angiotensin II type 2 (AT2) receptor: an enigmatic seven transmembrane receptor. *Front Biosci (Landmark Ed)* 14: 958-972.
- Portaels F, Meyers WM, Ablordey A, et al. (2008) First cultivation and characterization of *Mycobacterium ulcerans* from the environment. *PLoS Negl Trop Dis* 2(3): e178.
- Qin N, Olcese R, Bransby M, et al. (1999) Ca²⁺-induced inhibition of the cardiac Ca²⁺ channel depends on calmodulin. *Proc Natl Acad Sci U S A* 96(5): 2435-2438.
- Reeh PW (1986) Sensory receptors in mammalian skin in an in vitro preparation. *Neurosci Lett* 66(2): 141-146.
- Rivat C and Ballantyne J (2016) The dark side of opioids in pain management: basic science explains clinical observation. *Pain Rep* 1(2): e570.
- Ross BC, Marino L, Oppedisano F, et al. (1997) Development of a PCR assay for rapid diagnosis of *Mycobacterium ulcerans* infection. *J Clin Microbiol* 35(7): 1696-1700.
- Roura-Ferrer M, Etxebarria A, Solé L, et al. (2009) Functional implications of KCNE subunit expression for the Kv7.5 (KCNQ5) channel. *Cell Physiol Biochem* 24(5-6): 325-334.
- Royal P, Andres-Bilbe A, Ávalos Prado P, et al. (2019a) Migraine-Associated TRESK Mutations Increase Neuronal Excitability through Alternative Translation Initiation and Inhibition of TREK. *Neuron* 101(2): 232-245.e236.
- Royal P, Ávalos Prado P, Wdziekonski B, et al. (2019b) [Two-pore-domain potassium channels and molecular mechanisms underlying migraine]. *Biol Aujourdhui* 213(1-2): 51-57.

- Rubera I, Tauc M, Bidet M, et al. (1998) Chloride currents in primary cultures of rabbit proximal and distal convoluted tubules. *Am J Physiol* 275(5): F651-663.
- Ruscic KJ, Miceli F, Villalba-Galea CA, et al. (2013) IKs channels open slowly because KCNE1 accessory subunits slow the movement of S4 voltage sensors in KCNQ1 pore-forming subunits. *Proc Natl Acad Sci U S A* 110(7): E559-566.
- Sakya SA, Aboagye SY, Darko Otchere I, et al. (2016) Clinical and Laboratory Diagnosis of Buruli Ulcer Disease: A Systematic Review. *Can J Infect Dis Med Microbiol* 2016: 5310718.
- Sala-Rabanal M, Yurtsever Z, Berry KN, et al. (2017) Modulation of TMEM16A channel activity by the von Willebrand factor type A (VWA) domain of the calcium-activated chloride channel regulator 1 (CLCA1). *J Biol Chem* 292(22): 9164-9174.
- Sala-Rabanal M, Yurtsever Z, Nichols CG, et al. (2015) Secreted CLCA1 modulates TMEM16A to activate Ca(2+)-dependent chloride currents in human cells. *Elife* 4.
- Sandoz G, Douguet D, Chatelain F, et al. (2009) Extracellular acidification exerts opposite actions on TREK1 and TREK2 potassium channels via a single conserved histidine residue. *Proc Natl Acad Sci U S A* 106(34): 14628-14633.
- Sanguinetti MC, Curran ME, Zou A, et al. (1996) Coassembly of K(V)LQT1 and minK (IsK) proteins to form cardiac I(Ks) potassium channel. *Nature* 384(6604): 80-83.
- Sanguinetti MC, Jiang C, Curran ME, et al. (1995) A mechanistic link between an inherited and an acquired cardiac arrhythmia: HERG encodes the IKr potassium channel. *Cell* 81(2): 299-307.
- Sarfo FS, Phillips R, Wansbrough-Jones M, et al. (2016) Recent advances: role of mycolactone in the pathogenesis and monitoring of Mycobacterium ulcerans infection/Buruli ulcer disease. *Cell Microbiol* 18(1): 17-29.
- Scherr N, Bieri R, Thomas SS, et al. (2018) Targeting the Mycobacterium ulcerans cytochrome bc. *Nat Commun* 9(1): 5370.
- Schroeder BC, Cheng T, Jan YN, et al. (2008) Expression cloning of TMEM16A as a calcium-activated chloride channel subunit. *Cell* 134(6): 1019-1029.
- Schroeder BC, Waldegger S, Fehr S, et al. (2000) A constitutively open potassium channel formed by KCNQ1 and KCNE3. *Nature* 403(6766): 196-199.
- Seebom G, Strutz-Seebom N, Birkin R, et al. (2007) Regulation of endocytic recycling of KCNQ1/KCNE1 potassium channels. *Circ Res* 100(5): 686-692.
- Seo Y, Lee HK, Park J, et al. (2016) cAni9, A Novel Potent Small-Molecule ANO1 Inhibitor with Negligible Effect on ANO2. *PLoS One* 11(5): e0155771.
- Smith JS and Rajagopal S (2016) The β -Arrestins: Multifunctional Regulators of G Protein-coupled Receptors. *J Biol Chem* 291(17): 8969-8977.

- Smith MT, Anand P and Rice AS (2016) Selective small molecule angiotensin II type 2 receptor antagonists for neuropathic pain: preclinical and clinical studies. *Pain* 157 Suppl 1: S33-41.
- Smith MT, Woodruff TM, Wyse BD, et al. (2013) A small molecule angiotensin II type 2 receptor (AT₂R) antagonist produces analgesia in a rat model of neuropathic pain by inhibition of p38 mitogen-activated protein kinase (MAPK) and p44/p42 MAPK activation in the dorsal root ganglia. *Pain Med* 14(10): 1557-1568.
- Sondo E, Scudieri P, Tomati V, et al. (2014) Non-canonical translation start sites in the TMEM16A chloride channel. *Biochim Biophys Acta* 1838(1 Pt B): 89-97.
- Sones WR, Davis AJ, Leblanc N, et al. (2010) Cholesterol depletion alters amplitude and pharmacology of vascular calcium-activated chloride channels. *Cardiovasc Res* 87(3): 476-484.
- Song OR, Kim HB, Jouny S, et al. (2017) A Bacterial Toxin with Analgesic Properties: Hyperpolarization of DRG Neurons by Mycolactone. *Toxins (Basel)* 9(7).
- Splawski I, Shen J, Timothy KW, et al. (2000) Spectrum of mutations in long-QT syndrome genes. KVLQT1, HERG, SCN5A, KCNE1, and KCNE2. *Circulation* 102(10): 1178-1185.
- Stattin EL, Boström IM, Winbo A, et al. (2012) Founder mutations characterise the mutation panorama in 200 Swedish index cases referred for Long QT syndrome genetic testing. *BMC Cardiovasc Disord* 12: 95.
- Strutz-Seebohm N, Seebohm G, Fedorenko O, et al. (2006) Functional coassembly of KCNQ4 with KCNE-beta- subunits in *Xenopus* oocytes. *Cell Physiol Biochem* 18(1-3): 57-66.
- Sumners C and Gelband CH (1998) Neuronal ion channel signalling pathways: modulation by angiotensin II. *Cell Signal* 10(5): 303-311.
- Suzuki J, Fujii T, Imao T, et al. (2013) Calcium-dependent phospholipid scramblase activity of TMEM16 protein family members. *J Biol Chem* 288(19): 13305-13316.
- Suzuki J, Matsubara H, Urakami M, et al. (1993) Rat angiotensin II (type 1A) receptor mRNA regulation and subtype expression in myocardial growth and hypertrophy. *Circ Res* 73(3): 439-447.
- Takumi T, Ohkubo H and Nakanishi S (1988) Cloning of a membrane protein that induces a slow voltage-gated potassium current. *Science* 242(4881): 1042-1045.
- Tapper AR and George AL (2000) MinK subdomains that mediate modulation of and association with KvLQT1. *J Gen Physiol* 116(3): 379-390.
- Tauc M, Le Maout S and Poujeol P (1990) Fluorescent video-microscopy study of regulatory volume decrease in primary culture of rabbit proximal convoluted tubule. *Biochim Biophys Acta* 1052(2): 278-284.
- Thompson E, Eldstrom J, Westhoff M, et al. (2018) The I. *Biophys J* 115(9): 1731-1740.

- Tian Y, Kongsuphol P, Hug M, et al. (2011) Calmodulin-dependent activation of the epithelial calcium-dependent chloride channel TMEM16A. *FASEB J* 25(3): 1058-1068.
- Tien J, Peters CJ, Wong XM, et al. (2014) A comprehensive search for calcium binding sites critical for TMEM16A calcium-activated chloride channel activity. *Elife* 3.
- Tinel N, Diochot S, Borsotto M, et al. (2000) KCNE2 confers background current characteristics to the cardiac KCNQ1 potassium channel. *EMBO J* 19(23): 6326-6330.
- Trimmer JS (1998) Regulation of ion channel expression by cytoplasmic subunits. *Curr Opin Neurobiol* 8(3): 370-374.
- Turu G, Szidonya L, Gáborik Z, et al. (2006) Differential beta-arrestin binding of AT1 and AT2 angiotensin receptors. *FEBS Lett* 580(1): 41-45.
- Ulbrich MH and Isacoff EY (2007) Subunit counting in membrane-bound proteins. *Nat Methods* 4(4): 319-321.
- Vallon V, Grahammer F, Richter K, et al. (2001) Role of KCNE1-dependent K⁺ fluxes in mouse proximal tubule. *J Am Soc Nephrol* 12(10): 2003-2011.
- van Kesteren CA, van Heugten HA, Lamers JM, et al. (1997) Angiotensin II-mediated growth and antigrowth effects in cultured neonatal rat cardiac myocytes and fibroblasts. *J Mol Cell Cardiol* 29(8): 2147-2157.
- Vanoye CG, Welch RC, Tian C, et al. (2010) KCNQ1/KCNE1 assembly, co-translation not required. *Channels (Austin)* 4(2): 108-114.
- Venkatakrishnan AJ, Deupi X, Lebon G, et al. (2016) Diverse activation pathways in class A GPCRs converge near the G-protein-coupling region. *Nature* 536(7617): 484-487.
- Venkatakrishnan AJ, Deupi X, Lebon G, et al. (2013) Molecular signatures of G-protein-coupled receptors. *Nature* 494(7436): 185-194.
- Ventafriida V, Saita L, Ripamonti C, et al. (1985) WHO guidelines for the use of analgesics in cancer pain. *Int J Tissue React* 7(1): 93-96.
- Vetter DE, Mann JR, Wangemann P, et al. (1996) Inner ear defects induced by null mutation of the *isk* gene. *Neuron* 17(6): 1251-1264.
- Wang KW and Goldstein SA (1995) Subunit composition of minK potassium channels. *Neuron* 14(6): 1303-1309.
- Warth R, Garcia Alzamora M, Kim JK, et al. (2002) The role of KCNQ1/KCNE1 K(+) channels in intestine and pancreas: lessons from the KCNE1 knockout mouse. *Pflugers Arch* 443(5-6): 822-828.
- Waxman SG and Zamponi GW (2014) Regulating excitability of peripheral afferents: emerging ion channel targets. *Nat Neurosci* 17(2): 153-163.
- Westenskow P, Splawski I, Timothy KW, et al. (2004) Compound mutations: a common cause of severe long-QT syndrome. *Circulation* 109(15): 1834-1841.

- Williams JT, Ingram SL, Henderson G, et al. (2013) Regulation of μ -opioid receptors: desensitization, phosphorylation, internalization, and tolerance. *Pharmacol Rev* 65(1): 223-254.
- Wolf W, Meese K and Seedorf M (2014) Ist2 in the yeast cortical endoplasmic reticulum promotes trafficking of the amino acid transporter Bap2 to the plasma membrane. *PLoS One* 9(1): e85418.
- Xiao Q and Cui Y (2014) Acidic amino acids in the first intracellular loop contribute to voltage- and calcium- dependent gating of anoctamin1/TMEM16A. *PLoS One* 9(6): e99376.
- Xiao Q, Yu K, Perez-Cornejo P, et al. (2011) Voltage- and calcium-dependent gating of TMEM16A/Ano1 chloride channels are physically coupled by the first intracellular loop. *Proc Natl Acad Sci U S A* 108(21): 8891-8896.
- Xu X, Jiang M, Hsu KL, et al. (2008) KCNQ1 and KCNE1 in the IKs channel complex make state-dependent contacts in their extracellular domains. *J Gen Physiol* 131(6): 589-603.
- Xu X, Kanda VA, Choi E, et al. (2009) MinK-dependent internalization of the IKs potassium channel. *Cardiovasc Res* 82(3): 430-438.
- Yang YD, Cho H, Koo JY, et al. (2008) TMEM16A confers receptor-activated calcium-dependent chloride conductance. *Nature* 455(7217): 1210-1215.
- Yao H, Ji CC, Cheng YJ, et al. (2018) Mutation in KCNE1 associated to early repolarization syndrome by modulation of slowly activating delayed rectifier K. *Exp Cell Res* 363(2): 315-320.
- Yotsu RR, Murase C, Sugawara M, et al. (2015) Revisiting Buruli ulcer. *J Dermatol* 42(11): 1033-1041.
- Yotsu RR, Suzuki K, Simmonds RE, et al. (2018) Buruli Ulcer: a Review of the Current Knowledge. *Curr Trop Med Rep* 5(4): 247-256.
- Yu K, Whitlock JM, Lee K, et al. (2015) Identification of a lipid scrambling domain in ANO6/TMEM16F. *Elife* 4: e06901.
- Yu K, Zhu J, Qu Z, et al. (2014) Activation of the Ano1 (TMEM16A) chloride channel by calcium is not mediated by calmodulin. *J Gen Physiol* 143(2): 253-267.
- Zacharias DA, Violin JD, Newton AC, et al. (2002) Partitioning of lipid-modified monomeric GFPs into membrane microdomains of live cells. *Science* 296(5569): 913-916.
- Zhang H, Han GW, Batyuk A, et al. (2017a) Structural basis for selectivity and diversity in angiotensin II receptors. *Nature* 544(7650): 327-332.
- Zhang H, Unal H, Gati C, et al. (2015) Structure of the Angiotensin receptor revealed by serial femtosecond crystallography. *Cell* 161(4): 833-844.
- Zhang J and Pratt RE (1996) The AT2 receptor selectively associates with G α 2 and G α 3 in the rat fetus. *J Biol Chem* 271(25): 15026-15033.

- Zhang R, Sahu ID, Comer RG, et al. (2017b) Probing the interaction of the potassium channel modulating KCNE1 in lipid bilayers via solid-state NMR spectroscopy. *Magn Reson Chem* 55(8): 754-758.
- Zhao H, Sprunger LK and Simasko SM (2010) Expression of transient receptor potential channels and two-pore potassium channels in subtypes of vagal afferent neurons in rat. *Am J Physiol Gastrointest Liver Physiol* 298(2): G212-221.
- Zhou Y, Morais-Cabral JH, Kaufman A, et al. (2001) Chemistry of ion coordination and hydration revealed by a K⁺ channel-Fab complex at 2.0 Å resolution. *Nature* 414(6859): 43-48.

- Article 1: Royal, P., Andres-Bilbe, A., **Ávalos Prado, P.**, Verkest, C., Wdziekonski, B., Schaub, S., Baron, A., Lesage, F., Gasull, X., Levitz, J. and Sandoz, G. (2019). Migraine-Associated TRESK Mutations Increase Neuronal Excitability through Alternative Translation Initiation and Inhibition of TREK. *Neuron* 101, 232-245.e236.
- Article 2: **Ávalos Prado, P.**, Häfner, S., Comoglio, Y., Wdziekonski, B., Durantou, C., Attali, B., Barhanin, J. and Sandoz, G. (2020). KCNE1 is an auxiliary subunit of two distinct ion channel superfamilies. *Cell* 184, 1-11.
- Review 1: Royal, P., **Ávalos Prado, P.**, Wdziekonski, B. and Sandoz, G. (2019). Two-pore-domain potassium channels and molecular mechanisms underlying migraine. *Biol Aujourd'hui* 213, 51-57.
- Review 2: **Ávalos Prado, P.** and Sandoz, G. (2019). TREK for High-Speed and High-Frequency Conduction through the Axon. *Neuron* 104, 831-833.
- Review 3: Verkest, C., Häfner, S., **Ávalos Prado, P.**, Baron, A. and Sandoz, G. (2020). Migraine and Two-Pore-Domain Potassium Channels. *Neuroscientist*, 1073858420940949.
- Patent: **Ávalos Prado, P.**, Barhanin, J. and Sandoz, G. (2020). Therapeutic use of calcium-activated chloride channel peptide activator.

Migraine-Associated TRESK Mutations Increase Neuronal Excitability through Alternative Translation Initiation and Inhibition of TREK

Perrine Royal,^{1,2} Alba Andres-Bilbe,³ Pablo Ávalos Prado,^{1,2} Clément Verkest,^{2,4} Brigitte Wdziekonski,^{1,2} Sébastien Schaub,¹ Anne Baron,^{2,3} Florian Lesage,^{2,4} Xavier Gasull,³ Joshua Levitz,⁵ and Guillaume Sandoz^{1,2,6,*}

¹Université Côte d'Azur, CNRS, Inserm, Institut de Biologie Valrose, Nice, France

²Laboratories of Excellence, Ion Channel Science and Therapeutics, Nice, France

³Neurophysiology Laboratory, Department of Biomedicine, Medical School, Institute of Neurosciences, Universitat de Barcelona, IDIBAPS, Barcelona, Spain

⁴Université Côte d'Azur, CNRS, Institut de Pharmacologie Moléculaire et Cellulaire, Valbonne, France

⁵Department of Biochemistry, Weill Cornell Medicine, New York, NY, USA

⁶Lead Contact

*Correspondence: sandoz@unice.fr

<https://doi.org/10.1016/j.neuron.2018.11.039>

SUMMARY

It is often unclear why some genetic mutations to a given gene contribute to neurological disorders and others do not. For instance, two mutations have previously been found to produce a dominant negative for TRESK, a two-pore-domain K⁺ channel implicated in migraine: TRESK-MT, a 2-bp frameshift mutation, and TRESK-C110R. Both mutants inhibit TRESK, but only TRESK-MT increases sensory neuron excitability and is linked to migraine. Here, we identify a new mechanism, termed frameshift mutation-induced alternative translation initiation (fsATI), that may explain why only TRESK-MT is associated with migraine. fsATI leads to the production of a second protein fragment, TRESK-MT2, which co-assembles with and inhibits TREK1 and TREK2, two other two-pore-domain K⁺ channels, to increase trigeminal sensory neuron excitability, leading to a migraine-like phenotype in rodents. These findings identify TREK1 and TREK2 as potential molecular targets in migraine and suggest that fsATI should be considered as a distinct class of mutations.

INTRODUCTION

Migraine is a common, disabling neurological disorder with a genetic, environmental, and hormonal component with an annual prevalence estimated at ~15%. It is characterized by attacks of severe, usually unilateral, and throbbing headache and can be accompanied by nausea, vomiting, and photophobia. Migraine is clinically divided into two main subtypes: migraine with aura (MA), when a migraine is preceded by transient neurological disturbances that are usually visual, and migraine without

aura (MO). Cortical spreading depression (CSD) underlies the aura, although its precise relationship to headache is unclear. Activation and sensitization of trigeminal neurons (TG) leading to the release of pro-inflammatory peptides is likely a key component in pain initiation and transmission in migraine (Noseda and Burstein, 2013; Yan and Dussor, 2014).

Recent evidence points to a pivotal contribution of a variety of two-pore-domain potassium (K_{2P}) channels in chronic pain processing. The diverse K_{2P} channel family is made of 15 subtypes, which form 6 subfamilies. The activity of these channels drives the membrane potential toward the K⁺ equilibrium potential and therefore reduces cellular excitability. Expression of several K_{2P} channel subunits has been detected in nociceptive dorsal root ganglion and trigeminal neurons (Alloui et al., 2006; Bautista et al., 2008; Blin et al., 2016; Morenilla-Palao et al., 2014; Noël et al., 2009; Yamamoto et al., 2009). One subtype of K_{2P} channels that is highly expressed in sensory neurons, TRESK, has been directly linked to MA via a causally linked 2-bp frameshift mutation (F139WfsX24) identified in the KCNK18 gene, which causes premature truncation of TRESK ("TRESK-MT"; Lafrenière et al., 2010; Wood, 2010). This mutation segregated perfectly with the MA phenotype in a large pedigree and was shown to produce a non-functional protein that can serve as a dominant negative that functionally downregulates the wild-type (WT) TRESK channel (Lafrenière et al., 2010; Wood, 2010). TRESK-MT has been shown to induce hyperexcitability of TG neurons (Guo et al., 2014; Liu et al., 2013), which likely underscores its role in migraine. However, in subsequent genetic screening studies, another missense TRESK variant, C110R, was identified (Andres-Enguix et al., 2012). TRESK-C110R, similar to TRESK-MT, exerts a dominant-negative effect on WT-TRESK in heterologous cells, but expression of this mutant was found to have no effect on TG excitability (Guo et al., 2014). This absence of effect explains why this mutant was found in both migraine patients and control subjects (Guo et al., 2014). Therefore, despite the fact that both mutations lead to the same apparent effect on TRESK function, only TRESK-MT is able to increase TG excitability and is linked to migraine pathophysiology.



Classically a eukaryotic mRNA is thought to contain one translation start codon, which allows the production of a single protein species. However, in some cases, eukaryotic ribosomes can recognize several alternative translation start sites to induce the formation of several different proteins from the same mRNA (Kochetov, 2008). This alternative translation initiation is a means of expanding the proteome (Kochetov, 2008) and has been shown to increase the functional diversity of K_{2P} channels (Thomas et al., 2008), raising the possibility that it plays a role in TRESK-mediated migraine pathophysiology.

In this study, we addressed why TRESK-MT (F139WfsX24), but not TRESK-C110R, is able to increase TG excitability and, potentially, play a role in migraines. Using single-molecule fluorescence and chemical optogenetic methods, we found that TRESK is able to heterodimerize with 2 distantly related K_{2P} channels from another subfamily, TREK1 and TREK2, and that TRESK-MT strongly inhibits TRESK, TREK1, and TREK2 currents. In stark contrast, we show that TRESK-C110R is only able to inhibit TRESK, but not TREK1 or TREK2. Furthermore, we show, using double knockout (KO) mice for TREK1 and TREK2, that TRESK-MT increases TG neuronal excitability by inhibiting TREK1 and TREK2. Consistent with a role for TREK1 and TREK2 in migraine induction, we found that double-KO mice for TREK1 and TREK2 present, at rest, a migraine-like allodynia phenotype. These results resolve the contradictory lack of effect of TRESK-C110R, which targets only TRESK and not TREK1 or TREK2. Strikingly, we next find that the 2-bp frameshift mutation of TRESK-MT puts an alternative start codon in frame, which leads to the translation of a second TRESK fragment, termed MT2, which specifically co-assembles with TREK1 and TREK2 to downregulate their function, leading to the TG excitability increase. Consistent with a role for MT2 in migraine induction, we found that MT2 expression within the trigeminal ganglia induced a migraine-like allodynia phenotype in rat. Finally, we find that other previously uncharacterized migraine-associated TRESK mutations also produce multiple fragments via alternative translation initiation (ATI) that can have distinct effects on TRESK and TREK channels. Together, these findings identify frameshift-induced ATI (fsATI) as a mechanism initiated by TRESK mutations, which leads to two protein fragments with dominant-negative effects on distinct channel targets to, ultimately, increase sensory neuron excitability, which may contribute to migraine induction.

RESULTS

TRESK Heteromerizes with TREK1 and TREK2

Despite the fact that K_{2P} channels share a similar architecture and global function, they share a low level of sequence identity, even between members of the same subfamily. Surprisingly, this low level of identity does not preclude heteromerization, as we and others recently showed within the TREK subfamily (Blin et al., 2016; Hwang et al., 2014; Lengyel et al., 2016; Levitz et al., 2016). Based on this and the fact that TG neurons express many K_{2P} channels (TREK1, TREK2, TRAAK, TASK1, and TASK3; Bautista et al., 2008; Yamamoto et al., 2009), we hypothesized that the difference between TRESK mutants is due to their differential ability to modify the function of other K_{2P} chan-

nels through heteromerization. To assess the ability of TRESK to heteromerize with other K_{2P} channels that are expressed in TG neurons, we used the single-molecule pull-down (“SiMPull”) assay (Jain et al., 2012) to visualize individual antibody-immobilized protein complexes on polyethylene-glycol-passivated glass coverslips (Figure 1A). We co-expressed GFP-TRESK with either hemagglutinin HA-TRESK, HA-TREK1, HA-TREK2, HA-TRAAK, HA-TASK1, or HA-TASK3 and assessed their ability to co-immunoprecipitate (coIP) GFP-TRESK via an anti-HA antibody. HA-TRESK, HA-TREK1, and HA-TREK2, were able to coIP many fluorescent GFP-TRESK spots (Figures 1B and 1C), whereas no GFP-TRESK spots were observed for HA-TRAAK, HA-TASK1, or HA-TASK3 (Figure 1C), indicating that TRESK co-assembly with other K_{2P} channels is specific for TREK1 and TREK2. Importantly, controls showed that identical results were observed in two different non-ionic detergents (Figure 1C), that similar expression levels were seen for GFP-TRESK when co-expressed with HA-TREK1 or HA-TRESK (Figure S1A), that all HA-tagged K_{2P} constructs were able to pull down themselves (Figures S1B and S1C), and that pull-down was dependent on the presence of the anti-HA antibody (Figure S1D) and confirm that TREK1, TREK2, and TRESK can be co-expressed in the same cultured TG neurons using immunofluorescence and single-cell RT-PCR (Figure S1F).

We next used photobleaching step analysis (Ulbrich and Isacoff, 2007) to determine the stoichiometry of TREK1 and TRESK complexes to test the hypothesis that they form heterodimers. First, we confirmed that HA-GFP-TREK1 form homodimers in our assay by observing ~70% 2-step bleaching for each when expressed and immunoprecipitated alone with anti-HA antibodies (Figure S2A), consistent with the formation of strict dimers with a GFP maturation rate of ~80%. Then, we counted the number of GFP-TRESK subunits within a HA-TREK1/GFP-TRESK complex by observing bleaching steps of GFP-TRESK coIP with immobilized HA-TREK1 (Figure S2C). The majority of fluorescence intensity trajectories showed one bleaching step (~70%; Figure S2C). This distribution is similar to the one observed for HA-TREK1/GFP-TREK1 complexes (Figure S2B) and agrees well with a 1:1 stoichiometry showing that TREK1-TRESK is primarily a heterodimer.

To test the functionality of the TREK1-TRESK heterodimer, we developed a heterodimerization assay based on an engineered “photoswitchable conditional subunit” (TREK1-PCS) of TREK1. The TREK1-PCS is a TREK1 subunit where the C terminus has been deleted to produce endoplasmic reticulum retention, which can be rescued through co-assembly with a full-length subunit (Sandoz et al., 2012). Following co-assembly and surface targeting, TREK1-PCS can then optically control the channel via a tethered photoswitchable blocker (“MAQ”), which attaches to a genetically engineered cysteine. Therefore, gain of photosensitivity of an identified co-expressed TREK-interacting subunit allows for the verification of a functional heteromer with TREK1. As expected, expression of TREK1-PCS alone did not generate a photoswitchable current (Figure 1D), but co-expression with either TREK1 or TRESK induced a robust photoswitchable current (Figures 1E and 1F), indicating that the TRESK subunit is able to co-assemble with TREK1-PCS. Consistent with SiMPull data, no photocurrent was observed when TASK1 (Figure 1G)

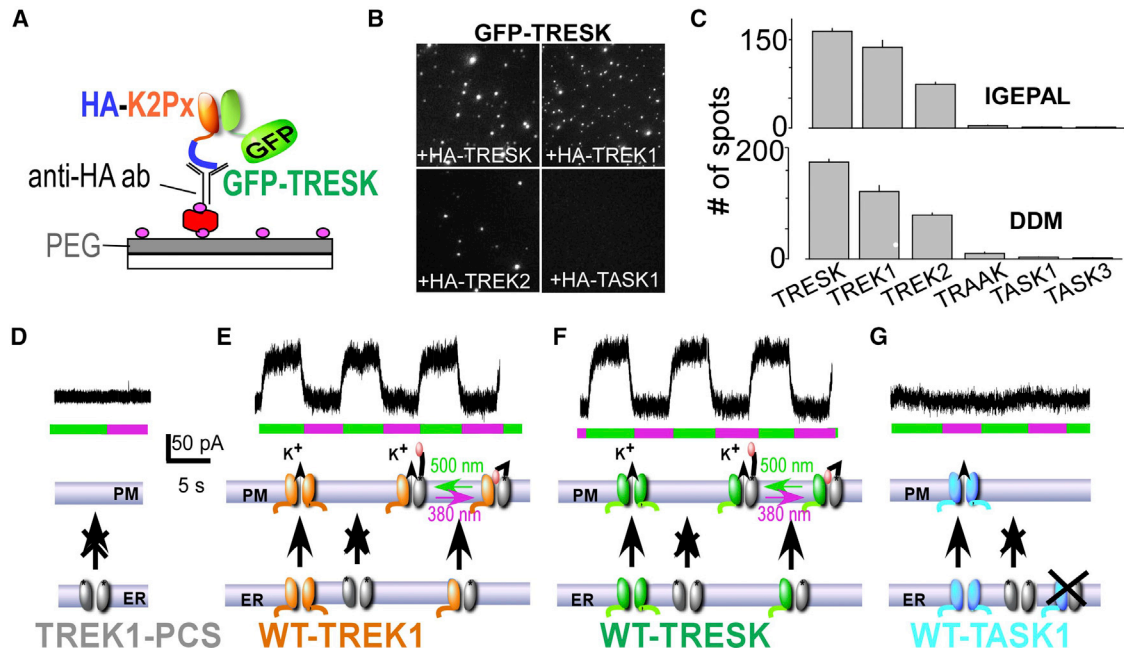


Figure 1. TRESK Heteromerizes Physically and Functionally with TREK1 and TREK2

(A) Schematic of single-molecule pull-down (SiMPull) of GFP-TRESK. HEK293T cells expressing GFP-TRESK and an HA-tagged K2P channel (“HA-K2Px”) were lysed and then immobilized on a polyethylene glycol (PEG)-passivated coverslip conjugated to a biotinylated anti-HA antibody.

(B and C) Representative images (B) (IGEPAL) and summary bar graphs (C) with 2 different detergents, IGEPAL and DDM, showing pull-down of GFP-TRESK by HA-TRESK, HA-TREK1, or HA-TREK2, but not by HA-TASK1, HA-TASK3, or HA-TRAAK. Data are represented as mean \pm SEM.

(D–G) Co-expression of TREK1-PCS with WT-TREK1 produces a heteromeric channel that traffics from the endoplasmic reticulum (ER) to the plasma membrane (PM) and which can be light gated due to attachment of a photoswitchable blocker to the TREK1-PCS. TREK1-PCS expression alone does not produce any photoswitchable current (D), but co-expression of TREK1 (E) or TRESK (F), but not TASK1 (G), leads to a photoswitchable current indicating that TREK1-TRESK form functional heteromers, but there is no functional assembly of TREK1 and TASK1.

See also [Figures S1](#), [S2](#), and [S3](#).

or TASK3 ([Figure S1E](#)) were co-expressed with TREK1-PCS. Furthermore, the bleaching step distribution of GFP-TREK1-PCS spots colPeped with immobilized HA-TREK1 is similar to HA-TREK1/GFP-TREK1; the majority of fluorescence spots showed one bleaching step (\sim 70%; [Figure S2D](#)), supporting the conclusion that the light-gated TREK1-PCS/TRESK current is carried by a TREK1-PCS/TRESK heterodimer with a common pore.

Next, to test the functional properties of the TREK1-TRESK heteromer, we constructed a linked, tandem dimer to have a uniform representation at the surface of the cell of the TREK1-TRESK heteromer ([Figure S3](#)). This heteromeric channel displayed properties that are a mix of those from TREK1 and TRESK homodimers. Notably, TRESK is insensitive to arachidonic acid and TREK1 is sensitive ([Figures S3A–S3C](#)) and TRESK-TREK1 tandems show an intermediate sensitivity to arachidonic acid ([Figure S3C](#)). Furthermore, similar to TRESK, but not TREK1, TRESK-TREK1 tandems showed sensitivity to intracellular calcium, as tested with ionomycin application ([Figures S3D](#) and [S3F](#)). Consistent with this, the light-gated TREK1-PCS/TRESK current is also calcium sensitive ([Figures S3E](#) and [S3F](#)), confirming that the light-gated TREK1-PCS/TRESK current is carried by a TREK1-TRESK heteromer with a common pore.

Having found that TREK can physically and functionally heteromerize with TRESK and that all three channel subtypes are

co-expressed in sensory neurons, we next investigated the ability of TRESK mutants to modify TREK1 and TREK2 currents.

TRESK-MT, but Not TRESK-C110R, Acts as a Dominant Negative on TREK1 and TREK2 Channels

As previously shown ([Andres-Enguix et al., 2012](#)), both TRESK-MT and TRESK-C110R exert a dominant-negative effect on whole-cell TRESK currents ([Figures 2A–2C](#)). Because TREK1 can co-assemble with TRESK ([Figure 1](#)), we addressed the impact of the MT and C110R variants on TREK1 current. We found that TRESK-C110R co-expression did not modify TREK1 current, whereas TRESK-MT co-expression induced a near-complete inhibition of TREK1 current ([Figures 2D–2F](#)). Similar to TREK1, TRESK-MT, but not TRESK-C110R, strongly inhibited TREK2 current ([Figures 2G–2I](#)). This dominant-negative effect is specific and likely dependent on co-assembly because TASK1, TASK3, and TRAAK, which do not colP with TRESK ([Figure 1](#)), were not sensitive to TRESK-MT co-expression ([Figure S4](#)). To address why TRESK-C110R does not modify TREK1 or TREK2 current, we used the SiMPull assay to test the ability of TRESK-C110R to physically interact with TREK1. We co-expressed HA-TREK1 with either GFP-TRESK or GFP-TRESK-C110R and tested their ability to be colPeped with HA-TREK1 via an anti-HA antibody. Whereas GFP-TRESK was able to be colPeped with HA-TREK1, leading to many fluorescent spots,

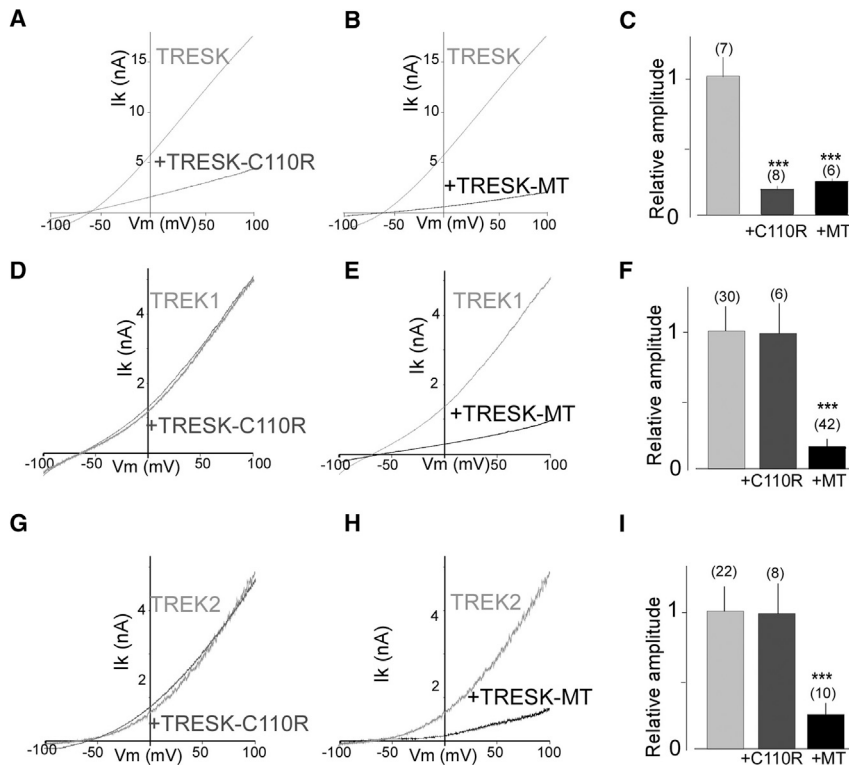


Figure 2. TRESK-MT, but Not TRESK-C110R, Acts as a Dominant Negative on TREK1 and TREK2 Channels

(A and B) Representative traces showing the effect of TRESK-C110R (A) and TRESK-MT (B) co-expression on TRESK current in HEK293T cells. Currents were elicited by voltage ramps (from -100 to 100 mV; 1 s duration).

(C) Bar graph summarizing the relative TRESK current amplitude at 0 mV for TRESK when TRESK-C110R and TRESK-MT are or not co-expressed. Data are represented as mean \pm SEM.

(D–F) Same as (A)–(C) for TREK1.

(G–I) same as (A)–(C) for TREK2. The numbers of cells tested are indicated in parentheses on the graphs. Student's *t* test (***) $p < 0.001$.

See also Figures S4 and S5.

very few spots were observed for GFP-TRESK-C110R (Figure S5A). This indicates that TREK1 can co-assemble with TRESK and that the C110R mutation leads to a drastic reduction of this association, explaining why TRESK-C110R has no effect on TREK1 current. Together, these data show that TRESK-MT can inhibit TRESK, TREK1, and TREK2, whereas TRESK-C110R is only able to inhibit TRESK. Based on the fact that TRESK-MT, but not TRESK-C110R, is able to induce TG neuron hyperexcitability (Guo et al., 2014; Liu et al., 2013), we hypothesized that TRESK-MT induces sensory neuron hyperexcitability primarily by acting on TREK1 and TREK2, not TRESK.

TRESK-MT Increases Neuronal Excitability through the Inhibition of TREK1 and TREK2

To investigate the role of TREK1 and TREK2 in the induction of TG hyperexcitability by TRESK-MT, we tested whether overexpression of GFP-TRESK-MT alters the passive and active electrophysiological properties of small-diameter (<25 μ m) TG neurons from wild-type or TREK1/TREK2 double-knockout (*TREK1*^{-/-}/*TREK2*^{-/-}) mice. As previously shown, TRESK-MT expression in WT TG neurons led to a decrease of the lamotrigine current (Figure S6), leading to an increase in excitability (Figure 3C), which included a decrease in the rheobase (74 ± 11 pA versus 47 ± 5 pA; $p < 0.05$ for TG neurons expressing GFP or TRESK-MT, respectively) and an increase in the number of action potentials (APs) evoked by suprathreshold current injections compared to control (Figures 3A and 3C). As shown in Figure 3B, neurons from *TREK1*^{-/-}/*TREK2*^{-/-} mice were more excitable than WT TG neurons. These neurons have a smaller lamotrigine current

(Figure S6), smaller rheobase (55 ± 6 pA; $p < 0.05$) and a significant increase in the number of APs evoked by suprathreshold current injections compared to WT TG neurons. Consistent with a role for TREK1 and 2 in mediating the effects of TRESK-MT, TRESK-MT overexpression did not alter the excitability of *TREK1*^{-/-}/*TREK2*^{-/-} mice (Figure 3D). *TREK1*^{-/-}/*TREK2*^{-/-} TG neurons showed no increase in the number of evoked APs or a reduction in rheobase

(55 ± 6 pA versus 53 ± 5 pA for TG neuron expressing GFP or TRESK-MT, respectively; $p > 0.5$). Together, these data strongly support a major role for TREK1 and TREK2 in the control of TG neuron excitability and support the idea that TRESK-MT differs functionally from TRESK-C110R in its ability to target TREK1 and TREK2 to increase the excitability of TG neurons, which is likely a crucial step in the induction of migraines.

TREK1^{-/-}/*TREK2*^{-/-} Mice Show a Mechanical Allodynia, which Is Not Increased by NO Donors

Having found that expression of the TRESK-MT mutant increases TG excitability through TREK1-TREK2 inhibition, we hypothesized that *TREK1*^{-/-}/*TREK2*^{-/-} mice would show an increased susceptibility to a migraine-related phenotype. Migraine is associated with an increase of the sensitivity to all sensory modalities, and cutaneous allodynia can be used as a quantifiable marker of migraine disorder (Bates et al., 2010; Verkest et al., 2018). One approach to model acute and chronic migraine is the quantification of this increase in response to known migraine triggers, such as nitric oxide (NO) donors (Bates et al., 2010), including isosorbide dinitrate (ISDN) (Verkest et al., 2018). We quantified ISDN-evoked mechanical allodynia in *TREK1*^{-/-}/*TREK2*^{-/-} and wild-type controls in acute and chronic conditions. In a first experiment, paw mechanical nociception thresholds were determined with a dynamic von Frey aesthesiometer before and during a 3-hr period after intraperitoneal injection of ISDN (10 mg/kg; Figure 3E; Bates et al., 2010; Verkest et al., 2018). In a second experiment, we assessed mechanical nociception thresholds in both *TREK1*^{-/-}/*TREK2*^{-/-} and wild-type controls

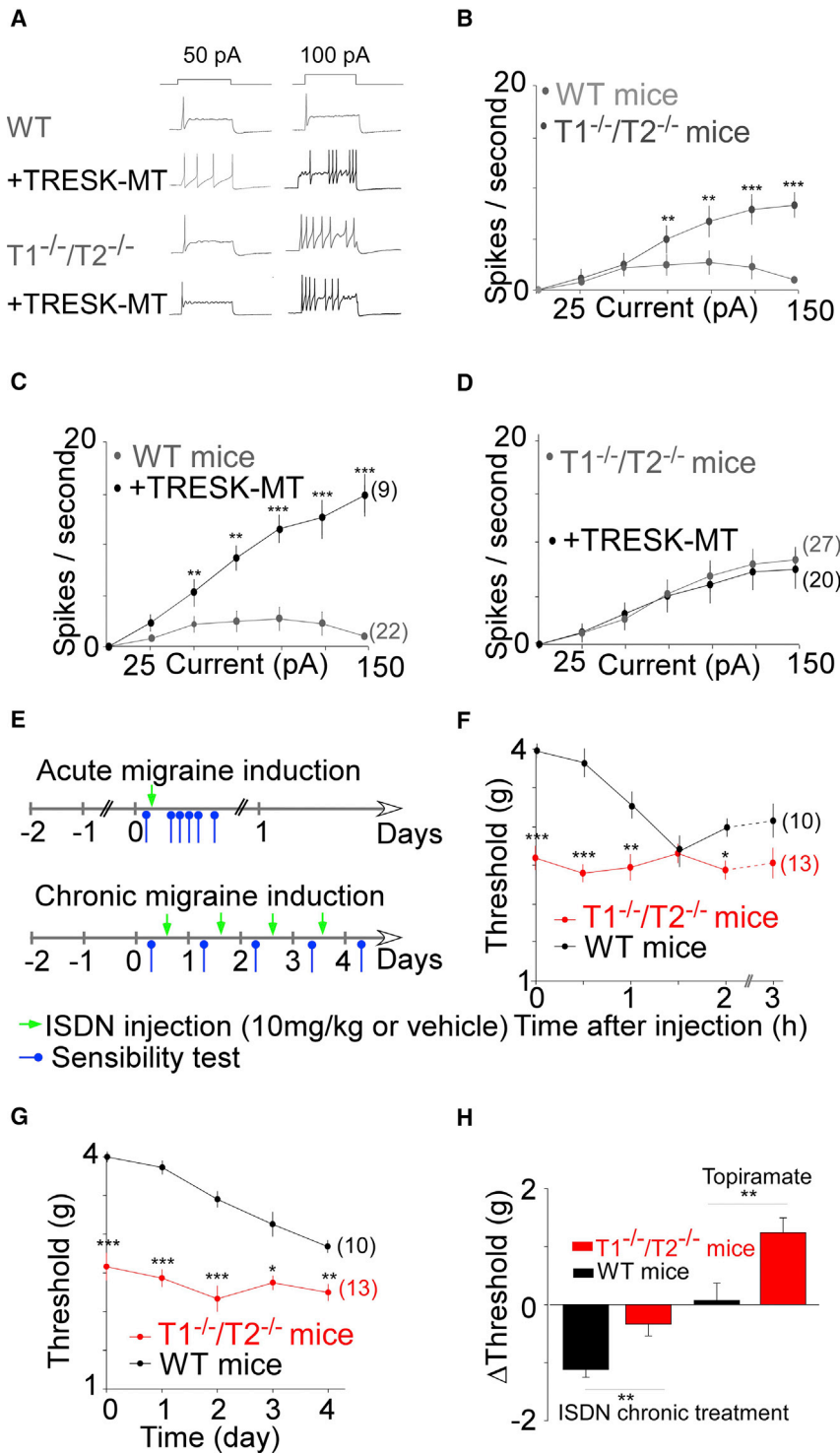


Figure 3. TREK1 and TREK2 Invalidation Increases Sensory Neuron Excitability and Mechanical Pain Perception

(A–D) $TREK1^{-/-}/TREK2^{-/-}$ TG neurons are more excitable than WT TG neurons and are not sensitive to TRESK-MT overexpression.

(A) Representative traces of action potentials (spikes) generated by incremental depolarizing current injections in small-diameter TG neurons.

(B) Input-output plots of spike frequency in response to 1-s depolarizing current injection in untransfected, small TG neurons from WT and $TREK1^{-/-}/TREK2^{-/-}$ double-KO mice.

(C and D) TRESK-MT acts as a dominant negative on TREK1 and TREK2 channels to increase excitability of TG neurons.

(C) Input-output plots of the spike frequency in response to 1-s depolarizing current injection in transfected small TG neurons from WT (C) and $TREK1^{-/-}/TREK2^{-/-}$ double-KO mice (D) show that an increase in excitability elicited by TRESK-MT is observed in WT, but not $T1^{-/-}/T2^{-/-}$, neurons.

The numbers of tested cells are indicated in parentheses on the plots and come from at least 4 different animals. Student's t test (* $p < 0.05$; ** $p < 0.01$; *** $p < 0.001$).

(E–H) $TREK1^{-/-}/TREK2^{-/-}$ double-knockout animals present a migraine-like hypersensitivity to mechanical stimuli.

(E) Schematic of experimental behavioral paradigms. Green arrows represent the injection of ISDN, a known migraine trigger. Blue arrows represent the measurement of mechanical sensitivity.

(F) Paw withdrawal mechanical threshold, assessed after the first ISDN injection, were significantly decreased in double-knockout animals and remained less than WT for the first 1.5 hr following ISDN injection.

(G) Mechanical responses, assessed prior to and after chronic ISDN injections, were significantly decreased in double-knockout animals.

(H) Variation (Δ Threshold (g)) of the paw withdrawal mechanical threshold induced by ISDN chronic treatment or by topiramate injection. Mechanical responses were assessed before and after ISDN chronic (4 days) treatment (left bars) and before and 2 hr after topiramate injection (right bars) in WT and $TREK1^{-/-}/TREK2^{-/-}$ double-knockout ISDN-nontreated mice. Numbers of mice tested are indicated in parentheses on the plots; Student's t test to compare WT versus $TREK1^{-/-}/TREK2^{-/-}$ mice (* $p < 0.05$; ** $p < 0.01$; *** $p < 0.001$). Data are represented as mean \pm SEM.

See also Figure S6.

by intraperitoneally injecting ISDN every day for four days as a model of chronic migraine-associated pain (Figure 3E). We found that, at rest, $TREK1^{-/-}/TREK2^{-/-}$ mice showed a decreased mechanical threshold compared to WT mice (2.6 ± 0.1 g versus 3.9 ± 0.1 g; $p < 0.001$). Notably, the basal mechanical threshold of

the injection of ISDN in $TREK1^{-/-}/TREK2^{-/-}$ mice does not induce any modification of the mechanical threshold, which remained significantly lower than in wild-type controls during the first 1.5 hr following ISDN injection (Figure 3F; $p < 0.001$ after 30 min and $p < 0.01$ after 1 hr with a linear mixed-effects model).

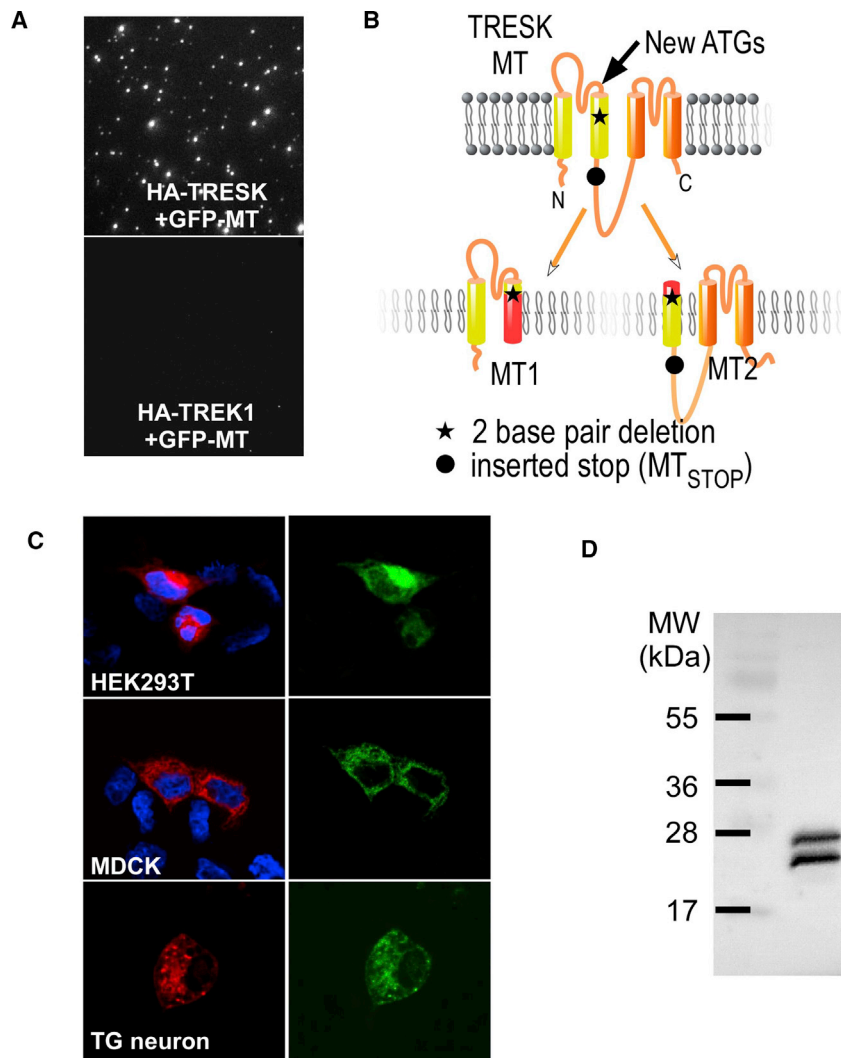


Figure 4. TRESK-MT Induces the Translation of a Second Protein, MT2

(A) Representative images from SiMPull experiments showing that GFP-TRESK-MT can be pulled down by HA-TRESK, but not by HA-TREK1.

(B) Cartoon showing the membrane topology of TRESK and the expected products induced by ATI in the TRESK-MT mutation. The region corresponding to aberrant sequences is shown in red.

(C) Co-synthesis of mCherry-MT1 and MT2-GFP products from the mCherry-TRESK-MT-GFP cDNA in HEK293T cells (top), MDCK (middle), and TG neurons (bottom). DAPI nuclear stain is shown in blue.

(D) Western blot against HA-TRESK-MT-HA probed with anti-HA antibodies from HEK293T cells lysate. See also Figure S10.

In the chronic migraine-associated pain assay, the mechanical thresholds remained significantly lower for *TREK1*^{-/-}/*TREK2*^{-/-} mice compared to wild-type controls, but the difference was strongly reduced (Δ mechanical threshold induced by 4 days ISDN treatment 0.33 ± 0.2 g in *TREK1*^{-/-}/*TREK2*^{-/-} versus 1.12 ± 0.1 g in WT mice; Figure 3G).

Having found that *TREK1*^{-/-}/*TREK2*^{-/-} mice show basal mechanical allodynia that cannot be further increased by an ISDN injection, we wondered whether a treatment used in prophylaxis in migraine patient, topiramate, could reverse this observed migraine-like phenotype as was observed in models of nitroglycerin (NO) donor-induced migraine (Pradhan et al., 2014) and in a model of ISDN-induced migraine in rats (Verkest et al., 2018). We assessed the mechanical nociception threshold in *TREK1*^{-/-}/*TREK2*^{-/-} mice before and 2 hr following the intraperitoneal injection of 30 mg/kg of topiramate. Treatment with topiramate reversed partially the chronic basal allodynia seen in *TREK1*^{-/-}/*TREK2*^{-/-} mice (Δ mechanical threshold of 1.2 ± 0.2 g; Figure 3H), as was previously observed for a nitroglycerin-evoked form of al-

lodynia (Pradhan et al., 2014). As a control, we tested non-treated ISDN WT mice and did not observe any significant shift of the mechanical threshold following topiramate treatment (Figure 3H).

These data demonstrate that, at rest, the *TREK1*^{-/-}/*TREK2*^{-/-} mice present an allodynia phenotype, which is similar to the phenotype observed in ISDN-treated WT animals. This is consistent with a role of TREK1/TREK2 in trigeminal sensory neuron hypersensitivity that is relevant to migraine, which is also supported by the reversion induced by topiramate, a drug used in the clinic to treat chronic migraine.

TRESK-MT Mutation Induces the Translation of a Second Protein, MT2

We next explored how TRESK-MT exerts its effects on TREK channels at the molecular level. The F139WfsX24 frameshift mutation

of TRESK-MT results in the premature truncation of the human TRESK protein from 384 amino acids (aas) to 162 aas. The truncated TRESK includes the first 138 aas of wild-type TRESK followed by a 24-aa aberrant sequence. The corresponding mutation has very similar effects on the mouse TRESK gene, generating a truncated protein with the first 149 aas of wild-type TRESK and followed by a 50-aa aberrant sequence at the C terminus (Figure 4B). We fused a GFP tag to the N terminus of the mouse TRESK-MT and tested its ability to be immobilized by HA-TRESK, HA-TREK1, or HA-TREK2 in the SiMPull assay. Surprisingly, only HA-TRESK was able to colIP GFP-TRESK-MT via an anti-HA antibody (Figure 4A). This result confirms that TRESK-MT associates with TRESK to induce its dominant-negative effect but raises the question of how TRESK-MT is able to inhibit TREK1 and TREK2 without direct association.

It has been hypothesized that ATI of eukaryotic mRNAs, including those that encode K_{2P} channels (Thomas et al., 2008), may provide a method to expand the proteome (Kochetov, 2008). A close examination of the nucleotide sequence of

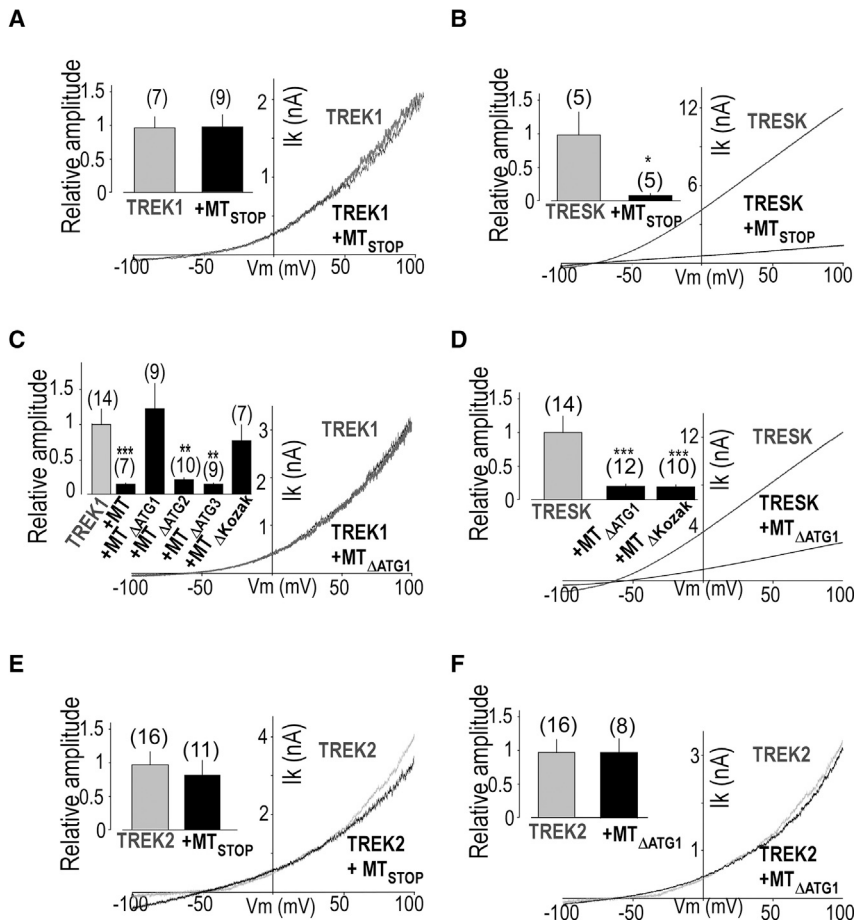


Figure 5. MT2 Mediates TREK1 Inhibition

(A) Representative traces showing the effect of introduction of a STOP codon at the beginning of the MT2 ORF within the 2-3 loop (TRESK-MT_{STOP}) on TREK1 current in HEK293T cells. Inset shows a summary of TREK1 relative current densities when TRESK-MT_{STOP} is co-expressed.

(B) Representative traces showing the effect of TRESK-MT_{STOP} on TRESK current. (Insets) TRESK relative current densities when TRESK-MT_{STOP} is co-expressed are shown.

(C) Representative traces showing the effect of introduction of a mutation of ATG at position +356 (Δ ATG1) on TREK1 current and summary bar graph showing the effect of mutation of candidate alternative start codons (Δ ATG1, Δ ATG2, or Δ ATG3) and mutation of the Kozak sequence surrounding ATG1 (Δ Kozak) in TRESK-MT. Currents were elicited by voltage ramps (from -100 to 100 mV; 1 s duration). (D) Representative traces showing the effect of TRESK-MT Δ ATG1 on TRESK current. (Insets) TRESK relative current densities when TRESK-MT Δ ATG1 is co-expressed are shown.

(E and F) same as (A) and (C) for TREK2. The numbers of cells tested are indicated in parentheses on the graphs. Cells come from at least two experimental days. Student's t test (* $p < 0.05$, ** $p < 0.01$, and *** $p < 0.001$) shows the difference between TREK1, TRESK, or TREK2 and TREK1, TRESK, or TREK2 when co-expressed with different TRESK-MT constructs. Data are represented as mean \pm SEM.

See also Figures S7 and S11.

TRESK-MT revealed that the F139WfsX24 frameshift mutation places two new ATG codons in frame with the reference open reading frame of TRESK (ATGs at position +356 and +407 for the human TRESK cDNA and +389 and +490 for the mouse cDNA). We hypothesized that one of these codons may serve as an ATI site that can lead to the formation of a second truncated TRESK protein, termed "MT2," that would include a short (either 2 or 19 aas) N-terminal aberrant sequence followed by the C-terminal part of TM2, including the 2-3 intracellular loop, TM3, P2 loop, TM4, and the C-terminal domains (Figure 4B). To test whether MT2 is co-translated with MT1, we introduced an N-terminal mCherry tag in frame with MT1 and a C-terminal GFP in frame with MT2 within the mouse TRESK-MT cDNA ("mCherry-TRESK-MT-GFP"). Expression of this construct led to HEK293T cells with both mCherry and GFP fluorescence, showing the co-translation of mCherry-MT1 and MT2-GFP (Figure 4C). This co-translation was observed in other cell lines, including MDCK cells (Figure 4C), as well as in primary TG neurons (Figure 4C). Next, we introduced an N-terminal HA tag in frame with MT1 and another one in frame with MT2 within the mouse TRESK-MT cDNA ("HA-TRESK-MT-HA"). Lysate from cells transfected with HA-TRESK-MT-HA was probed in a western blot with anti-HA antibodies, and 2 bands, with a similar intensity, corresponding to the expected molecular weights for

MT1 (~23 kDa) and MT2 (~29 kDa) were detected (Figure 4D). Together, these data clearly show that TRESK-MT leads to the production of two distinct fragments of TRESK.

To probe the function of MT2, we introduced a stop codon into the MT2 open reading frame (ORF) of TRESK-MT at the beginning of the 2-3 loop (Figure 4B), inducing the loss of expression of MT2 (Figure S7A). As shown in Figure 5, whereas the introduction of the stop codon in the MT2 ORF did not change the ability of TRESK-MT to inhibit TRESK current (Figure 5B), this stop codon abolished the ability of TRESK-MT to produce a dominant-negative functional effect on TREK1 (Figure 5A). We next confirmed the importance of this second ORF by mutating, in TRESK-MT, the putative ATI start codons one by one. Mutation of the first ATG abolished the ability of TRESK-MT to inhibit TREK1 (Figure 5C), but not TRESK (Figure 5D), whereas mutation of the second ATG did not alter the ability of TRESK-MT to inhibit TREK1 current (Figures 5C and S7B). These data indicate that the ATI site is the first internal ATG. As a control, we mutated a third ATG, which is also present in the WT-TRESK sequence, and found that it did not change the ability of TRESK-MT to inhibit both TRESK and TREK1 currents (Figures 5C and S7C). Similar to TREK1, introduction of a stop codon into the MT2 ORF or mutation of the first ATG also abolished the inhibition of TREK2 by TRESK-MT (Figures 5E and 5F). To further

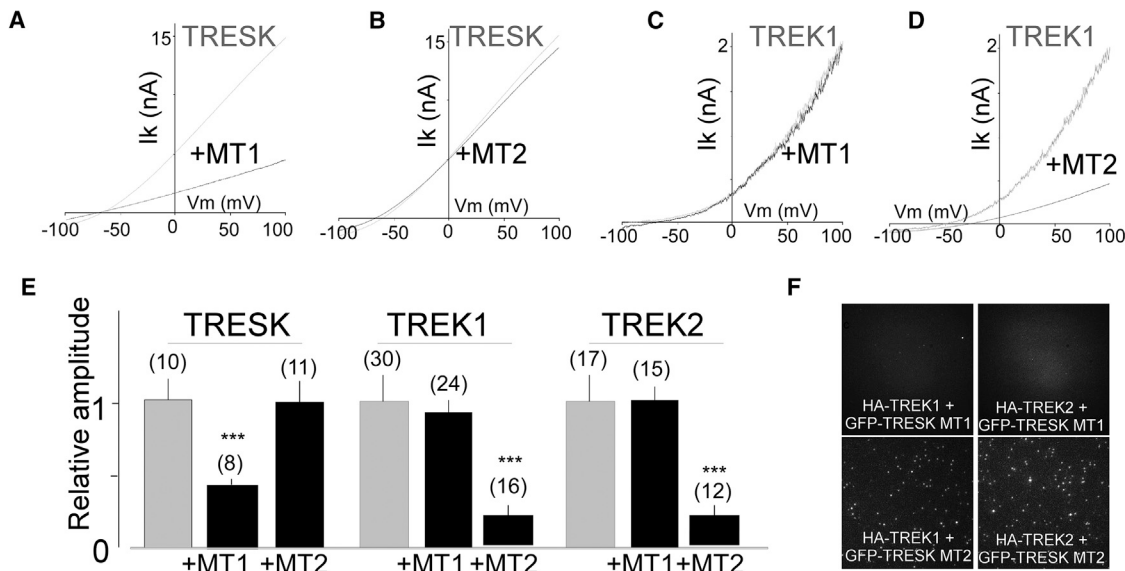


Figure 6. MT1 Acts as Dominant Negative on TRESK, whereas MT2 Acts as a Dominant Negative on TREK1 and TREK2 Channels

(A–D) Representative traces showing the effect of TRESK-MT1 (A and C) or TRESK-MT2 (B and D) co-expression on TRESK (A and B) or TREK1 (C and D) currents in HEK293T cells. Currents were elicited by voltage ramps (from -100 to 100 mV; 1 s duration).

(E) Bar graph summarizing the relative TRESK, TREK1, and TREK2 current amplitudes at 0 mV when MT1 or MT2 are co-expressed. The numbers of cells tested are indicated in parentheses on the graphs. Cells come from at least two experimental days. Student's *t* test (** $p < 0.001$). Data are represented as mean \pm SEM. (F) Representative images showing that GFP-MT2, but not GFP-MT1, can be pulled down by HA-TREK1 and HA-TREK2 via an anti-HA antibody in the SiMPull assay with HEK293T cells.

See also Figures S7, S8, and S11.

demonstrate that the first ATG serves as a start codon, we mutated the potential Kozak sequence GCTATGG to CCTATGC and found that alteration of the Kozak sequence strongly reduced the inhibitory effect of TRESK-MT on TREK1 current (Figures 5C and S7D) without affecting the effect on TRESK (Figures 5D and S7E).

MT2, but Not MT1, by Acting as a Dominant Negative on TREK1 and TREK2 Channels, Increases Neuronal Excitability of WT Small TG Neurons, Leading to Facial Allodynia

To independently express MT1 and MT2 for functional characterization, we sub-cloned both ORFs into separate mammalian expression vectors. Co-expression of MT2 with TRESK did not modify TRESK current (Figures 6B and 6E), and MT1 co-expression induced a ~ 3 -fold decrease of the current, which was similar to what was observed for the co-expression of the full TRESK-MT construct (Figures 6A and 6E). On the contrary, co-expression of MT1 did not modify TREK1 current (Figures 6C and 6E), but co-expression of MT2 induced a ~ 4 -fold decrease of the current, similar to what was observed with co-expression of the full TRESK-MT construct (Figures 6D and 6E). Similar results were obtained for TREK2 (Figures 6E and S8). Consistent with the functional data, we found that GFP-MT2 is colPed with HA-TREK1 or HA-TREK2 in the SiMPull assay (Figure 6F).

To validate the physiological role of interaction between TREK1, TREK2, and MT2, we tested the functional effect of MT2 in TG neurons. Whereas MT1 expression did not alter the excitability of WT TG neurons (Figures 7A and 7B), MT2

increased it significantly (Figures 7A and 7C). In fact, MT1 did not modify the rheobase (74 ± 11 pA versus 79 ± 5 pA; $p > 0.5$ for TG neurons expressing GFP or MT1, respectively) and did not modify the number of APs evoked by suprathreshold current injections compared to control. Conversely, MT2 expression in WT TG neurons led to an increase in excitability (Figure 7), which included a decrease in the rheobase (74 ± 11 pA versus 55 ± 5 pA; $p < 0.05$ for TG neurons expressing GFP or MT2, respectively; $p < 0.05$) and an increase in the number of APs evoked by suprathreshold current injections compared to control (Figures 7A and 7C). We confirmed that this effect is linked to TREK1 and TREK2 because MT2 overexpression failed to increase the excitability of *TREK1*^{-/-}/*TREK2*^{-/-} TG neurons (Figure 7D).

Having found that MT2, by inhibiting TREK1 and TREK2, is sufficient to increase TG excitability, we asked whether MT2 expression in TG ganglia would induce a migraine-related phenotype. We conducted behavioral experiments in rats in which MT2 was virally overexpressed within the trigeminal ganglia. Rats allowed to test the mechanical pain threshold on the face, which is directly linked to TG excitability, constituting a relatively direct, reliable, and quantifiable marker of migraine disorder in clinical contexts as well as in NO-induced migraine (Pradhan et al., 2014; Kopruszinski et al., 2017; Harris et al., 2017). As shown in Figure 7F, MT2 expression in TG ganglia (Figure S9) significantly increased the facial mechanical threshold (3.3 ± 0.4 g versus 7.7 ± 0.4 g; $p < 0.001$). Furthermore, as was seen for the *TREK1*^{-/-}/*TREK2*^{-/-} mice, the basal mechanical facial threshold of MT2-expressing rats is similar to the threshold

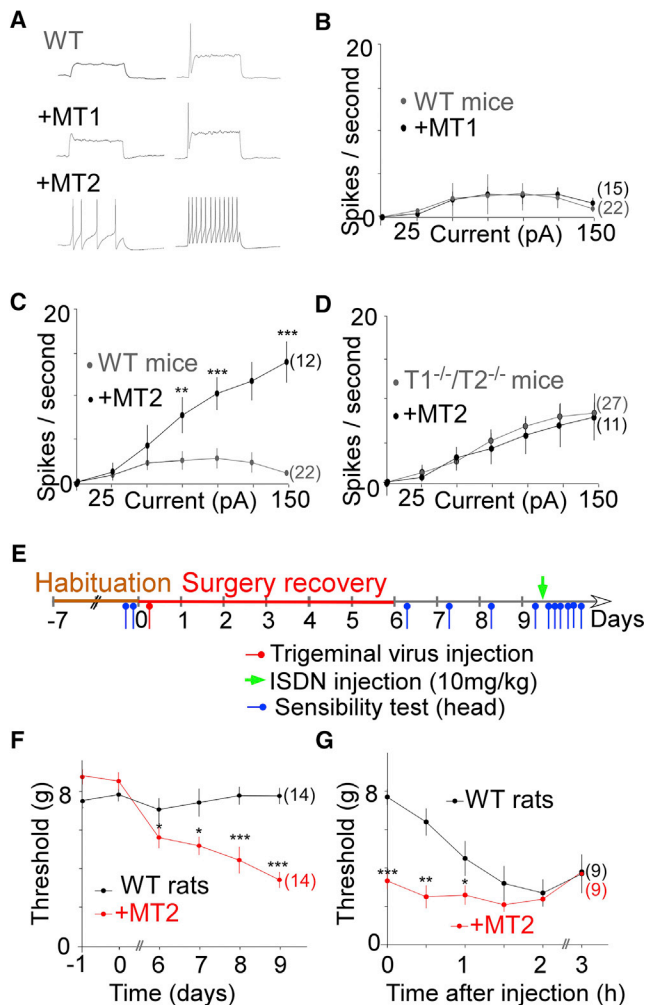


Figure 7. MT2, but Not MT1, Increases Neuronal Excitability of WT Small TG Neurons through TREK1 and TREK2 Inhibition

(A) Representative traces showing spikes generated by incremental depolarizing current injections (+50 pA and +100 pA) in small-diameter TG neurons. (B and C) Input-output plots of spike frequency in response to 1-s depolarizing current injections in WT small-diameter TG neurons transfected with either GFP (“WT”), the GFP-tagged MT1 subunit (“MT1”; B), or the GFP-tagged MT2 subunit (“MT2”; C).

(D) Input-output plots of spike frequency show a lack of effect of GFP-MT2 expression on TG neurons from TREK1/TREK2 double-KO mice ($T1^{-/-}/T2^{-/-}$).

(E–G) MT2 overexpression in TG leads to facial mechanical allodynia in rats. (E) Schematic of experimental behavioral paradigms. After a week of habituation, rats were injected with 10 μ L of AAV2 encoding for either MT2 + GFP or GFP.

(F) Face withdrawal mechanical threshold assessed after trigeminal virus infection encoding either GFP (WT rat condition) or MT2.

(G) Face withdrawal mechanical threshold, assessed after the first ISDN injection. The threshold for MT2-expressing rats was significantly decreased before the injection and remained less than WT for the first 1.5 hr following ISDN injection. The numbers of tested cells and rats are indicated in parentheses on the plots. Mice neurons come from at least 5 different animals. Student’s t test (* $p < 0.05$, ** $p < 0.01$, and *** $p < 0.001$). Data are represented as mean \pm SEM.

See also Figure S9.

observed 1.5, 2, and 3 hr after acute ISDN injection in WT rats. Having found that MT2 overexpression induced allodynia, we quantified ISDN-evoked mechanical allodynia and found that MT2 overexpression in TG neurons prevents any further effect of ISDN on facial allodynia. This loss of effect of NO donors may be due to the fact that the “ceiling” level of allodynia has already been reached.

Together, these data demonstrate that, at rest, the overexpression of MT2 leads to an increase in TG excitability and a chronic cutaneous allodynia to a similar level to what is observed following NO-donor injection. This is also similar to the allodynia observed in $TREK1^{-/-}/TREK2^{-/-}$ double-KO mice (Figure 3).

MT2-Producing Alternative Translation Initiation Is Found in Other Migraine-Associated TRESK Mutants

Having found that MT2 is responsible for the migraine-associated increase in TG excitability and induction of a migraine-like phenotype through the inhibition of TREK1 and TREK2, we anticipated that other frameshift mutations may exist that place the ATG at position +356 in frame with the reference open reading frame of TRESK. Such mutations would lead to the formation of MT2. This mutation could be either a 2-bp deletion or 1-bp insertion in the region between the ATG at position +356 and the ATG at position +427 (Figure S10). We used the Exome Aggregation Consortium (ExAC) database (Lek et al., 2016) and found one variant (Y121LfsX44) with a T duplication (+1 pb; c.361dupT) that places the AT1 site in frame with the TRESK ORF (Figure S9). We introduced this insertion into the mCherry-TRESK-GFP (mCherry-TRESK-c.361dupT-GFP) sequence and found, similar to mCherry-TRESK-MT-GFP (Figure 4C), that this construct led to HEK293T cells with both mCherry and GFP fluorescence (Figure 8A) due to the co-translation of both MT1 and MT2 proteins. Similar to TRESK-MT, this mutant is able to inhibit TRESK, TREK1, and TREK2 (Figure 8). As was seen for TRESK-MT (Figure 5), introduction of a stop codon into the MT2 ORF (TRESK c.361dupT_{STOP}) of this mutant abolished its ability to inhibit TREK1 and TREK2 (Figure 8), but not TRESK. Because this Y121LfsX44 mutation leads to the same molecular effects as TRESK-MT on TREK function, we hypothesized that it may be associated with a migraine phenotype. To address this, we looked in the ClinVar database (Landrum et al., 2016) and found that this mutant has been correlated with a migraine phenotype (RCV000490385.1).

DISCUSSION

Although initial findings of migraine-associated mutations of TRESK represented a major breakthrough (Lafrenière et al., 2010), a direct relationship between TRESK channel disruption and migraine has been challenged based on the discovery of a TRESK mutation (C110R) that produces a dominant-negative form of TRESK but is found in a control cohort population (Andres-Enguix et al., 2012). The presence of this mutation in control individuals indicates that a single non-functional TRESK variant alone may not be sufficient to cause migraines, consistent with the genetic complexity of this disorder. In this study, we have addressed this controversy and found that the migraine-associated

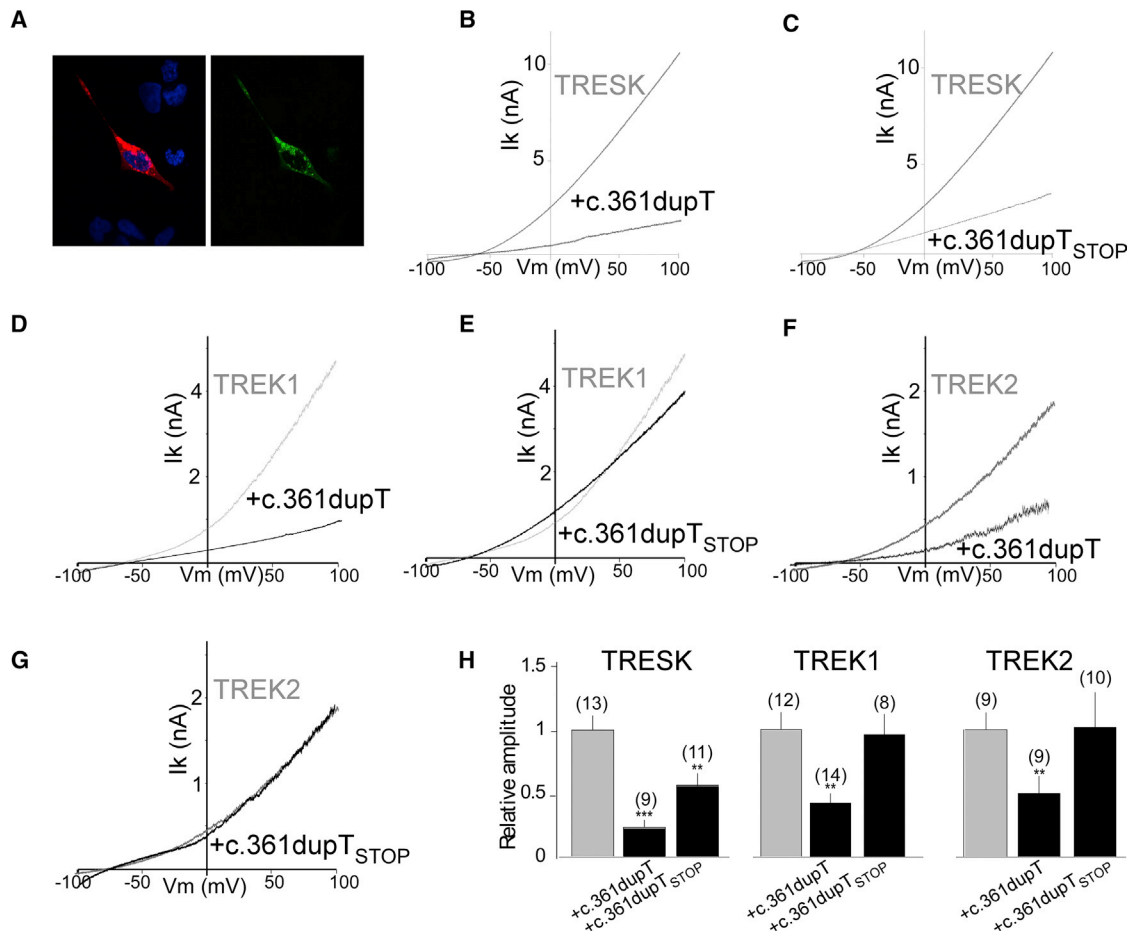


Figure 8. TRESK-c.361dupT (Y121LfsX44) Acts as a Dominant Negative to Reduce Both TRESK and TREK1 Current

(A) Co-synthesis of mCherry-MT1 and MT2-GFP products from the mCherry-TRESK-c.361dupT-GFP cDNA in HEK293T cells.

(B and C) Representative traces showing the effect of TRESK c.361dupT (B) and TRESK c.361dupT_{STOP} (C) co-expression on TRESK current. Currents were elicited by voltage ramps (from -100 to 100 mV; 1 s duration).

(D and E) Same as (B) and (C) for TREK1.

(F and G) same as (A) and (B) for TREK2.

(H) Bar graph summarizing the relative TRESK, TREK1, and TREK2 current amplitudes at 0 mV for TRESK, TREK1, and TREK2 when TRESK c.361dupT and TRESK c.361dupT_{STOP} are co-expressed. The numbers of cells tested are indicated in parentheses on the graphs. Cells come from at least two experimental days. Student's t test (** $p < 0.01$ and *** $p < 0.001$). Data are represented as mean \pm SEM.

See also [Figure S10](#).

mutation of TRESK exerts its effects on sensory neurons by associating and serving as a dominant negative not only for TRESK but also for TREK1 and TREK2 channels. In stark contrast, TRESK-C110R is not able to regulate TREK channels. Consistent with a function of TREK1 and TREK2 in TRESK-MT-induced migraine, the *TREK1*^{-/-}/*TREK2*^{-/-} mice show a migraine-like hypersensitivity to mechanical stimuli. Surprisingly, we find that migraine-associated frameshift mutations of TRESK induce alternative translation initiation that allows the formation of a second product, MT2, which mediates the dominant-negative action on TREK1 and TREK2 when overexpressed. This dominant-negative action on TREK1 and TREK2, ultimately, leads to an increase in TG neuron excitability and a migraine-like hypersensitivity to facial mechanical stimuli. Supporting

this phenomenon as a general mechanism, we found another migraine-associated frameshift mutation in TRESK that produces a similar ORF shift, which also leads to the formation of MT2. Together, these findings support a role of fsATI and for TREK potassium channels as a key part of sensory neuron excitability and the underlying cellular mechanism of migraine.

We and others (Blin et al., 2016; Hwang et al., 2014; Lengyel et al., 2016; Levitz et al., 2016) have recently shown that K_{2P} channels are able to form both homodimeric and heterodimeric potassium channels. In this study, we show that TREK and TRESK readily assemble as heteromers. To co-assemble natively, TRESK and TREK must be expressed in the same cells. We and others have found that TG neurons from mice can co-express TREK1, TREK2, and TRESK (Bautista et al., 2008), and it

has been confirmed that TREK1 and TRESK are also co-expressed in human TG neurons (Flegel et al., 2015). Recent single-cell RNA sequencing data on dorsal root ganglion (DRG) sensory neurons from mice have also shown that co-expression of TRESK with TREK-2 and/or TREK-1 occurs in some subtypes of sensory neurons involved in pain signaling, including peptidergic and non-peptidergic subtypes (Usoskin et al., 2015; Zeisel et al., 2018). Single-channel recordings also identified these channels in medium- and small-sized sensory neurons of the DRG, which are likely involved in nociception (Kang et al., 2005). In this study, we have supported these previous findings by using immunohistochemistry and single-cell RT-PCR (Figure S1), as well as pharmacology (Figure S6), to confirm the co-expression of TRESK and TREK channels in sensory neurons. Nevertheless, the relative expression levels of TREK and TRESK in TG neurons are, as is the case for the DRG, likely variable, and therefore, we expect a differential population of homo and heteromers from cell to cell. Expression studies with single-cell precision are ultimately needed to precisely determine which subpopulations co-express different relative amounts of each channel. We show that this TRESK-TREK heteromer is a functional dimer because one TRESK is able to co-assemble with one TREK subunit to form a heterodimeric channel with a common pore using a photoswitchable conditional TREK1 (Sandoz et al., 2012). This is quite surprising given that TREK1/2 and TRESK are in different K_{2P} channel subfamilies and only show low sequence identity of ~19.7% (Sano et al., 2003). We previously found that all members of the TREK channel subfamily (TREK1, TREK2, and TRAAK) can co-assemble but that TREK was unable to interact with TASK channels. Similar to the other reported heteromers, TREK1-TRESK heterodimers show unique biophysical behavior that blends the properties of the parent subunits. Notably, TREK1-TRESK is both arachidonic-acid- and calcium-sensitive. In this study, we also show that TRESK does not heteromerize with three other K_{2P} channels, one from the TREK subfamily, TRAAK, and two from the TASK subfamily, TASK1 and TASK3. Together, this indicates that not all pairs of K_{2P} channel subunits are able to interact and that there are indeed rules of interaction that remain to be deciphered. Future work will be needed to determine the molecular mechanisms and structural interfaces that mediate specific K_{2P} heteromer assembly and the associated functional consequences of heteromerization.

TRESK channels are expressed in the DRG and show their highest expression levels in TG. In DRG and TG, TRESK is most abundant in the small- and medium-size sensory neurons (Dobler et al., 2007; Lafrenière et al., 2010). In TG neurons, introduction of TRESK-MT has been shown to reduce the lamotrigine-sensitive K^+ current, leading to an increase in excitability (Guo et al., 2014; Liu et al., 2013). This increase of TG excitability cannot be explained by TRESK inhibition because TRESK-C110R, which also strongly inhibits wild-type TRESK, does not inhibit the lamotrigine-sensitive K^+ current and does not increase TG excitability, explaining its lack of involvement in migraine (Guo et al., 2014). TREK1 and TREK2 are also expressed in DRG and show high expression levels in TG (Blin et al., 2016; Yamamoto et al., 2009). Furthermore, TREK1 and TREK2 have recently been shown to also be lamotrigine sensi-

tive (Walsh et al., 2016; Figure S6). We found that TRESK-MT inhibits TREK1 and TREK2 to increase TG excitability, showing that TREK1 and TREK2 control TG neuron excitability. To address the impact of this sensory neuron excitability increase, linked to TREK1 and TREK2 inhibition, we tested *TREK1^{-/-}/TREK2^{-/-}* mice for their susceptibility to a migraine-like phenotype. Migraine is associated with increased sensitivity to all sensory modalities, and it appears that cutaneous allodynia can be used as a quantifiable marker of migraine disorder (Bates et al., 2010). Increase of basal mechanical hyperalgesia induced by TREK1 and TREK2 invalidation, to a similar level compared to WT animals after ISDN injection, is in agreement with a KO-induced increase of sensory neuron excitability that is relevant to migraine (Brennan et al., 2013). Furthermore, trigeminal overexpression of MT2 in rats also induced a chronic facial allodynia. This facial allodynia can be a facial hypersensitivity without migraine; however, orbitofacial allodynia is clearly accepted as a reflection of the activity of TG neurons and therefore relevant to migraine (Pradhan et al., 2014; Kopruszinski et al., 2017; Harris et al., 2017). Nevertheless, inhibition of TREK1/TREK2 by TRESK-MT2 fragments will depend on its physiological expression and remains to be demonstrated without overexpression. Topiramate was previously shown to inhibit NO-donor-induced acute or basal chronic allodynia (Pradhan et al., 2014). We found that topiramate was able to partially reverse TREK1-TREK2 invalidation-induced allodynia, which is consistent with its action as a prophylactic migraine therapy (Pradhan et al., 2014). Therefore, these results seem to indicate that the dysfunction of TREK1 and TREK2, and not of TRESK alone, contributes to the increase of TG excitability, which may lead to an alteration of pain processing like during migraine, suggesting that TREK1, TREK2, and TREK-TRESK heterodimers should be considered as new targets for migraine treatment.

An important remaining question is: how can TREK1 and TREK2 dysfunction lead to migraine phenotypes? Importantly, the TRESK-MT mutant has been found in migraine with aura phenotype (Lafrenière et al., 2010). Aura has been linked to CSD, which precedes the activation of TG neurons (Noseda and Burstein, 2013). TREK1 and TREK2 channel activity, by reducing TG excitability, may serve as a brake to prevent the pathological activation of TG neurons during the early stages of CSD. In patients expressing TRESK-MT, this mechanism may be reduced or eliminated, enhancing the activation of TG neurons, thus leading to migraines. Fitting the model in which an increase in TG excitability is the primary underlying cause of headaches, the TRESK-MT proband described in the original Lafrenière paper (Lafrenière et al., 2010; OMIM no. 613656) also showed migraine headaches in isolation without a preceding aura.

Most importantly, this study led us to uncover an undescribed mechanism involving alternative translation initiation. We provide evidence that the 2-bp deletion observed for TRESK-MT introduces an in-frame start codon with the reference open reading frame of TRESK, allowing the formation of MT2, the TRESK fragment responsible for the increase in TG excitability. Translation initiation of most eukaryotic mRNAs follows a linear scanning mechanism where the 40S ribosome is recruited to the

5' cap structure of the mRNA followed by downstream movement until an initiation codon is encountered (Kozak, 1999). In these cases, the translation initiation site is the first cap-proximal start codon for methionine (AUG). In most eukaryotic mRNA, this first AUG is embedded into the Kozak consensus sequence [A/G]-XX-ATGG (Kozak, 1984a, 1984b; Jackson et al., 2010). However, if the first AUG is used inefficiently, some ribosomes read through the site without recognition; this leaky scanning can result in translation initiation at a downstream position (Thomas et al., 2008). This has been observed for TREK1, where the second strong ATI site allows the physiological formation of a TREK1 channel with a shorter N terminus that leads to altered TREK1 ion selectivity (Thomas et al., 2008). Similar to what was seen with TREK1, the TRESK ATG at position +356 is embedded into the Kozak consensus sequence (GCTATGG), which may explain why this ATG can serve as an ATI. To further determine why the ATG at position +356 is able to serve as an ATI, we submitted the TRESK-MT sequence to TIS Miner and the ATGpr algorithms (Nishikawa et al., 2000), and both algorithms predicted that the ATG at position +356 is a strong start codon and it is the second possible start codon after ATG at position +1. Furthermore, we found that Kozak sequence mutation significantly reduced the TRESK-MT effect on TREK1 current. This indicates that leaky scanning may explain the generation of TRESK-MT2.

At the physiological level, ATI is thought to increase protein functional diversity, as is also the case with RNA splicing. For example, it was recently shown in osteogenesis imperfecta (OI) disease, that a causative missense mutation of c.-14C > T of the cDNA encoding IFITM5 creates an upstream ATG (ACG at position -15 was mutated to give ATG) in the 5' UTR in frame with IFITM5, which can serve as an ATI site, resulting in addition of an N-terminal 15-aa sequence (Lazarus et al., 2014). Here, we find that an ATG embedded by a strong Kozak sequence, downstream of the ATG at position +1, can be put in frame by a frameshift mutation to induce the translation of a second truncated protein. In the present work, this second product was found to target TREK1 and TREK2 to increase TG neuron excitability and to produce mechanical allodynia, linking this mutant to migraine. This represents the first example where a frameshift mutation downstream of an ATG start codon at position +1 creates a new ORF, allowing the production of a second product that is at the origin of a physiological disturbance. To see whether this fsATI is a general phenomenon in TRESK, we predicted that any mutations before the stop codon ATG at position +427 that put the ATG at position +356 in frame would induce the formation of an MT2 that would lead to disease. Indeed, we demonstrate that another frameshift mutation, c.361dupT (Y121LfsX44), also leads to the formation of MT2 and is correlated to migraine (Clinvar, RCV000490385.1). It is not possible to make any causal statements from this observation, but it is worth noting that this is the only other TRESK mutation that has been linked to a migraine phenotype. Together, this work shows that different frameshift mutations downstream of the first start codon can lead to ATI to produce a second protein that can carry the physiological function, suggesting that this mechanism may be widespread in nature and therefore needs to be

considered when analyzing frameshift mutations linked to human disorders.

STAR★METHODS

Detailed methods are provided in the online version of this paper and include the following:

- **KEY RESOURCES TABLE**
- **CONTACT FOR REAGENT AND RESOURCE SHARING**
- **EXPERIMENTAL MODEL AND SUBJECT DETAILS**
 - Knock-out mice
 - HEK cells
 - *Xenopus* oocytes
 - Rats
 - WT mice
- **METHOD DETAILS**
 - Behavioral experiments
 - Electrophysiology
 - Immunocytochemistry
 - Molecular Biology, Cell Culture and Gene Expression
 - PCR amplification and quantification
 - Primary cultures of mouse TG neurons
 - Single Molecule Pulldown (SiMPull)
 - Single cell reverse transcription
 - Trigeminal neurons RNA extraction and reverse transcription
 - Vector preparation
 - Western blot analysis
- **QUANTIFICATION AND STATISTICAL ANALYSIS**
 - Single Molecule Pulldown
 - Electrophysiology
 - Animal experiment
 - Quantitative PCR

SUPPLEMENTAL INFORMATION

Supplemental Information includes eleven figures and can be found with this article online at <https://doi.org/10.1016/j.neuron.2018.11.039>.

ACKNOWLEDGMENTS

We thank Michel Vivaudou, Rainer Waldman, Bernard Mari, Kevin Le Brigand, Eric Lingueglia, Michel Lanteri-Minet, Emile Piquet, and Maximilian Furthauer for helpful discussion. The work was supported by a grant to G.S. by the ATP-AVENIR funds and the Fondation pour la Recherche Medicale (Equipe labellisée FRM 2017, FRM DEQ20170336753 and ANR AT2R-TRAAK-Bioanalgesics ANR-17-CE18-0001 and ANR-17-ERC2-0023) as well as grants to G.S. and F.L. from the Agence Nationale de la Recherche (Laboratory of Excellence "Ion Channel Science and Therapeutics," grant ANR-11-LABX-0015-01 and ANR Dynaselect, grant ANR-14-CE13-0010). The work was also supported by grants from Ministerio de Ciencia, Innovacion y Universidades and Instituto de Salud Carlos III of Spain FIS PI14/00141 and FIS PI17/00296 (to X.G.), RETIC RD16/0008/0014 (to X.G.), and Generalitat de Catalunya 2017SGR737 (to X.G.). We thank A. Monteil and C. Lemmers from the Vectorology facility, PVM, Biocampus Montpellier, CNRS UMS3426 for virus production. The microscopy was done in the Prism facility, "Plateforme PRISM - IBV-CNRS UMR 7277- INSERM U1091-UNS." The help of Magali Mondin is acknowledged. Histopathological analyses were performed on the Experimental Histopathology Platform of iBV, CNRS UMR7277-INSERM U1091-UNS. The help of Samah REKIMA is acknowledged.

AUTHOR CONTRIBUTIONS

Conceptualization, P.R., X.G., J.L., and G.S.; Methodology, P.R., A.B., A.A.-B., C.V., F.L., J.L., X.G., and G.S.; Investigation, P.R., A.A.-B., P.A.P., C.V., B.W., J.L., and G.S.; Writing – Original Draft, J.L. and G.S.; Writing – Review and Editing, P.R., A.B., F.L., X.G., J.L., and G.S.; Funding Acquisition, G.S.; Project Administration, G.S.

DECLARATION OF INTERESTS

Patent applications have been filed on TREK1/2 as potential targets to treat migraine (application with InsermTransfert).

Received: April 16, 2018

Revised: October 3, 2018

Accepted: November 20, 2018

Published: December 17, 2018

REFERENCES

- Alloui, A., Zimmermann, K., Mamet, J., Duprat, F., Noël, J., Chemin, J., Guy, N., Blondeau, N., Voilley, N., Rubat-Coudert, C., et al. (2006). TREK-1, a K⁺ channel involved in polymodal pain perception. *EMBO J.* *25*, 2368–2376.
- Andres-Enguix, I., Shang, L., Stansfeld, P.J., Morahan, J.M., Sansom, M.S., Lafrenière, R.G., Roy, B., Griffiths, L.R., Rouleau, G.A., Ebers, G.C., et al. (2012). Functional analysis of missense variants in the TRESK (KCNK18) K channel. *Sci. Rep.* *2*, 237.
- Bates, E.A., Nikai, T., Brennan, K.C., Fu, Y.H., Charles, A.C., Basbaum, A.I., Ptáček, L.J., and Ahn, A.H. (2010). Sumatriptan alleviates nitroglycerin-induced mechanical and thermal allodynia in mice. *Cephalalgia* *30*, 170–178.
- Bautista, D.M., Sigal, Y.M., Milstein, A.D., Garrison, J.L., Zorn, J.A., Tsuruda, P.R., Nicoll, R.A., and Julius, D. (2008). Pungent agents from Szechuan peppers excite sensory neurons by inhibiting two-pore potassium channels. *Nat. Neurosci.* *11*, 772–779.
- Blin, S., Ben Soussia, I., Kim, E.J., Brau, F., Kang, D., Lesage, F., and Bichet, D. (2016). Mixing and matching TREK/TRAAK subunits generate heterodimeric K₂P channels with unique properties. *Proc. Natl. Acad. Sci. USA* *113*, 4200–4205.
- Brennan, K.C., Bates, E.A., Shapiro, R.E., Zyuzin, J., Hallows, W.C., Huang, Y., Lee, H.-Y., Jones, C.R., Fu, Y.-H., Charles, A.C., et al. (2013). Casein kinase II mutations in familial migraine and advanced sleep phase. *Sci. Transl. Med.* *5*, 183ra156, 1–11.
- Dobler, T., Springauf, A., Tovornik, S., Weber, M., Schmitt, A., Sedlmeier, R., Wischmeyer, E., and Döring, F. (2007). TRESK two-pore-domain K⁺ channels constitute a significant component of background potassium currents in murine dorsal root ganglion neurons. *J. Physiol.* *585*, 867–879.
- Flegel, C., Schöbel, N., Altmüller, J., Becker, C., Tannapfel, A., Hatt, H., and Gisselmann, G. (2015). RNA-seq analysis of human trigeminal and dorsal root ganglia with a focus on chemoreceptors. *PLoS ONE* *10*, e0128951.
- Guo, Z., Liu, P., Ren, F., and Cao, Y.Q. (2014). Nonmigraine-associated TRESK K⁺ channel variant C110R does not increase the excitability of trigeminal ganglion neurons. *J. Neurophysiol.* *112*, 568–579.
- Guyon, A., Tardy, M.P., Rovère, C., Nahon, J.L., Barhanin, J., and Lesage, F. (2009). Glucose inhibition persists in hypothalamic neurons lacking tandem-pore K⁺ channels. *J. Neurosci.* *29*, 2528–2533.
- Harris, H.M., Carpenter, J.M., Black, J.R., Smitherman, T.A., and Sufka, K.J. (2017). The effects of repeated nitroglycerin administrations in rats; modeling migraine-related endpoints and chronification. *J. Neurosci. Methods* *284*, 63–70.
- Hwang, E.M., Kim, E., Yarishkin, O., Woo, D.H., Han, K.S., Park, N., Bae, Y., Woo, J., Kim, D., Park, M., et al. (2014). A disulphide-linked heterodimer of TWIK-1 and TREK-1 mediates passive conductance in astrocytes. *Nat. Commun.* *5*, 3227.
- Jackson, R.J., Hellen, C.U., and Pestova, T.V. (2010). The mechanism of eukaryotic translation initiation and principles of its regulation. *Nat. Rev. Mol. Cell Biol.* *11*, 113–127.
- Jain, A., Liu, R., Xiang, Y.K., and Ha, T. (2012). Single-molecule pull-down for studying protein interactions. *Nat. Protoc.* *7*, 445–452.
- Johansen, F.F., Lambolez, B., Audinat, E., Bochet, P., and Rossier, J. (1995). Single cell RT-PCR proceeds without the risk of genomic DNA amplification. *Neurochem. Int.* *26*, 239–243.
- Kang, D., Choe, C., and Kim, D. (2005). Thermosensitivity of the two-pore domain K⁺ channels TREK-2 and TRAAK. *J. Physiol.* *564*, 103–116.
- Kochetov, A.V. (2008). Alternative translation start sites and hidden coding potential of eukaryotic mRNAs. *BioEssays* *30*, 683–691.
- Kopruszinski, C.M., Xie, J.Y., Eyde, N.M., Remeniuk, B., Walter, S., Stratton, J., Bigal, M., Chichorro, J.G., Dodick, D., and Porreca, F. (2017). Prevention of stress- or nitric oxide donor-induced medication overuse headache by a calcitonin gene-related peptide antibody in rodents. *Cephalalgia* *37*, 560–570.
- Kozak, M. (1984a). Compilation and analysis of sequences upstream from the translational start site in eukaryotic mRNAs. *Nucleic Acids Res.* *12*, 857–872.
- Kozak, M. (1984b). Point mutations close to the AUG initiator codon affect the efficiency of translation of rat preproinsulin in vivo. *Nature* *308*, 241–246.
- Kozak, M. (1999). Initiation of translation in prokaryotes and eukaryotes. *Gene* *234*, 187–208.
- Lafrenière, R.G., Cader, M.Z., Poulin, J.F., Andres-Enguix, I., Simoneau, M., Gupta, N., Boisvert, K., Lafrenière, F., McLaughlan, S., Dubé, M.P., et al. (2010). A dominant-negative mutation in the TRESK potassium channel is linked to familial migraine with aura. *Nat. Med.* *16*, 1157–1160.
- Landrum, M.J., Lee, J.M., Benson, M., Brown, G., Chao, C., Chitipiralla, S., Gu, B., Hart, J., Hoffman, D., Hoover, J., et al. (2016). ClinVar: public archive of interpretations of clinically relevant variants. *Nucleic Acids Res.* *44* (D1), D862–D868.
- Lazarus, S., McInerney-Leo, A.M., McKenzie, F.A., Baynam, G., Broley, S., Cavan, B.V., Munns, C.F., Puijts, J.E., Sillence, D., Terhal, P.A., et al. (2014). The IFITM5 mutation c.-14C > T results in an elongated transcript expressed in human bone; and causes varying phenotypic severity of osteogenesis imperfecta type V. *BMC Musculoskelet. Disord.* *15*, 107.
- Lek, M., Karczewski, K.J., Minikel, E.V., Samocha, K.E., Banks, E., Fennell, T., O'Donnell-Luria, A.H., Ware, J.S., Hill, A.J., Cummings, B.B., et al.; Exome Aggregation Consortium (2016). Analysis of protein-coding genetic variation in 60,706 humans. *Nature* *536*, 285–291.
- Lengyel, M., Cziráj, G., and Enyedi, P. (2016). Formation of functional heterodimers by TREK-1 and TREK-2 two-pore domain potassium channel subunits. *J. Biol. Chem.* *291*, 13649–13661.
- Levitz, J., Royal, P., Comoglio, Y., Wdziekonski, B., Schaub, S., Clemens, D.M., Isacoff, E.Y., and Sandoz, G. (2016). Heterodimerization within the TREK channel subfamily produces a diverse family of highly regulated potassium channels. *Proc. Natl. Acad. Sci. USA* *113*, 4194–4199.
- Liu, P., Xiao, Z., Ren, F., Guo, Z., Chen, Z., Zhao, H., and Cao, Y.Q. (2013). Functional analysis of a migraine-associated TRESK K⁺ channel mutation. *J. Neurosci.* *33*, 12810–12824.
- Long, H., Liao, L., Zhou, Y., Shan, D., Gao, M., Huang, R., Yang, X., and Lai, W. (2017). A novel technique of delivering viral vectors to trigeminal ganglia in rats. *Eur. J. Oral Sci.* *125*, 1–7.
- Morenilla-Palao, C., Luis, E., Fernández-Peña, C., Quintero, E., Weaver, J.L., Bayliss, D.A., and Viana, F. (2014). Ion channel profile of TRPM8 cold receptors reveals a role of TASK-3 potassium channels in thermosensation. *Cell Rep.* *8*, 1571–1582.
- Nishikawa, T., Ota, T., and Isogai, T. (2000). Prediction whether a human cDNA sequence contains initiation codon by combining statistical information and similarity with protein sequences. *Bioinformatics* *16*, 960–967.
- Noël, J., Zimmermann, K., Busserolles, J., Deval, E., Alloui, A., Diochot, S., Guy, N., Borsotto, M., Reeh, P., Eschalier, A., and Lazdunski, M. (2009). The mechano-activated K⁺ channels TRAAK and TREK-1 control both warm and cold perception. *EMBO J.* *28*, 1308–1318.

- Nosedá, R., and Burstein, R. (2013). Migraine pathophysiology: anatomy of the trigeminovascular pathway and associated neurological symptoms, cortical spreading depression, sensitization, and modulation of pain. *Pain* 154, S44–S53.
- Pradhan, A.A., Smith, M.L., McGuire, B., Tarash, I., Evans, C.J., and Charles, A. (2014). Characterization of a novel model of chronic migraine. *Pain* 155, 269–274.
- Sandoz, G., Levitz, J., Kramer, R.H., and Isacoff, E.Y. (2012). Optical control of endogenous proteins with a photoswitchable conditional subunit reveals a role for TREK1 in GABA(B) signaling. *Neuron* 74, 1005–1014.
- Sano, Y., Inamura, K., Miyake, A., Mochizuki, S., Kitada, C., Yokoi, H., Nozawa, K., Okada, H., Matsushime, H., and Furuichi, K. (2003). A novel two-pore domain K⁺ channel, TRESK, is localized in the spinal cord. *J. Biol. Chem.* 278, 27406–27412.
- Thomas, D., Plant, L.D., Wilkens, C.M., McCrossan, Z.A., and Goldstein, S.A. (2008). Alternative translation initiation in rat brain yields K2P2.1 potassium channels permeable to sodium. *Neuron* 58, 859–870.
- Ulbrich, M.H., and Isacoff, E.Y. (2007). Subunit counting in membrane-bound proteins. *Nat. Methods* 4, 319–321.
- Usoskin, D., Furlan, A., Islam, S., Abdo, H., Lönnberg, P., Lou, D., Hjerling-Leffler, J., Haeggström, J., Kharchenko, O., Kharchenko, P.V., et al. (2015). Unbiased classification of sensory neuron types by large-scale single-cell RNA sequencing. *Nat. Neurosci.* 18, 145–153.
- Verkest, C., Piquet, E., Diochot, S., Dauvois, M., Lanteri-Minet, M., Lingueglia, E., and Baron, A. (2018). Effects of systemic inhibitors of acid-sensing ion channels 1 (ASIC1) against acute and chronic mechanical allodynia in a rodent model of migraine. *Br. J. Pharmacol.* 175, 4154–4166.
- Walsh, Y., Leach, M.J., Veale, E.L., and Mathie, A. (2016). Identified regions of TREK and TRESK two pore domain potassium channels critical for inhibition by sipatragine and lamotrigine. *Proc. Physiol. Soc.* 37, PCB259.
- Wood, H. (2010). Migraine: familial migraine with aura is associated with a mutation in the TRESK potassium channel. *Nat. Rev. Neurol.* 6, 643.
- Yamamoto, Y., Hatakeyama, T., and Taniguchi, K. (2009). Immunohistochemical colocalization of TREK-1, TREK-2 and TRAAK with TRP channels in the trigeminal ganglion cells. *Neurosci. Lett.* 454, 129–133.
- Yan, J., and Dussor, G. (2014). Ion channels and migraine. *Headache* 54, 619–639.
- Zeisel, A., Hochgerner, H., Lönnberg, P., Johnsson, A., Memic, F., van der Zwan, J., Häring, M., Braun, E., Borm, L.E., La Manno, G., et al. (2018). Molecular architecture of the mouse nervous system. *Cell* 174, 999–1014.e22.

STAR★METHODS

KEY RESOURCES TABLE

REAGENT or RESOURCE	SOURCE	IDENTIFIER
Antibodies		
Anti-HA-7 (western)	Sigma	Cat# H9658
anti-TRESK	abcam	Cat# ab96868; RRID:AB_10863722
Atto 488	Sigma-Aldrich	Cat# 41051; RRID:AB_260092
Biotinylated anti-HA clone 16B12	BioLegend	Cat# 901501; RRID:AB_901501
Cy3	abcam	Cat# ab146452
Cy5	abcam	Cat# ab146454
TREK1	Blin et al., 2016	N/A
TREK2	Blin et al., 2016	N/A
Bacterial and Virus Strains		
MT2-IRES2EGFP in pAAV	This paper	Vectorology facility, PVM, Biocampus Montpellier
IRES2EGFP in pAAV	This paper	Vectorology facility, PVM, Biocampus Montpellier
Biological Samples		
Mice trigeminal ganglia	This paper	N/A
Rat trigeminal ganglia	This paper	N/A
Chemicals, Peptides, and Recombinant Proteins		
Biotin-PEG	Laysan Bio	Item# Biotin-PEG-SVA-3400
Collagenase type II	ThermoFisher	Cat#17101015
Dako Fluorescent Mounting medium	Dako Corporation	Code S3023
DMEM media	ThermoFisher	Cat# 10566-016
FBS	Sigma-Aldrich	Cat# F9665
ISDN Risordan®	Sanofi	N/A
Laminin	Sigma-Aldrich	Cat# L2020
Lipofectamine 2000	Invitrogen	Cat#11668027
Moloney murine leukemia virus reverse transcriptase	Invitrogen	Cat# 28025013
NeutrAvidin	ThermoFisher	Cat# 31000
PEG	Laysan Bio	Item# MPEG-SVA-5000
Polybrene	Sigma-Aldrich	Cat# TR-1003
Poly-L-lysine	Sigma-Aldrich	Cat#P4707
Protease inhibitors	Roche Diagnostics	Cat#4693116001
Random hexamers	ThermoFisher	Cat# N8080127
SuperScript II	ThermoFisher	Cat# 18064014
Topiramate	Sigma-Aldrich	Cat# T0575
Trypsin	Sigma-Aldrich	Cat# T1763
Critical Commercial Assays		
mMESSAGE mMACHINE T7 Transcription Kit	Invitrogen	Cat # AM1344
Nucleospin RNA Plus XS kit	MACHEREY-NAGEL GmbH & Co. KG	Cat# 740990.50
PowerUp SYBR Green Master Mix	ThermoFisher	Cat# A25742
Experimental Models: Cell Lines		
HEK293T	ATCC	Cat#CRL11268
Mouse primary neurons	This paper	N/A
<i>X. laevis</i> oocytes	This paper	N/A

(Continued on next page)

Continued		
REAGENT or RESOURCE	SOURCE	IDENTIFIER
Experimental Models: Organisms/Strains		
Mouse: C57BL/6J	Charles River Laboratories	Strain Code 027
Mouse: TREK1/TREK2 dKO	Guyon et al., 2009	N/A
Rat: Sprague Dawley	Janvier Labs	Strain RjHan:SD
Oligonucleotides		
GAPDH sens cctggagaaacctgccaagtatga	This paper	N/A
GAPDH reverse tgctgttgaagtgcaggaga	This paper	N/A
TREK1 forward catcttcacctgttgctg	This paper	N/A
TREK1 reverse atcatgctcagaacagctgc	This paper	N/A
TREK2 forward aacagtggtgccatctcg	This paper	N/A
TREK2 reverse ccagcaaagaagaaggcact	This paper	N/A
TRESK forward ctgcttccttgctgcctg	This paper	N/A
TRESK reverse aagaagagagcgtcaggaa	This paper	N/A
Recombinant DNA		
pcDNA3.1-GFP-X	This paper	N/A
pCMV-HA-X	This paper	N/A
pIRES2eGFP	Clontech	Cat#6029-1
Software and Algorithms		
Fiji/ImageJ	NIH	https://imagej.net/Fiji/Downloads
pClamp	Molecular Devices	http://mdc.custhelp.com/app/answers/detail/a_id/20260/~/axon%E2%84%A2-pclamp%E2%84%A2-11-electrophysiology-data-acquisition-%26-analysis-software
SigmaPlot	Systat Software Inc.	https://systatsoftware.com/products/sigmaplot/
Other		
Axioplan 2 Imaging Microscope	Zeiss	https://www.micro-shop.zeiss.com/?s=16103145829fcb6&l=en&p=us&f=a&i=10027
Axopatch 200A amplifier	Molecular Devices	https://fr.moleculardevices.com/products/axon-patch-clamp-system/amplifiers/axon-instruments-patch-clamp-amplifiers#ref
Camera EMCCD iXon	Andor	https://andor.oxinst.com/products/ixon-emccd-cameras
Dagan TEV-200A	Cornerstone	http://www.dagan.com/tev-200a.htm
Dynamic plantar aesthesiometer	Ugo Basil	Cat#: 37450
von Frey filaments	Bioseb	Modèle: Bio-VF-M

CONTACT FOR REAGENT AND RESOURCE SHARING

Further information and requests for resources and reagents should be directed to and will be fulfilled by the Lead Contact, Guillaume Sandoz (sandoz@unice.fr).

EXPERIMENTAL MODEL AND SUBJECT DETAILS

Knock-out mice

Mice lacking TREK1 and TREK2 were generated as described ([Guyon et al., 2009](#)). Null mutations were backcrossed against the C57BL/6J inbred strain for 10+ generations prior to establishing the breeding cages to generate subjects for this study. Age- and sex-matched C57BL/6J WT mice, aged 9-12 weeks, were obtained from Charles River Laboratories (Wilmington, MA).

HEK cells

HEK (human embryonic kidney) 293T cells were purchased from ATCC and maintained at 37°C, in 5% CO₂ in high glucose DMEM containing 10% fetal bovine serum and used from passage 10 to 40. One splitting per week was made on 35 mm diameter dishes.

Xenopus oocytes

Xenopus leavis oocytes were collected from female *Xenopus leavis* (agreement # 35382015121816318324V7) and dissociated using collagenase type IV (Levitz et al., 2016). Oocytes were injected with 50 nL of a cRNA at a concentration of 1 μg/μL and maintained at 18°C in ND96 solution (96 mM NaCl, 2 mM KCl, 2 mM MgCl₂, 1.8 mM CaCl₂, 5mM HEPES, pH 7.4). Oocytes were used 1 to 3 days after injections.

Rats

Experiments were performed on male Sprague Dawley rats (Janvier Labs) weighing 250 to 400 g (mean weight: 337 ± 16 g, 6 to 9 weeks old), and on male knock-out mice for TREK1 and TREK2 (weighting 20-25 g 7- to 13-weeks-old). Animals were housed in a 12 hour light-dark cycle with food and water available *ad libitum*. Animal procedures were approved by the Institutional Local Ethical Committee and authorized by the French Ministry of Research and the Spanish Ministry of Research according to the European Union regulations and the Directive 2010/63/EU (Agreements C061525 and 01550.03). Animals were sacrificed at experimental end points by CO₂ euthanasia.

WT mice

All mouse experiments were conducted according to national and international guidelines and have been approved by the local ethical committee (CIEPAL NCE). The C57BL/6J breeders were maintained on a 12 h light/dark cycle with constant temperature (23–24°C), humidity (45%–50%), and food and water *ad libitum* at the animal facility of Valrose.

METHOD DETAILS

Behavioral experiments

Drug administration and virus injection

For the topiramate experiment, mice were injected intraperitoneally with topiramate once at a dose of 30 mg/kg and mechanical nociception thresholds were assessed every 30 minutes for two hours after the injection.

The procedures of virus trigeminal injections are described by Long et al. (Long et al., 2017). Briefly, following general anesthesia with a cocktail of ketamine and xylazine (100 mg/kg and 10 mg/kg respectively *i.p.*), rats were shaved on the right side, which is the injected side, and placed on a warmed surgical plate. The site of injection was determined using a notch between the condylar process and the ipsilateral angular process. The depth of injection was 9 mm. Antibiotics were used 5 days following injections. Viral vector suspension (10 μL, 10¹¹ transduction unit) containing 6 μg/mL of Polybrene was injected slowly over 1 min. Rats in the experimental group (randomly selected, n = 14) received 10 μL of viral vector containing the MT2 protein sequence, while those in the control group (randomly selected, n = 14) received the same amount of EGFP viral vector. Injections were made in a blind way for the behavior experimenter. Epifluorescence imaging and qPCR were performed to verify successful transduction of trigeminal ganglia by viral vector.

Mechanical sensitivity measurements

The face mechanical sensitivity was measured using calibrated von Frey filaments (Bioseb, France). Unrestrained rats placed in individual plastic boxes on top of a wire surface were trained over one week to stimulation on the periorbital area, following a progressive protocol, starting with non-noxious filaments during the first 3 days of training. The face withdrawal force threshold (g) was determined by the filament evoking at least three responses over five trials, starting with lower force filaments. Basal values were determined 2 days before experiments. Animals showing an outlier threshold for the basal value were excluded from the study.

The hindpaw mechanical sensitivity was evaluated with a dynamic plantar aesthesiometer (Ugo Basile, Italy). Unrestrained mice were placed in 10 individual plastic boxes on top of a wire surface. The mouse hindpaw was submitted to a force ramp up to 7.5 g during 10 s, the paw withdrawal force threshold (g) was assessed in three consecutive trials with at least 3–5 min between the trials and averaged to select animals. Basal values were determined 2 days before experiments. Animals showing an outlier threshold for the basal value were excluded from the study.

Migraine rodent models

The rodent model of NO-induced migraine was induced by intraperitoneal (*i.p.*) injection of ISDN (Risordan®, Sanofi) at 10mg/kg, a long-lasting NO donor. The vehicle control used in these experiments was 0.9% saline. The acute mechanical allodynia induced by a single ISDN injection was followed on the hindpaw for mice and on the face for rats before (basal value) and for 3 hours after injection, every 30 minutes. Animals showing an outlier threshold for the basal value were excluded from the study. Chronic mechanical allodynia was induced by a single daily injection of ISDN during 4 days. The hindpaw extra-cephalic mechanical sensitivity was measured each day before the ISDN *i.p.* injection for mice. Topiramate was tested on chronic mechanical allodynia on the 5th day and effects were followed every 30 min during 2 hours after injection in mice. Experiments were made on two batches of animals in duplicate.

Electrophysiology

HEK293T cell electrophysiology was performed 24–72 h after Lipofectamine transfection (with 1 to 1.6 μg DNA) in solution containing (in mM): 145 mM NaCl, 4 mM KCl, 1 mM MgCl_2 , 2 mM CaCl_2 and 10 mM HEPES. For co-expression of K2P channels and mutant channels, a DNA ratio of 1:1 was used. Glass pipettes of resistance between 3 and 6 $\text{M}\Omega$ were filled with intracellular solution containing (in mM): 140 KCl, 10 HEPES, 5 EGTA, 3 MgCl_2 , pH 7.4. Cells were patch clamped using an Axopatch 200A (Molecular Devices) amplifier in the whole cell mode. Currents were elicited by voltage-ramps (from -100 to 100 mV, 1 s in duration) and the current density was calculated at 0 mV.

Oocyte two-electrode voltage clamp electrophysiology was performed in a 0.3-mL perfusion chamber; a single oocyte was impaled with two standard microelectrodes (1–2.5 $\text{M}\Omega$ resistance) filled with 3 M KCl, and maintained under voltage clamp using a Dagan TEV 200 amplifier in standard ND96 solution [96 mM NaCl, 2 mM KCl, 1.8 mM CaCl_2 , 2 mM MgCl_2 , 5 mM HEPES pH 7.4 with NaOH]. For the high K^+ solution contained 80 mM K^+ , 78 mM NaCl was replaced by KCl. Stimulation of the preparation, data acquisition, and analysis were performed using pClamp software (Molecular Devices).

Neuronal excitability was studied in small-diameter TG neurons transfected with 1 μg of the pIRES2EGFP vector containing the X insert in which there is no N-terminal tag on the insert and EGFP is co-translated as a transfection marker or the pIRES2EGFP control plasmid with Lipofectamine 2000. Extracellular solution contained (in mM): 135 NaCl, 5 KCl, 2 CaCl_2 , 1 MgCl_2 , 5 HEPES, 10 glucose, pH 7.4 with NaOH, 310 mOsm. The pipette solution contained the following (in mM): 140 K-gluconate, 10 NaCl, 2 MgCl_2 , 5 EGTA, 10 HEPES, 2 ATP-Mg, 0.3 GTP-Na, 1 CaCl_2 pH 7.3 with KOH, 290 mOsm. Recording pipettes had < 4.5 $\text{M}\Omega$ resistance. Series resistance (< 20 $\text{M}\Omega$) was not compensated. Signals were filtered at 10 kHz and digitized at 20 kHz. After establishing whole-cell access, membrane capacitance was determined with amplifier circuitry. The amplifier was then switched to current-clamp mode to measure resting membrane potential (V_{rest}). Neurons were excluded from analysis if the V_{rest} was higher than -40 mV or if the input resistance was smaller than 200 $\text{M}\Omega$. To test neuronal excitability, neurons were held at V_{rest} and injected with 1 s depolarizing currents in 25 pA incremental steps until at least 1 action potential (AP) was elicited.

Immunocytochemistry

Transfected neurons on coverslips were fixed with PBS containing 4% paraformaldehyde for 15 minutes at room temperature (RT), then permeabilized with PBS and 0.1% Triton X-100 (PBST) and blocked for 1h with 5% horse serum (HS) in PBST. Primary and secondary antibodies were diluted in PBST and 5% HS and incubated for 1h at RT. Three 5-min washes with PBST were carried out between each incubation step and at the end of the procedure. Coverslips were mounted in Dako Fluorescent Mounting medium (Dako Corporation, Carpinteria, CA, USA). The following antibodies were used: rabbit anti-TREK1 and TREK2 (Blin et al., 2016), anti-TRESK (ab96868, abcam) conjugated with Cy3 (ab146452, abcam), Cy5 (ab146454, abcam) and Atto 488 (Sigma) respectively. Microscopy analysis and data acquisition were carried out with an Axioplan 2 Imaging Microscope (Zeiss®).

Molecular Biology, Cell Culture and Gene Expression

Channel DNA was used in the pIRES2eGFP, pcDNA3.1 and pCMV-HA vectors. HEK293T cells were maintained in DMEM with 5% FBS on poly-L-lysine-coated glass coverslips in 12 well plates. Cells were transiently co-transfected using Lipofectamine 2000 (Invitrogen) with a total of 1–1.6 μg of DNA total per 35 mm dish. When two genes were co expressed, a ratio of 1:1 DNA was used.

PCR amplification and quantification

Semiquantitative PCR were performed to determine the relative levels of TREK1, TREK2, and TRESK after RNA extraction and reverse transcription using primers described below. qPCR (10 μL) was performed using the aforementioned reverse-transcribed cDNA (4 μL) and the primers for TREK1 (forward: catcttcacacctgttgctg, reverse: atcatgctcagaacagctgc, 240 pb), TREK2 (forward: aacagtgggtgccatcttcg, reverse: ccagcaaagaagaaggcact, 276 pb), TRESK (forward: ctgcttccttgctgcctg, reverse: aagaagagagcgctcaggaa, 256 pb) and GAPDH (forward: cctggagaaacctgccaagtatga, reverse: tgctgtgaagtcgcaggaga) as a reference. After initial denaturation at 95°C for 15 s, 40 cycles of amplification (95°C for 15 s and 60°C for 1 minute) were performed.

Quantitative PCR were performed to determine the levels of GFP after inoculation of adenovirus vectors containing GFP MT2 sequences into trigeminal ganglia using the same protocol with specific primers for the GFP (forward: aagctgaccctgaagttcatctgc, reverse: cttgtagtgccctgccttgaa).

Analysis were made using the GAPDH as the housekeeping gene along with the $2^{-\Delta\Delta\text{Ct}}$ Calculation Method.

Primary cultures of mouse TG neurons

Trigeminal ganglion tissues were collected from postnatal day 8 mice of either sex and treated with 2 mg/ml collagenase type II (Worthington) for ~ 2 hours, followed by 2.5 mg/ml trypsin for 15 min. Neurons were dissociated by triturating with fire-polished glass pipettes and seeded on polylysine/laminin coated coverslips. The DMEM-based culture medium contained 10% fetal bovine serum and 2mM GlutaMAX (Invitrogen). Neurons were transfected at 1 *d in vitro* (DIV) with 1 μg of DNA using Lipofectamine 2000 (Invitrogen). Transfected neurons were identified by the green fluorescence and patch clamp recordings were performed between DIV 3 and 5.

Single Molecule Pulldown (SiMPull)

For SiMPull experiments, a DNA ratio of 1:1 was used, with a total quantity of 1 μg . 24 hours after transfection, HEK 293T cells were harvested from coverslips by incubating with Ca^{2+} -free PBS buffer for 20–30 minutes followed by gentle pipetting. Cells were lysed in buffer containing (in mM): 150 NaCl, 10 Tris pH 7.5, 1 EDTA, protease inhibitor cocktail (Thermo Scientific) and 1.5% IGEPAL (Sigma) or 1% DDM (Sigma). After 30–60 minute incubation at 4°, lysate was centrifuged for 20 minutes at 12,500 g and the supernatant was collected. Coverslips passivated with PEG (~99%)/ biotin-PEG (~1%) and treated with NeutrAvidin (Pierce) were prepared as described (Jain et al., 2012). 15 nM biotinylated anti-HA antibody (clone 16B12, BioLegend) was applied for 20 minutes and then washed out. Antibody dilutions and washes were done in T50 buffer with BSA containing (in mM): 50 NaCl, 10 Tris pH 7.5, and 0.1 mg/mL BSA. Lysate, diluted in lysis buffer containing 0.04% IGEPAL, was then applied to the chamber and washed away following brief incubation (~2 minutes). Single molecules were imaged using a 488 nm Argon laser on a total internal reflection fluorescence microscope with a 60x objective (Olympus). We recorded the emission light after an additional 3x magnification and passage through a double dichroic mirror and an emission filter (525/50 for GFP) with a back-illuminated EMCCD camera (Andor iXon DV-897 BV). Recordings were made in blind for the experimenter before being analyzed.

Single cell reverse transcription

The procedures of single cell RT-PCR are adapted from Johansen et al. (Johansen et al., 1995). The content of each cell was aspirated into the patch pipette by applying negative pressure. The flow of the cytosol in the pipette as well as the aspiration of the nucleus was controlled under the microscope. Only cell samples which included the nucleus were investigated in the present study.

The pipette was then released from the holder and mounted on a syringe to expel its content into a test tube. To the ~6.5 μL of the pipette-content expelled into the test tube was added 3.5 μL of a solution containing random hexamers (Invitrogen, 5 μM final concentration), dithiothreitol (DTT, final concentration 10 mM), the four deoxyribonucleotide triphosphates (dNTP, Thermo Fisher, final 0.5 mM each), 20 U ribonuclease inhibitor (Promega), and 100 U Moloney murine leukemia virus reverse transcriptase (Invitrogen).

The total 10 μL reaction was incubated for 1 h at 35°C for synthesis of single stranded cDNA, and then kept on ice until PCR.

Trigeminal neurons RNA extraction and reverse transcription

Total RNA was isolated from trigeminal neurons in suspension using a Nucleospin RNA Plus XS kit (from MACHEREY-NAGEL GmbH & Co. KG) according to the manufacturer's protocols and 1 μg of RNA was reverse transcribed (with 10 nM random hexamers for 5 min at 65°C, then with 10 mM DTT, 0.5 mM each dNTP, 100 U SuperScript II (Invitrogen) 42°C for 50 min). Subsequently, the cDNA was quantified by qPCR with PowerUp SYBR Green Master Mix (ThermoFisher).

Vector preparation

Adenovirus vector (DJ) encoding an IRES2EGFP or MT2-IRES2EGFP were used. Following linearization, this vector was recombined with the mouse version of the MT2 protein. The recombinant was amplified with PCR, and DNA sequencing was performed to verify the DNA sequence. Viral vectors were packaged and harvested by transfection of HEK293T cells, followed by quantification of the viral titer through quantitative PCR. In addition, as a control, an adenovirus vector containing only the IRES2EGFP sequence was used.

Western blot analysis

24 to 48 hours after transfection using 1 μg DNA with Lipofectamine 2000, HEK293T cells were homogenized in PBS containing saponin (0.5% w/v), Triton X-100 (0.5% w/v) and protease inhibitors (Roche Diagnostics, Basel, Switzerland). Lysates were clarified by centrifugation at 20 000 g for 30 min. Proteins were separated on 10% SDS polyacrylamide gel and blotted onto nitrocellulose membrane (Hybond-C extra, Amersham Biosciences, Freiburg, Germany). Detection was carried out using mouse monoclonal antibody clone HA-7 against the HA epitope (Sigma-Aldrich).

QUANTIFICATION AND STATISTICAL ANALYSIS

Single Molecule Pulldown

Movies of 250–500 frames were acquired at frame rates of 10–30 Hz. The imaged area was 13 \times 13 μm^2 . At least 5 movies were recorded for each condition and data was analyzed using custom software. Multiple independent experiments (at least 3 times) were performed for each condition. Representative datasets are presented to quantitatively compare conditions tested on the same day.

Electrophysiology

The numbers of cells tested are indicated in parentheses on top of graphs in each figure. Cells come from at least 3 batches of experiment. Student's t test (* $p < 0.05$, ** $p < 0.01$, *** $p < 0.001$) are performed between the different conditions tested (indicated in each figure's legend). For neurons, the cells come from at least 4 different animals. When the data did not follow a normal distribution, Mann-Whitney U test were assessed.

Animal experiment

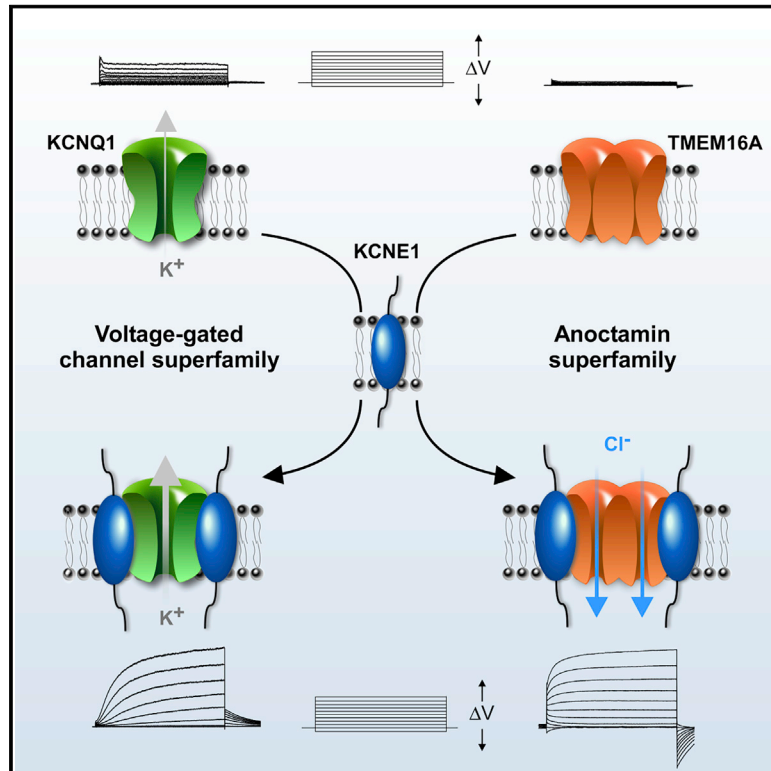
Numbers of mice and rats tested are indicated in parentheses in each figure. Student's t test to compare WT versus *TREK1*^{-/-}/*TREK2*^{-/-} mice (*p < 0.05, **p < 0.01, ***p < 0.001).

Quantitative PCR

Analysis were made using the GAPDH as the housekeeping gene along with the 2- $\Delta\Delta$ Ct Calculation Method. n represents the number of single cells tested.

KCNE1 is an auxiliary subunit of two distinct ion channel superfamilies

Graphical Abstract



Authors

Pablo Ávalos Prado, Stephanie Häfner, Yannick Comoglio, ..., Bernard Attali, Jacques Barhanin, Guillaume Sandoz

Correspondence

sandoz@unice.fr

In Brief

KCNE1, a β -subunit of the cardiac KCNQ1 channel belonging to the voltage-dependent channel superfamily, serves also as an auxiliary subunit of the anoctamin superfamily member TMEM16A, a calcium-activated chloride channel. By interacting with TMEM16A, KCNE1 induces a voltage-dependent current in the absence of intracellular calcium elevation dynamically regulated by angiotensin II in native tissue.

Highlights

- KCNE1 can serve as an auxiliary subunit of two superfamilies of ion channels
- KCNE1 is an auxiliary subunit of the TMEM16A chloride channel
- TMEM16A-KCNE1 channel mediates a voltage-gated Cl⁻ current independently of Ca²⁺
- KCNE1 S38G and R32H polymorphisms abolish the KCNE1-TMEM16A Cl⁻ current

Article

KCNE1 is an auxiliary subunit of two distinct ion channel superfamilies

Pablo Ávalos Prado,^{1,2} Stephanie Häfner,^{1,2} Yannick Comoglio,^{1,2} Brigitte Wdziekonski,^{1,2} Christophe Duranton,^{2,3} Bernard Attali,⁴ Jacques Barhanin,^{2,3} and Guillaume Sandoz^{1,2,5,*}

¹Université Côte d'Azur, CNRS, INSERM, iBV, Nice, France

²Laboratories of Excellence, Ion Channel Science and Therapeutics, Nice, France

³Université Côte d'Azur, CNRS, LP2M, Medical Faculty, Nice, France

⁴Department of Physiology and Pharmacology, Sackler Faculty of Medicine and Sagol School of Neurosciences, Tel Aviv University, Tel Aviv, Israel

⁵Lead Contact

*Correspondence: sandoz@unice.fr

<https://doi.org/10.1016/j.cell.2020.11.047>

SUMMARY

Determination of what is the specificity of subunits composing a protein complex is essential when studying gene variants on human pathophysiology. The pore-forming α -subunit KCNQ1, which belongs to the voltage-gated ion channel superfamily, associates to its β -auxiliary subunit KCNE1 to generate the slow cardiac potassium I_{Ks} current, whose dysfunction leads to cardiac arrhythmia. Using pharmacology, gene invalidation, and single-molecule fluorescence assays, we found that KCNE1 fulfils all criteria of a bona fide auxiliary subunit of the TMEM16A chloride channel, which belongs to the anoctamin superfamily. Strikingly, assembly with KCNE1 switches TMEM16A from a calcium-dependent to a voltage-dependent ion channel. Importantly, clinically relevant inherited mutations within the TMEM16A-regulating domain of KCNE1 abolish the TMEM16A modulation, suggesting that the TMEM16A-KCNE1 current may contribute to inherited pathologies. Altogether, these findings challenge the dogma of the specificity of auxiliary subunits regarding protein complexes and questions ion channel classification.

INTRODUCTION

KCNE1 is a 129-residue peptide, with a single short hydrophobic membrane spanning domain and carboxy- and amino-terminal domains facing toward the intracellular and extracellular side, respectively (Takumi et al., 1988). When injected in *Xenopus laevis* oocytes, KCNE1 produces a slowly activating K^+ current (Takumi et al., 1988). For this reason, KCNE1 was initially believed to be the minimal sequence that could encode for a K^+ channel (Goldstein and Miller, 1991; Wang and Goldstein, 1995). Experiments using other heterologous cell models questioned this finding, because expression of KCNE1 alone is not able to induce current in mammalian cell lines (Lesage et al., 1993). This enigma was resolved by the discovery that *Xenopus* oocytes express endogenous KCNQ1 channels, which are modulated by KCNE1 (Barhanin et al., 1996; Sanguinetti et al., 1996). These experiments showed that KCNE1 does not encode for a pore-forming α -subunit but for an ancillary (β) subunit of the voltage-dependent potassium KCNQ1 channel. Association between KCNQ1 and KCNE1 underlies the slow repolarizing component in the cardiac action potential (I_{Ks}) (Barhanin et al., 1996; Sanguinetti et al., 1996). In addition to the K^+ current described above, a voltage-dependent Cl^- current was

observed upon injection of cRNA of KCNE1 in *Xenopus* oocytes (Attali et al., 1993), and up to now, the molecular identity of this current has remained elusive.

Ca^{2+} -activated Cl^- channels (CaCCs), belonging to the anoctamin protein superfamily, play a major role in cell physiology, including signal transduction, regulation of cardiac and neuronal excitability, epithelial secretion, and muscle contraction, among others (Hartzell et al., 2005; Pedemonte and Galletta, 2014). TMEM16A was the first member of this superfamily to be cloned by three independent laboratories, using different approaches (Caputo et al., 2008; Schroeder et al., 2008; Yang et al., 2008). Ten anoctamin members have been found in mammals, but only TMEM16A and TMEM16B have been demonstrated to be full CaCCs, whereas the rest of the family operates as scramblases that rapidly and bidirectionally translocate lipids maintaining the asymmetry of the plasma membrane (Falzone et al., 2018; Pedemonte and Galletta, 2014). The structure of TMEM16A has been recently elucidated, defining the channel as a homodimer constituted of ten transmembrane domains per subunit (Dang et al., 2017; Peters et al., 2018). TMEM16A represents the major chloride channel in *Xenopus* oocytes (Schroeder et al., 2008), where it mediates fast polyspermy block (Wozniak et al., 2018). Nevertheless, no β -subunit has been identified for this channel up to now.

Because of its high expression in *Xenopus* oocytes (Schroeder et al., 2008), we hypothesize in the present manuscript that KCNE1 may serve as a β -subunit of the pore-forming TMEM16A α -subunits to induce the voltage-gated Cl^- current, which was described almost 30 years ago (Attali et al., 1993). We demonstrate here that KCNE1 interacts physically with TMEM16A with a $2\alpha:2\beta$ stoichiometry using electrophysiology in heterologous and native systems and single molecule pull-down assays. This interaction induces a sustained voltage-dependent chloride current in the absence of elevated cytoplasmic Ca^{2+} , which, physiologically, responds to the blood pressure regulating renin-angiotensin system in proximal tubule cells. Importantly, we find that clinically relevant inherited polymorphisms within the KCNE1-regulating domain, including the common S38G polymorphism, abolish the KCNE1-dependent regulation of TMEM16A, indicating that this current may contribute to inherited pathologies such as cardiac arrhythmia. Our results demonstrate that KCNE1 fulfils all criteria of an auxiliary subunit of chloride channels. Therefore, KCNE1 associates with and modulates two distinct classes of protein superfamilies: the voltage-gated ion channels and the anoctamins. This finding should be considered when analyzing functional impacts of KCNE1 gene variants on human pathophysiology.

RESULTS

KCNE1 shifts TMEM16A from a calcium-dependent to a voltage-dependent Cl^- channel

To test the ability of KCNE1 to regulate TMEM16A, we used the heterologous HEK293T cell model, which expresses neither TMEM16A nor KCNE1 endogenously. Whereas transfection of HEK293T cells with either TMEM16A or KCNE1 alone produced no significant current, co-expression of both proteins induced a voltage-dependent current, whose density was of 18.1 ± 2.8 pA/pF at +100 mV (Figures 1A and 1B). The reversal potential was -4.8 ± 1.3 mV, which is similar to the expected reversal Cl^- potential in the experimental conditions used. This chloride current was inhibited by niflumic acid (NFA), T16Ainh-A01 (Davis et al., 2013), and also by Ani9, the most specific TMEM16A inhibitor (Seo et al., 2016; Figures 1C and 1D). As expected, the TMEM16A-KCNE1 current presented higher permeability for large anions with lower hydration energy, as it has been shown before for TMEM16A alone in the presence of calcium (Table S1; Caputo et al., 2008; Schroeder et al., 2008; Yang et al., 2008). In addition, the channel does not become cation permeable, because replacement of the external solution by a 15 mM NaCl solution supplemented with D-mannitol allowed us to determine a $P_{\text{Na}}/P_{\text{Cl}}$ of ~ 0.1 . This value is consistent with the calculated prediction through the Goldman-Hodgkin-Katz equation in our conditions (see Equation 1 in the STAR methods) and similar to the reported value (Yang et al., 2008; Peters et al., 2018). This suggests that KCNE1 switches TMEM16A from a calcium-dependent to a voltage-dependent chloride channel.

To preclude the possibility that KCNE1 activates endogenous calcium channels, we conducted similar experiments in the presence of the fast calcium chelator BAPTA (Figures 1E and 1F). As shown in Figure 1F, BAPTA did not affect the voltage-dependent current evoked by the TMEM16A-KCNE1 complex. To rule out a

potential modulation of endogenous calcium channels by KCNE1 leading to TMEM16A activation, we co-expressed KCNE1 with the Ca^{2+} -activated SK4 channel, which has a similar calcium sensitivity as TMEM16A (Cao and Houamed, 1999). KCNE1 overexpression did not induce any increase of the SK4 current in the absence of calcium (Figures 1G and 1H). Altogether, these results exclude an implication of intracellular Ca^{2+} in the KCNE1-induced and voltage-dependent activation of TMEM16A.

TMEM16A does not have any obvious classical voltage-sensor domains, but several cytoplasmic and transmembrane domains have been shown to be implicated in its regulation by voltage, including the first intracellular loop (Xiao et al., 2011) and the sixth transmembrane domain (TM6) (Peters et al., 2018). To determine which domain is involved in the KCNE1-induced voltage-gating of the channel, we first tested the effect of KCNE1 on the mutation ${}_{444}\text{EEEE}_{447}/{}_{444}\text{AAAA}_{447}$ that is known to abolish the intrinsic TMEM16A voltage-dependence (Xiao et al., 2011). The mutation ${}_{444}\text{EEEE}_{447}/{}_{444}\text{AAAA}_{447}$ did not prevent channel regulation by KCNE1, ruling out the hypothesis that KCNE1 modifies the gating of TMEM16A by acting on the intrinsic voltage-dependence linked to this domain (Figure S1). We then tested the role of the TMEM16A TM6 domain using two TMEM16A mutants bearing the TM6 mutations I637A and Q645A, which enable the channel to be activated in the absence of calcium (Peters et al., 2018). As expected, these two mutants produced current in the absence of elevated Ca^{2+} , but no additional effect was observed upon co-expression of KCNE1 (Figures 2A–2C). The absence of an additive effect strongly supports the idea that KCNE1 modulates channel gating by acting on the TM6 conformation. This conformation mimics a single Ca^{2+} occupancy state as it has been demonstrated for both mutations (Figures 2B and 2C; Peters et al., 2018). Supporting this, we found that the conductance versus V_m curve observed for TMEM16A + KCNE1 overlaps with the curve obtained with TMEM16A alone at moderate calcium concentrations (0.5 μM) (Figure 2D). Despite of their ability to enable channel activation in the absence of calcium, the TM6 I637A and Q645A mutants are still modulated by Ca^{2+} (Peters et al., 2018). Therefore, we assessed the calcium sensitivity of the TMEM16A-KCNE1 current. Similarly to both mutants, TMEM16A-KCNE1 presented a calcium sensitivity (Figures 2E, 2F, and S2) reinforcing the idea that KCNE1 modulates channel gating by acting on the TM6 conformation. We also evaluated the impact of KCNE1 co-expression on channel density and found that there was no effect of KCNE1 on it. In fact, at saturating calcium concentrations no difference in current densities was observed between cells expressing TMEM16A alone and TMEM16A + KCNE1 (Figure 2F).

TMEM16A activation by KCNE1 involves physical interaction

To be considered as an auxiliary subunit, a protein has to interact directly and stably with the α -subunits. To test the physical association between KCNE1 and TMEM16A, we used the recently developed single molecule pull-down (SiMPull) assay (Jain et al., 2011; Levitz et al., 2016; Royal et al., 2019). By direct visualization of antibody-immobilized protein complexes (Figures 3A and 3E), this technique allows one to determine the composition

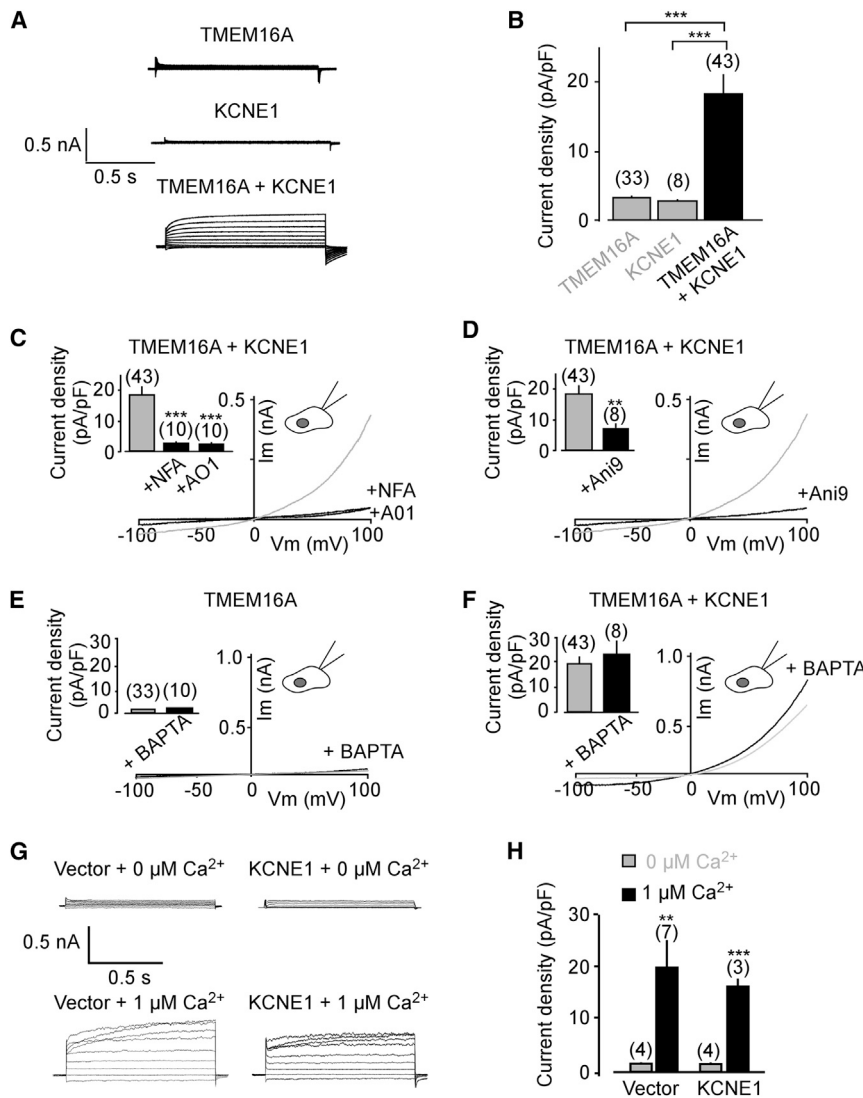


Figure 1. KCNE1 converts the CaCC TMEM16A into a voltage-dependent chloride channel

(A) Representative current traces showing the effect of expression of either KCNE1 or TMEM16A or both TMEM16A and KCNE1 in HEK293T cells. Traces were generated using pulses between -100 and +100 mV at 20 mV intervals from a holding potential of -80 mV.

(B) Summary of current densities obtained at +100 mV.

(C and D) Representative traces showing the effect of application of either niflumic acid (NFA) (100 μ M, C), T16A(inh)A01 (10 μ M, D) or Ani9 (300 nM, D).

(E and F) Representative traces of TMEM16A alone (E) or co-expressed with KCNE1 (F) in the presence of 1 mM of BAPTA. Currents were elicited by voltage-ramps (from -100 to +100 mV, 1 s duration), insets show a summary of current densities obtained at +100 mV.

(G and H) KCNE1 co-expression does not activate SK4 current.

(G) Representative current traces obtained from HEK293T cells co-transfected with SK4 and either an empty vector or KCNE1 in the presence or absence of 1 μ M cytosolic Ca^{2+} . Traces were generated using pulses between -100 and +100 mV at 20-mV intervals from a holding potential of -80 mV.

(H) Summary of current densities obtained at +100 mV. Mann-Whitney test (** $p < 0.01$, *** $p < 0.001$). Mean \pm SEM. See also [Figure S3](#) and [Table S1](#).

and stoichiometry within single protein complexes by counting fluorophore bleaching (Jain et al., 2011; Levitz et al., 2016; Royal et al., 2019). After co-transfection with the two putative partners KCNE1 and TMEM16A, one of them fused to an HA affinity tag and the other to a GFP label, and subsequent pull-down, we observed many fluorescent spots for both conditions, TMEM16A-GFP + HA-KCNE1 (Figure 3B) and KCNE1-GFP + HA-TMEM16A (Figure 3F). This demonstrates a physical interaction between KCNE1 and TMEM16A. Importantly, when HA-KCNE1 or HA-TMEM16A were not co-expressed, no proteins fused to GFP were isolated (Figures 3I–3L), confirming the specificity of the HA-antibody that we used in our SiMPull assays. By analyzing bleaching steps for immobilized HA-KCNE1-TMEM16A-GFP complexes, we were able to determine the number of TMEM16A-GFP subunits within the complex. We found that the majority of fluorescence intensity trajectories showed two-step bleaching (~70%), with the remaining spots bleaching in one step (~20%) or occasionally three steps

most complexes presented two bleaching steps (~65%) and some remaining spots bleached in one (~25%) and three steps (~10%) (Figures 3G and 3H). This distribution corresponds to the presence of two KCNE1-GFP subunits within the protein complex. Therefore, two KCNE1 subunits assemble with two TMEM16A subunits (Dang et al., 2017; Takumi et al., 1988), following a $2\alpha:2\beta$ stoichiometry.

The KCNEs-dependent regulation of TMEM16A is not restricted to KCNE1

The anoctamin family is constituted of ten members, but only TMEM16A and TMEM16B have been demonstrated to be full CaCCs (Schroeder et al., 2008). We assessed the ability of the KCNE1 to modulate the TMEM16B current. Co-expression of TMEM16B with KCNE1 did not induce any chloride current at rest, nor did any other KCNE subunit (Figure S3A). The KCNE family comprises five members that show a similar structure despite their low homology (Crump and Abbott, 2014). The

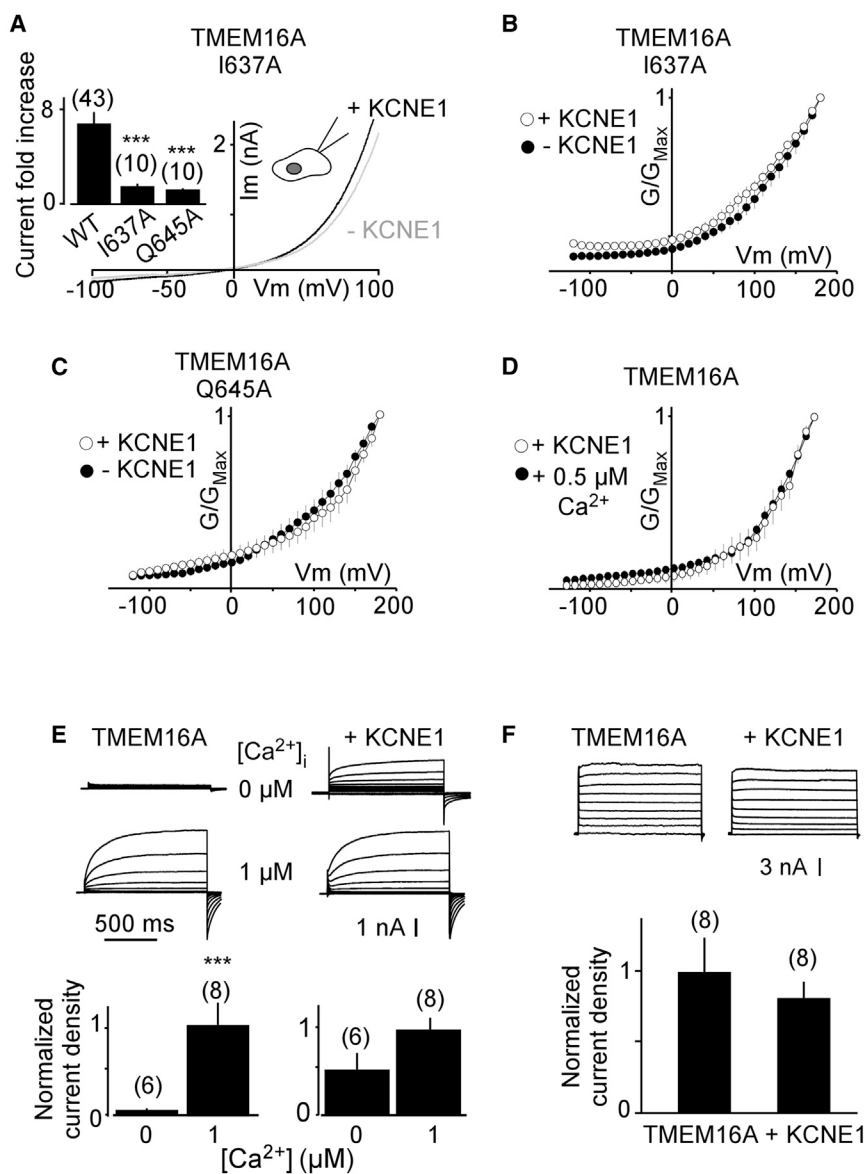


Figure 2. I637A and Q645A in the TM6 of TMEM16A are key residues for channel regulation by KCNE1 and calcium

(A) Representative current traces showing the effect of expression of either TMEM16A I637A alone or TMEM16A I637A + KCNE1 in HEK293T cells. Currents were elicited by voltage-ramps (from -100 to $+100$ mV, 1 s duration), insets show a summary of current density fold increase induced by KCNE1 co-expression at $+100$ mV in the wild-type and TM6 mutant forms.

(B and C) KCNE1 does not modify the voltage sensitivity of TMEM16A-TM6 I637A and Q645A mutants. G/G_{Max} versus V_m curves for I637A (B) and Q645A (C) mutants expressed alone or co-expressed with KCNE1 in whole-cell patch clamp. (D) TMEM16A activation at a moderate calcium concentration. G/G_{Max} versus V_m curves for TMEM16A alone in the presence of $0.5 \mu\text{M Ca}^{2+}$ and TMEM16A co-expressed with KCNE1.

(E and F) Calcium sensitivity of TMEM16A-KCNE1 channel complex.

(E) Whole cell current traces showing TMEM16A and TMEM16A + KCNE1 currents in the presence or absence of $1 \mu\text{M [Ca}^{2+}]_i$. Bar graph represents relative current densities of TMEM16A and TMEM16A + KCNE1 at the two different calcium concentrations.

(F) Sample traces from whole-cell patch-clamp recording of HEK293T cells expressing either TMEM16A alone or co-expressed with KCNE1, stepped from -80 to $+80$ mV in 20 mV steps from a holding potential of -80 mV at saturating $[Ca^{2+}]_i$. Bar graph represents normalized current densities of TMEM16A and TMEM16A + KCNE1 at a saturating calcium concentration showing a similar maximal current amplitude with or without KCNE1. Mann-Whitney test ($***p < 0.001$). Mean \pm SEM. See also [Figures S1 and S2](#).

different members of this family have been found to differently regulate the KCNQ1 channel (Bendahhou et al., 2005). We studied TMEM16A regulation by the different KCNE subunits and observed that, as demonstrated for KCNE1, only KCNE5 was able to induce a sustained chloride current in the absence of intracellular elevation of Ca^{2+} (Figures S3B and S3C). KCNE5 was also found to interact with TMEM16A at the single molecule level (Figures S3D and S3E).

The complex KCNE1-TMEM16A generates voltage-dependent Cl^- currents in proximal convoluted tubule cells

To be considered as a bona fide auxiliary subunit, the protein must interact with the alpha subunits in a native environment. To confirm that KCNE1 is an auxiliary subunit of TMEM16A in native tissue and to eliminate possible artifacts due to heterolo-

gous overexpression, we took advantage of kidney proximal convoluted tubule (PCT) cells obtained from wild-type and *kcnk1* knockout (KO) mice (Barrière et al., 2003). PCT cells are considered as a relevant model as they naturally co-express both TMEM16A and KCNE1 (Faria et al., 2014; Vallon et al., 2001) and do not necessitate any genetic manipulation to record TMEM16A currents. Moreover, while no modification of the K^+ current was found in PCT cells from *kcnk1* KO mice compared to wild-type, a DIDS (4,4'-diisothiocyanostilbene-2,2'-disulfonic acid)-sensitive Cl^- conductance was impaired (Barrière et al., 2003). We confirmed the loss of current, whose reversal potential was similar to the expected Cl^- reversal potential in *kcnk1* null PCT cells (18.07 ± 1.21 pA/pF versus 5.37 ± 0.56 pA/pF for PCT cells from wild-type and KO mice, respectively) (Figure 4A). This current was inhibited by NFA (4.51 ± 0.28 pA/pF), T16Ainh-AO1 (5.52 ± 0.72 pA/pF), and Ani9 (2.88 ± 0.38 pA/pF) (Figures 4B–4D). Moreover, knock down of TMEM16A by a previously validated small interfering RNA (siRNA) transfection (Sala-Rabanal et al., 2017) in wild-type PCT cells significantly reduced the

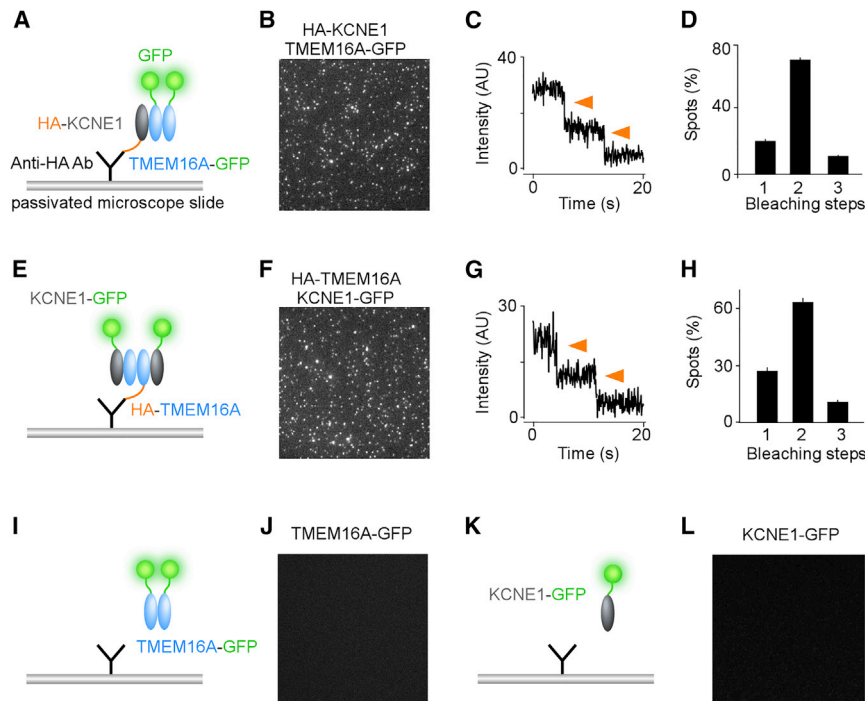


Figure 3. KCNE1 and TMEM16A interact in a 2 α :2 β complex

(A) Schematic of single molecule pull-down (SiM-Pull) assay of TMEM16A. Lysates of HEK293T cells co-expressing TMEM16A-GFP and HA-tagged KCNE1 were immobilized on a PEG-passivated coverslip conjugated to a biotinylated anti-HA antibody.

(B) Representative TIRF image of single molecules showing the pull-down of TMEM16A-GFP by HA-KCNE1.

(C) Representative trace showing two photobleaching steps (orange arrows) of TMEM16A-GFP (a.u., arbitrary units).

(D) Summary of photobleaching step distribution for TMEM16A-GFP.

(E–H), same as (A)–(D) for the SiMPull of KCNE1-GFP by HA-TMEM16A.

(I–L) Specificity of the anti-HA antibody.

(I–J) SiMPull assay with TMEM16A-GFP in the absence of HA-KCNE1.

(K and L) SiMPull assay with KCNE1-GFP in the absence of HA-TMEM16A.

See also Figure S3.

Cl^- current amplitude (4.23 ± 0.48 pA/pF) (Figure 4E). This demonstrates the involvement of TMEM16A subunits in the channel complex responsible for the herein studied Cl^- current. A rescue experiment by KCNE1 transfection of *kcne1*^{-/-} cells fully restored the voltage-dependent Cl^- current (21.59 ± 1.38 pA/pF) (Figure 4F), showing that the absence of chloride current in these cells was only due to the KO of *kcne1* and not due to any modification that might occur during the culture process.

The KCNE1-TMEM16A voltage-dependent Cl^- current in proximal convoluted tubule cells is dynamically regulated by the renin-angiotensin system

Both *kcne1*^{-/-} and *tmem16a*^{-/-} mice exhibit an increased hematocrit value and dehydration due to enhanced water loss (Valion et al., 2001; Faria et al., 2014), which suggests a functional role of the KCNE1-TMEM16A complex in water reabsorption and consequently in blood pressure regulation. In the renal proximal tubule, these processes are regulated by the renin-angiotensin system that activates AT1R leading to PKC pathway stimulation. This pathway increases Na^+ transport through activation of the apical Na^+/H^+ exchanger 3 (NHE3) (Harris and Young, 1977; Lara et al., 2008; Li et al., 2011). To keep the electroneutrality, Na^+ transport needs notably Cl^- as a counter ion. We hypothesized that the KCNE1-TMEM16A channels may carry this Cl^- current

Application of angiotensin II (AngII), the natural ligand of angiotensin II receptor type 1 (AT1R), on wild-type PCT cells led to an ~ 3 -fold increase in chloride current with a reversal potential that was similar to the expected Cl^- reversal potential (Figure 5A). AngII application on *kcne1*^{-/-} PCT cells failed to produce any current increase (6.5 ± 0.6 pA/pF versus 6.6 ± 1.1 pA/pF, $p > 0.9$) (Figure 5B), demonstrating that this AngII-induced chloride

current is dependent on KCNE1. Moreover, knock down of TMEM16A by siRNA transfection (Sala-Rabanal et al., 2017) in wild-type PCT cells prevented this Cl^- current increase (9.21 ± 1.07 pA/pF versus 10.03 ± 1.1 pA/pF) (Figure 5C), and Ani9 application fully inhibited it (68.69 ± 8.77 versus 8.92 ± 1.25 pA/pF) (Figure 5D). Together, this demonstrates that the Cl^- current enhanced by AngII is dependent on KCNE1 and is carried by TMEM16A, showing an endogenous role for the KCNE1-TMEM16A channel in the renin-angiotensin system.

In the proximal tubule, AT1R has been shown to couple to protein kinase A (PKA) (Crajoinas et al., 2016) and protein kinase C (PKC) (Lara et al., 2008) pathways. As shown in Figure S4A, application of the PKA agonist 8-(4-chlorophenylthio) adenosine 3',5'-cyclic monophosphate (CPT-cAMP) on wild-type PCT cells did not alter the Cl^- current (21.60 ± 3.03 pA/pF versus 19.69 ± 2.03 pA/pF, $p > 0.5$), whereas phorbol 12-myristate 13-acetate (PMA), a PKC agonist, led to a similar Cl^- current increase as observed for AT1R activation (27.13 ± 2.04 pA/pF versus 83.47 ± 14.81 pA/pF) (Figure S4B). This indicates that AT1R activates the PKC pathway to enhance the KCNE1-TMEM16A current. Moreover, this regulation is KCNE1-dependent, because *kcne1*^{-/-} PCT cells did not respond to PMA (5.59 ± 1.14 pA/pF versus 9.19 ± 1.97 pA/pF, $p > 0.1$) (Figure S4C), because it was also seen for AngII.

To address how KCNE1 confers the ability of TMEM16A to be activated by AngII through PKC pathway, we reconstituted the system in HEK293T cells. First, we validated the model: AngII did not modify the TMEM16A current when co-expressed with AT1R alone (Figure S5A) but induced an ~ 2.5 -fold increase of the TMEM16A-KCNE1 chloride current on cells co-expressing KCNE1-TMEM16A and AT1R (Figure S5B). As observed in PCT cells, PMA, but not CPT-cAMP, induced an ~ 3 -fold increase of the TMEM16A-KCNE1 chloride current (20.31 ± 3.31

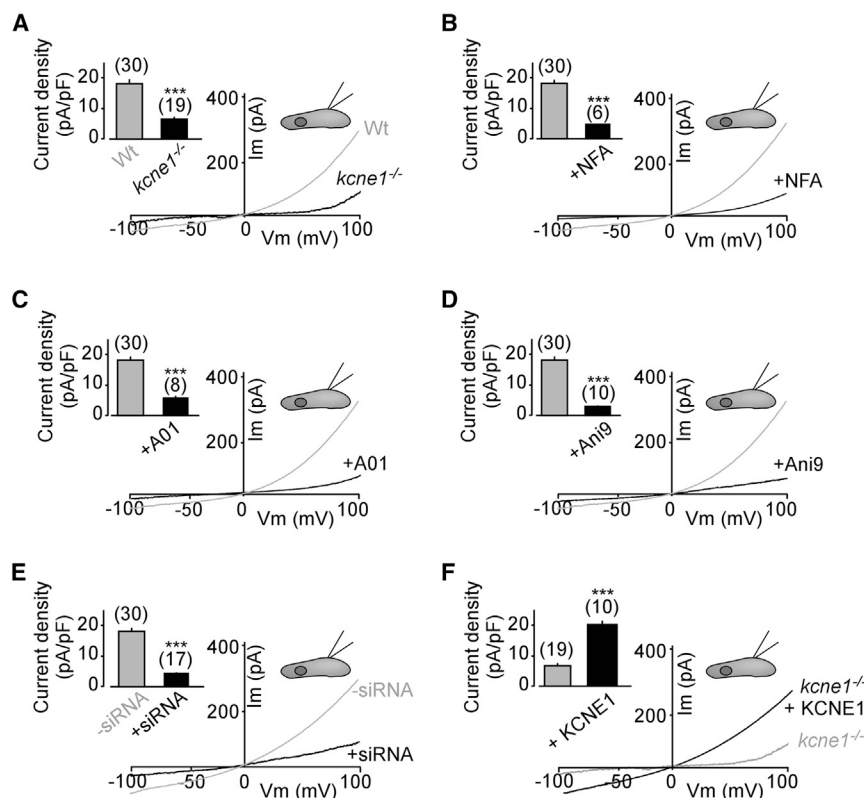


Figure 4. KCNE1-TMEM16A complex creates a voltage-dependent chloride current in proximal convoluted tubule (PCT) cells

(A) Representative traces obtained from wild-type and *kcne1*^{-/-} PCT cells.

(B–D) Representative traces from wild-type cells after incubation with NFA (100 μ M, B), A01 (10 μ M, C), (5 μ M Ani9, D).

(E) Trace obtained after transfection with siRNA against TMEM16A.

(F) Trace obtained from a *kcne1*^{-/-} PCT cell after transfection with KCNE1 cDNA. Currents were generated by voltage-ramps (from -100 to $+100$ mV, 1 s duration). Insets show current densities. Mann-Whitney test (***) $p < 0.001$. Mean \pm SEM.

(Figure 6B). By contrast, deletion of the full N-terminal domain suppressed the ability of KCNE1 to regulate TMEM16A (6.56 ± 0.89 pA/pF) (Figure 6B). No effect was observed for the partial N-terminal truncations, neither for Δ Nt16 (25.43 ± 4.46 pA/pF) nor for Δ Nt30 (25.23 ± 6.62 pA/pF) (Figure 6C). This demonstrates that the domain essential for TMEM16A activation is included in the sequence of the 13 residues preceding the transmembrane domain from L30 to L42. This result is in line with the previous

versus 63.12 ± 10.39 pA/pF) (Figures S5C and S5D), confirming an involvement of PKC. Substitution of the KCNE1-serine S102, a known PKC-targeted residue (Kanda et al., 2011; Xu et al., 2009), by an alanine abolished the regulation of the channel by AT1R and PKC (Figures S5E and S5F). Therefore, it is the phosphorylation of KCNE1 at residue S102 that promotes the TMEM16A-KCNE1 current following AT1R and PKC activation. Furthermore, replacement of S102 by an aspartate residue, mimicking a phosphorylated serine (Kanda et al., 2011; Xu et al., 2009), induced an ~ 3.5 -fold increase of the current (20.31 ± 3.31 versus 74.88 ± 24.38 pA/pF) (Figure S5G) similar to the current increase induced by either PKC or AT1R activation, confirming the pivotal role of KCNE1-S102 phosphorylation in the TMEM16A-KCNE1 chloride current regulation. These data demonstrate that in addition to the modification of channel gating, KCNE1 brings a regulation to TMEM16A by AT1R through PKC activation.

The N-terminal pre-transmembrane domain of KCNE1 is key for TMEM16A regulation

KCNE1 is a single transmembrane protein with an extracellular N-terminal domain and a C-terminal domain within the cytosol (Takumi et al., 1988). To determine the interacting site with TMEM16A, we produced a series of truncated KCNE1 forms (Figure 6A) and tested them for their ability to regulate TMEM16A. Truncation of the KCNE1 C-terminal domain (the last 80 residues of the C terminus) did not abolish the KCNE1-mediated TMEM16A regulation (25.04 ± 4.9 pA/pF, $p > 0.15$)

observation, that a partial deletion of KCNE1, including eight of the 13 amino acids of this sequence (KCNE1 Δ_{11-38}), abolished the KCNE1-induced chloride current in *Xenopus* oocytes (Attali et al., 1993). To check if this small domain is sufficient to recapitulate the properties of the entire KCNE1 on the TMEM16A current, we used a corresponding synthetic peptide (Nter13), bearing the L30–L42 sequence. In HEK293T cells only expressing TMEM16A, application of 100 μ M Nter13 elicited an Ani9-sensitive current (15.48 ± 3.25 pA/pF) (Figures 6D, S6A, and S6B). Again, the reversal potential was similar to the current observed when the full KCNE1 is co-expressed, whereas no effect was observed by application of a scrambled peptide (Figure 6D).

KCNE1 polymorphisms within the TMEM16A-interacting sequence suppress the Cl⁻ current

Previous works have identified two common KCNE1 polymorphisms, S38G and R32H, within the 13-residue extracellular domain. Although these polymorphisms may be related to cardiac arrhythmia, they do not or just weakly affect the cardiac I_{Ks} current generated by KCNE1-KCNQ1 (Crump and Abbott, 2014; Westenskow et al., 2004; Yao et al., 2018). We therefore tested the potential of these two KCNE1 variants to regulate TMEM16A. The disease-related mutation T7I, which does not belong to the regulating 13-residue domain, was used as a control. Whereas mutation T7I did not alter the KCNE1-dependent regulation of TMEM16A (24.69 ± 1.57 pA/pF) (Figures 7C and 7D), both R32H and S38G mutations abolished the ability of

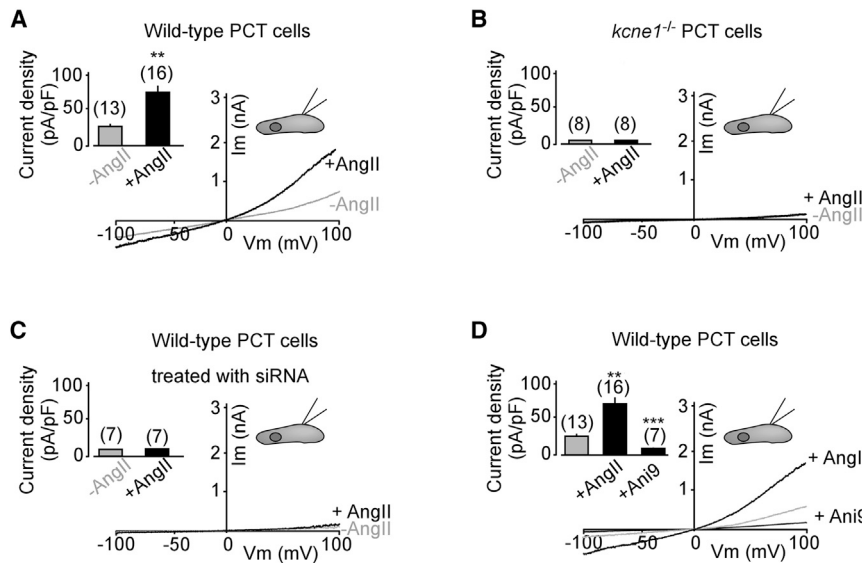


Figure 5. Activation of a KCNE1-dependent chloride current by the renin-angiotensin system in proximal tubule cells

(A–C) Representative current traces showing the effect of AngII application (100 nM) on wild-type (A), *kcne1*^{-/-} (B) and wild-type PCT cells treated with a siRNA against TMEM16A (C).

(D) Inhibition of wild-type PCT cells stimulated with AngII by Ani9 (5 μM). Inset: current densities obtained at +100 mV. Representative traces of *kcne1*^{-/-} PCT cells before and after treatment with AngII. Mann-Whitney test (**p < 0.01, ***p < 0.001). Mean ± SEM.

See also [Figures S4 and S5](#).

cardiac arrhythmias (Barhanin et al., 1996; Crump and Abbott, 2014; Sanguinetti et al., 1995, 1996). Cross-modulation by β-subunits of pore-forming α-subunits from the same superfamily of ion channels was shown for Na_v and K_v channels (Marionneau et al., 2012; Nguyen et al., 2012).

KCNE1 to modulate the TMEM16A current properties (5.69 ± 1.18 pA/pF and 6.96 ± 0.78 pA/pF for R32H and S38G) (Figures 7C and 7D). This finding suggests a potential role of the KCNE1-TMEM16A complex in human diseases.

DISCUSSION

Most ion channels are assembled as complexes of a pore-forming α-subunit, associated with auxiliary (β) subunits. In this study, we demonstrate that KCNE1, classically considered as a β-subunit of the cardiac KCNQ1 pore-forming subunit belonging to the voltage-dependent K_v channel superfamily, also serves as an auxiliary subunit of the anoctamin superfamily channel TMEM16A, a Ca²⁺-activated Cl⁻ channel (CaCC). By stably interacting with TMEM16A following a 2α:2β stoichiometry, KCNE1 induces a voltage-dependent current in the absence of intracellular elevation of calcium. Furthermore, we show that the presence of KCNE1 in the TMEM16A channel complex is essential for the dynamic regulation by the blood pressure-regulating renin-angiotensin system in proximal tubule cells. KCNE1 polymorphisms within the TMEM16A-interacting domain abolish its ability to regulate TMEM16A, suggesting a possible implication of this voltage-dependent chloride current in human diseases.

β-subunits of ion channels are important molecular players providing a source of electrical signaling diversity in cells. Although they cannot induce native currents per se, they associate with pore-forming subunits of ion channels and modulate their pharmacological and biophysical characteristics. Their physiological importance is reflected by the large number of diseases linked to their mutations, such as muscular pathologies, epilepsy, and cardiac arrhythmias (Adelman, 1995; Cannon, 2007; Crump and Abbott, 2014; Verguit et al., 2015). KCNE1 is a famous example of a K_v β-subunit, which associates with KCNQ1 and hERG to control both I_{Ks} and I_{Kr} components of the cardiac action potential. More than sixty KCNE1 gene variants have been reported to be associated with human diseases, particularly with

Na_vβ₁ coordinates the control of K_v and Na_v channels, which derive from the same ancestor (Moran et al., 2015) and belong to the superfamily of voltage-gated ion channels. Our results demonstrate auxiliary subunit-cross-modulation of two different superfamilies, which are phylogenetically not related: the voltage-gated channels and the anoctamins.

This cross-regulation concerns not only the KCNE member 1 of the KCNE subunit family, but also the KCNE member 5. Despite the fact that we did not find a significant alignment of the KCNE1's 13 residues sequence in the KCNE5 sequence, both subunits interact with TMEM16A and both seem to have a similar activating effect on the Cl⁻ current. A similar effect does not necessarily mean an identical mode of action and it is possible that they differ in their manner to regulate TMEM16A. This has been already described for K_v channel regulation by the different KCNE members. For instance, both KCNE4 and KCNE5 provoke the same inhibition of KCNQ1 channels, but whereas KCNE4 inhibits the binding of the channel activator calmodulin, KCNE5 shifts the voltage-dependence of KCNQ1 toward highly depolarized potentials (Angelo et al., 2002; Ciampa et al., 2011) rendering the channel non-functional at physiological potentials. Future studies will aim to fully characterize these regulations and interactions between KCNE and TMEM16 members. Our results demonstrate auxiliary subunit-cross-modulation of two different superfamilies, which are phylogenetically not related: the voltage-gated channels and the anoctamins.

We found that, by interacting with TMEM16A, KCNE1 modifies the gating of this anoctamin member, switching it from a calcium-dependent to a voltage-dependent channel. Our experiments with different Ca²⁺ chelators and with the Ca²⁺-activated SK4 channel as a very sensitive reporter demonstrated that activation of this CaCC is independent from any rise of cytosolic Ca²⁺, the natural activator of the channel in the absence of KCNE1 (Caputo et al., 2008; Schroeder et al., 2008; Yang et al., 2008). We also discarded a potential

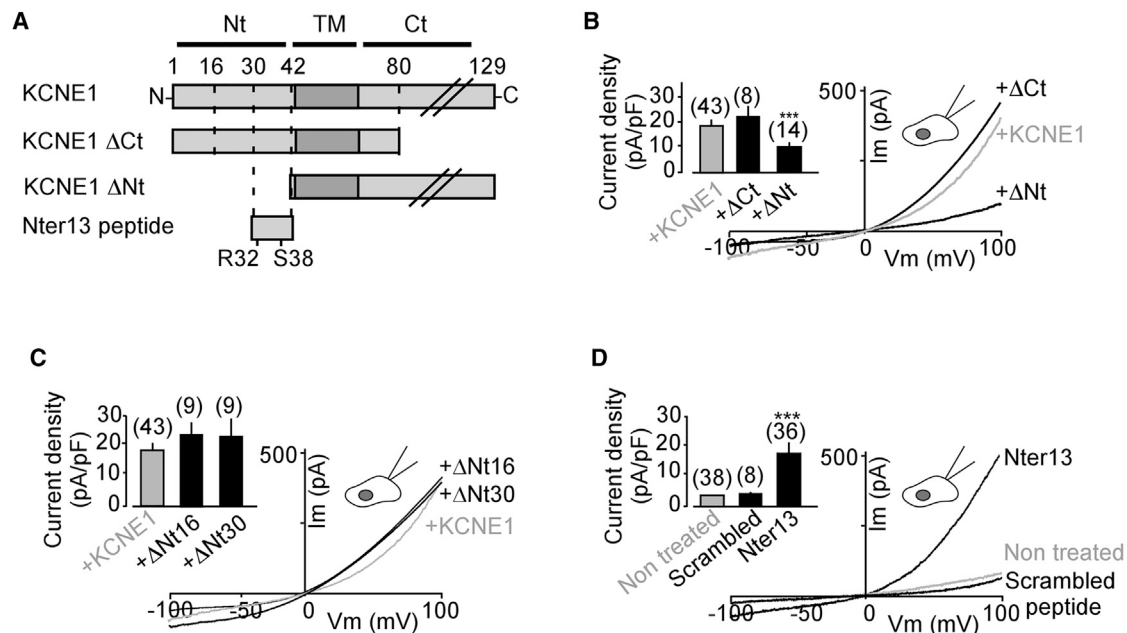


Figure 6. The pre-transmembrane domain (Nter13) of KCNE1 is sufficient for KCNE1-induced TMEM16A conversion

(A) Cartoon depicting KCNE1 truncated forms used to determine the domains implicated in TMEM16A interaction.

(B and C) Representative traces obtained from HEK293T cells co-expressing TMEM16A and KCNE1ΔCt, KCNE1ΔNt (B), KCNE1ΔNt16, or KCNE1ΔNt30 (in which the first 16 and 30 residues were deleted, respectively, C).

(D) Representative traces showing the effect of the Nter13 and a scrambled peptide on a HEK293T cell expressing TMEM16A alone. Currents were elicited by voltage-ramps from -100 to $+100$ mV, 1 s duration). Insets show the summary of current densities obtained for the different conditions at $+100$ mV. Mann-Whitney test ($***p < 0.001$). Mean \pm SEM.

See also Figure S6.

increase of cell surface expression of TMEM16A when KCNE1 is present. An absent current density increase at a saturating Ca^{2+} concentration in the presence of KCNE1 shows that this protein does not stabilize the channel at the cell surface, as it was previously described for CLCA1 (Sala-Rabanal et al., 2017), but rather modifies channel gating. Recently, the TMEM16A-TM6 segment was reported to play a crucial role in voltage and calcium sensing (Peters et al., 2018). The TM6 was shown to be flexible allowing it to adopt several stable conformations that would condition the channel activity mode. Its key function was demonstrated by showing that two mutations within the TM6 (I637A and Q645A) enable channel activation by membrane depolarization in the absence of calcium, as KCNE1 does (Peters et al., 2018). The absence of an additive effect of KCNE1 when co-expressed with the two TM6 mutants supports an overlapping mechanism. KCNE1 may modulate channel activity by modifying the TM6 conformation, placing the channel in a voltage-dependent mode and enabling the channel to be activated independently of Ca^{2+} . Clearly, the voltage-dependent chloride channel superfamily is not restricted to the ClC family, but extends to the anoctamin family when combined with KCNE1. This also shows that the difference between Ca^{2+} and voltage-dependent channels is not strict and that we should rather consider a continuum of biophysical properties.

Whereas the KCNQ1-KCNE1 stoichiometry remains a matter of debate (Morin and Kobertz, 2008; Murray et al., 2016; Nakajo et al.,

2010; Plant et al., 2014), we found that the TMEM16A-KCNE1 complex is composed of $2\alpha:2\beta$ subunits by using the SiMPull assay. We have shown that this complex is formed in HEK cells upon heterologous expression, but we also demonstrated its presence in native kidney cells, where it mediates a Cl^{-} conductance that is sensitive to TMEM16A inhibitors. This Cl^{-} conductance cannot be recorded in KCNE1 KO cells or in cells in which TMEM16A has been knocked down, and it is rescued in these cells by KCNE1 re-expression upon transfection. The TMEM16A-KCNE1 channel may participate in the volume regulation of PCT cells, as the regulatory volume decrease (RVD) typically observed after a hypo-osmotic shock in cells issued from *kcne1*^{-/-} mice is reduced (Barrière et al., 2003). This lack of RVD was attributed to the loss of a chloride conductance and not to the loss of the KCNQ1-KCNE1 K^{+} current, as it was anticipated at that time. At the whole animal level, *kcne1*^{-/-} and *tmem16a*^{-/-} mice exhibit similar phenotypes such as an increased hematocrit value and dehydration due to enhanced water loss (Vallon et al., 2001; Faria et al., 2014). The renin-angiotensin system is involved in blood pressure regulation by notably increasing water and salt reabsorption through activation of AT1R, enhancing the transport of Na^{+} and its counter ion Cl^{-} . In line with this, our results demonstrate that the KCNE1-TMEM16A chloride current in proximal tubule cells increases upon activation of the renin-angiotensin system. This indicates that the KCNE1-TMEM16A chloride current is, at least partially, the AngII-dependent Cl^{-} KCNE1-TMEM16A current, in which TMEM16A is the pore-forming α -subunit and

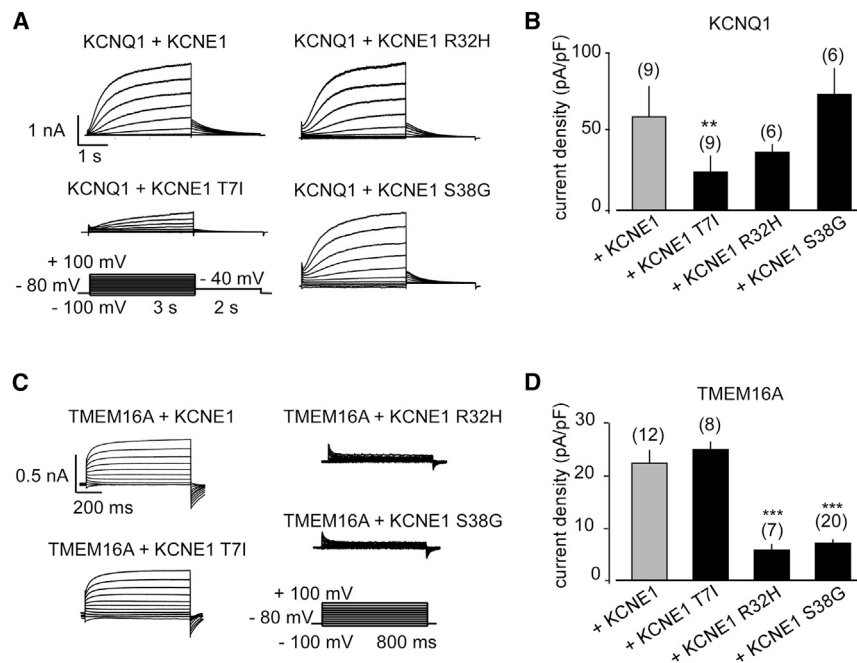


Figure 7. KCNE1 S38G and R32H do not impair the KCNQ1 regulation, but abolish TMEM16A regulation

(A) Current traces of whole-cell patch-clamp recordings from cells transfected with KCNQ1 alone and co-transfected with KCNE1 or KCNE1 R32H or KCNE1 S38G or KCNE1 T7I.

(B) Summary of current densities obtained for the different conditions at +40 mV.

(C and D) Same as (A) and (B), with cells co-expressing TMEM16A and the different KCNE1 forms. Current densities were calculated at +100 mV. Mann-Whitney test (** $p < 0.01$, *** $p < 0.001$). Mean \pm SEM.

KCNE1 the β -subunit. Therefore, TMEM16A-KCNE1 association is not only found upon recombinant overexpression, but can also be observed in native cells, notably in renal PCT cells, in which the complex responds to the renin-angiotensin system involved in physiological blood pressure regulation.

Our detailed study of the signaling pathway, linking the renin-angiotensin system activation to the Cl^- TMEM16A-KCNE1 current, demonstrates that it is the phosphorylation of the KCNE1 β -subunit that confers the ability to TMEM16A α -subunit to be stimulated by AngII. In fact, phosphorylation of KCNE1-S102 is responsible for the totality of the effect observed upon AngII binding on AT1R. Therefore, KCNE1 mediates a dynamic channel regulation by involving intracellular PKC-dependent pathways. Interestingly, the PKC-targeted S102 residue was shown to lead to a reduced I_{Ks} current, carried by KCNQ1-KCNE1 complex, when phosphorylated (Kanda et al., 2011; Xu et al., 2009).

Our electrophysiological assays, using truncated forms of KCNE1 and synthetic peptides based on the β -subunit, allowed us to determine the crucial role of the N terminus of KCNE1 in TMEM16A regulation. More specifically, we have observed that the segment closer to the transmembrane domain of KCNE1 is necessary and sufficient to recapitulate the action of the entire KCNE1 on the TMEM16A current. The synthetic peptide generated on the basis of this segment's sequence is the first designed TMEM16A agonist and may be useful for clinical applications. Notably, activation of an apical chloride channel such as TMEM16A triggers the secretion of water, which makes TMEM16A-targeted activators potential drug candidates for treatment of cystic fibrosis or dry eye syndromes.

The KCNE1 N-terminal 13-amino acid segment bears at least two residues that are subject topolymorphisms (R32H and S38G) related with cardiac arrhythmias (Crump and Abbott, 2014). Whereas several clinically relevant KCNE1 variants were

found to modify its ability to regulate KCNQ1, providing a link between these mutations and polymorphisms with cardiac arrhythmias, the KCNE1 S38G poorly impairs KCNQ1 regulation by KCNE1 (Yao et al., 2018). We found that the KCNE1 S38G as well as the R32H mutants lost their ability to regulate TMEM16A, suggesting a potential role of this chloride current in cardiac arrhythmias.

Along this line, a recent study performed in canine heart suggests a protective role for TMEM16A against risk of arrhythmias by reducing spatial and temporal heterogeneity of cardiac repolarization and early after-depolarization (Hegyi et al., 2017). To sum up, we have found that KCNE1, a well-known auxiliary subunit of voltage-dependent K^+ channels, fulfills the four needed conditions to be considered as an auxiliary subunit of the anoctamin anion channel superfamily (Adelman, 1995; Arikath and Campbell, 2003; Cannon, 2007; Gurnett and Campbell, 1996; Trimmer, 1998): first, KCNE1 does not show any ion channel activity by itself, second, KCNE1 and TMEM16A interact directly and stably with a fixed stoichiometry ($2\alpha:2\beta$), third, KCNE1 modifies drastically the TMEM16A function enabling the channel to work in the absence of elevated cytosolic calcium, and fourth, KCNE1 regulates TMEM16A in native tissue. Therefore, KCNE1 is a bona fide auxiliary subunit of two distinct classes of ion channel superfamilies which are not phylogenetically related: the voltage-gated cation channel and the anoctamin superfamily. Finally, the TMEM16A-KCNE1 association should be considered when analyzing outcomes of clinically relevant KCNE1 mutations, as emphasized by the finding that two known cardiac arrhythmia-related KCNE1 variants, including S38G, lost their ability to regulate TMEM16A.

STAR★METHODS

Detailed methods are provided in the online version of this paper and include the following:

- KEY RESOURCES TABLE
- RESOURCE AVAILABILITY
 - Lead contact
 - Materials availability

- Data and code availability
- **EXPERIMENTAL MODEL AND SUBJECT DETAILS**
 - HEK293T cells
 - PCT cells
- **METHOD DETAILS**
 - Molecular biology and gene expression
 - Electrophysiology
 - Single Molecule Pulldown assay
- **QUANTIFICATION AND STATISTICAL ANALYSIS**

SUPPLEMENTAL INFORMATION

Supplemental Information can be found online at <https://doi.org/10.1016/j.cell.2020.11.047>.

ACKNOWLEDGMENTS

We thank Prof. Lily Yeh Jan for providing us the clone encoding TMEM16A-GFP (isoform a) (RefSeq: NM_001242349.1) and Prof. Criss Hartzell for sharing the clone encoding the TMEM16A_{444EEEE447/444AAAA447} mutant. We also thank Prof. Harald Janovjak, Prof. Josh Levitz, and Dr. Michel Vivaudou for fruitful discussion. The experiments requiring microscope imaging were performed at the PRISM facility, “PRISM-IBV-CNRS UMR 7277-INSERM U1091-UNS.” This work was supported by a grant to G.S. by the Fondation pour la Recherche Medicale (Equipe labellisée FRM 2017, FRM DEQ20170336753) the Agence Nationale de la Recherche (AT2R-TRAAK-Bio-analgesics ANR-17-CE18-0001 and ANR-17-ERC2-0023), the Laboratory of Excellence “Ion Channel Science and Therapeutics” (ANR-11-LABX-0015-01), and the French government, through the UCAJEDI Investments in the Future project managed by the National Research Agency (ANR) with the reference number ANR-15-IDEX-01. The work was also supported by a grant to P.A.P. by the Fondation pour la Recherche Medicale (FRM 2019, FDT201904008083) and to S.H. (Ville de Nice). This work was further supported by a grant from the Israel Science Foundation (ISF 1365/17) to B.A.

AUTHOR CONTRIBUTIONS

Conceptualization, P.A.P., S.H., J.B., and G.S.; Methodology, P.A.P., S.H., J.B., B.A., and G.S.; Investigation, P.A.P., B.W., S.H., and Y.C.; Resources, C.D.; Writing – Original Draft, P.A.P., S.H., J.B., B.A., and G.S.; Writing – Review & Editing, P.A.P., S.H., J.B., B.A., and G.S.; Funding Acquisition, G.S.; Project Administration, G.S.

DECLARATION OF INTERESTS

The authors declare no competing interests.

Received: April 27, 2020

Revised: October 22, 2020

Accepted: November 25, 2020

Published: December 28, 2020

REFERENCES

- Adelman, J.P. (1995). Proteins that interact with the pore-forming subunits of voltage-gated ion channels. *Curr. Opin. Neurobiol.* *5*, 286–295.
- Angelo, K., Jespersen, T., Grunnet, M., Nielsen, M.S., Klaerke, D.A., and Olesen, S.P. (2002). KCNE5 induces time- and voltage-dependent modulation of the KCNQ1 current. *Biophys. J.* *83*, 1997–2006.
- Arikath, J., and Campbell, K.P. (2003). Auxiliary subunits: essential components of the voltage-gated calcium channel complex. *Curr. Opin. Neurobiol.* *13*, 298–307.
- Attali, B., Guillemare, E., Lesage, F., Honoré, E., Romey, G., Lazdunski, M., and Barhanin, J. (1993). The protein IsK is a dual activator of K⁺ and Cl⁻ channels. *Nature* *365*, 850–852.
- Barhanin, J., Lesage, F., Guillemare, E., Fink, M., Lazdunski, M., and Romey, G. (1996). K(V)LQT1 and IsK (minK) proteins associate to form the I(Ks) cardiac potassium current. *Nature* *384*, 78–80.
- Barrière, H., Rubera, I., Belfodil, R., Tauc, M., Tonnerieux, N., Poujeol, C., Barhanin, J., and Poujeol, P. (2003). Swelling-activated chloride and potassium conductance in primary cultures of mouse proximal tubules. Implication of KCNE1 protein. *J. Membr. Biol.* *193*, 153–170.
- Bendahhou, S., Marionneau, C., Haurogne, K., Larroque, M.M., Derand, R., Szuts, V., Escande, D., Demolombe, S., and Barhanin, J. (2005). In vitro molecular interactions and distribution of KCNE family with KCNQ1 in the human heart. *Cardiovasc. Res.* *67*, 529–538.
- Cannon, S.C. (2007). Physiologic principles underlying ion channelopathies. *Neurotherapeutics* *4*, 174–183.
- Cao, Y.J., and Houamed, K.M. (1999). Activation of recombinant human SK4 channels by metal cations. *FEBS Lett.* *446*, 137–141.
- Caputo, A., Caci, E., Ferrera, L., Pedemonte, N., Barsanti, C., Sondo, E., Pfeiffer, U., Ravazzolo, R., Zegarra-Moran, O., and Galletta, L.J. (2008). TMEM16A, a membrane protein associated with calcium-dependent chloride channel activity. *Science* *322*, 590–594.
- Ciampa, E.J., Welch, R.C., Vanoye, C.G., and George, A.L., Jr. (2011). KCNE4 juxtamembrane region is required for interaction with calmodulin and for functional suppression of KCNQ1. *J. Biol. Chem.* *286*, 4141–4149.
- Crajoinas, R.O., Polidoro, J.Z., Carneiro de Moraes, C.P., Castelo-Branco, R.C., and Girardi, A.C. (2016). Angiotensin II counteracts the effects of cAMP/PKA on NHE3 activity and phosphorylation in proximal tubule cells. *Am. J. Physiol. Cell Physiol.* *311*, C768–C776.
- Crump, S.M., and Abbott, G.W. (2014). Arrhythmogenic KCNE gene variants: current knowledge and future challenges. *Front. Genet.* *5*, 3.
- Dang, S., Feng, S., Tien, J., Peters, C.J., Bulkley, D., Lolicato, M., Zhao, J., Zuberbühler, K., Ye, W., Qi, L., et al. (2017). Cryo-EM structures of the TMEM16A calcium-activated chloride channel. *Nature* *552*, 426–429.
- Davis, A.J., Shi, J., Pritchard, H.A., Chadha, P.S., Leblanc, N., Vasilikostas, G., Yao, Z., Verkman, A.S., Albert, A.P., and Greenwood, I.A. (2013). Potent vasorelaxant activity of the TMEM16A inhibitor T16A(inh)-A01. *Br. J. Pharmacol.* *168*, 773–784.
- Falzone, M.E., Malvezzi, M., Lee, B.C., and Accardi, A. (2018). Known structures and unknown mechanisms of TMEM16 scramblases and channels. *J. Gen. Physiol.* *150*, 933–947.
- Faria, D., Rock, J.R., Romao, A.M., Schweda, F., Bandulik, S., Witzgall, R., Schlatter, E., Heitzmann, D., Pavenstädt, H., Herrmann, E., et al. (2014). The calcium-activated chloride channel Anoctamin 1 contributes to the regulation of renal function. *Kidney Int.* *85*, 1369–1381.
- Goldstein, S.A., and Miller, C. (1991). Site-specific mutations in a minimal voltage-dependent K⁺ channel alter ion selectivity and open-channel block. *Neuron* *7*, 403–408.
- Gurnett, C.A., and Campbell, K.P. (1996). Transmembrane auxiliary subunits of voltage-dependent ion channels. *J. Biol. Chem.* *271*, 27975–27978.
- Harris, P.J., and Young, J.A. (1977). Dose-dependent stimulation and inhibition of proximal tubular sodium reabsorption by angiotensin II in the rat kidney. *Pflügers Arch.* *367*, 295–297.
- Hartzell, C., Putzier, I., and Arreola, J. (2005). Calcium-activated chloride channels. *Annu. Rev. Physiol.* *67*, 719–758.
- Hegyi, B., Horváth, B., Vácsi, K., Gönczi, M., Kistamás, K., Ruzsnavszky, F., Veress, R., Izu, L.T., Chen-Izu, Y., Bányász, T., et al. (2017). Ca²⁺-activated Cl⁻ current is antiarrhythmic by reducing both spatial and temporal heterogeneity of cardiac repolarization. *J. Mol. Cell. Cardiol.* *109*, 27–37.
- Jain, A., Liu, R., Ramani, B., Arauz, E., Ishitsuka, Y., Ragunathan, K., Park, J., Chen, J., Xiang, Y.K., and Ha, T. (2011). Probing cellular protein complexes using single-molecule pull-down. *Nature* *473*, 484–488.
- Kanda, V.A., Purtell, K., and Abbott, G.W. (2011). Protein kinase C downregulates I(Ks) by stimulating KCNQ1-KCNE1 potassium channel endocytosis. *Heart Rhythm* *8*, 1641–1647.

- Lara, L.S., Correa, J.S., Lavelle, A.B., Lopes, A.G., and Caruso-Neves, C. (2008). The angiotensin receptor type 1-Gq protein-phosphatidylinositol phospholipase C-beta-protein kinase C pathway is involved in activation of proximal tubule Na⁺-ATPase activity by angiotensin(1-7) in pig kidneys. *Exp. Physiol.* **93**, 639–647.
- Lesage, F., Attali, B., Lakey, J., Honoré, E., Romey, G., Faurobert, E., Lazdunski, M., and Barhanin, J. (1993). Are *Xenopus* oocytes unique in displaying functional IsK channel heterologous expression? *Receptors Channels* **1**, 143–152.
- Levitz, J., Royal, P., Comoglio, Y., Wdziekowski, B., Schaub, S., Clemens, D.M., Isacoff, E.Y., and Sandoz, G. (2016). Heterodimerization within the TREK channel subfamily produces a diverse family of highly regulated potassium channels. *Proc. Natl. Acad. Sci. USA* **113**, 4194–4199.
- Li, H., Weatherford, E.T., Davis, D.R., Keen, H.L., Grobe, J.L., Daugherty, A., Cassis, L.A., Allen, A.M., and Sigmund, C.D. (2011). Renal proximal tubule angiotensin AT1A receptors regulate blood pressure. *Am. J. Physiol. Regul. Integr. Comp. Physiol.* **301**, R1067–R1077.
- Marionneau, C., Carrasquillo, Y., Norris, A.J., Townsend, R.R., Isom, L.L., Link, A.J., and Nerbonne, J.M. (2012). The sodium channel accessory subunit Navβ1 regulates neuronal excitability through modulation of repolarizing voltage-gated K⁺ channels. *J. Neurosci.* **32**, 5716–5727.
- Moran, Y., Barzilai, M.G., Liebeskind, B.J., and Zakon, H.H. (2015). Evolution of voltage-gated ion channels at the emergence of Metazoa. *J. Exp. Biol.* **218**, 515–525.
- Morin, T.J., and Kobertz, W.R. (2008). Counting membrane-embedded KCNE beta-subunits in functioning K⁺ channel complexes. *Proc. Natl. Acad. Sci. USA* **105**, 1478–1482.
- Murray, C.I., Westhoff, M., Eldstrom, J., Thompson, E., Emes, R., and Fedida, D. (2016). Unnatural amino acid photo-crosslinking of the IKs channel complex demonstrates a KCNE1:KCNQ1 stoichiometry of up to 4:4. *eLife* **5**, e11815.
- Nakajo, K., Ulbrich, M.H., Kubo, Y., and Isacoff, E.Y. (2010). Stoichiometry of the KCNQ1 - KCNE1 ion channel complex. *Proc. Natl. Acad. Sci. USA* **107**, 18862–18867.
- Nguyen, H.M., Miyazaki, H., Hoshi, N., Smith, B.J., Nukina, N., Goldin, A.L., and Chandry, K.G. (2012). Modulation of voltage-gated K⁺ channels by the sodium channel β1 subunit. *Proc. Natl. Acad. Sci. USA* **109**, 18577–18582.
- Pedemonte, N., and Galletta, L.J. (2014). Structure and function of TMEM16 proteins (anoctamins). *Physiol. Rev.* **94**, 419–459.
- Peters, C.J., Gilchrist, J.M., Tien, J., Bethel, N.P., Qi, L., Chen, T., Wang, L., Jan, Y.N., Grabe, M., and Jan, L.Y. (2018). The Sixth Transmembrane Segment Is a Major Gating Component of the TMEM16A Calcium-Activated Chloride Channel. *Neuron* **97**, 1063–1077.
- Plant, L.D., Xiong, D., Dai, H., and Goldstein, S.A. (2014). Individual IKs channels at the surface of mammalian cells contain two KCNE1 accessory subunits. *Proc. Natl. Acad. Sci. USA* **111**, E1438–E1446.
- Royal, P., Andres-Bilbe, A., Ávalos Prado, P., Verkest, C., Wdziekowski, B., Schaub, S., Baron, A., Lesage, F., Gasull, X., Levitz, J., and Sandoz, G. (2019). Migraine-Associated TRESK Mutations Increase Neuronal Excitability through Alternative Translation Initiation and Inhibition of TREK. *Neuron* **101**, 232–245.
- Sala-Rabanal, M., Yurtsever, Z., Berry, K.N., Nichols, C.G., and Brett, T.J. (2017). Modulation of TMEM16A channel activity by the von Willebrand factor type A (VWA) domain of the calcium-activated chloride channel regulator 1 (CLCA1). *J. Biol. Chem.* **292**, 9164–9174.
- Sanguinetti, M.C., Jiang, C., Curran, M.E., and Keating, M.T. (1995). A mechanistic link between an inherited and an acquired cardiac arrhythmia: HERG encodes the IKr potassium channel. *Cell* **81**, 299–307.
- Sanguinetti, M.C., Curran, M.E., Zou, A., Shen, J., Spector, P.S., Atkinson, D.L., and Keating, M.T. (1996). Coassembly of K(V)LQT1 and minK (IsK) proteins to form cardiac I(Ks) potassium channel. *Nature* **384**, 80–83.
- Schneider, C.A., Rasband, W.S., and Eliceiri, K.W. (2012). NIH Image to ImageJ: 25 years of image analysis. *Nat. Methods* **9**, 671–675.
- Schroeder, B.C., Cheng, T., Jan, Y.N., and Jan, L.Y. (2008). Expression cloning of TMEM16A as a calcium-activated chloride channel subunit. *Cell* **134**, 1019–1029.
- Seo, Y., Lee, H.K., Park, J., Jeon, D.K., Jo, S., Jo, M., and Namkung, W. (2016). Ani9, A Novel Potent Small-Molecule ANO1 Inhibitor with Negligible Effect on ANO2. *PLoS ONE* **11**, e0155771.
- Takumi, T., Ohkubo, H., and Nakanishi, S. (1988). Cloning of a membrane protein that induces a slow voltage-gated potassium current. *Science* **242**, 1042–1045.
- Trimmer, J.S. (1998). Regulation of ion channel expression by cytoplasmic subunits. *Curr. Opin. Neurobiol.* **8**, 370–374.
- Ulbrich, M.H., and Isacoff, E.Y. (2007). Subunit counting in membrane-bound proteins. *Nat. Methods* **4**, 319–321.
- Vallon, V., Grahmmer, F., Richter, K., Bleich, M., Lang, F., Barhanin, J., Völkl, H., and Warth, R. (2001). Role of KCNE1-dependent K⁺ fluxes in mouse proximal tubule. *J. Am. Soc. Nephrol.* **12**, 2003–2011.
- Vergult, S., Dheedene, A., Meurs, A., Faes, F., Isidor, B., Janssens, S., Gautier, A., Le Caignec, C., and Menten, B. (2015). Genomic aberrations of the CACNA2D1 gene in three patients with epilepsy and intellectual disability. *Eur. J. Hum. Genet.* **23**, 628–632.
- Vetter, D.E., Mann, J.R., Wangemann, P., Liu, J., McLaughlin, K.J., Lesage, F., Marcus, D.C., Lazdunski, M., Heinemann, S.F., and Barhanin, J. (1996). Inner ear defects induced by null mutation of the *isk* gene. *Neuron* **17**, 1251–1264.
- Wang, K.W., and Goldstein, S.A. (1995). Subunit composition of minK potassium channels. *Neuron* **14**, 1303–1309.
- Westenskow, P., Splawski, I., Timothy, K.W., Keating, M.T., and Sanguinetti, M.C. (2004). Compound mutations: a common cause of severe long-QT syndrome. *Circulation* **109**, 1834–1841.
- Wozniak, K.L., Phelps, W.A., Tembo, M., Lee, M.T., and Carlson, A.E. (2018). The TMEM16A channel mediates the fast polyspermy block in *Xenopus laevis*. *J. Gen. Physiol.* **150**, 1249–1259.
- Xiao, Q., Yu, K., Perez-Cornejo, P., Cui, Y., Arreola, J., and Hartzell, H.C. (2011). Voltage- and calcium-dependent gating of TMEM16A/Ano1 chloride channels are physically coupled by the first intracellular loop. *Proc. Natl. Acad. Sci. USA* **108**, 8891–8896.
- Xu, X., Kanda, V.A., Choi, E., Panaghie, G., Roepke, T.K., Gaeta, S.A., Christini, D.J., Lerner, D.J., and Abbott, G.W. (2009). MinK-dependent internalization of the IKs potassium channel. *Cardiovasc. Res.* **82**, 430–438.
- Yang, Y.D., Cho, H., Koo, J.Y., Tak, M.H., Cho, Y., Shim, W.S., Park, S.P., Lee, J., Lee, B., Kim, B.M., et al. (2008). TMEM16A confers receptor-activated calcium-dependent chloride conductance. *Nature* **455**, 1210–1215.
- Yao, H., Ji, C.C., Cheng, Y.J., Chen, X.M., Liu, L.J., Fan, J., and Wu, S.H. (2018). Mutation in KCNE1 associated to early repolarization syndrome by modulation of slowly activating delayed rectifier K⁺ current. *Exp. Cell Res.* **363**, 315–320.
- Zacharias, D.A., Violin, J.D., Newton, A.C., and Tsien, R.Y. (2002). Partitioning of lipid-modified monomeric GFPs into membrane microdomains of live cells. *Science* **296**, 913–916.

STAR★METHODS

KEY RESOURCES TABLE

REAGENT or RESOURCE	SOURCE	IDENTIFIER
Antibodies		
Biotinylated anti-HA clone 16B12	BioLegend	Cat# 901501; RRID: AB_2565023
Chemicals, Peptides, and Recombinant Proteins		
8-(4-Chlorophenylthio) adenosine 3',5'-cyclic monophosphate (CPT-cAMP)	Sigma-Aldrich	Cat# C3912
Angiotensin II	Tocris	Cat# 1158
Ani9	Sigma- Aldrich	Cat# 1813
Biotin-PEG-Succinimidyl Valerate	Laysan Bio	Item# Biotin-PEG-SVA-5000
BSA	Euromedex	Cat# 04-100-812-C
Collagen	This paper	N/A
Dexamethasone	Sigma-Aldrich	Cat# D4902
DMEM	GIBCO	Cat# 41965-039
DMEM/F12	Sigma-Aldrich	Cat# 6421
DPBS	GIBCO	Cat# 14190-169
EGF	Sigma-Aldrich	Cat# E4127
FBS	Dutscher	Cat# S1900-500
Glutamine	GIBCO	Cat# 25030-081
HEPES	GIBCO	Cat# 15630-080
IGEPAL	Sigma-Aldrich	Cat# I8896
ITS	Sigma-Aldrich	Cat# I3146
Lipofectamine 2000	Invitrogen	Cat#11668027
mPEG-Succinimidyl Valerate	Laysan Bio	Item# MPEG-SVA-5000
NeutrAvidin	ThermoFisher	Cat# 31000
Niflumic acid	Sigma-Aldrich	Cat# N0630
Nter13	GenScript	N/A
Penicillin-Streptomycin	GIBCO	Cat# 15140-122
Phorbol 12-myristate 13-acetate (PMA)	Sigma-Aldrich	Cat# P8139
Poly-L-lysine	Sigma-Aldrich	Cat# P4707
Protease inhibitor	Roche Diagnostics	Cat# 4693116001
Protease inhibitors	Roche Diagnostics	Cat# 04 693 116 001
Scrambled Peptide	GenScript	N/A
T3	Sigma-Aldrich	Cat# T0281
Trypsin	Sigma-Aldrich	Cat# T1763
Trypsin-EDTA	GIBCO	Cat# 25300-054
Deposited Data		
Raw and analyzed data	This paper	https://doi.org/10.17632/k74mpd5p5n.1
Experimental Models: Cell Lines		
HEK293T cells	ATCC	Cat#CRL11268
PCT cells	Barrière et al., 2003 ; Vetter et al., 1996	N/A
Oligonucleotides		
KCNE1 (forward): TATGAATTCACCATGAT CCTGTCTAACACCACA	Sigma-Aldrich	N/A

(Continued on next page)

Continued

REAGENT or RESOURCE	SOURCE	IDENTIFIER
KCNE1 (reverse): TAGTCGACTCATGGGGA AGGCTTCGTCTCAGGA	Sigma-Aldrich	N/A
KCNE1 T71 (internal forward) TATGAATTCACCATGATCCT GTCTAACACCATAGCGGTGA	Sigma-Aldrich	N/A
KCNE1 T71 (internal reverse) ATACTCGAGTCATGGGGAAGGCTTCGTCT	Sigma-Aldrich	N/A
KCNE1 R32H (internal forward) GGCCTGGCCCACAGGTCCCCCGC	Sigma-Aldrich	N/A
KCNE1 R32H (internal reverse) GGGGGACCTGTGGGCCAGGCCCGA	Sigma-Aldrich	N/A
KCNE1 S38G (internal forward) CCCCGCAGCGGTGACGGCAAGCTG	Sigma-Aldrich	N/A
KCNE1 S38G (internal reverse) CTTGCCGTCACCGCTCGGGGGGA	Sigma-Aldrich	N/A
KCNE1 ΔCt (forward) TATGAATTCACCATGATCCTGTCTAACACCACA	Sigma-Aldrich	N/A
KCNE1 ΔCt (reverse) ATACTCGAGCTAGTTGAATGGGTCGTTCGAG	Sigma-Aldrich	N/A
KCNE1 ΔNt (forward) TATCTCGAGACCATGGAGGCCCTCTACGTC	Sigma-Aldrich	N/A
KCNE1 ΔNt (reverse) ATAGAATTCTCATGGGGAAGGCTTCGTCTC	Sigma-Aldrich	N/A
KCNE1 ΔNt16 (forward) TATCTCGAGACCATGCTGTGGCAGGAGACA	Sigma-Aldrich	N/A
KCNE1 ΔNt16 (reverse) ATAGAATTCTCATGGGGAAGGCTTCGTCTC	Sigma-Aldrich	N/A
KCNE1 ΔNt30 (forward) TATCTCGAGACCATGGCCCGAGGTCCCCC	Sigma-Aldrich	N/A
KCNE1 ΔNt30 (reverse) ATAGAATTCTCATGGGGAAGGCTTCGTCTC	Sigma-Aldrich	N/A
HA-KCNE1 (forward) TATGAATTCTTATCCTGTCTAACACCACAGCG	Sigma-Aldrich	N/A
HA-KCNE1 (reverse) ATACTCGAGTCATGGGGAAGGCTTCGTCT	Sigma-Aldrich	N/A
KCNE1-GFP (forward) TATGCTAGCCATGATCCTGTCTAACACCAC	Sigma-Aldrich	N/A
KCNE1-GFP (reverse) ATAGGATCCCTAGACTCGAGCGGCCCA	Sigma-Aldrich	N/A
KCNE1-GFP (internal forward) AGACGAAGCCTTCCCA GTGAGCAAGGGCGAGGAG	Sigma-Aldrich	N/A
KCNE1-GFP (internal reverse) CTCCTCGCCCTTGCTCACTGGGGAAGGCTTCGTCT	Sigma-Aldrich	N/A
KCNE1 S102A (internal forward) CGGGTCCTGGAGGCCTACAGGTCGTGC	Sigma-Aldrich	N/A
KCNE1 S102A (internal reverse) GCACGACCTGTAGGCCTCCAGGACCCG	Sigma-Aldrich	N/A
KCNE1 102D (internal forward) CGGGTCCTGGAGGACTACAGGTCGTGC	Sigma-Aldrich	N/A
KCNE1 S102D (internal reverse) GCACGACCTGTAGTCTCCAGGACCCG	Sigma-Aldrich	N/A

(Continued on next page)

Continued

REAGENT or RESOURCE	SOURCE	IDENTIFIER
TMEM16A (forward): TATCTCGAGACCATGAGGGTCCCCGAGAAGTA	Sigma-Aldrich	N/A
TMEM16A (reverse): ATAGAATTCCTACAGCGCGTCCCCAT	Sigma-Aldrich	N/A
TMEM16A I637A (internal forward): CTGAGCATCGCTATGCTGGGCAAG	Sigma-Aldrich	N/A
TMEM16A I637A (internal reverse): GCCCAGCATAGCGATGCTCAGCTG	Sigma-Aldrich	N/A
TMEM16A Q645A (internal forward): CAGCTAATCGCGAACAATCTCTTC	Sigma-Aldrich	N/A
siRNA targeting sequence TMEM16A	Santa Cruz Biotechnology	sc-76687
Recombinant DNA		
pCMV-HA-X	Clontech	631604
pcDNA3.1-GFP-X	Royal et al., 2019	N/A
pIRES2eGFP	Clontech	6029-1
pcDNA3.1	ThermoFisher	V79020
mTMEM16A ₄₄₄ EEEE/AAAA ₄₄₇	Provided by Criss Hartzell	N/A
mTMEM16A	Provided by Dr Lily Yeh Jan	N/A
hKCNE1	Barhanin et al., 1996	N/A
Software and Algorithms		
Fiji/ImageJ, v1.8	NIH, Schneider et al., 2012	https://imagej.nih.gov/ij/
pCLAMP 10, pCLAMP 11	Molecular Devices	N/A
MaxChelator	https://somapp.ucdmc.ucdavis.edu/pharmacology/bers/maxchelator/	N/A
SigmaPlot v11	Systat Software Inc.	N/A
Other		
Axioplan 2 Imaging Microscope	Zeiss	http://www.micro-shop.zeiss.com/de/de/
Axopatch 200B amplifier	Molecular Devices	N/A
Micromanipulator MP225	Sutter Instrument	https://www.wpi-europe.com/products/micromanipulators/motorised-manipulators/mp-225.aspx
Digidata 1550B	Molecular Devices	N/A
Perfusion	ValveLink 8.2	https://www.autom8.com/perfusion-systems-overview/valvelink8-2-controller/
Camera EMCCD iXon	Andor	https://andor.oxinst.com/products/ixon-emccd-cameras
sCMOS camera Zyla 4.2+	Andor	https://andor.oxinst.com/products/scmos-camera-series/zyla-4-2-scmos
Nikon TiE/Yokogawa W1 Microscope	Nikon	N/A

RESOURCE AVAILABILITY

Lead contact

Further information and requests for resources and reagents should be directed to and will be fulfilled by the Lead Contact, Guillaume Sandoz (sandoz@unice.fr).

Materials availability

This study did not generate new unique reagents.

Data and code availability

Source data for the main and supplemental figures in the paper is available at Mendeley <https://doi.org/10.17632/k74mpd5p5n.1>.

EXPERIMENTAL MODEL AND SUBJECT DETAILS

HEK293T cells

HEK293T (ATCC, #CRL11268) cells were maintained in DMEM supplemented with 10% FBS in 35 mm dishes. At 70%–80% confluency they were transiently co-transfected using lipofectamine 2000 (Invitrogen) or the calcium phosphate method with a total amount of 1 and 3.5 μg of DNA, respectively, and seeded on 18 mm diameter poly-L-lysine-coated glass coverslips in 12 well plates. Cells were recorded or used for SiMPull experiments 24 h – 48 h after their transfection.

PCT cells

Proximal convoluted tubule (PCT) cells originating from either wild-type or *kcne1*^{-/-} mice (inbred 129Sv) (Vetter et al., 1996) were prepared as described previously (Barrière et al., 2003). Culture were maintained in DMEM/F12 (Sigma) supplemented with 1% FBS (Dutscher), 5 mg/l insulin, 5 mg/l transferrin, 30 nM sodium selenite (ITS, Sigma), 2 mM glutamine, 10 nM triiodothyronine (T3, Sigma), 20 mM HEPES (GIBCO), 50 nM dexamethasone (Sigma) and 10 $\mu\text{g}/\text{l}$ EGF (Sigma). At 70%–80% confluency they were transiently transfected using the calcium phosphate method with a total amount of 3.5 μg of DNA and seeded on collagen-coated glass coverslips.

METHOD DETAILS

Molecular biology and gene expression

mTMEM16A splice variant “a” (kindly provided by Dr Lily Yeh Jan, RefSeq: NM_001242349.1), mTMEM16A₄₄₄EEEE/AAAA₄₄₇ (kindly provided by Dr Criss Hartzell) and hKCNE1 cDNA (RefSeq: NM_000219.5) were subcloned in pIRES2eGFP, pcDNA3.1, pCDNA3.1-GFP-X and pCMV-HA vectors. Truncations and mutations were generated by PCR. For SiMPull experiments, HA-tags were fused to the N terminus of sequences, whereas GFP-tags were fused to the C-terminal part.

Electrophysiology

HEK293T and PCT cell electrophysiology was performed 24 – 48 h after transfection. For whole-cell patch-clamp experiments, cells were recorded in a bath solution containing (in mM) 150 NaCl, 5 KCl, 2 CaCl₂ and 10 HEPES, pH 7.4. The glass pipettes (2–5 M Ω of resistance) were filled with (in mM) 5 NaCl, 135 CsCl, 2 MgCl₂, 5 EGTA, 10 HEPES, pH 7.3. Concentrations of AngII, PMA, CPT-cAMP and of the different inhibitors used are indicated in the respective figure legends with incubation times ranging from 20 to 40 min. For siRNA experiments cells were transfected overnight with 50 pmol siRNA using lipofectamine 2000 and recorded the next day. Total calcium concentration was calculated with Maxchelator (<https://somapp.ucdmc.ucdavis.edu/pharmacology/bers/maxchelator/>) for a temperature of 20°C. HEK293T and PCT cells were recorded at room temperature in voltage-clamp mode using an Axopatch 200B (Molecular Devices) amplifier. Signals were filtered at 10 kHz and digitalized at 20 kHz. Whole-cell currents were elicited by voltage-ramps (from –100 to +100 mV, 1 s) and I-V stimulation pulses (from –100 to +100 mV in 20 mV increments, 1 s each pulse), holding the cells at –80 mV. Current densities were measured at +100 mV.

For inside-out recordings, the extracellular (pipette) solution contained (in mM) 140 NaCl, 10 HEPES and 0.1 EGTA. The intracellular (bath) solution had the same composition as the pipette solutions for recordings in absence of Ca²⁺. A saturating Ca²⁺ solution (~20 μM Ca²⁺) was prepared by adding 0.12 mM of CaCl₂ to the bath solution. Non-saturating solutions included (in mM) 1 EGTA and 0.59, 0.79, 0.89, 0.94 of CaCl₂ to obtain 0.1 μM , 0.25 μM , 0.5 μM and 1 μM free-Ca²⁺ solutions, respectively. The pH of inside-out solutions was adjusted to 7.4 with NaOH. Cell recordings, data acquisition and analysis of electrophysiology were performed using pClamp software (Molecular Devices).

For anion permeability experiments, cells were recorded using a pipette filled with CsCl 140 mM. The permeability ratio P_X/P_{Cl} was calculated from the reversal potential shift (ΔE_r) given by the Goldman-Hodgkin-Katz equation (Equation 1), when replacing extracellular Cl⁻ with ion X⁻,

$$\Delta E_r = E_{rX} - E_{rCl} = \frac{RT}{zF} \ln \frac{P_X [X^-]_o}{P_{Cl} [Cl^-]_o} \quad \text{Equation 1}$$

in which, E_{rX} and E_{rCl} represent the reversal potentials of ions X⁻ and Cl⁻, and [X⁻]_o and [Cl⁻]_o represent concentrations of ions X⁻ and Cl⁻ in the bath solution, respectively.

Single Molecule Pulldown assay

For SiMPull assays, we followed the protocol previously described by Jain et al. (2011). Briefly, HEK293T cells co-transfected with an HA-tagged bait protein and a GFP-fused prey protein (applying the widely used eGFP A206K mutant which greatly reduces homodimerization events) (Zacharias et al., 2002) were lysed in a buffer containing (in mM): 150 NaCl, 10 Tris pH 7.5, 1 EDTA, protease inhibitor cocktail (Roche-Diagnostics) and 1.5% IGEPAL (Sigma). Lysates were collected and pulled-down on coverslips passivated with PEG (99%) and biotin-PEG (1%) and treated with neutravidin (1.4 mg/mL, ThermoFisher) and biotinylated anti-HA antibody (15 nM, BioLegend). Several washes with T50 buffer (in mM: 50 NaCl, 10 Tris, 20 EDTA; 0.1 mg/mL BSA, pH 7.5) were performed

to avoid unspecific protein binding. Finally, single molecule complexes were imaged using a 488 nm Argon laser in total internal reflection fluorescence microscopy with a 100x objective (Nikon). $13 \times 13 \mu\text{m}^2$ movies of 250 frames were acquired at frame rates of 10–30 Hz and analyzed using Fiji software (NIH). Multiple independent experiments were performed for each condition and only the spots which were fully bleached at the end of the illumination were considered. Representative datasets are presented to quantitatively compare the different conditions.

QUANTIFICATION AND STATISTICAL ANALYSIS

Analysis of obtained currents in whole-cell and inside-out recordings was performed using ClampFit. For analysis of ramp traces and I-V traces cursors were set at 100 mV, where we extracted the average current. Signals were filtered at 10 kHz and digitalized at 20 kHz. Statistical details can be found in the figure legends and in the main text. Reported n values can be found in the figure legends. For SiMPull experiments a minimum of 15 movies per condition was acquired in at least two independent experiments. Per movie, at least 50 bleaching traces were analyzed. Statistical analysis was performed in SigmaPlot and Excel.

Supplemental Figures

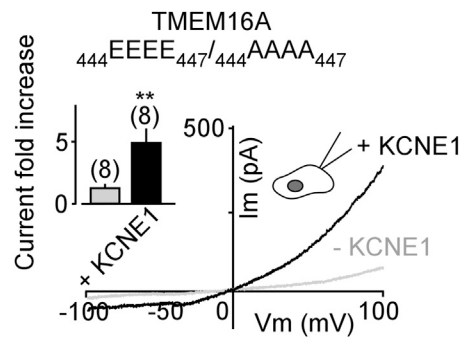


Figure S1. KCNE1 does not shift the intrinsic voltage-dependence of TMEM16A, related to Figure 2

Representative current traces showing the effect of expression of either TMEM16A_{444EEEE_{447/444}AAAA₄₄₇} alone or TMEM16A_{444EEEE_{447/444}AAAA₄₄₇} and KCNE1 in HEK293T cells. Currents were elicited by voltage-ramps (from -100 to $+100$ mV, 1 s duration), insets show a summary of current density fold increase induced by KCNE1 co-expression obtained at $+100$ mV. Mann-Whitney test (** $p < 0.01$). Mean \pm SEM.

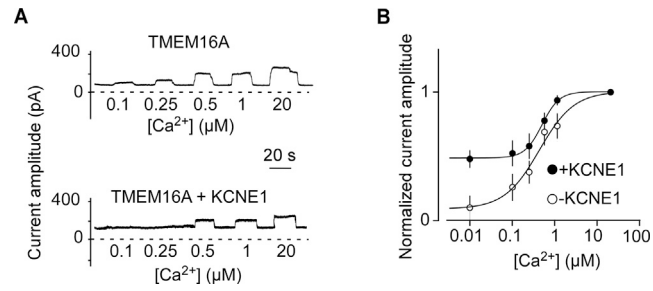


Figure S2. Calcium sensitivity of the TMEM16A-KCNE1 channel complex, related to Figure 2

(A) Representative current traces of TMEM16A-CaCC in inside-out patch configuration in response to various intracellular calcium concentrations. (B) Calcium dose-response of TMEM16A channel.

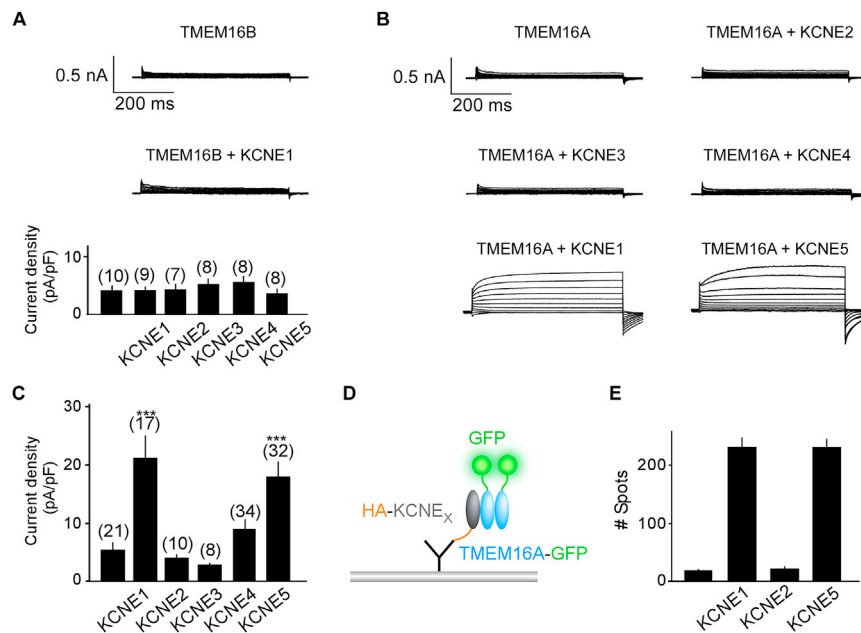


Figure S3. KCNE5 interacts with and shifts the TMEM16A channel from a calcium to a voltage-dependent mode, related to Figures 1 and 3
 (A) Representative current traces showing the effect of expression of TMEM16B alone or with KCNE1. Traces were generated using pulses between -100 and $+100$ mV at 20 mV intervals from a holding potential of -80 mV. Bar graph represents the current density obtained at $+100$ mV for TMEM16B expressed alone or with the different KCNE subunits. (B) Representative current traces showing the effect of expression of TMEM16A alone or with KCNE1, KCNE2, KCNE3, KCNE4 or KCNE5. Traces were generated using pulses between -100 and $+100$ mV at 20 mV intervals from a holding potential of -80 mV. (C) Bar graph representing the current density obtained at $+100$ mV for TMEM16A expressed alone or with the different KCNE subunits. (D) Schematic of single molecule pull-down (SiMPull) assay. Lysates of HEK293T cells co-expressing TMEM16A-GFP and HA-tagged KCNE1, KCNE2 or KCNE5 were immobilized on a PEG-passivated coverslip conjugated to a biotinylated anti-HA antibody. (E) Bar graph showing the number of spots within the field of view obtained for the SiMPull assay of TMEM16A-GFP expressed alone or with HA-tagged KCNE1, KCNE2 or KCNE5.

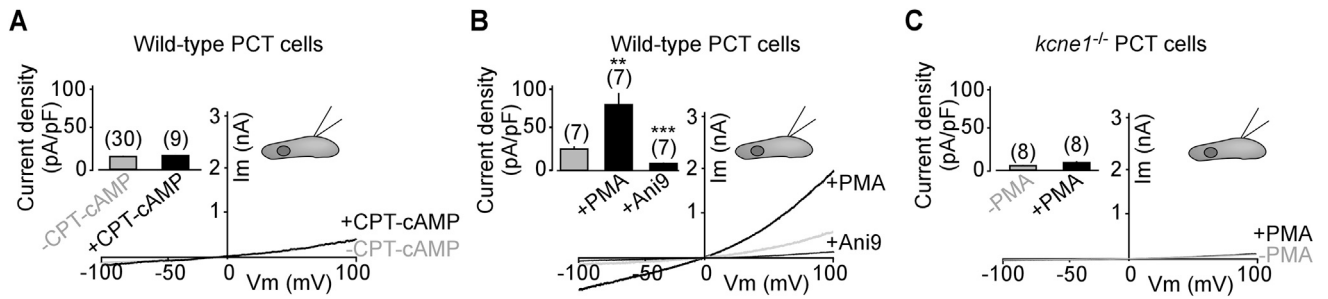


Figure S4. The KCNE1-TMEM16A current is stimulated by activation of PKC, related to Figure 5

(A) Representative current traces showing the effect of CPT-cAMP (500 μ M) on wild-type PCT cells. (B-C) Representative current traces showing the effect of PMA application (100 nM) on wild-type PCT cells (B), on PCT cells treated with Ani9 (5 μ M) after exposure to PMA, and on *kcne1*^{-/-} PCT cells (C). Inset, current densities obtained at +100 mV. Mann-Whitney test (** $p < 0.01$, *** $p < 0.001$). Mean \pm SEM.

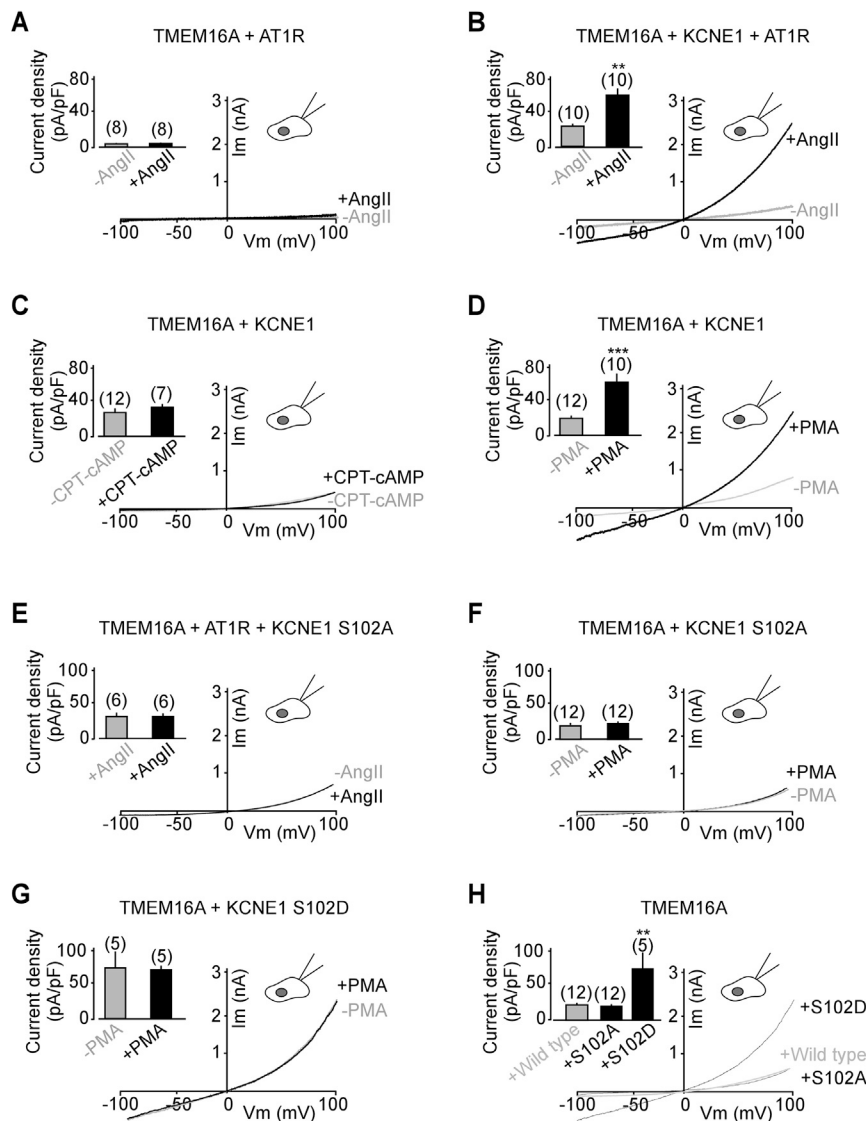


Figure S5. The KCNE1-TMEM16A current is stimulated by the renin-angiotensin system in HEK293T cells through KCNE1-S102 phosphorylation, related to Figure 5

(A, B) Representative current traces showing the effect of AngII application on cells co-expressing TMEM16A and AT1R (A) and co-expressing TMEM16A, AT1R and KCNE1 (B). (C, D) Representative current traces showing the effect of CPT-cAMP (500 μ M, C) and PMA (100 nM, D) application on cells co-expressing TMEM16A and KCNE1. Inset, current densities obtained at +100 mV. (E-F) KCNE1-Ser102 is targeted by PKC to enhance the TMEM16A-KCNE1 chloride current upon AngII binding to AT1R. (E) Application of AngII in HEK293T cells co-expressing TMEM16A, AT1R and KCNE1 S102A does not regulate the chloride current. (F, G) Effect of PMA (100 nM) addition on HEK293T cells co-expressing TMEM16A and KCNE1 S102A (F) or KCNE1 S102D (G). (H) Comparison of current densities obtained from cells co-expressing TMEM16A with either wild-type KCNE1 or KCNE1 S102A or KCNE1 S102D. Inset, current densities obtained at +100 mV. Mann-Whitney test (** $p < 0.01$, *** $p < 0.001$). Mean \pm SEM.

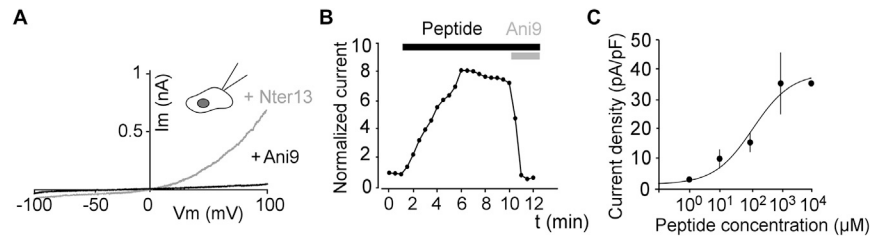


Figure S6. Nter13 peptide is sufficient to switch the functioning mode of TMEM16A, related to Figure 6

(A) Representative traces showing the effect of Nter13 peptide application (100 μM) and its reversion by Ani9 (5 μM) on a HEK293T cell expressing TMEM16A alone. (B) Effect of Nter13 peptide on TMEM16A current over time followed by inhibition through co-application of Ani9 in HEK293T cells. (C) Concentration-response curve representing the current density observed for different peptide concentrations in HEK293T cells expressing TMEM16A. Mean \pm SEM.

ARTICLE

Canaux potassiques à deux domaines P (K2P) et migraine

Perrine Royal^{1,2}, Pablo Ávalos Prado^{1,2}, Brigitte Wdziekonski^{1,2}, et Guillaume Sandoz^{1,2,*}

¹ Université Côte d'Azur, CNRS, INSERM, Institut de Biologie Valrose, Parc Valrose, 06108 Nice, France

² Laboratories of Excellence, Ion Channel Science and Therapeutics, Nice, France

Reçu le 4 juin 2019

Résumé – La migraine est un désordre neurologique qui affecte 15 % de la population mondiale. Les crises migraineuses sont liées, entre autres, à l'hyperexcitabilité électrique des neurones trigéminaux. Leur activité électrique est contrôlée par les canaux potassiques à deux domaines P (K2P) dont l'importance dans l'induction du contrôle de l'excitabilité a récemment été mise en évidence par la découverte d'une version mutée de l'un d'eux TRESK, le mutant TRESK-MT, qui est lié à la migraine. Cette découverte a été controversée à la suite du séquençage d'autres canaux TRESK mutés non fonctionnels qui ne sont pas liés à la migraine. Notre étude montre que les mutations délétères du gène TRESK impliquées dans la migraine entraînent la formation de deux protéines au lieu d'une (comme attendu du gène non muté), *via* un nouveau mécanisme appelé fsATI (initiation alternative de la traduction induite par déplacement du cadre de lecture). L'une est inactive et l'autre, en ciblant d'autres canaux K2P, TREK1 et TREK2, stimule fortement l'activité électrique des neurones provoquant ainsi des crises migraineuses. Cette découverte a permis l'identification de deux nouvelles cibles dans le traitement de la migraine, TREK1 et TREK2, et suggère que les mutations induisant une traduction alternative due à un déplacement du cadre de lecture (fsATI) doivent être considérées comme une classe distincte de mutations lors de l'étude des mutations impliquées dans les pathologies humaines.

Mots clés : canaux ioniques, excitabilité, hétéromérisation, douleur, migraine

Abstract – **Two-pore-domain potassium channels and molecular mechanisms underlying migraine.** Migraine is a common, disabling neurological disorder with genetic, environmental and hormonal components and a prevalence estimated at ~15%. Migraine episodes are notably related, among several factors, to electric hyperexcitability in sensory neurons. Their electrical activity is controlled by ion channels that generate current, specifically by the two-pore-domain potassium, K2P, channels, which inhibit electrical activity. Mutation in the gene encoding TRESK, a K2P channel, causes the formation of TRESK-MT1, the expected non-functional C-terminal truncated TRESK channel, and an additional unexpected protein, TRESK-MT2, which corresponds to a non-functional N-terminal truncated TRESK channel, through a mechanism called frameshift mutation-induced Alternative Translation Initiation (fsATI). TRESK-MT1 is inactive but TRESK-M2 targets two other ion channels, TREK1 and TREK2, inducing a great stimulation of the neuronal electrical activity that may cause migraines. These findings identify TREK1 and TREK2 as potential molecular targets for migraine treatment and suggest that fsATI should be considered as a distinct class of mutations.

Keywords: ion channels, excitability, heteromerization, pain, migraine

Introduction

Il est difficile de comprendre pourquoi des mutations génétiques délétères du même gène se trouvent être ou ne pas être associées à une pathologie. La migraine est un désordre neurologique handicapant qui affecte 15 % de la population. Une attaque migraineuse se traduit par des maux de tête, ayant un caractère pulsatile, d'une durée de

4 à 72 h, accompagnés d'une hypersensibilité à de nombreux stimuli tels que la lumière ou le son pouvant mener à des nausées voire des vomissements. Les migraines sont cliniquement divisées en deux sous-types : la migraine avec aura (MA), quand elle est précédée de perturbations neurologiques transitoires, telles que des auras visuelles, et la migraine sans aura (MO). La dépression corticale envahissante est sous-jacente aux auras, bien que la relation de causalité n'ait pas encore été élucidée. La migraine est une maladie complexe liée, entre

*Auteur correspondant : sandoz@unice.fr

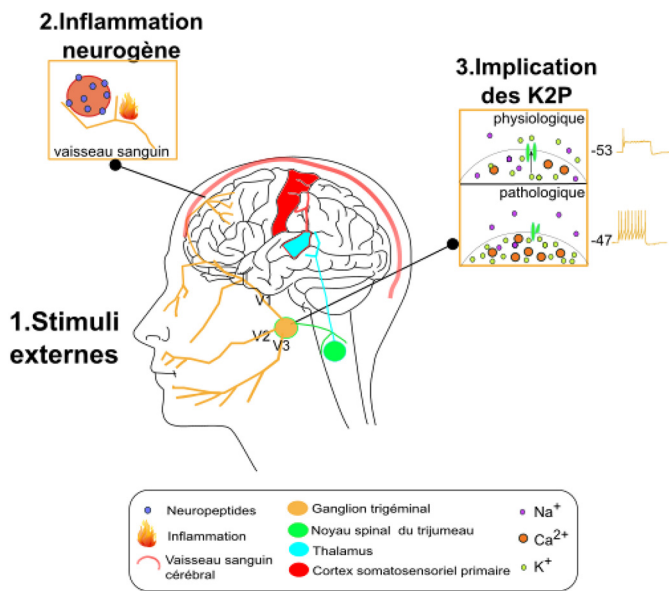


Figure 1. Représentation schématique soulignant les mécanismes qui contribuent à la pathogenèse de la migraine. 1. La migraine est déclenchée lorsqu'une vague électrique, initiée par des stimuli endogènes et exogènes, va perturber le système de modulation sensorielle dans le cerveau pour finalement activer les premières divisions du système trigéminal (V1/2/3). 2. Cette activation stimule le relargage de neuropeptides comme le CGRP, à l'origine d'une dilatation vasculaire et d'une inflammation. Il en résulte une facilitation de la transmission du signal douloureux par ces mêmes divisions jusqu'aux corps cellulaires situés dans les ganglions trigéminaux. 3. À ce niveau, des mutations dans le gène *kenk18* et les dérégulations conséquentes des canaux K2P potentialisent l'hyperexcitabilité neuronale et la transmission de la douleur. En haut : en condition physiologique, la protéine TRESK fonctionnelle contrôle activement la conductance potassique et stabilise le potentiel de membrane négatif, et par conséquent l'équilibre du sodium (Na⁺) et du calcium (Ca²⁺). En bas : la mutation de TRESK détruit cet équilibre en empêchant l'efflux de K⁺, pour finalement faciliter l'émission de potentiels d'actions, renforçant la transmission de l'information nociceptive et le relargage des différents neurotransmetteurs des voies correspondantes (adapté d'Albury *et al.*, 2017).

autres, à l'hyperexcitabilité électrique des neurones sensoriels de la face appelés neurones trigéminaux. Cette activation et la sensibilisation qui en découle mènent à un relargage de peptides pro-inflammatoires (Messlinger *et al.*, 2011), composants clé dans l'initiation et la transmission de la migraine (Figure 1). Cette excitabilité électrique est sous le contrôle des canaux ioniques.

Les canaux ioniques

Les cellules constituant tout organisme sont délimitées par une bicouche lipidique appelée membrane plasmique. Celle-ci isole l'intérieur de la cellule du milieu extracellulaire. Les molécules chargées telles que les ions ne peuvent traverser cette barrière hydrophobe que par l'intermédiaire de protéines transmembranaires. Des protéines enzymatiques intégrées à cette membrane utilisent l'énergie de l'ATP pour générer une distribution asymétrique (gradient

de concentration) des ions de part et d'autre de cette membrane. La pompe Na⁺/K⁺ ATPase, qui est responsable de la mise en place des gradients de Na⁺ et K⁺, est l'exemple le plus connu. L'énergie électrochimique produite par ces gradients est utilisée par la cellule pour transporter des molécules (de l'extérieur vers l'intérieur et inversement), et pour générer des signaux électriques. Ces derniers nécessitent des structures membranaires particulières que l'on appelle canaux ioniques, lesquels sont le plus souvent spécifiques d'un seul type d'ion. Par exemple, lors de l'ouverture de canaux sélectifs du K⁺, ce cation, plus concentré à l'intérieur qu'à l'extérieur, a tendance à sortir, créant ainsi une différence de potentiel entre les milieux intra- et extra-cellulaires, qui peut être calculée par l'équation de Nernst. Dans une cellule non excitée, ou au repos, le potentiel de membrane est très proche du potentiel d'équilibre de l'ion K⁺ (E_k). La raison en est que, dans cet état, les canaux K⁺ sont pratiquement les seuls ouverts. Par conséquent, ce sont eux qui imposent le potentiel de repos. C'est la raison pour laquelle l'intérieur de la cellule est polarisé négativement au repos. À l'inverse, l'ouverture des canaux sélectifs pour le Na⁺ ou le Ca²⁺ entraîne une entrée de ces cations dans la cellule, ce qui déplace le potentiel de membrane vers des valeurs plus positives, traduisant une dépolarisation de la cellule. Les signaux électriques générés par ces gradients sont l'un des moyens mis en place par la cellule pour réguler son activité en réponse à différents types de stimuli. La première fonction parfaitement décrite pour les canaux ioniques est la génération et la propagation des signaux électriques (potentiel d'action, PA) le long des axones. Dès le début des années cinquante, Hodgkin et Huxley expliquèrent les mécanismes de la genèse et de la propagation du PA. En particulier, un PA n'est possible que grâce à l'association de plusieurs conductances ioniques : sodiques, potassiques et parfois calciques. À chacun de ces canaux est associée une phase du PA. La phase de dépolarisation est due à l'ouverture des canaux sodiques. Cette dépolarisation ouvre les canaux calciques dépendants du potentiel et responsables de la phase plateau. La phase de repolarisation est déclenchée par l'ouverture des canaux potassiques dépendants du potentiel de membrane et/ou du calcium.

Les canaux potassiques

Les canaux potassiques ne sont pas seulement impliqués dans la genèse d'un potentiel d'action, ils sont également à l'origine de nombreuses fonctions physiologiques. Les rôles physiologiques des canaux potassiques ont pu être mis en évidence grâce aux énormes progrès de la biologie moléculaire qui sont intervenus au cours de ces trente dernières années. L'émergence des techniques de clonage a permis l'étude de la régulation et des propriétés électrophysiologiques et pharmacologiques de nombreux canaux ioniques. Les canaux potassiques sont régulés par une grande variété de stimuli chimiques (pH, osmolarité, oxygène, anesthésiques), physiques (activité électrique, pression, température) et biologiques (ATP, calcium, protéine G, acides gras, kinases, phosphatases). Dans les cellules excitables, l'activité de ces

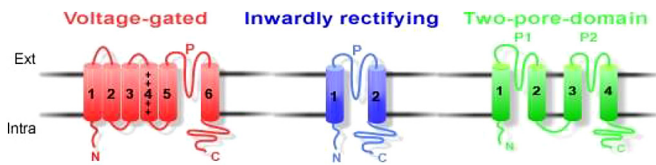


Figure 2. Topologie de canaux potassiques KP. Les canaux voltage-dépendants (en rouge) possèdent six domaines transmembranaires et un domaine P (pore). Les canaux rectifiants entrants (en bleu) ont deux domaines transmembranaires et un domaine P. Les canaux à deux domaines P (K2P, en vert) possèdent quatre domaines transmembranaires et donc deux domaines pore (P1 et P2).

canaux joue un rôle important dans le contrôle de l'excitabilité et dans la génération et la fréquence des PA. Ils sont impliqués dans divers processus physiologiques tels que la mémoire, la neuroprotection, le contrôle respiratoire, la contraction musculaire, la sécrétion d'hormones et de neurotransmetteurs, la régulation du rythme cardiaque. Certains de ces canaux sont la cible des anesthésiques généraux ou volatils. Dans les cellules non excitables, les canaux potassiques sont impliqués dans le contrôle du volume cellulaire, la prolifération et l'apoptose. Afin d'assurer toutes ces fonctions, il existe une importante diversité moléculaire de canaux potassiques présentant des modes de régulation distincts. En effet, il existe chez l'homme au moins 77 gènes qui codent pour ces canaux. Certains de ces canaux sont régulés par une dépolarisation cellulaire, d'autres par une déformation mécanique de la membrane ou encore par une élévation de la concentration de calcium intracellulaire, etc. Au niveau structural, les canaux potassiques sont des complexes protéiques transmembranaires. Chaque sous-unité composante possède un ou deux domaines P, et c'est l'assemblage de quatre domaines P qui permet de former un pore perméable aux ions (Figure 2). Le domaine P correspond à une séquence d'acides aminés entre deux hélices transmembranaires qui traverse partiellement la membrane plasmique. Cette partie transmembranaire contient le filtre de sélectivité aux ions potassium. Chez les mammifères, les sous-unités composant ces canaux contiennent deux, quatre ou six/sept segments transmembranaires. Les membres des familles de canaux à deux ou six/sept segments transmembranaires se caractérisent par la présence d'une seule boucle P alors que les canaux à quatre segments transmembranaires contiennent deux domaines P. Comme il faut quatre boucles P pour former un canal fonctionnel, les canaux à un domaine P (K1P, à deux ou six/sept segments transmembranaires) se tétramérisent en homo- ou hétéro-tétramère alors que les canaux à deux domaines P (K2P, à quatre segments transmembranaires) se dimérisent.

La famille des canaux K2P dans les neurones

Ces canaux sont à l'origine d'un courant dit de fond. Le rôle principal de ce courant est la mise en place et le maintien du potentiel de repos des cellules et ainsi le

contrôle de l'excitabilité cellulaire. En effet, quand ces canaux sont ouverts, ils laissent passer des ions K^+ du milieu intracellulaire vers le milieu extracellulaire, ce qui entraîne un déplacement de charges positives de l'intérieur vers l'extérieur de la cellule, générant une hyperpolarisation cellulaire (cellule peu excitable). À l'inverse, la fermeture de ces canaux entraîne une dépolarisation de la cellule (cellule fortement excitable). Il existe quinze gènes codant pour ces canaux K2P. Les quinze membres de la famille partagent la même structure : quatre segments transmembranaires, deux boucles P et des extrémités carboxy- et amino-terminales intracellulaires. On peut classer ces quinze canaux en six grandes sous-familles en fonction des homologies de séquences et des propriétés fonctionnelles (Figure 3). La première sous-famille se compose des canaux TWIK1 (*Tandem of P domains in Weak Inwardly rectifying K^+ channel*), TWIK2 et KCNK7 ; la deuxième se compose des canaux TREK1 (*TWIK Related K^+ channel*), TREK2 et TRAAK (*TWIK Related Arachidonic Acid stimulated K^+ channel*) ; la troisième comprend TASK3 (*TWIK-related Acid Sensing K^+ channel*), TASK1 et TASK5 ; la quatrième, THIK1 (*TWIK related Halothane Inhibited K^+ channel*) et THIK2 ; la cinquième, TALK1 (*TWIK-related Alkaline-pH-Activated K^+ channel*), TALK2 et TASK2 ; et la sixième sous-famille ne possède qu'un seul membre, le canal TRESK (*TWIK-Related Spinal cord K^+ channel*). Ces différentes sous-familles de canaux se caractérisent par des propriétés fonctionnelles qui leur sont propres.

Canaux potassiques à deux domaines P et neurones trigéminaux

Le système trigéminovasculaire est constitué de neurones trijumeaux et des vaisseaux (généralement cérébraux) qu'ils innervent. Les corps cellulaires bipolaires de ces neurones sont situés dans le ganglion du trijumeau (TG). Les axones périphériques projettent sur les structures crâniennes et les vaisseaux sanguins cérébraux alors que les axones projetant au niveau central atteignent notamment le noyau *spinalis caudalis trigeminalis*. L'activation des terminaisons sensorielles des neurones innervant les vaisseaux méningés provoque la libération de neuropeptides tels que la substance P et le CGRP. Il en résulte une vasodilatation et une inflammation qui sensibilisent les neurones trigéminaux impliqués dans la douleur. Cette sensibilisation permet à ces neurones de répondre anormalement à des stimulations qui sont normalement non douloureuses. Le message douloureux est alors transmis au niveau supérieur ce qui induit la migraine. L'hyperexcitabilité électrique de ces neurones sensoriels de la face joue donc un rôle clé dans la physiopathologie migraineuse.

L'excitabilité des neurones trigéminaux est notamment placée sous le contrôle de six canaux potassiques K2P : TASK1, TASK3, TREK1, TREK2, TRAAK et TRESK. L'importance de ces canaux dans le contrôle de l'excitabilité des neurones trigéminaux, et, ainsi, dans

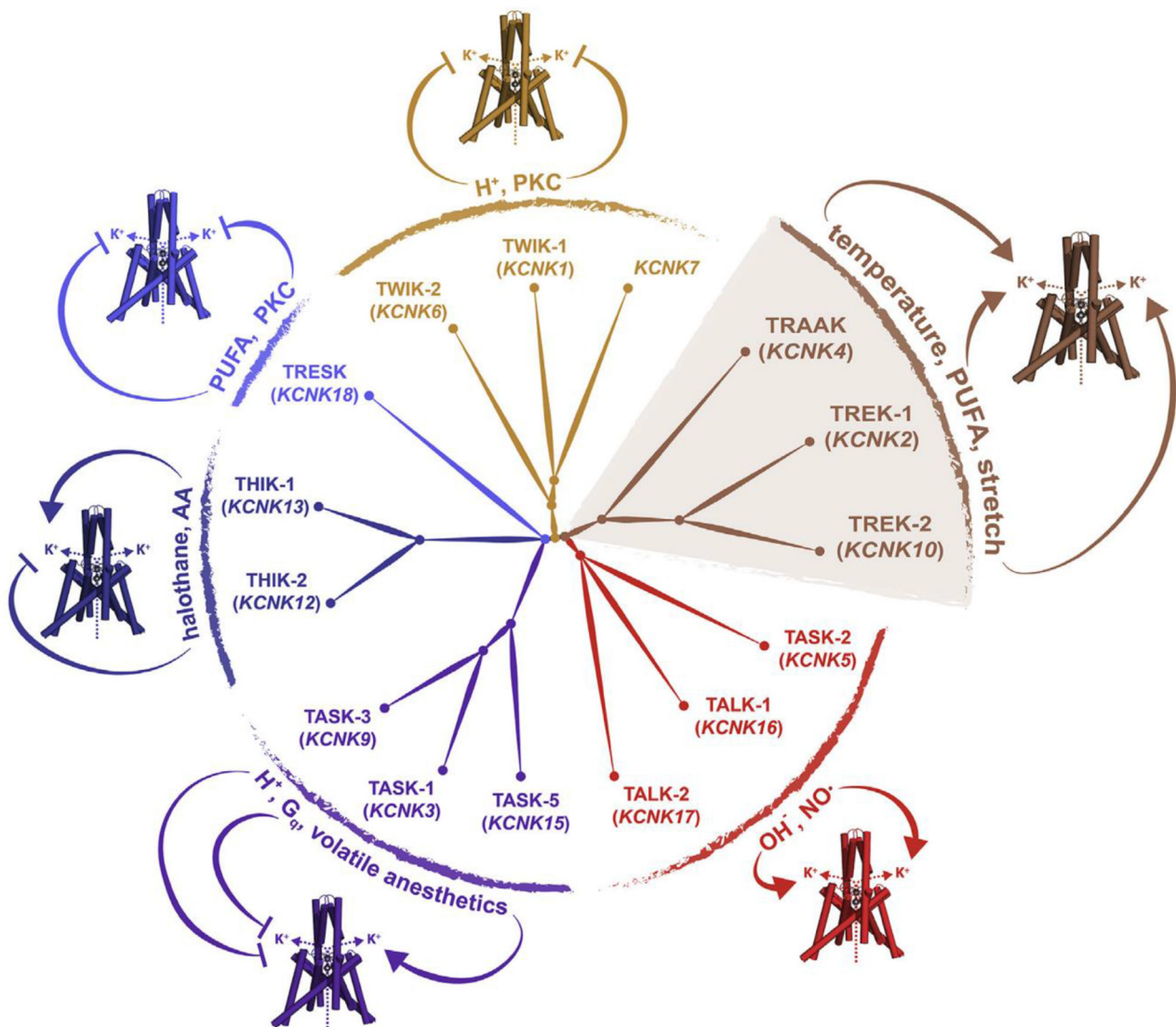


Figure 3. Dendrogramme de la famille des canaux potassiques à deux domaines P. L'effet de différents stimuli sur les courants de chaque sous-famille K2P est indiqué. PUFA, acides gras poly-insaturés; PKC, protéine kinase C; AA, acide arachidonique.

l'induction de la migraine, a récemment été mise en évidence par la découverte d'une version mutée du canal TRESK qui est liée à la migraine (Lafrenière *et al.*, 2010).

Le canal TRESK et la migraine – « la controverse »

La protéine mutée TRESK-MT, résultant d'une délétion de deux paires de bases (F139WfsX24) dans le gène *KCNK18*, est en corrélation parfaite avec un phénotype migraineux sur plusieurs générations (Lafrenière *et al.*, 2010). Cette mutation déplace le cadre de lecture et induit ainsi la formation d'un canal tronqué au niveau de sa partie carboxy-terminale. Ce canal mutant, en plus d'être non fonctionnel, agit comme dominant négatif du canal TRESK sauvage, de telle sorte que TRESK-MT abolit le courant généré par ce dernier. En accord avec l'implication de cette mutation dans la migraine, les neurones trigéminaux exprimant ce canal

mutant voient leur excitabilité augmentée, ce qui explique l'induction de la migraine (Liu *et al.*, 2013). Cependant, des études subséquentes ont décrit une autre mutation TRESK-C110R, qui, comme TRESK-MT, conduit à la formation d'un canal non fonctionnel agissant comme dominant négatif sur le canal sauvage (Andres-Enguix *et al.*, 2012). Bien que TRESK-C110R et TRESK-MT semblent être similaires fonctionnellement, seule la mutation TRESK-MT est associée à une augmentation de l'excitabilité neuronale et à un phénotype migraineux. En effet, l'expression du mutant TRESK-C110R dans des neurones de ganglions trigéminaux n'induit pas une augmentation de l'excitabilité, ce qui pourrait expliquer pourquoi ce mutant est retrouvé à la fois chez des personnes migraineuses et chez les sujets contrôles (Guo *et al.*, 2014). Comment deux mutations génétiques délétères du même gène TRESK peuvent-elles être, ou ne pas être, associées à la migraine ?

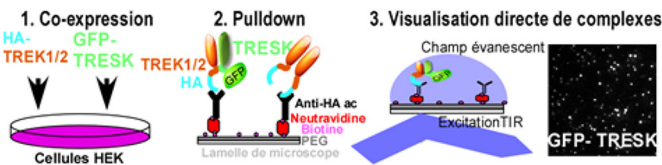


Figure 4. TRESK hétéromérise avec TREK1 et TREK2. Des cellules HEK exprimant GFP-TRESK et TREK1/2 fusionné à un marqueur HA sont lysées et immobilisées sur une lamelle passivée avec du polyéthylène glycol (PEG) conjugué avec un anticorps biotinylé anti-HA. La figure illustre les différentes étapes jusqu'à la visualisation des complexes TRESK-TREK (cf. [Royal et al., 2019](#) pour la description complète des techniques utilisées).

Le canal TRESK peut s'hétéromériser

Comme décrit précédemment, les canaux K2P sont actifs à l'état de dimère. La famille K2P est composée de 15 membres et certains d'entre eux sont capables de former des hétéro-dimères ([Levitz et al., 2016](#)). Nous avons émis l'hypothèse selon laquelle la différence entre les deux mutants TRESK-MT et TRESK-C110R pouvait provenir de leur capacité à réguler de manière différente les autres canaux K2P au travers de l'hétéromérisation.

L'utilisation de la technique de précipitation en molécule unique, le *SiMPull* ([Jain et al., 2012](#)), nous a permis de montrer que TRESK était capable de s'hétéromériser avec d'autres canaux K2P, notamment TREK1 et TREK2, aussi exprimés dans les neurones trigéminaux ([Figure 4](#)).

Ayant démontré que TRESK pouvait s'hétéromériser avec TREK1 et TREK2, nous avons testé la capacité des mutants TRESK (TRESK-MT et TRESK-C110R) à réguler TREK1 et TREK2. Les études fonctionnelles utilisant l'électrophysiologie révèlent que TRESK-MT, mais pas TRESK-C110R, est capable d'inhiber TREK1 et TREK2. Ainsi, le mutant impliqué dans la migraine, en plus de sa capacité à inactiver TRESK, peut inhiber TREK1 et TREK2, alors que le mutant TRESK-C110R, qui n'est pas impliqué dans la migraine, ne modifie pas les courants TREK1/2. Ce résultat nous a amenés à tester l'importance de TREK1 et TREK2 dans le contrôle de l'excitabilité des neurones trigéminaux et leur implication dans l'augmentation d'excitabilité induite par l'expression de TRESK-MT. Pour ce faire, nous avons généré des souris dont les gènes *TREK1* et *TREK2* sont invalidés. L'enregistrement de neurones trigéminaux des souris *TREK1^{-/-}/TREK2^{-/-}* a permis de montrer que l'absence d'expression de ces canaux génère un état basal hyperexcitable identique à celui observé dans les neurones exprimant TREK-MT. De plus, la surexpression de TRESK-MT dans ces neurones n'est plus capable d'augmenter leur excitabilité, démontrant que TRESK-MT augmente l'excitabilité *via* l'inhibition de TREK1 et TREK2. Ainsi, la différence entre le mutant impliqué dans la migraine et celui qui ne l'est pas réside dans la capacité du premier à inhiber TREK1 et TREK2. Les canaux TREK1 et TREK2 ayant un rôle de frein de l'excitabilité, il en résulte une augmentation de l'excitabilité des neurones trigéminaux induisant ainsi la migraine.

Enfin, nous avons testé le comportement des souris dont TREK1 et TREK2 ont été invalidés génétiquement et avons trouvé qu'elles présentent un phénotype migraineux qui disparaît sous l'action de médicaments utilisés pour traiter les migraines chroniques. C'est donc l'inhibition de TREK1 et TREK2, mais pas de TRESK, qui conduit à la migraine, ouvrant ainsi de nouvelles pistes pour le traitement de cette pathologie.

L'initiation alternative de la traduction induite par un déplacement du cadre de lecture

La mutation TRESK-MT est censée générer un canal tronqué non fonctionnel, appelé TRESK-MT1. Alors que le canal TRESK sauvage est capable d'interagir avec TREK1 et TREK2 dans un essai de précipitation en molécules uniques, TRESK-MT, dépourvu de la partie carboxy-terminale de TRESK, ne l'est pas. Si l'inhibition de TREK1/2 observée dans les cellules co-exprimant TRESK-MT ne vient pas de TRESK-MT1, il faut envisager l'implication d'un autre mécanisme. Normalement, un ARNm va permettre de produire une protéine. Mais dans certains cas, cette loi n'est pas suivie ([Kozak, 1999](#)). En effet, un site d'initiation de la traduction alternatif peut parfois être reconnu par les ribosomes et induire la synthèse d'une deuxième protéine à partir du même ARNm. Nous avons trouvé la présence d'un tel site d'initiation alternatif spécifiquement dans la séquence de TRESK-MT. Ce site alternatif a été mis en évidence par la délétion de deux paires de bases. Cette nouvelle protéine, appelée TRESK-MT2, correspond à un canal TRESK tronqué au niveau de sa partie N-terminale et donc non fonctionnel. L'existence de ce second transcrit a été mise en évidence par une série d'expériences de biologie cellulaire et de biochimie ([Royal et al., 2019](#)). Nous avons appelé fsATI (pour *frameshift mutation-induced Alternative Translation Initiation*) ce nouveau mécanisme de mise en place d'un site alternatif de la traduction par un déplacement du cadre de lecture ([Figure 5](#)). Nous avons testé, par une technique de précipitation en molécules uniques, la capacité de TRESK-MT2 à interagir avec TREK1 et TREK2 et avons trouvé que ce mutant s'associe fortement à ces deux canaux K2P. Nous avons alors recherché l'effet fonctionnel de cette interaction et avons trouvé que TRESK-MT2 était capable d'inhiber les canaux TREK1 et TREK2. En outre, les résultats obtenus sur les neurones trigéminaux sauvages montrent que l'inhibition de TREK1 et TREK2 par TRESK-MT2 induit une forte augmentation de l'excitabilité de ces neurones, similaire à celle observée dans les neurones dont TREK1 et TREK2 ont été invalidés.

L'inhibition de TREK1 et TREK2 par TRESK-MT2 induit l'hyperexcitabilité

Ayant trouvé que l'inhibition de TREK1 et TREK2 était induite par TRESK-MT2, nous avons voulu savoir si l'expression de TRESK-MT2 était suffisante pour induire un phénotype migraineux, comme celui observé chez les

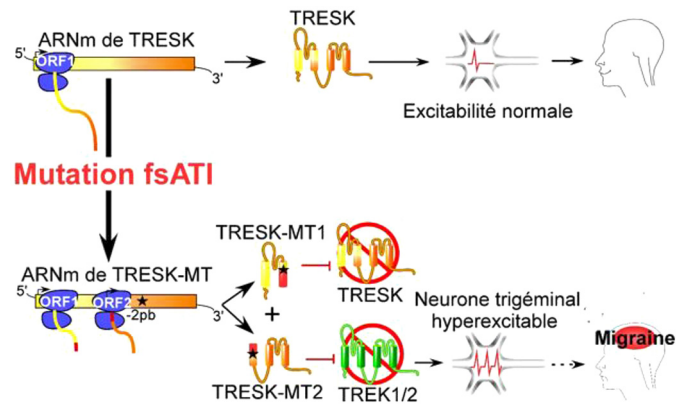


Figure 5. TRESK-MT provoque une migraine *via* l'inhibition de TREK1 et TREK2 par la protéine tronquée TRESK-MT2. En haut, excitabilité physiologique, normale, des neurones trigéminaux exprimant la forme sauvage de TRESK. En bas, les personnes portant la forme mutée du canal TRESK (TRESK-MT, symbolisée par une étoile noire) présentent une allodynie liée à la migraine. Le gène muté, par un mécanisme appelé fsATI, est traduit en deux protéines, TRESK-MT1 et TRESK-MT2. TRESK-MT1 va inhiber TRESK alors que TRESK-MT2 va cibler TREK1 et TREK2, menant à une hyperexcitabilité neuronale et à un phénotype migraineux.

patients portant la mutation TRESK-MT. Pour ce faire, nous avons surexprimé TRESK-MT2 dans les neurones trigéminaux grâce à des vecteurs viraux et avons testé le phénotype migraineux. La migraine peut être générée *via* l'utilisation de molécules donneuses d'oxyde nitrique comme l'isosorbide dinitrate. La migraine ainsi induite s'accompagne d'une hypersensibilité faciale, directement reliée à la sensibilité des nerfs trijumeaux innervant la face, qui peut être mesurée avec des filaments de von Frey. Ainsi, la sensibilité faciale de ces rats est utilisée comme un index reflétant le phénotype migraineux. Après une semaine d'infection, pour laisser le temps au virus d'exprimer TRESK-MT2, nous avons observé que les rats infectés présentaient une hypersensibilité faciale. Cette dernière est similaire à celle observée chez les rats soumis à une induction de migraine par les donneurs d'oxyde nitrique. Cette expérience confirme que la protéine TRESK-MT2 est suffisante pour induire le phénotype migraineux observé chez les patients.

TRESK-MT est-il le seul mutant de type fsATI ?

TRESK-MT est la première illustration d'une mutation qui induit la formation de deux protéines à partir d'un même ARN, au lieu d'une seule comme attendu, à la suite d'un déplacement du cadre de lecture. Afin de savoir si ce nouveau mécanisme de transmission de maladie héréditaire était, ou non, un cas isolé, nous avons cherché dans les bases de données publiques si d'autres mutations de type délétion de paires de bases pouvaient, comme la mutation TRESK-MT, créer un site alternatif de traduction. Nous avons trouvé une autre mutation du canal TRESK capable de créer un site alternatif d'initiation de la traduction. Nos données de biologie cellulaire et de biochimie confirment que cette mutation Y121LfsX44 conduit à la production de deux protéines (MT1 et MT2) et induit l'inhibition des canaux TREK1 et TREK2. Afin de savoir si cette mutation était liée à la maladie, nous avons alors confronté cette séquence aux bases de données cliniques et avons

trouvé que cette mutation est la seule mutation de TRESK qui a également été liée à un phénotype migraineux dans des cohortes de populations asiatiques. La co-expression avec TREK1 dans un système d'expression hétérologue conduit à des résultats similaires : la production de deux protéines et l'inhibition des canaux TREK1 démontrant que la mutation TRESK-MT n'est pas un cas isolé.

Conclusion

Ces travaux démontrent que la différence entre les mutants du canal TRESK non fonctionnels qui sont – ou non – impliqués dans la migraine réside dans leur capacité à inhiber TREK1 et TREK2 en plus de TRESK. TREK1 et TREK2 constituent ainsi de nouvelles cibles pour le traitement de cette pathologie. D'autre part, ces travaux nous ont permis de découvrir un nouveau mécanisme de transmission de maladie génétique appelé « fsATI », qui doit maintenant être pris en compte dans l'étude des mutations impliquées dans les pathologies humaines.

Références

- Albury, C.L., Stuart, S., Haupt, L.M., Griffiths, L.R. (2017). Ion channelopathies and migraine pathogenesis. *Mol Genet Genomics*, 292, 729-739.
- Andres-Enguix, I., Shang, L., Stansfeld, P.J., Morahan, J.M., Sansom, M.S.P., Lafrenière, R.G., Roy, B., Griffiths, L.R., Rouleau, G.A., Ebers, G.C., Cader Z.M., Tucker S.J. (2012). Functional analysis of missense variants in the TRESK (KCNK18) K channel. *Sci Rep*, 2, 237.
- Guo, Z., Liu, P., Ren, F., Cao, Y.-Q. (2014). Nonmigraine-associated TRESK K⁺ channel variant C110R does not increase the excitability of trigeminal ganglion neurons. *J Neurophysiol*, 112, 568-579.
- Jain, A., Liu, R., Xiang, Y.K., Ha, T. (2012). Single-molecule pull-down for studying protein interactions. *Nat Protoc*, 7, 445-452.

- Kozak, M. (1999). Initiation of translation in prokaryotes and eukaryotes. *Gene*, 234, 187-208.
- Lafrenière, R.G., Cader, M.Z., Poulin, J.-F., Andres-Enguix, I., Simoneau, M., Gupta, N., Boisvert, K., Lafrenière, F., McLaughlan, S., Dubé, M.-P., Marcinkiewicz M.M., Ramagopalán S., Ansoorge O., Brais B., Sequeiros J., Pereira-Monteiro J. M., Griffiths L.R., Tucker S.J., Ebers G., Rouleau G.A. (2010). A dominant-negative mutation in the TRESK potassium channel is linked to familial migraine with aura. *Nat Med*, 16, 1157-1160.
- Levitz, J., Royal, P., Comoglio, Y., Wdziekonski, B., Schaub, S., Clemens, D.M., Isacoff, E.Y., Sandoz, G. (2016). Heterodimerization within the TREK channel subfamily produces a diverse family of highly regulated potassium channels. *Proc Natl Acad Sci USA*, 113, 4194-4199.
- Liu, P., Xiao, Z., Ren, F., Guo, Z., Chen, Z., Zhao, H., Cao, Y.-Q. (2013). Functional analysis of a migraine-associated TRESK K⁺ channel mutation. *J Neurosci*, 33, 12810-12824.
- Messlinger, K., Fischer, M.J.M., Lennerz, J.K. (2011). Neuropeptide effects in the trigeminal system: Pathophysiology and clinical relevance in migraine. *Keio J Med*, 60, 82-89.
- Royal, P., Andres-Bilbe, A., Prado, P.Á., Verkest, C., Wdziekonski, B., Schaub, S., Baron, A., Lesage, F., Gasull, X., Levitz, J., Sandoz G. (2019). Migraine-associated TRESK mutations increase neuronal excitability through alternative translation initiation and inhibition of TREK. *Neuron*, 101, 232-245.e6.

Citation de l'article : Royal, P., Ávalos Prado, P., Wdziekonski, B., et Sandoz, G. (2019). Canaux potassiques à deux domaines P (K2P) et migraine. *Biologie Aujourd'hui*, **213**, 51-57

The study by Ng et al. (2019) revealed a mechanism by which the signal elicited by pheromone is amplified in the ORNs that promote courtship behavior (see Figure 1). The mechanism involves PPK25, a member of DEG/ENaC channels that plays a key role in signal amplification and transduction. The CBM in PPK25 channel directly interacts with calmodulin during the rise of the intracellular calcium level, which is spurred by the activation of a ligand-gated OR, eventually generating signal amplification. Interestingly, the CBM is also found in other species, including mouse and human, and the DEG/ENaC channels are expressed in different types of sensory neurons that mediate mechanosensation, baro-reception, proprioception, nociception, and taste reception. This work will provide a foundation for understanding signal amplification in other neuron types.

REFERENCES

- Benton, R., Vannice, K.S., Gomez-Diaz, C., and Vosshall, L.B. (2009). Variant ionotropic glutamate receptors as chemosensory receptors in *Drosophila*. *Cell* 136, 149–162.
- Buck, L.B. (1996). Information coding in the vertebrate olfactory system. *Annu. Rev. Neurosci.* 19, 517–544.
- Grosjean, Y., Rytz, R., Farine, J.P., Abuin, L., Cortot, J., Jefferis, G.S., and Benton, R. (2011). An olfactory receptor for food-derived odours promotes male courtship in *Drosophila*. *Nature* 478, 236–240.
- Lin, H.H., Cao, D.S., Sethi, S., Zeng, Z., Chin, J.S.R., Chakraborty, T.S., Shepherd, A.K., Nguyen, C.A., Yew, J.Y., Su, C.Y., and Wang, J.W. (2016). Hormonal Modulation of Pheromone Detection Enhances Male Courtship Success. *Neuron* 90, 1272–1285.
- Ng, R., Salem, S.S., Wu, S.T., Wu, M., Lin, H.H., Shepherd, A.K., Joiner, W.J., Wang, J.W., and Su, C.Y. (2019). Amplification of *Drosophila* Olfactory Responses by a DEG/ENaC Channel. *Neuron* 104, this issue, 947–959.
- Sato, K., Pellegrino, M., Nakagawa, T., Nakagawa, T., Vosshall, L.B., and Touhara, K. (2008). Insect olfactory receptors are heteromeric ligand-gated ion channels. *Nature* 452, 1002–1006.
- Sato, K., Tanaka, K., and Touhara, K. (2011). Sugar-regulated cation channel formed by an insect gustatory receptor. *Proc. Natl. Acad. Sci. USA* 108, 11680–11685.
- Starostina, E., Liu, T., Vijayan, V., Zheng, Z., Siwicki, K.K., and Pikielny, C.W. (2012). A *Drosophila* DEG/ENaC subunit functions specifically in gustatory neurons required for male courtship behavior. *J. Neurosci.* 32, 4665–4674.
- Vosshall, L.B., and Stocker, R.F. (2007). Molecular architecture of smell and taste in *Drosophila*. *Annu. Rev. Neurosci.* 30, 505–533.
- Wicher, D., Schäfer, R., Bauernfeind, R., Stensmyr, M.C., Heller, R., Heinemann, S.H., and Hansson, B.S. (2008). *Drosophila* odorant receptors are both ligand-gated and cyclic-nucleotide-activated cation channels. *Nature* 452, 1007–1011.

TREK for High-Speed and High-Frequency Conduction through the Axon

Pablo Ávalos Prado^{1,2,*} and Guillaume Sandoz^{1,2,*}

¹Université Côte d'Azur, CNRS, INSERM, iBV, Nice, France

²Laboratories of Excellence, Ion Channel Science and Therapeutics, Nice, France

*Correspondence: pablo.avalos-prado@univ-cotedazur.fr (P.Á.P.), sandoz@unice.fr (G.S.)

<https://doi.org/10.1016/j.neuron.2019.11.015>

In this issue of *Neuron*, Kanda et al. (2019) find that the two-pore domain potassium channels TRAAK and TREK1 drive axonal action potential repolarization for high-speed and high-frequency nervous impulses in mammalian myelinated nerves.

An action potential (AP) corresponds to a fast modification of the membrane potential, which rapidly rises and then falls, driven in the soma by the sequential activation of the voltage-dependent Na⁺ and the voltage-dependent K⁺ channels. In neurons, the main function of the AP is cell-to-cell communication by its propagation along the axon toward synaptic boutons. In non-myelinated axon, the AP travels by regenerating itself (Hodgkin, 1937). The AP induces a sufficient depolarization of the neighbor region inducing the activation of the voltage-dependent

Na⁺ channels allowing AP regeneration. This AP propagation has a maximum speed of ~1 m/s. Fast AP propagation requires myelin sheaths. Myelin is a multilamellar membrane that enwraps the axon in segments separated by intervals known as nodes of Ranvier (NRs). Myelin presents a high electrical resistance that prevents the AP conduction along the myelinated segments. However, the current carried at near distance, through the axon cable properties, generates a sufficient depolarization at subsequent NRs allowing AP regeneration. This prop-

agation, known as saltatory conduction, allows a propagation of the AP over 100 m/s.

Since Hodgkin and Huxley established the first ionic conductances of the AP in giant squid axon, AP generation and transmission in the nervous system has been a subject of continuous study. Nevertheless, 80 years after their experiments, the molecular identity of the channels underlying AP propagation and regeneration at the NRs in mammals is still a matter of conjecture. Whereas some research suggests that



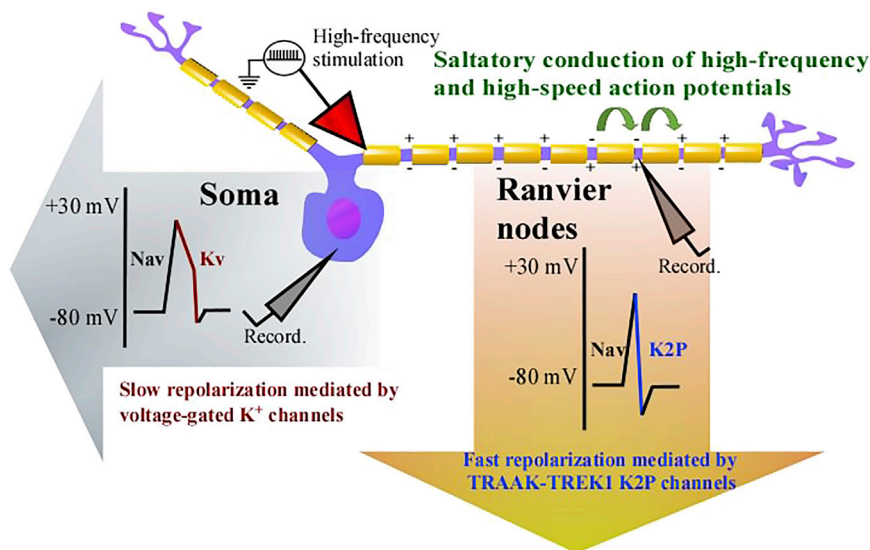


Figure 1. TREK1-TRAAK Channels Mediate Rapid Action Potential Repolarization Enabling Fast Saltatory Action Potential Conduction in Mammal Myelinated Axons

Recordings of action potentials (APs) in different regions of a pseudo-unipolar trigeminal neuron of mammal. At the soma, during high-frequency stimulation, APs are long due to the slow repolarization phase mediated by voltage-gated K⁺ channels. At the nodes of Ranvier, this process is faster because it is mainly driven by background K2P channels that rapidly set the resting potential to very negative values. Rapid regeneration of APs and very hyperpolarized membrane potential allow high-frequency and high-speed saltatory conduction of nervous impulses through myelinated axons.

AP depolarization and repolarization in both soma and NRs are carried by Na⁺ and K⁺ voltage-dependent channels, respectively (Bean, 2007), others suggest that there is no K⁺ channel implication in AP in intact NRs (Chiu and Ritchie, 1980). One important issue concerning this debate has been the lack of reliable tools to address the molecular identity of ion currents of APs at NRs. Standard patch-clamp pipettes often fail to access this region due to the presence of myelinating cells and tiny perineural tissue surrounding the nodes. In this issue of *Neuron*, Kanda and co-workers have developed an “*in situ*” pressure-patch-clamp technique that overcomes this problem allowing to directly patch-clamp intact NRs (Kanda et al., 2019). This novel system finely controls the internal pressure of the patch-clamp pipette, enabling the cleaning of the surface areas around NRs of intact rat trigeminal axons and the making of proper seals.

Once sealed, the application of different ion channel blockers on trigeminal A β -afferent nerves showed two interesting findings. First, as expected, when the voltage-gated Na⁺ channel inhibitor

TTX was applied, the inward-depolarizing currents were completely abolished, matching with previous works showing that voltage-dependent Na⁺ channels are required for saltatory conduction (Caldwell et al., 2000). Second, addition of TEA and intracellular Cs⁺, two typical blockers of voltage-gated K⁺ channels, elongated AP repolarization in soma but not in NRs. This last result confirmed that molecular actors involved in AP propagation at mammal myelinated axons differ from those that are used at the soma.

When Kanda et al. (2019) looked in more detail into the ionic current kinetics at A β -afferent nerves, they noticed the presence of a fast non-inactivating outward current following depolarizing that was not inhibited by classical voltage-gated K⁺ or Cl⁻ channel blockers. However, the changes in extracellular K⁺ concentration altered the reversal potential. These properties made two-pore domain K⁺ (K2P) channels good candidates for carrying this outward current. In fact, K2P channels create non-inactivating K⁺ currents that are nearly instantaneous and are strongly expressed within the nervous system. In neurons, K2P channels

serve as a hub for the generation and regulation of the negative resting membrane potential (Noël et al., 2011). Their importance is reflected by the large number of neurological diseases related to dysfunction of these channels, such as depression (Heurteaux et al., 2006) and migraine (Royal et al., 2019).

In order to narrow down what members of the K⁺ leak currents at NRs, Kanda et al. (2019) performed whole-cell and single-channel experiments to show that this current is mechano- and thermosensitive. This regulation is consistent with the poly-modal gating of the TWIK-related K⁺ (TREK) channel subfamily, which includes TREK1, TREK2, and TRAAK (Noël et al., 2011). Moreover, immunocytochemistry data revealed the presence of TREK1 and TRAAK, but not of TREK2, in NRs. Because TREK1 and TRAAK subunits tend to combine and generate heterodimers with intermediate functional properties when they are co-expressed in heterologous systems (Levitz et al., 2016), Kanda et al. (2019) wondered whether this mechanism could be also present in myelinated nerves. As the single-channel K⁺ conductance in trigeminal A β -afferent axons was similar to the one observed in TREK1-TRAAK heterodimers in heterologous system, Kanda and co-workers concluded that the K⁺ leak current in NRs is mostly carried by TREK1-TRAAK heterodimers, with a minor participation of TRAAK and TREK1 homodimers.

Henceforth, the role of TREK1 and TRAAK K2P channels in AP propagation at NRs is nicely demonstrated genetically by injecting specific shRNA and pharmacologically using TREK channel blockers and activators. The inhibition of TREK1-TRAAK led to an increase of the AP duration, a depolarization of the resting membrane potential and a decrease of the nodal membrane input resistance, demonstrating that TREK1 and TRAAK channels are also important regulators of intrinsic membrane properties.

Furthermore, as myelinated A β -afferent nerves constitute one of the fastest carriers of sensory information in the nervous system (Djouhri and Lawson, 2004), Kanda et al. (2019) also searched to elucidate whether TREK1-TRAAK nodal rapid repolarization was consistent with high-frequency and high-speed impulses of

these fibers. Patch-clamp recordings showed AP broadening in a frequency-dependent manner in soma but not in axon of trigeminal A β -afferent nerves. Also, in contrast with soma, high-frequency stimulation did not alter the rate of success to generate AP. This superiority of the axon for high-fidelity reproduction in the shape of the AP underlying the high AP success rate was strongly reduced in axons of neurons in which TREK1-TRAAK were genetically and pharmacologically inhibited. Finally, to challenge *in vivo* the functional role of TREK1-TRAAK channel in velocity and fidelity of firing, Kanda and co-workers performed whisker tactile behavioral tests in rats in which TREK1-TRAAK were genetically depleted using shRNA in D2 whisker hair follicles. As tactile stimuli are conducted by myelinated A β -afferent nerves (Djouhri and Lawson, 2004), they expected that invalidation of TREK1 and/or TRAAK would impair sensory responses. Indeed, rats injected with specific shRNAs showed a strong decrease of tactile response in comparison with the scrambled shRNA control group. This *in vivo* test reinforced the strong *in vitro* evidence, proving that mechano-sensitive and thermosensitive K2P channels are crucial for nervous conduction.

To conclude, Kanda et al. (2019) have demonstrated by genetic and pharmacological invalidation approaches that fast AP repolarization in mammal NRs is mediated by TREK1-TRAAK heterodimeric channels. Furthermore, by setting the

resting membrane potential at very negative values, they increased the number of responsive voltage-gated Na⁺ channels by enabling fast recovery from their inactivated state. This mechanism explains the high-frequency fidelity and high-speed conduction through the NRs of myelinated afferent nerves (Figure 1). *In vivo*, behavioral experiments confirmed this observation, as tactile stimuli are mainly conducted by trigeminal A β -afferent myelinated nerves at high frequency and high speed (Djouhri and Lawson, 2004). This work ends the old debate about whether AP in the nervous system is carried by the same ion channels in soma and NRs, where the AP is regenerated and conducted, pointing out the importance of K2P channels in neuronal transmission. Nevertheless, whether this repolarization mechanism in myelinated axons is shared by other classes in the animal kingdom is still uncertain because in amphibians, it involves voltage-gated K⁺ channels. This question and the elucidation of additional contributors to the AP propagation at NRs may be solved with the novel pressure-patch-clamp technique.

REFERENCES

- Bean, B.P. (2007). The action potential in mammalian central neurons. *Nat. Rev. Neurosci.* 8, 451–465.
- Caldwell, J.H., Schaller, K.L., Lasher, R.S., Peles, E., and Levinson, S.R. (2000). Sodium channel Na(v)1.6 is localized at nodes of ranvier, dendrites, and synapses. *Proc. Natl. Acad. Sci. USA* 97, 5616–5620.
- Chiu, S.Y., and Ritchie, J.M. (1980). Potassium channels in nodal and internodal axonal membrane of mammalian myelinated fibres. *Nature* 284, 170–171.
- Djouhri, L., and Lawson, S.N. (2004). Abeta-fiber nociceptive primary afferent neurons: a review of incidence and properties in relation to other afferent A-fiber neurons in mammals. *Brain Res. Brain Res. Rev.* 46, 131–145.
- Heurteaux, C., Lucas, G., Guy, N., El Yacoubi, M., Thümmel, S., Peng, X.D., Noble, F., Blondeau, N., Widmann, C., Borsotto, M., et al. (2006). Deletion of the background potassium channel TREK-1 results in a depression-resistant phenotype. *Nat. Neurosci.* 9, 1134–1141.
- Hodgkin, A.L. (1937). Evidence for electrical transmission in nerve: Part I. *J. Physiol.* 90, 183–210.
- Kanda, H., Ling, J., Tomomura, S., Noguchi, K., Matalon, S., and Gu, J.G. (2019). TREK-1 and TRAAK are principal K⁺ channels at the nodes of Ranvier for rapid action potential conduction on mammalian myelinated afferent nerves. *Neuron* 104, this issue, 960–971.
- Levitz, J., Royal, P., Comoglio, Y., Wdziekonski, B., Schaub, S., Clemens, D.M., Isacoff, E.Y., and Sandoz, G. (2016). Heterodimerization within the TREK channel subfamily produces a diverse family of highly regulated potassium channels. *Proc. Natl. Acad. Sci. USA* 113, 4194–4199.
- Noël, J., Sandoz, G., and Lesage, F. (2011). Molecular regulations governing TREK and TRAAK channel functions. *Channels (Austin)* 5, 402–409.
- Royal, P., Andres-Bilbe, A., Ávalos Prado, P., Verkest, C., Wdziekonski, B., Schaub, S., Baron, A., Lesage, F., Gasull, X., Levitz, J., and Sandoz, G. (2019). Migraine-Associated TRESK Mutations Increase Neuronal Excitability through Alternative Translation Initiation and Inhibition of TREK. *Neuron* 101, 232–245.e6.

Migraine and Two-Pore-Domain Potassium Channels

The Neuroscientist
1–17
© The Author(s) 2020
Article reuse guidelines:
sagepub.com/journals-permissions
DOI: 10.1177/1073858420940949
journals.sagepub.com/home/nro



Clément Verkest^{1,2,3*}, Stephanie Häfner^{1,2*},
Pablo Ávalos Prado^{1,2*}, Anne Baron^{2,3},
and Guillaume Sandoz^{1,2}

Abstract

Migraine is a common, disabling neurological disorder with a genetic, environmental, and hormonal component with an annual prevalence estimated at ~15%. It is characterized by attacks of severe, usually unilateral and throbbing headache, and can be accompanied by nausea, vomiting, and photophobia. Migraine is clinically divided into two main subtypes: migraine with aura, when it is preceded by transient neurological disturbances due to cortical spreading depression (CSD), and migraine without aura. Activation and sensitization of trigeminal sensory neurons, leading to the release of pro-inflammatory peptides, is likely a key component in headache pain initiation and transmission in migraine. In the present review, we will focus on the function of two-pore-domain potassium (K_{2P}) channels, which control trigeminal sensory neuron excitability and their potential interest for developing new drugs to treat migraine.

Keywords

migraine, trigeminal sensory neurons, K_{2P} channels, KCNK, heterodimerization, frameshift mutation-induced alternative translation initiation (fsATI), allodynia, Kozac sequence, excitability

Introduction

Migraine is one of the most common diseases worldwide, affecting nearly 15% of the global population, with a women to men ratio of 3:1. Its societal and economic burden is considerable (Burch and others 2015). Migraine manifests as a unilateral throbbing headache and is accompanied by multiple symptoms such as nausea, vomiting, photophobia, phonophobia, or cutaneous allodynia. The migraine attack is often split into four different phases following a temporal pattern that can last for several days: premonitory, aura, headache, and postdrome phase (Goadsby and others 2017) (Fig. 1). The premonitory phase can begin as early as 3 days before the headache and is characterized by fatigue, mood changes, food craving, and yawning (Goadsby and others 2017). Around less than one-third of patients will develop an aura before the headache, which consists of visual and sensory disturbances that will last from several minutes to a few hours. The underlying event is thought to be a cortical spreading depression (CSD), a wave of brief depolarization followed by a long-lasting depression of neuronal activity that propagates slowly in the brain (Charles and Baca 2013). Then, the headache phase will start, lasting from 4 to 72 hours. The migraine attack resolves with a postdrome phase, lasting from hours to days, and consisting of residual

headache, fatigue, and impaired cognitive functions (Bose and others 2018). In addition to the presence or not of aura, the frequency of headaches is used to further differentiate episodic migraine (headache with or without aura that occurs 1–14 days per month, for at least 3 months) or chronic migraine patients (at least 15 days of headache per month for at least 3 months) (Adams and others 2015). A broad array of symptoms contributes to the disability associated with migraine attacks and indicates involvement of brain regions in homeostatic, autonomic, emotional, and sensory processing, thus highlighting a wide involvement of the nervous system in migraine (Goadsby and others 2017; Vila-Pueyo 2018). Imaging studies have confirmed that these non-pain symptoms and changes in the brain are not simply responses to pain but can exist in the absence of

¹CNRS, INSERM, iBV, Université Côte d'Azur, Nice, France

²Laboratories of Excellence, Ion Channel Science and Therapeutics Nice, France

³Université Côte d'Azur, CNRS, INSERM, Institut de Pharmacologie Moléculaire et Cellulaire, Valbonne, France

*These authors contributed equally to this work.

Corresponding Author:

Guillaume Sandoz, CNRS, INSERM, iBV, Université Côte d'Azur, 28 av de valrose, Nice, 06100, France.
Email: sandoz@unice.fr

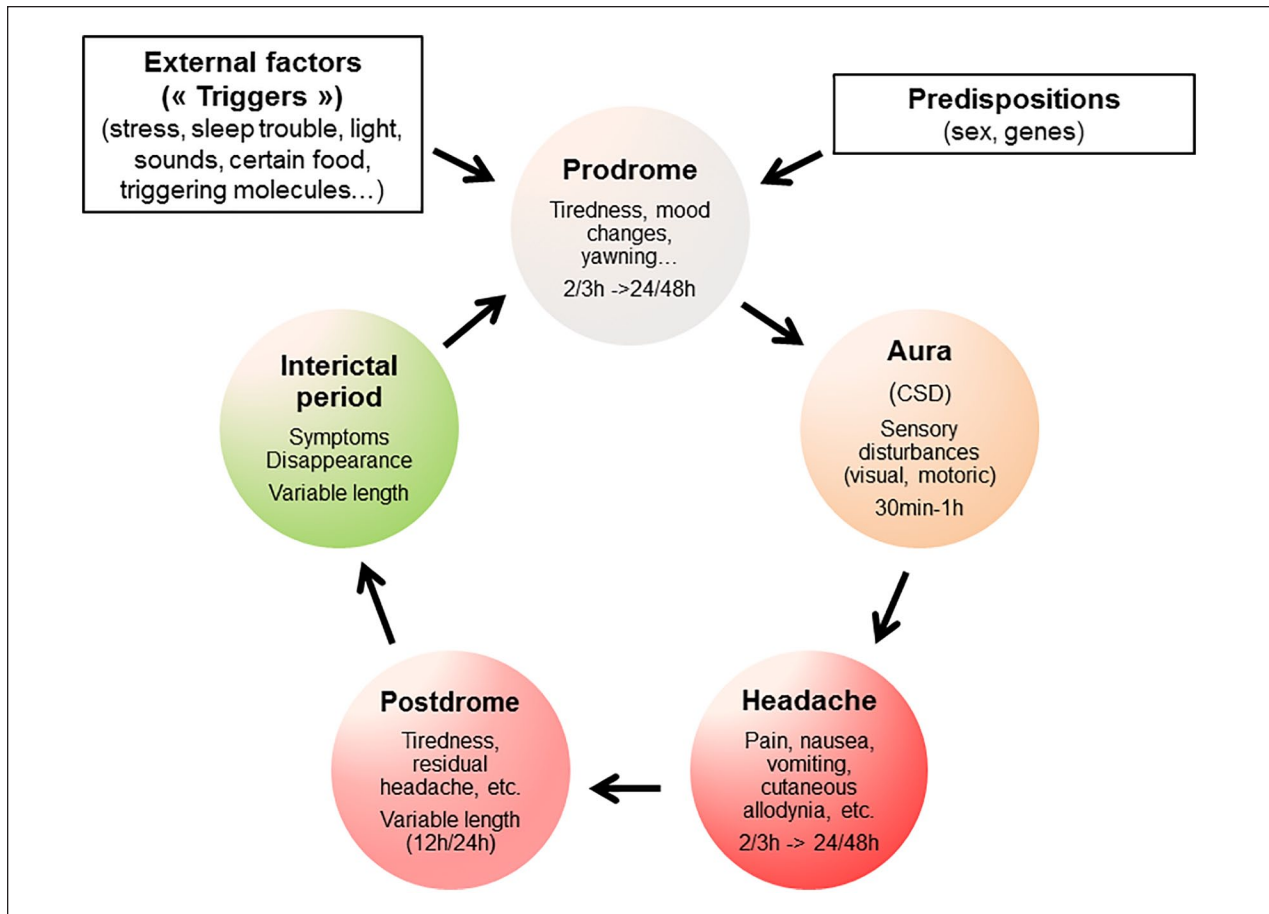


Figure 1. Schematic display of the migraine crisis and its associated symptoms. A combination of external factors and predispositions are underlying the generation of a migraine attack. The different phases (red circles) have variable length and are characterized by multiple, sometimes overlapping symptoms. The interictal period (green circle) corresponds to the end of migraine-associated symptoms. The duration of this phase is variable and will depend on many factors such as medication overuse or inappropriate behavior leading to a longer exposure to potential triggering factors. As such, chronic migraine patients have a considerably reduced interictal period.

headache and produce functional imaging changes on their own (Denuelle and others 2007; Schulte and May 2016). Therefore, migraine can be considered as a broad sensory disorder. Migraine patients display abnormal responses toward pain (Nahman-Averbuch and others 2019) or light (Bernstein and others 2019). Other differences lie on responses that should be adaptive but become impaired or maladaptive, such as altered brainstem processing (Vila-Pueyo and others 2019), changes in gray matter volume (Coppola and others 2017), impaired adaptive cerebral hemodynamic mechanisms (Frederiksen and others 2019), habituation deficiency (Coppola and others 2005) or metabolic impairment (Gross and others 2019). Due to the nature of the triggers reported by patients (stress, sleep disorder, etc.) (Karsan and Goadsby 2018; Turner and Houle 2018) and a clear involvement of the hypothalamus in the early phases of the attack, migraine is considered as a

deregulated response toward various stressful stimuli, highlighting the difficulty of the brain to keep a physiological and stable state. Thus, migraine has been described as a pathophysiology of allostasis (i.e., the responses that help to maintain physiological stability) (Borsook and others 2012). Despite the broad impact of migraine, the understanding of several aspects of its pathophysiology and underlying mechanisms remain unclear.

Initiation of Migraine Attacks: Triggering Factors and Genetic Aspects

Triggering Factors

Among various external factors able to trigger migraine attacks, stress is the most reported (Turner and Houle 2018).

In clinical and preclinical context, methods for inducing a migraine attack include the injection of triggering molecules, like the calcitonin gene-related peptide (CGRP), for which elevated levels have been measured in patients during migraine attacks (Edvinsson and others 2018), nitric oxide (NO) donors or pituitary adenylate-cyclase activating peptide (PACAP) (Al-Karagholi and others 2019; Ashina and others 2017a; Ashina and others 2017b; De Felice and others 2010; De Felice and Porreca, 2009; Guo and others 2016; Liu and others 2013). However, NO donors, for example, are triggers in migraine patients but poorly affect healthy volunteers (Schytz and others 2010). Nevertheless, in certain experimental conditions (doses and combined use of provocative drugs, duration of treatment), a higher proportion of healthy individuals may develop a genuine migraine attack, suggesting the existence of a putative “migraine threshold” (Olesen and Ashina 2015).

Genetic Aspects

Early studies on the genetics of migraine have led to the identification of several genes responsible for rare cases of familial hemiplegic migraine (FHM). This includes FHM1, a gain-of-function mutation affecting the alpha subunit of the voltage-gated calcium channel $Ca_v2.1$ (CACNA1A) leading to an increase in synaptic transmission (van den Maagdenberg and others 2004), FHM2, a loss-of-function mutation targeting the alpha 2 subunit of the astrocytic Na^+/K^+ ATP-dependent pump (ATP1A2) and resulting in an impaired clearance of synaptic glutamate (De Fusco and others 2003) and FHM3, impairing the alpha subunit of the voltage-gated sodium channel $Na_v1.1$ (SCN1A) (Dichgans and others 2005; Zerimech and others 2020). However, those mutations are also linked to other diseases such as dyskinesia, ataxia, or mental retardation. Furthermore, they only account to a minor proportion of migraine patients (around 1 of 10,000) (Ducros 2013). Another gene whose loss of function has been recently associated with migraine is KCNK18, which encodes the two-pore-domain (K_{2p}) potassium channel TRESK (Twik-related spinal cord K^+ channel) (Lafrenière and others 2010). The mutation in this gene was the only one that has been linked to a “common” migraine phenotype. Nevertheless, the latter was a matter of controversy until recently (Pettingill and others 2019; Royal and others 2019, see below).

Due to their contribution to neuronal excitability, a genomic study has explored the potential involvement of hundreds of ion transport genes in migraine pathology (Nyholt and others 2008). However, a significant gene variant has not been identified. In the last years, larger scale genome-wide association studies (GWAS) have made important contributions to identify genetic components involved in

migraine, resulting in new hypotheses regarding migraine pathophysiology (Nyholt and others 2017). Further studies provided evidence that common types of migraine are genetically complex: multiple genetic variants with small effect sizes act together with environmental factors to confer migraine susceptibility (Gormley and others 2018). Interestingly, those studies have identified other variants in genes encoding K_{2p} channels, namely KCNK5 (TASK2, Twik-related acid sensing K^+ channel) (Gormley and others 2016) and KCNK4 (TRAAK, Twik-related arachidonic acid stimulated K^+ channel). It is also of note that migraine has a genetic overlap with psychiatric disorders, especially depression, in which K_{2p} channels have been also shown to play a role (Djillani and others 2019; Heurteaux and others, 2006).

Anatomy: Focus on the Migraine Pain Pathway

Multiple sensory symptoms arise during a migraine attack, being the headache the most prominent one. It is now well established that migraine headache is the result of the activation and sensitization (decreasing response threshold and increasing response strengths) of trigeminal neurons and, to a lesser extent, cervical nociceptive C (non-myelinated) and $A\delta$ (myelinated) fibers that innervate cranial meninges and their blood vessels (Khan and others 2019; Strassman and others 1996). This ensemble is commonly referred to the trigeminovascular system (Fig. 2). The pathway starts in trigeminal sensory neurons whose cell bodies are located in the trigeminal ganglia (TG) and send peripheral axons to the meningeal dura mater and the surrounding blood vessels through the ophthalmic branch of the trigeminal nerve (V1). Central axons from TG neurons project to the trigeminal nucleus caudalis (TNC) (Uddman and others 1985). This nucleus integrates signals from projections coming from periorbital skin and pericranial muscles. The ascending axon projections of TNC transmit nociceptive information to diverse hypothalamic, brainstem and basal ganglia nuclei that could explain different migraine related symptoms such as vomiting, nausea and yawning (Burstein and others 2015). Additionally, trigeminovascular nociceptive information is subject to extensive modulation by multiple descending neurons from different brain regions (Goadsby and others 2017), including various brainstem nuclei, notably the Locus coeruleus and Periaqueductal Grey (Edelmayer and others 2009; Vila-Pueyo and others 2019), the hypothalamus (Goadsby and others 2017) or the cerebral cortex (Noseda and others 2010).

Activation of trigeminal and innervating fibers in meninges is thought to initiate a neurogenic and sterile inflammation, owing to the dense population of various vasoactive neuropeptides (i.e., CGRP, PACAP, and substance P) within sensory neurons and to the proximity of

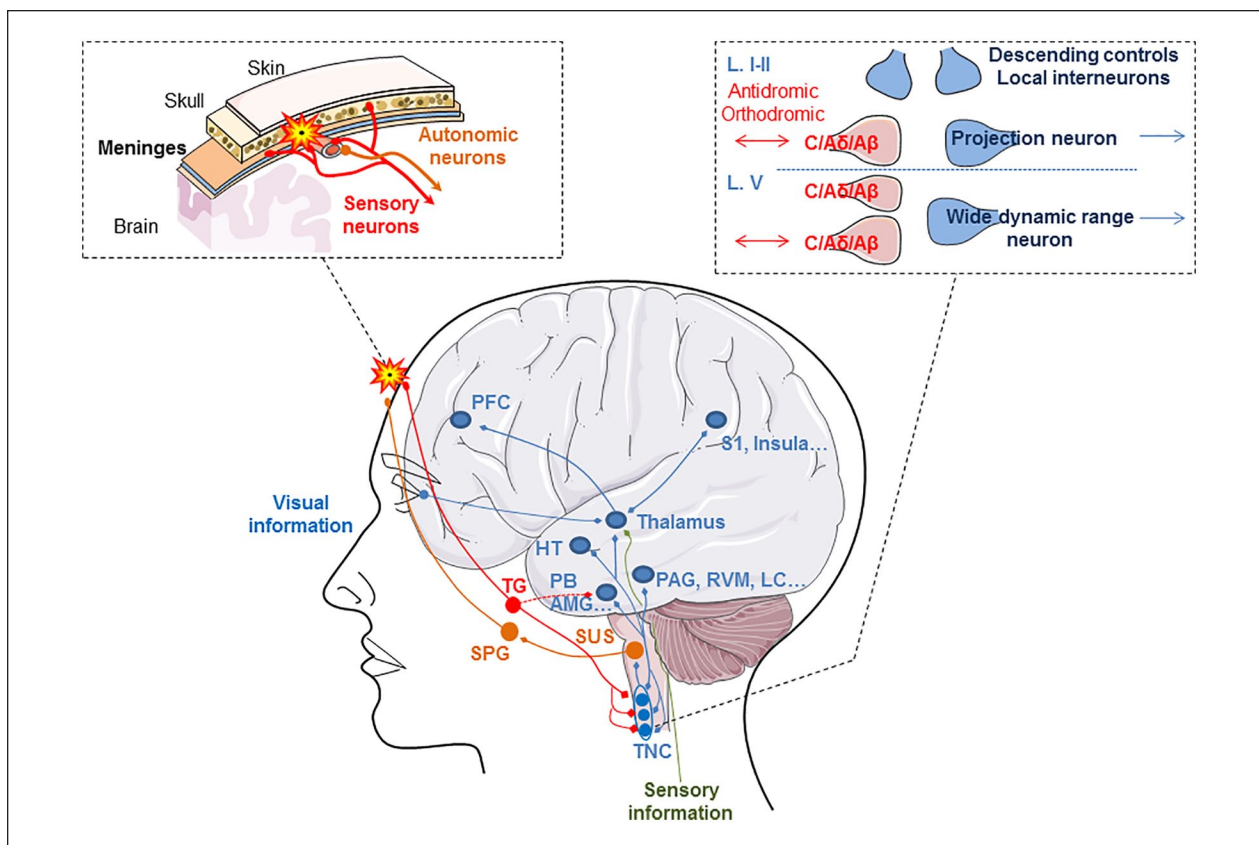


Figure 2. Migraine pathophysiology: Anatomy of the trigeminovascular pathway. The migraine attack begins in trigeminal ganglion (TG), whose axons (red lines) project to meningeal dura mater blood vessels through the ophthalmic branch stimulating the production of vasoactive neuropeptides. Nociceptive information is then carried from meninges to the rest of the brain through sensory and autonomic neurons. A second group of axons from TG targets the trigeminal nucleus caudalis (TNC), which also receives information from anterior and posterior parts of head and upper neck (red lines). TNC conveys then the inputs to diverse nuclei at limbic system, basal ganglia, hypothalamus, cortex, and thalamus (blue lines). The thalamus also integrates stimuli detected from the outside and from internal organs (green lines). Additional nuclei are believed to contribute to migraine headache. Activation of the sphenopalatine ganglion (SPG) (orange lines) may stimulate antidromic sensory fibers converging to the superior salivatory nucleus (SUS), which contains cell bodies involved in the parasympathetic autonomic vasodilator pathway.

blood vessels, immune cells (Edvinsson and others 2018; Levy and others 2019; Rua and McGavern 2018) and autonomic neuron fibers (Harriott and Gold 2009). Meningeal sensory neurons are equipped with a rich set of receptors and ion channels, allowing them to be exquisitely sensitive and to respond to a broad range of chemical and mechanical stimuli (Bonnet and others 2019; Burgos-Vega and others 2016; Levy and others 2019). There is now growing evidence that an inflammatory component might sustain nociceptor activation and sensitization, through the action of protons, cytokines, or neurotrophic factors and their downstream targets (van Dongen and others 2017).

However, the initiating event leading to the activation of meningeal sensory neurons in the context of a migraine attack remains unclear. Regarding migraine with aura,

CSD was shown to activate meningeal nociceptors, being also linked to a meningeal inflammation (Boly and others 2002; Hadjikhani and others 2020; Karatas and others 2013). A more likely explanation combines extensive modulation of trigeminovascular information, predetermined hyperexcitable migraine brain and increase of nociceptive information by external triggering factors (Bree and Levy 2018; Kunkler and others 2018). Nowadays, it is well-established that trigeminal neuron hyperexcitability is a key factor for migraine headache generation and some associated symptoms (throbbing headache, cutaneous allodynia, some autonomic symptoms) through its role in the development of peripheral and central sensitization at various levels of the migraine pain network (Olesen and others 2009; Strassman and others 1996).

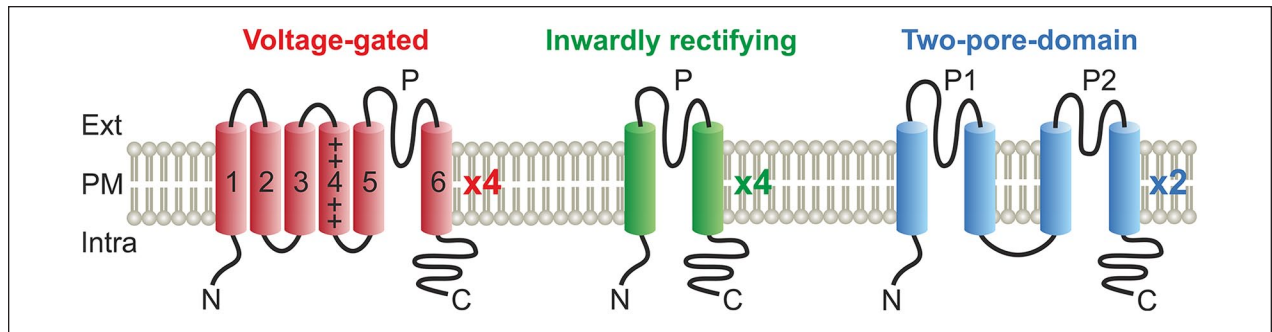


Figure 3. Membrane topology of potassium channels. Voltage-gated channels (red) possess six transmembrane domains and one pore domain (P). Some of them also present a seventh transmembrane segment. The inward rectifier channels (green) consist of two transmembrane domains and one pore domain (P), like the voltage-dependent channels they are active as tetramers. The two-pore-domain potassium channels (blue) possess four transmembrane domains and two pore domains (P1 and P2) and are active as dimers.

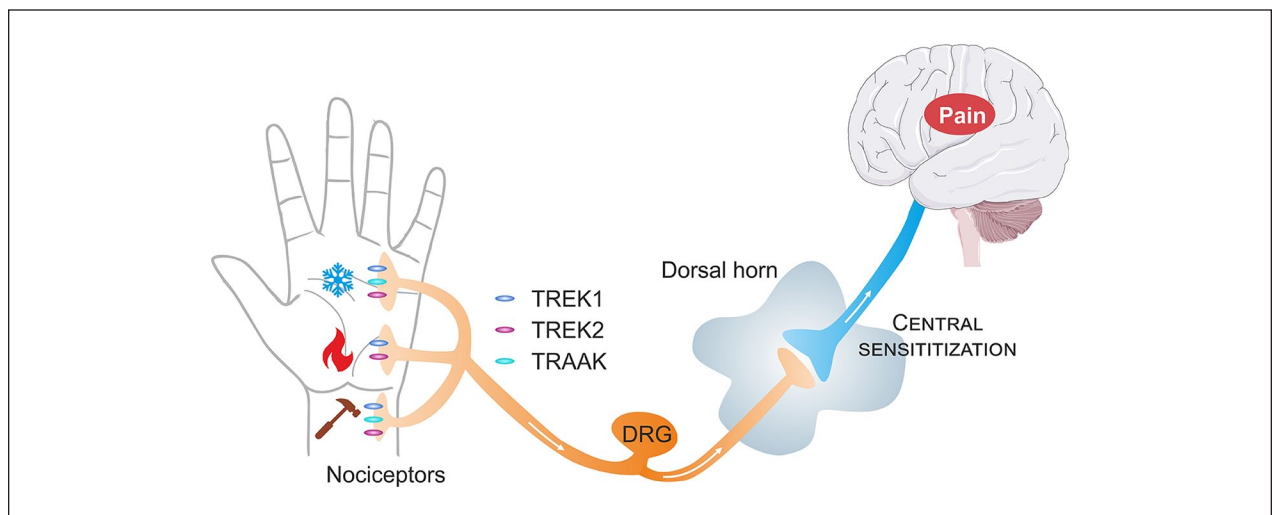


Figure 4. TREK channel members are involved in several polymodal ways of pain perception. Thermal and mechanical stimuli are detected by several TREK channels expressed in nociceptors (along with other ASIC, TRP, and piezo channels). They are primary sensors of a nervous signal that is sent to the cortex where it is integrated as a pain signal. DRG = dorsal root ganglion.

K_{2P} Channels and Pain

K_{2P} channels constitute one of the major families of K^+ channels. Its members share a dimeric structure with four transmembrane domains and two pore loops per subunit. Because of the two pore loops per subunit, these channels are not active as tetramer but as dimer (Fig. 3). K_{2P} channels exhibit a “background” K^+ conductance that is time- and voltage-independent and brings the resting membrane potential of cells toward the K^+ potential equilibrium. Therefore, they serve as a hub for the regulation of neuronal excitability by setting the resting membrane potential below the firing threshold in excitable cells. Furthermore, they were recently shown to contribute to neuronal high firing frequency

and high-speed conduction along myelinated axons by driving action potential repolarization (Ávalos Prado and Sandoz 2019; Brohawn and others 2019; Kanda and others 2019). Fifteen genes have been found to encode for this channel family that can be subdivided into six subfamilies depending of their sequence homology and biophysical properties (Box 1). K_{2P} channels play a central and active role in the response of cells to extracellular and intracellular signals as diverse as G-protein coupled receptor (GPCR) signaling, pH, and membrane stretch. They have been shown to participate in multiple physiological and pathological aspects of peripheral pain perception. Notably, they have been implicated in thermal and mechanical nociception (Fig. 4, Noël and others 2009) and also in inflammatory, neuropathic,

cancer, and recently, migraine pain (Alloui and others 2006; Descoeur and others 2011; Lafrenière and others 2010). This group mainly includes TWIK1, the members of the TREK subfamily (TREK1, TREK2, and TRAAK), the TASK subfamily members (TASK1 and TASK3) and TRESK (Li and Toyoda 2015). They are all expressed throughout the nervous system along the pain

pathway in various populations of dorsal root ganglia (DRG) or TG sensory neurons. It is worth to note that they are enriched in small and unmyelinated neurons that are mainly involved in noxious stimuli detection (e.g., peptidergic, non-peptidergic, itch, or cold-sensitive) (Acosta and others 2014; Alloui and others 2006; Pereira and others 2014).

Box I. Ion Channel Heteromerization and Means to Study It.

Heteromultimerization is a classical mechanism commonly used to increase the diversity of protein complexes. Despite the fact that K_{2P} channels share rather low sequence identity, it has been demonstrated that heteromerization is possible between different K_{2P} members. The first hints that pointed to the general possibility of a heteroassembly of K_{2P} members were reported in 2002 (Czirják and Enyedi 2002) when co-expression of TASK1 and TASK3 in *Xenopus* oocytes led to functional channels with intermediate channel properties. After, the existence of native TASK1/TASK3 dimers was proven in mammalian motoneurons (Berg and others 2004). Later, it was shown that these channels also dimerize with a member of a different subfamily, namely TWIK1 (Plant and others 2012), and several studies reported potential dimers of TWIK1/TREK1 (Mi Hwang and others 2014), THIK1/THIK2 (Blin and others 2014), TREK1/TREK2/TRAAK (Blin and others 2016; Levitz and others 2016), TASK1/TALK2 (Suzuki and others 2017), and finally, TREK1/TREK2/TRESK (Royal and others 2019). Nevertheless, not all K_{2P} subunits of the K_{2P} family are able to dimerize to form functional channels, but the compilation of a full K_{2P} interactome is impeded by the great variety of channel properties as well as the absence of specific pharmacology. The toolbox to study K_{2P} channel dimerization ranges from electrophysiology recordings of co-expressed or tandem-linked channels to fluorescence resonance energy transfer (FRET) assays or fluorescence imaging of co-localization experiments. The use of such various technical approaches has led to controversies in the field, for example for the TREK1-TWIK1 dimers, which has been described as the main potassium conductance in astrocytes (Hwang and others 2014), whereas this dimer was shown not to exist in a previous study (Plant 2012). To address the question of protein assembly, a new technology allowing direct visualization at single molecule level has been developed, the so-called single molecule pulldown (SiMPull) assay (Jain and others 2011), based on antibody-mediated immunoprecipitation of protein subunits carrying an affinity tag (e.g., HA [Human influenza hemagglutinin]) on passivated coverslips (Fig. B1-1). These proteins serve as bait molecules which can capture their respective fluorescence tagged protein partners. The visualization of this interaction is then carried out by total internal reflection fluorescence (TIRF) microscopy. The combination of biochemical immunoprecipitation with single molecule fluorescence microscopy allows to systematically test all K_{2P} interactions among the 120 that can be expected from the combination of the 15 members of the K_{2P} channel family (Fig. B1-2).

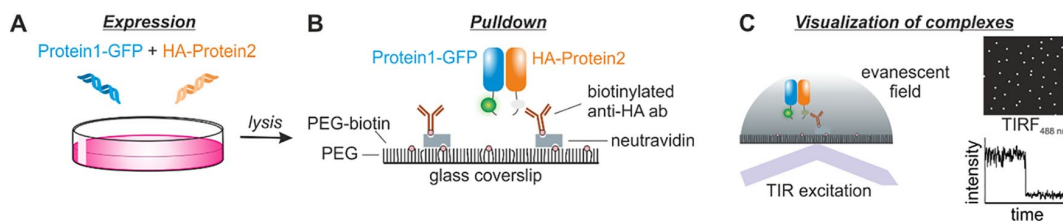
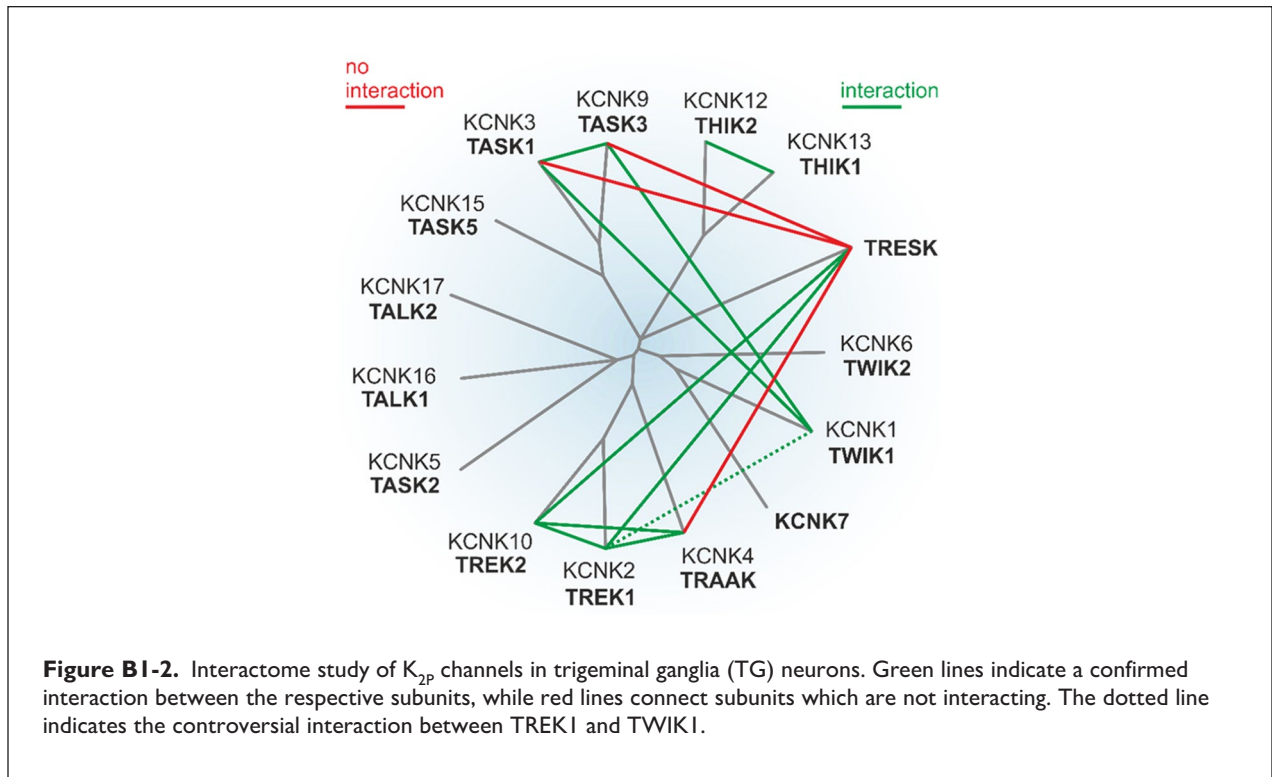


Figure B1-1. Principle of the single molecule pulldown assay. (A) To study the interaction of two proteins of interest, a protein with a fluorescence tag like the green fluorescent protein (GFP) is co-expressed with a second protein exhibiting an affinity tag like HA. (B) After lysis of the cells, the lysate is applied in flow chambers on passivated coverslips containing surface tethered antibodies. (C) The presence of GFP-tagged proteins allows the visualization of single protein complexes by TIRF (total internal reflection fluorescence) microscopy and subunit counting by observation of bleaching events.

Box I. (continued)

Box I. (continued) **K_{2p} Channels and Migraine**

With the identification of the FHM genes in the late 1990s and in the mid-2000s, a subsequent large-scale study was conducted by Nyholt and colleagues investigating the potential contribution to migraine pathology of common variations affecting several ion transport-related genes. Though none of the studied variants reached a statistical threshold, two K_{2p} channels (TREK1 and THIK2) were preliminarily selected as promising candidates in a Finnish cohort (Nyholt and others 2008). A pioneer study clearly linking K_{2p} channels and migraine led to the identification of a frameshift mutation in the gene encoding for TRESK channel, the F139WfsX24 mutation (TRESK-MT). This mutation, segregating perfectly with migraine with aura phenotype (and sometime without aura), was shown to produce a non-functional protein that served as a dominant-negative form of the wild-type (WT) TRESK channel (Lafrenière and others 2010) explaining its genetic dominant role. TRESK-MT has been shown to induce hyperexcitability of TG neurons (Guo and others 2014; Liu and others 2013), which likely underscores its role in migraine. Furthermore, the causative role of this mutation was emphasized by an elegant study with human nociceptive neurons derived from induced pluripotent

stem cells from migraine patients. In fact, these neurons are hyperexcitable and CRISPR-Cas9 engineering, for correcting the F139WfsX24 mutation, reversed the neuronal hyperexcitability (Pettingill and others 2019). However, in a subsequent genetic screening study, another missense TRESK variant, C110R, was identified (Andres-Enguix and others 2012). The TRESK-C110R mutation, similarly to TRESK-MT, was shown to produce a non-functional channel which exerts a dominant negative effect on the WT-TRESK channel in heterologous cells, but unexpectedly this mutant was found to have no effect on TG excitability when overexpressed (Guo and others 2014) and in human derived C110R mutant neurons (Pettingill and others 2019). This absence of effect elucidates why this mutant was found in both migraine and control subjects. We have recently shown in rodent that, even though both mutations lead to the same apparent deleterious effect on TRESK function, only TRESK-MT is able to functionally inhibit two other members of the K_{2p} channel family (Fig. 5). Inhibition of TREK1 and TREK2 channels activity then induces TG hyperexcitability and subsequent migraine pathophysiology (Fig. 6) (Royal and others 2019; see below). It is worth to note that a new TRESK mutation was just published to generate migraine and intellectual disability

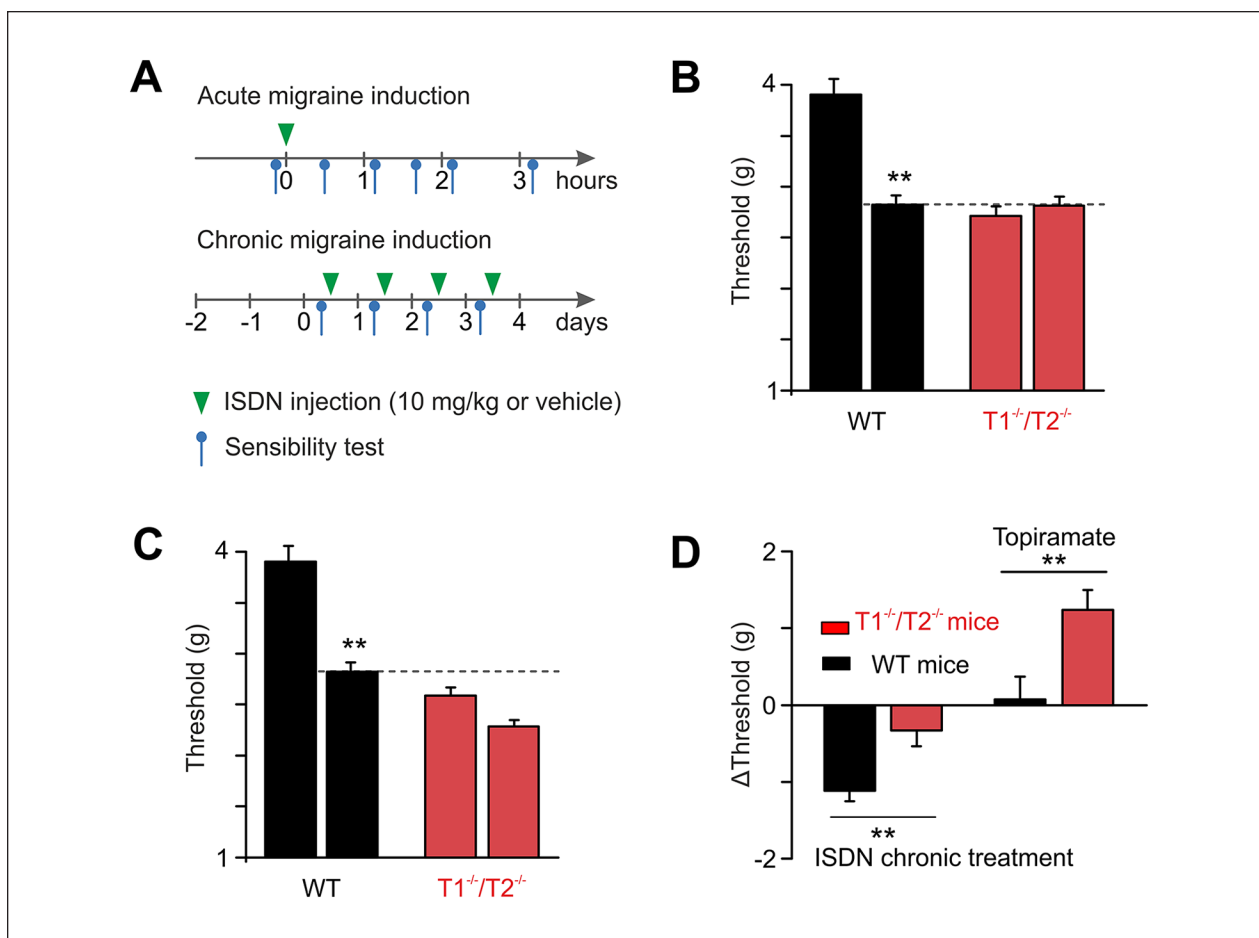


Figure 5. TREK1^{-/-}/TREK2^{-/-} double knockout animals present a migraine-like phenotype. (A) Schematic of experimental behavioral paradigms. Green arrows represent the injection of ISDN (isosorbide dinitrate), an established migraine trigger. Blue arrows represent measurements of mechanical sensitivity (Dallel and others 2018). (B) Bar graph representing the paw withdrawal mechanical thresholds assessed 1.5 hours after ISDN injection. The wild-type (WT) mice present a significant decreased paw withdrawal, whereas no modification was observed for double knockout animals (T1^{-/-}/T2^{-/-}). (C) Mechanical responses, assessed prior to and after chronic ISDN injection (4 days), were significantly decreased in WT animals, whereas no significant change of allodynia was observed in T1^{-/-}/T2^{-/-} animals. (D) Variation Δ Threshold (g) of the paw withdrawal mechanical threshold induced by ISDN chronic treatment or topiramate injection. Mechanical responses were assessed before and after chronic ISDN treatment (4 days, left bars), and before and two hours after topiramate injection (right bars) in ISDN-non-treated WT and T1^{-/-}/T2^{-/-} mice (from Royal and others 2019).

(W101R; Imbrici and others 2020). This mutation generates a non-functional channel, which acts as dominant-negative on WT-TRESK. Further works are needed to investigate their role on TREK channels.

K_{2p} Channels, Heteromerization, and TG Excitability

Even though K_{2p} channels share a low level of sequence identity, it has been recently shown that heteromerization is not rare between K_{2p} members, increasing functional diversity (Blin and others 2016; Levitz and others 2016).

Heteroassembly can occur not only within the same subfamily but also between different subfamily members, as was shown for the dimerization of TRESK with TREK1 and TREK2 in TG neurons (Royal and others 2019). The question, why only TRESK-MT, and not TRESK-C110R leads to an inhibition of TREK1 and TREK2, was solved by the discovery of a new mechanism allowing transmission of inherited diseases through an alternative translation initiation induced by a frameshift mutation in TRESK-MT called frameshift mutation induced alternative translation initiation (fsATI, Box 2; Royal and others 2019).

Box 2. Frameshift-Mutation-Induced Alternative Translation Initiation.

The TRESK-MT mutation, induced by the frameshift F139WfsX24, is expected to encode for a non-functional channel, as it is truncated by its C-terminal part. The WT-TRESK channel was shown to interact with TREK1 and TREK2 in SiMPull assays, whereas the TRESK-MT channel was not (Royal and others 2019). If the inhibition of the TREK1/2 current by co-expression of TRESK-MT did not have its origin in a co-assembly with this truncated channel form, there must be another explanation.

It has been assumed for a long time that one eukaryotic mRNA leads to the production of one single protein and that the variety of protein isoforms derived from one gene is evoked by alternative splicing or transcription from alternative promoters. The dogma of the existence of a unique translation start site was rebutted by Marilyn Kozak, who described that in certain cases, the rule of one mRNA—one protein is not followed as strictly (Kozak 1999). In fact, ribosomes can recognize an alternative initiation site and induce the generation of a second protein coming from the same RNA.

The canonical translation usually starts by binding of the 40S ribosomal subunit, initiator tRNA and several initiating factors (e.g., eIF4E) at the 5' cap structure, a 7-methylguanosine (m^7G) which precedes all eukaryotic mRNAs. The formation of this so-called pre-initiation complex is followed by linear scanning of the mRNA for an AUG initiation codon that is located in the right context which is in most eukaryotic mRNAs given by the Kozak sequence (A/G-XX-ATGG (Kozak 1987). Subsequent binding of the 60S ribosomal subunit to the translation initiation site (TIS) then initiates the protein translation. However, if the context of the first AUG on the mRNA is not optimal (i.e., not fully matching the Kozak sequence), the codon might be skipped, and the translation will start at a downstream AUG which has a more optimal context. This mechanism is also referred to as leaky scanning (Kochetov, 2008).

Such mechanism increases the diversity of proteins derived from one gene and has been already nicely described for K_{2p} channels in 2008 (Thomas and others 2008). In this study, an alternative translation initiation site in the TREK1 channel expressed in rat brain has been found to lead to a second truncated channel isoform missing the first 56 amino acids. This Δ 1-56 TREK1 channel is able to form functional homodimers as pseudo-heterodimers with the full-length protein which leads to various channel isoforms with alternate open probability, conductance, and permeability properties. Here, the second AUG was embedded in a stronger Kozak sequence which is recognized more efficiently as the first AUG. The study impressively demonstrated, how leaky scanning of ion channel genes like KCNK2 can effectively contribute to the regulation of CNS excitability.

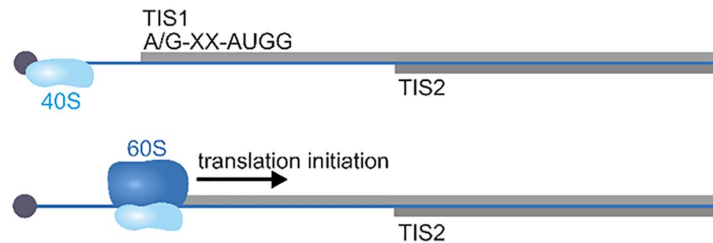
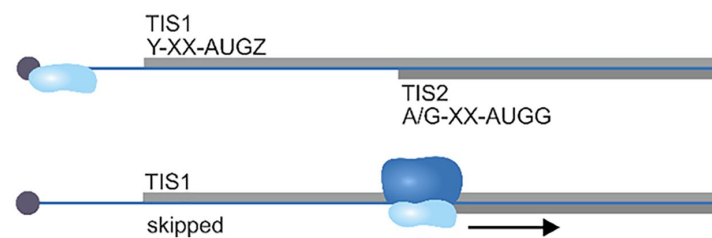
A Canonical linear scanning**B** Leaky scanning

Figure B2-I. Two common examples of eukaryotic translation initiation. (A) In the linear scanning model, the 40S ribosomal subunit binds to the 5' m^7G cap followed by subsequent scanning of the mRNA for an AUG codon, ideally embedded in a Kozak sequence (A/G-XX-**AUGG**), which serves as TIS. After assembly with the 60S ribosomal subunit, translation is initiated. (B) If the first scanned AUG is embedded in a suboptimal Kozak sequence (Y-XX-**AUGZ**, Y and Z representing Kozak-deviant bases), it is not efficiently recognized, and the scanning will proceed until the next suitable TIS is detected.

Box 2. (continued)

In the case of the *KCNK18* gene encoding for TRESK, a second AUG in a strong Kozak context can be found at position +356, yet ahead of a very short open-reading frame (ORF2). The frameshift in TRESK-MT, which is induced by deletion of two base pairs (c.410_411delCT), puts the AUG of ORF2 in frame with the C-terminal part of the full length TRESK. As the AUG of ORF2 is also embedded in an environment matching the Kozak sequence, the frameshift leads to the efficient translation of a second protein that corresponds to a TRESK-channel truncated by its N-terminus and therefore, non-functional (TRESK-MT2). The existence of this second transcript was elicited by several cell biological and biochemical assays (Royal and others 2019). We named the newly described mechanism, which is inducing an alternative translation site by displacing the open reading frame, fsATI (frameshift-mutation-induced alternative translation initiation).

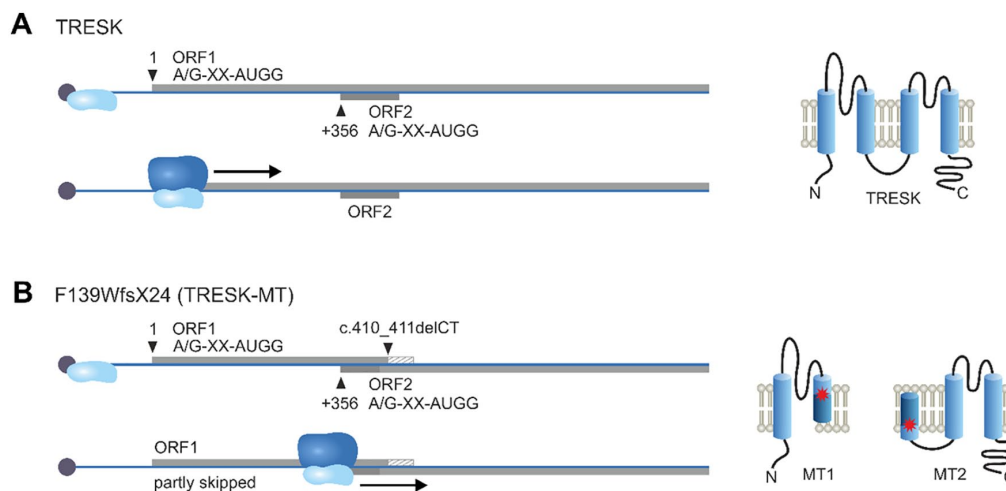


Figure B2-2. Principle of the frameshift-induced alternative translation initiation. (A) Organization of ORF1 and ORF2 on mRNA of WT-TRESK. (B) The deletion of two base pairs by the c.410_411delCT mutation results to a premature translation stop in ORF1 (TRESK-MT1). Coincidentally, the start codon of ORF2 at +356 is put in frame with the ORF of TRESK, inducing the translation of MT2.

The TRESK-MT mutation leads, through fsATI, to the production of two protein fragments instead of one, as expected (Box 1): TRESK-MT1, which corresponds to the expected C-terminal truncated TRESK channel and inhibits TRESK, and TRESK-MT2, which corresponds to an N-terminal truncated TRESK channel. TRESK-MT2, by co-assembling and inhibiting TREK1 and TREK2, induces TG sensory neuron hyperexcitability (Fig. 5). Overexpression of TRESK-MT2 in rat TG neurons, using virus, is sufficient to induce a chronic facial mechanical allodynia related to chronic migraine, an effect which has not been seen with MT1 (Royal and others 2019). Interestingly, fsATI was also found for another TRESK mutant (Y121LfsX44), which is the only other TRESK mutation related to migraine in humans (Domitrz and others 2016; Rainero and others 2014; Royal and others 2019). This mutation also leads to the production of a similar TRESK-MT2 (Royal and others 2019). The fundamental role of TREK1 and TREK2 in migraine induction has been further supported by TREK1/TREK2 double knock-out (KO) mice (Fig. 5). They exhibit a chronic migraine-like

cutaneous mechanical allodynia phenotype which can be reversed by Topiramate, a drug used in clinic to treat migraine (Royal and others 2019). This suggests, that, in human, migraine is due to the dysfunction of TREK1 and TREK2 and their respective heteromers with mutated TRESK, but not due to TRESK invalidation alone (Fig. 6).

In parallel, other preclinical studies in rodents have further confirmed a key involvement of K_{2p} channels in trigeminal nociception and migraine-related headache. Recently, TRESK invalidation was shown to increase peptidergic trigeminal neurons excitability (Guo and others 2019) and to enhance headache behavior induced by application of inflammatory mediators in the meninges (Pettingill and others 2019). These results would favor that TRESK is sufficient to generate migraine. Nevertheless, the findings by Guo and others and Pettingill and others also fits with TREK1 and TREK2 implication. In fact, by only targeting TRESK, TRESK-MT1, and C110R, the sensory neuron excitability is not altered (Guo and others 2014; Pettingill and others 2019; Royal and others 2019), whereas genetic

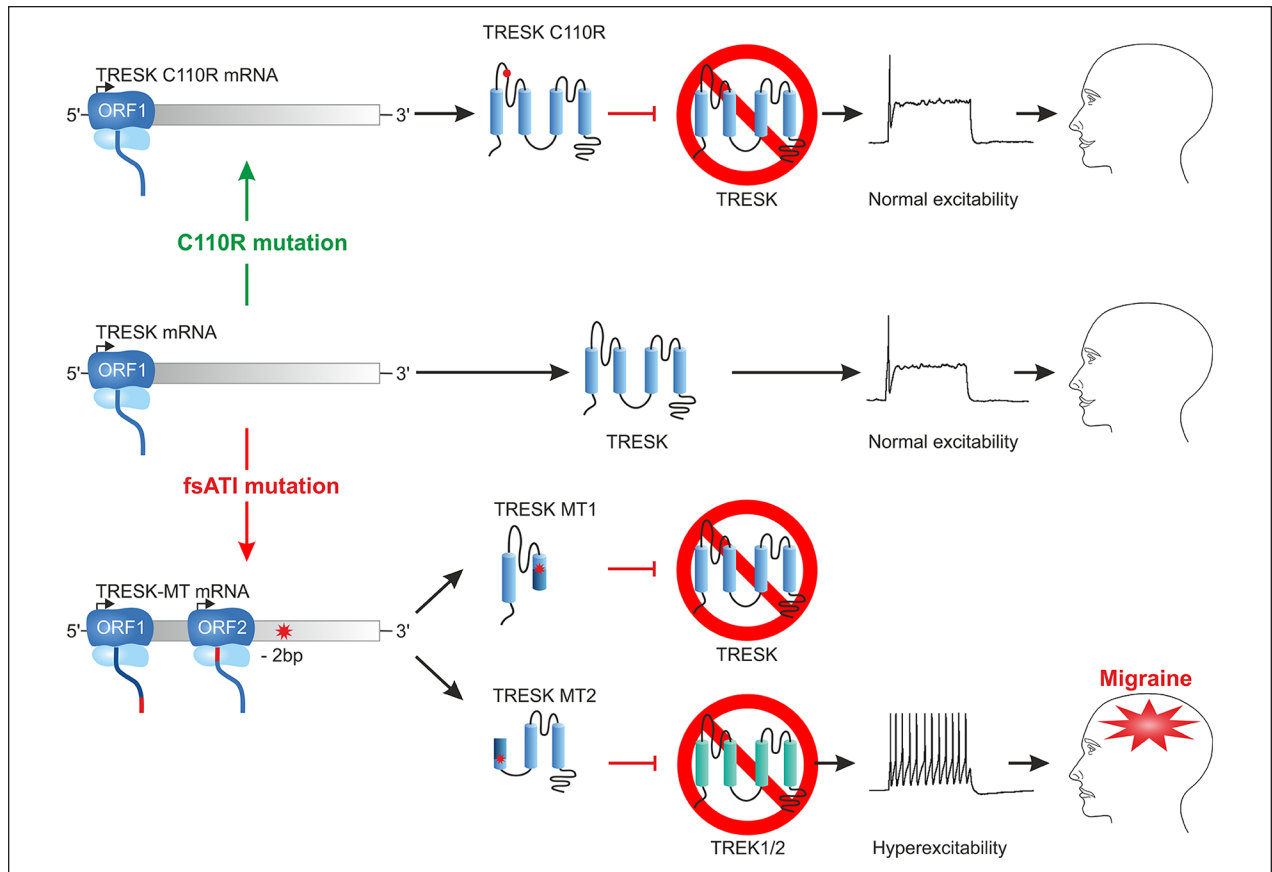


Figure 6. TRESK-MT causes migraine via inhibition of TREK1 and TREK2 by TRESK-MT2. Top: TRESKC110R targets only TRESK, which is not sufficient to induce an increase of trigeminal sensory neuron excitability and therefore does lead to migraine. Middle: the excitability of trigeminal neurons in the presence of the wild version of TRESK is normal. Bottom: the TRESK-MT mutation generates an ATI (see Box 1) resulting in the formation of two proteins, TRESK-MT1 and TRESK-MT2. TRESK-MT1 inhibits TRESK, while TRESK-MT2 targets TREK1 and TREK2. Inhibition of TREK1 and TREK2 leads to neuronal hyperexcitability causing a migraine phenotype.

inactivation affects TRESK homodimers as well as heterodimers (TRESK-TREK1, TRESK-TREK2) and therefore also TREK1 and TREK2 expression and composition at the cell surface (the equilibrium is modified). These differences between gene inactivation and dominant negative (affecting only TRESK) may explain why TRESK inactivation modifies TG excitability and induces a migraine phenotype. All in all, migraine-like behavior in rodents seems to involve both TRESK, TREK1 and TREK2 monomeric channels and TRESK-TREK heterodimeric channels.

Finally, in addition to these channels, TASK3 is also predominant in TG neurons, where it co-localizes with TRESK, TREK1, and TREK2 (Yamamoto and others 2009). Nevertheless, there is no evidence of TASK3 participation in migraine attacks. It is worth mentioning that TASK3 was not found to heteromerize with TRESK, TREK1, and TREK2 (Levitz and others 2016; Royal and others 2019).

Toward New Treatments for Migraine Involving K_{2P} Channels Targeting

Migraine therapy aims not only to terminate or to relieve acute attacks but also to prevent the evolution from episodic toward chronic migraine. Several drugs are used but present several side effects (Tables 1 and 2), for example, Topiramate may be used to treat chronic migraine but it has severe well-known side effects, including ataxia, confusion, diplopia, dizziness, drowsiness, dysphasia, fatigue, memory impairment, and others. Given the importance of CGRP as a migraine trigger, the use of monoclonal antibodies against this peptide represents one of the most effective treatments against the disease. Up to now, three different humanized monoclonal antibodies against CGRP pathway have been tested and exhibited excellent results: fremanezumab and galcanezumab, which target CGPR, and erenumab, which targets CGRP receptors (Fig. 7). All

Table 1. Current Prevent Treatments of Migraine, Their Targets, and Proposed Mechanisms of Action.

Preventive Treatment	Targets	Possible Mechanism of Action
Beta blockers (propranolol)	β 1-2 receptor antagonist	Stress reduction, neuronal modulation (descending controls), vascular effects
Antiepileptics (valproate, topiramate, levetiracetam, flunarizine, gabapentine)	Valproate: Na_v antagonist Topiramate: acts on Na_v , Ca_v , and carbonic anhydrase, modulates GABA-A and kainate receptors Levetiracetam: acts on SV2A (vesicular protein), Ca_v Flunarizine: calmodulin blocker, H1R, 5HTR, and D2R antagonist Gabapentine: Ca_v ($\alpha 2\delta$) antagonist	Decrease in neuronal excitation Decrease in neuronal excitation Decrease in neuronal excitation, modulation of neuronal activity Reduces neuronal excitation, modulation of neuronal activity Reduces neuronal excitation
Antidepressors (tricyclic: amitriptyline, SNRIs: venlafaxine)	Amitriptyline: prevents monoamine reuptake, multiple potential secondary targets (5HTR, H1-2R, α 1R, Ca_v , Na_v , K_v , etc.) Venlafaxine: prevents monoamine reuptake	Multiple actions: Decrease in neuronal excitation, modulation of neuronal activity Modulation of neuronal activity
5HTR antagonists (pizotifen, methysergide)	5HT2R antagonists	Modulation of neuronal activity
Botulinum toxin	Exocytosis of neurotransmitter vesicle	Multiple actions: muscle contraction, neuronal modulation (TRP trafficking, synaptic transmission)
ACE inhibitors (lisinopril, candesartan)	Lisinopril: ACE blocker (reduces production of angiotensin II) Candesartan: AT1R antagonist	Multiple actions: Modulation of neuronal activity (autonomic and sensory), vascular effect
Anti-CGRP (erenumab, fremanezumab)	Erenumab: antibody directed against CGRP receptor Fremanezumab: antibody against CGRP peptide	Modulation of neuronal function (neurotransmission, neuromodulation)

Table 2. Current Treatments of Acute Migraine, Their Targets, and Proposed Mechanisms of Action.

Acute Treatment	Targets	Possible Mechanism of Action
First-line analgesics (paracetamol, NSAID)	Paracetamol: multiple targets (modulation of K_v7 , TRPV1, $\text{Ca}_v3.2$, COXs) NSAID: inhibition COXs	Multiple actions: Decrease in neuronal excitation, modulation of neuronal activity Reduction of the production of inflammatory molecules (prostaglandins, etc.)
Triptans (sumatriptan)	5HT1B/5HT1D agonists	Modulation of neuronal function, other cells (vascular for 5HT1B)
Dihydroergotamine	5HT1B/5HT1D agonists	Like triptans, with a potential central and vascular effect
CGRP antagonists (rimegepant, ubrogepant)	CGRP receptor antagonist	Modulation of neuronal function (neurotransmission, neuromodulation)
Ditans (Lasmiditan)	5HT1F/5HT1D agonist	Modulation of neuronal function (neurotransmission, neuromodulation)

three products have demonstrated efficacy for the preventive treatment of chronic and episodic migraine and can be periodically self-administered (Spindler and Ryan 2020). In addition, they support the fact that an intervention at the level of the peripheral nervous system is sufficient to target migraine headache. Nevertheless, general side effects caused by monoclonal antibody drugs cannot be excluded

such as flu-like symptoms and allergic reactions in addition to the “specific” side effects such as dizziness, joint pain or pruritus and erythema.

Given their abundant expression in DRG, TG sensory and primary afferent neurons, drugs targeting K_{2p} channels constitute a promising therapy not only for the treatment of migraine and its associated pain but also of inflammatory,

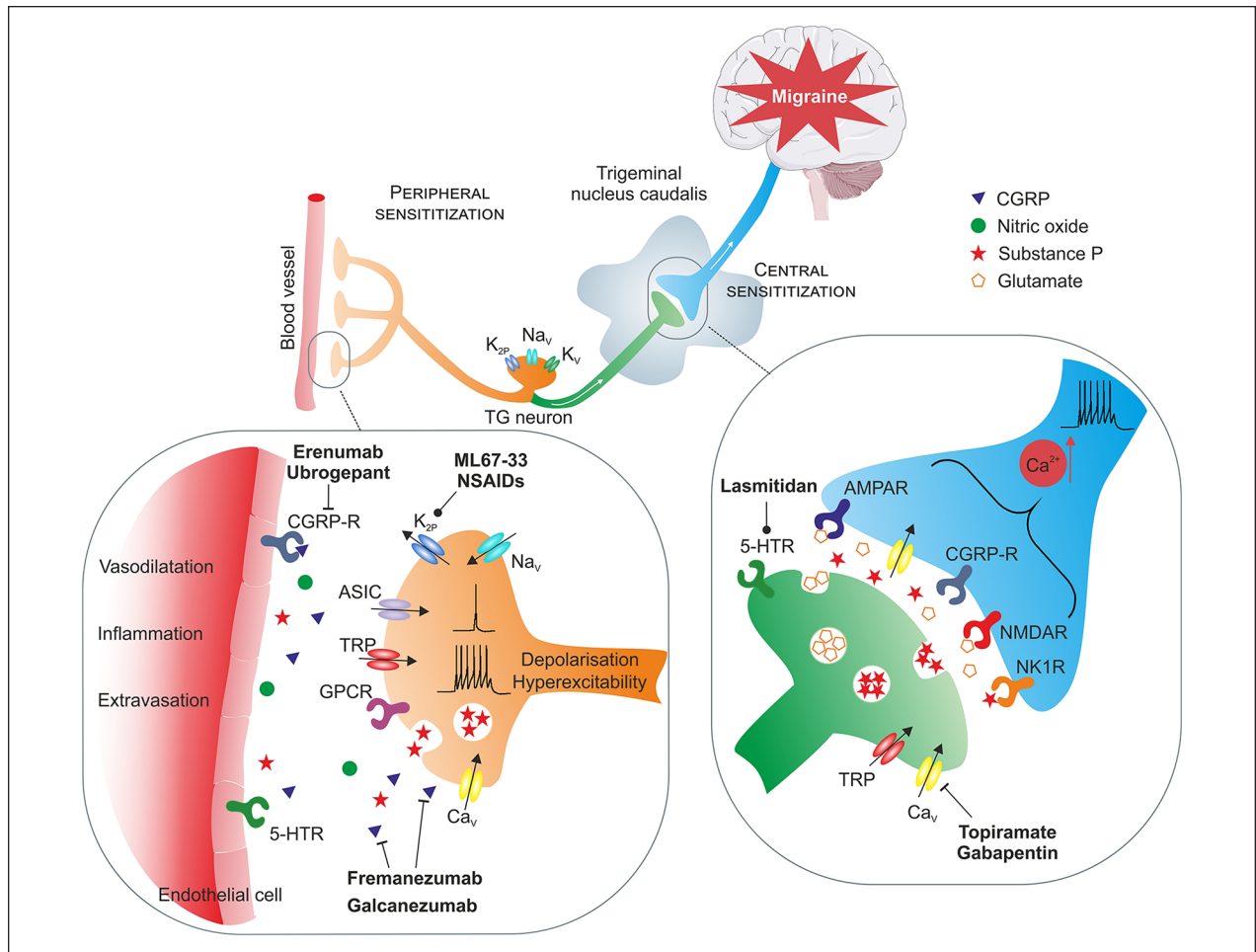


Figure 7. Main targets of currently used and potential future drugs for treating migraine headache. The analgesic action is mainly exerted by influencing several classes of receptors (ion channels, GPCRs, etc.) at multiple levels of the migraine pain pathway (peripheral trigeminal sensory neurons, TNC second order and higher neurons in the brain). They are principally acting on the neuronal hyperexcitability and the sensitization associated to migraine headache. Multiple drugs will aim at limiting the excessive depolarization through the blockade of inward cation flux (e.g., antiepileptics) or, on the opposite, through the activation of hyperpolarizing potassium channels (e.g., potential K_{2p} agonists). Other classes act on the neuronal modulation (e.g., CGRP antibodies) or neurotransmitters release (e.g., triptans).

neuropathic or cancer pains (Alloui and others 2006; Descoeur and others 2011; Noël and others 2009; Pereira and others 2014). This idea is strengthened by the fact that K_{2p} channels have been shown to be involved in other diseases such as depression (Heurteaux and others 2006), which severely affect 10% of the population suffering from migraine disorders, and that some drugs targeting K_{2p} channels have been proved to be effective against migraine, such as cloxyquin through TRESK activation (Pettingill and others 2019).

As previously shown, at least three K_{2p} channels subunits and their respective heteromers have been proved to be involved in the normal physiology and pathophysiology of migraine. TRESK, TREK1, and TREK2 containing channels seem to serve as a hub to set the negative resting potential of TG neurons (Dobler and others 2007;

Lafrenière and others 2010; Royal and others 2019). Thus, specific pharmacology targeting these channels should be potentially relevant for the development of anti-migraine treatment. Furthermore, targeting heterodimers would allow to reach higher specificity. Currently, only a small number of agonists of the aforementioned channels have been studied to be effective for migraine treatment. Among them, the anti-leukotriene agent Montelukast for asthma management has been demonstrated to act as a well-tolerated and prophylactic agent against acute migraine episodes at dosages of 10 to 20 mg per day (Sheftell and others 2000). Its efficacy may lie in its ability to specifically activate TRESK and TRESK heteromer channels (Wright and others 2019).

During migraine, experimental studies have demonstrated an increase of prostaglandin 2 (PGE2) in

the trigeminovascular system, where their receptors are distributed along TG and TNC neurons and induce vasodilation of cranial vessels (Antonova and others 2013). PGE2 is also known to be a potent inhibitor of TREK1 channels (Honoré 2007). Non-steroidal anti-inflammatory drugs (NSAIDs), which represent another widespread treatment to manage headache in acute migraine, may eventually avoid TREK1 inhibition.

Finally, although they have not yet been clinically tested, a number of selective activators of K_{2p} channels should also be considered for chronic migraine prevention. Among them, it is worth mentioning ML67-33, a well-known specific activator of TREK1, TREK2, and TRAAK channels, that exhibit an EC_{50} in micromolar range (Bagriantsev and others 2013). Further development of selective agents targeting specific heterodimers involving TRESK may be considered to increase specificity and to reduce secondary drug effects.

Concluding Remarks

Migraine is a common and disabling disease associated with disorders in neuronal excitability and cerebral blood flow. The complexity of the underlying processes which are not yet fully understood still render migraine treatment difficult. Currently, it is assumed that migraine headache is triggered by TG neuron activation. Hyperexcitability of TG fibers evokes release of vasoactive neuropeptides that enhance vasodilation causing neurogenic inflammation. This leads to a pain response to be conveyed to higher brain centers, including cortex, hypothalamic, brainstem and basal ganglia nuclei. The mechanisms leading to trigeminal hyperexcitability have not been fully elucidated until very recently.

K_{2p} channels, namely homo- and heterodimers of TRESK, TREK1, and TREK2, seem to play a key role in TG neuronal excitability and are therefore promising targets for migraine treatment. The discovery of a new type of translation initiation, generating several protein forms that can regulate other channels by heteromerization, clarified the understanding of K_{2p} channel implication in this disease. Henceforth, the novel role of K_{2p} channels in migraine, as well as their ability to generate functional and non-functional heterodimers, provides motivation for developing a deeper understanding of their function and organization within the plasma membrane and demonstrates that they have to be now taken into consideration for the development of highly specific pharmacological agents to treat migraine.

Declaration of Conflicting Interests

The author(s) declared no potential conflicts of interest with respect to the research, authorship, and/or publication of this article.

Funding

The author(s) disclosed receipt of the following financial support for the research, authorship, and/or publication of this article: This work was supported by a grant to G.S. by the Fondation pour la Recherche Medicale (Equipe labellisée FRM 2017, FRM DEQ20170336753 and ANR AT2R-TRAAK-Bioanalgesics ANR-17-CE18-0001) as well as Laboratory of Excellence “Ion Channel Science and Therapeutics,” grant ANR-11-LABX-0015-01 and the French government, through the UCAJEDI Investments in the Future project managed by the National Research Agency (ANR) with the reference number ANR-15-IDEX-01. The work was also supported by a grant to P.A.P. by the Fondation pour la Recherche Medicale (FRM 2019, FDT201904008083).

ORCID iDs

Clément Verkest  <https://orcid.org/0000-0001-8612-8002>

Stephanie Häfner  <https://orcid.org/0000-0003-0501-2193>

Guillaume Sandoz  <https://orcid.org/0000-0003-1251-0852>

References

- Acosta C, Djouhri L, Watkins R, Berry C, Bromage K, Lawson SN. 2014. TREK2 expressed selectively in IB4-binding C-fiber nociceptors hyperpolarizes their membrane potentials and limits spontaneous pain. *J Neurosci* 34(4):1494–509.
- Adams AM, Serrano D, Buse DC, Reed ML, Marske V, Fanning KM, and others. 2015. The impact of chronic migraine: The Chronic Migraine Epidemiology and Outcomes (CaMEO) Study methods and baseline results. *Cephalalgia* 35(7):563–78.
- Al-Karagholi MA, Hansen JM, Guo S, Olesen J, Ashina M. 2019. Opening of ATP-sensitive potassium channels causes migraine attacks: a new target for the treatment of migraine. *Brain* 142(9):2644–54.
- Alloui A, Zimmermann K, Mamet J, Duprat F, Noël J, Chemin J, and others. 2006. TREK-1, a K^+ channel involved in polymodal pain perception. *EMBO J* 25(11):2368–76.
- Andres-Enguix I, Shang L, Stansfeld PJ, Morahan JM, Sansom MS, Lafrenière RG, and others. 2012. Functional analysis of missense variants in the TRESK (KCNK18) K channel. *Sci Rep* 2:237.
- Antonova M, Wienecke T, Olesen J, Ashina M. 2013. Prostaglandins in migraine: update. *Curr Opin Neurol* 26(3):269–75.
- Ashina M, Dodick D, Goadsby PJ, Reuter U, Silberstein S, Zhang F, and others. 2017a. Erenumab (AMG 334) in episodic migraine: Interim analysis of an ongoing open-label study. *Neurology* 89(12):1237–43.
- Ashina M, Hansen JM, Á Dunga BO, Olesen J. 2017b. Human models of migraine—short-term pain for long-term gain. *Nat Rev Neurol* 13(12):713–24.
- Ávalos Prado P, Sandoz G. 2019. TREK for high-speed and high-frequency conduction through the axon. *Neuron* 104(5):831–3.
- Bagriantsev SN, Ang KH, Gallardo-Godoy A, Clark KA, Arkin MR, Renslo AR, and others. 2013. A high-throughput functional screen identifies small molecule regulators of

- temperature- and mechano-sensitive K₂P channels. *ACS Chem Biol* 8(8):1841–51.
- Berg AP, Talley EM, Manger JP, Bayliss DA. 2004. Motoneurons express heteromeric TWIK-related acid-sensitive K⁺ (TASK) channels containing TASK-1 (KCNK3) and TASK-3 (KCNK9) subunits. *J Neurosci* 24(30):6693–702.
- Bernstein CA, Nir RR, Noseda R, Fulton AB, Huntington S, Lee AJ, and others. 2019. The migraine eye: distinct rod-driven retinal pathways' response to dim light challenges the visual cortex hyperexcitability theory. *Pain* 160(3):569–78.
- Blin S, Ben Soussia I, Kim E-J, Brau F, Kang D, Lesage F, and others. 2016. Mixing and matching TREK/TRAAK subunits generate heterodimeric K₂P channels with unique properties. *Proc Natl Acad Sci U S A* 113(15):4200–5.
- Blin S, Chatelain FC, Feliciangeli S, Kang D, Lesage F, Bichet D. 2014. Tandem pore domain halothane-inhibited K⁺ channel subunits THIK1 and THIK2 assemble and form active channels. *J Biol Chem* 289(41):28202–12.
- Bolay H, Reuter U, Dunn AK, Huang Z, Boas DA, Moskowitz MA. 2002. Intrinsic brain activity triggers trigeminal meningeal afferents in a migraine model. *Nat Med* 8(2):136–42.
- Bonnet C, Hao J, Osorio N, Donnet A, Penalba V, Ruel J, and others. 2019. Maladaptive activation of Nav1.9 channels by nitric oxide causes triptan-induced medication overuse headache. *Nat Commun* 10(1):4253.
- Borsook D, Maleki N, Becerra L, McEwen B. 2012. Understanding migraine through the lens of maladaptive stress responses: a model disease of allostatic load. *Neuron* 73(2):219–34.
- Bose P, Karsan N, Goadsby PJ. 2018. The migraine prodrome. *Continuum (Minneapolis Minn)* 24(4, Headache):1023–31.
- Bree D, Levy D. 2018. Development of CGRP-dependent pain and headache related behaviours in a rat model of concussion: implications for mechanisms of post-traumatic headache. *Cephalalgia* 38(2):246–58.
- Brohawn SG, Wang W, Handler A, Campbell EB, Schwarz JR, MacKinnon R. 2019. The mechanosensitive ion channel TRAAK is localized to the mammalian node of Ranvier. *Elife* 8:e50403.
- Burch RC, Loder S, Loder E, Smitherman TA. 2015. The prevalence and burden of migraine and severe headache in the United States: updated statistics from government health surveillance studies. *Headache* 55(1):21–34.
- Burgos-Vega CC, Ahn DD, Bischoff C, Wang W, Horne D, Wang J, and others. 2016. Meningeal transient receptor potential channel M8 activation causes cutaneous facial and hindpaw allodynia in a preclinical rodent model of headache. *Cephalalgia* 36(2):185–93.
- Burstein R, Noseda R, Borsook D. 2015. Migraine: multiple processes, complex pathophysiology. *J Neurosci* 35(17):6619–29.
- Charles AC, Baca SM. 2013. Cortical spreading depression and migraine. *Nat Rev Neurol* 9(11):637–44.
- Coppola G, Petolicchio B, Di Renzo A, Tinelli E, Di Lorenzo C, Parisi V, and others. 2017. Cerebral gray matter volume in patients with chronic migraine: correlations with clinical features. *J Headache Pain* 18(1):115.
- Coppola G, Vandenheede M, Di Clemente L, Ambrosini A, Fumal A, De Pasqua V, and others. 2005. Somatosensory evoked high-frequency oscillations reflecting thalamocortical activity are decreased in migraine patients between attacks. *Brain* 128(Pt 1):98–103.
- Czirják G, Enyedi P. 2002. Formation of functional heterodimers between the TASK-1 and TASK-3 two-pore domain potassium channel subunits. *J Biol Chem* 277(7):5426–32.
- Dallel R, Descheemaeker A, Luccarini P. 2018. Recurrent administration of the nitric oxide donor, isosorbide dinitrate, induces a persistent cephalic cutaneous hypersensitivity: a model for migraine progression. *Cephalalgia* 38(4):776–85.
- De Felice M, Ossipov MH, Wang R, Lai J, Chichorro J, Meng I, and others. 2010. Triptan-induced latent sensitization: a possible basis for medication overuse headache. *Ann Neurol* 67(3):325–37.
- De Felice M, Porreca F. 2009. Opiate-induced persistent pronociceptive trigeminal neural adaptations: potential relevance to opiate-induced medication overuse headache. *Cephalalgia* 29(12):1277–84.
- De Fusco M, Marconi R, Silvestri L, Atorino L, Rampoldi L, Morgante L, and others. 2003. Haploinsufficiency of ATP1A2 encoding the Na⁺/K⁺ pump alpha2 subunit associated with familial hemiplegic migraine type 2. *Nat Genet* 33(2):192–6.
- Denuelle M, Fabre N, Payoux P, Chollet F, Geraud G. 2007. Hypothalamic activation in spontaneous migraine attacks. *Headache* 47(10):1418–26.
- Descocq J, Pereira V, Pizzoccaro A, Francois A, Ling B, Maffre V, and others. 2011. Oxaliplatin-induced cold hypersensitivity is due to remodelling of ion channel expression in nociceptors. *EMBO Mol Med* 3(5):266–78.
- Dichgans M, Freilinger T, Eckstein G, Babini E, Lorenz-Depiereux B, Biskup S, and others. 2005. Mutation in the neuronal voltage-gated sodium channel SCN1A in familial hemiplegic migraine. *Lancet* 366(9483):371–7.
- Djillani A, Mazella J, Heurteaux C, Borsotto M. 2019. Role of TREK-1 in health and disease, focus on the central nervous system. *Front Pharmacol* 10:379.
- Dobler T, Springauf A, Tovornik S, Weber M, Schmitt A, Sedlmeier R, and others. 2007. TRESK two-pore-domain K⁺ channels constitute a significant component of background potassium currents in murine dorsal root ganglion neurones. *J Physiol* 585(Pt 3):867–79.
- Domitz I, Kosiorek M, Żekanowski C, Kamińska A. 2016. Genetic studies of Polish migraine patients: screening for causative mutations in four migraine-associated genes. *Hum Genomics* 10:3.
- Ducros A. 2013. Genetics of migraine [in French]. *Rev Neurol (Paris)* 169(5):360–71.
- Edelmayer RM, Vanderah TW, Majuta L, Zhang ET, Fioravanti B, De Felice M, and others. 2009. Medullary pain facilitating neurons mediate allodynia in headache-related pain. *Ann Neurol* 65(2):184–93.
- Edvinsson L, Haanes KA, Warfvinge K, Krause DN. 2018. CGRP as the target of new migraine therapies - successful translation from bench to clinic. *Nat Rev Neurol* 14(6):338–50.

- Frederiksen SD, Haanes KA, Warfvinge K, Edvinsson L. 2019. Perivascular neurotransmitters: regulation of cerebral blood flow and role in primary headaches. *J Cereb Blood Flow Metab* 39(4):610–32.
- Goadsby PJ, Holland PR, Martins-Oliveira M, Hoffmann J, Schankin C, Akerman S. 2017. Pathophysiology of migraine: a disorder of sensory processing. *Physiol Rev* 97(2):553–622.
- Gormley P, Anttila V, Winsvold BS, Palta P, Esko T, Pers TH, and others. 2016. Meta-analysis of 375,000 individuals identifies 38 susceptibility loci for migraine. *Nat Genet* 48(8):856–66.
- Gormley P, Kurki MI, Hiekkala ME, Veerapen K, Häppölä P, Mitchell AA, and others. 2018. Common variant burden contributes to the familial aggregation of migraine in 1,589 families. *Neuron* 98(4):743–753.e4.
- Gross EC, Klement RJ, Schoenen J, D'Agostino DP, Fischer D. 2019. Potential protective mechanisms of ketone bodies in migraine prevention. *Nutrients* 11(4):811.
- Guo S, Vollesen AL, Olesen J, Ashina M. 2016. Premonitory and nonheadache symptoms induced by CGRP and PACAP38 in patients with migraine. *Pain* 157(12):2773–81.
- Guo Z, Liu P, Ren F, Cao YQ. 2014. Nonmigraine-associated TRESK K⁺ channel variant C110R does not increase the excitability of trigeminal ganglion neurons. *J Neurophysiol* 112(3):568–79.
- Guo Z, Qiu CS, Jiang X, Zhang J, Li F, Liu Q and others. 2019. TRESK K. *eNeuro* 6(4).
- Hadjikhani N, Albrecht DS, Mainero C, Ichijo E, Ward N, Granziera C, and others. 2020. Extra-axial inflammatory signal in parameninges in migraine with visual aura. *Ann Neurol* 87(6):939–49.
- Harriott AM, Gold MS. 2009. Contribution of primary afferent channels to neuropathic pain. *Curr Pain Headache Rep* 13(3):197–207.
- Heurteaux C, Lucas G, Guy N, El Yacoubi M, Thümmler S, Peng XD, and others. 2006. Deletion of the background potassium channel TREK-1 results in a depression-resistant phenotype. *Nat Neurosci* 9(9):1134–41.
- Honoré E. 2007. The neuronal background K2P channels: focus on TREK1. *Nat Rev Neurosci* 8(4):251–61.
- Hwang EM, Kim E, Yarishkin O, Woo DH, Han KS, Park N, and others. 2014. A disulphide-linked heterodimer of TWIK-1 and TREK-1 mediates passive conductance in astrocytes. *Nat Commun* 5:3227.
- Imbrici P, Nematian-Ardestani E, Hasan S, Pessia M, Tucker SJ, D'Adamo MC. 2020. Altered functional properties of a missense variant in the TRESK K⁺ channel (KCNK18) associated with migraine and intellectual disability. *Pflugers Arch*. Epub May 12. doi:10.1007/s00424-020-02382-5
- Jain A, Liu R, Ramani B, Arauz E, Ishitsuka Y, Raganathan K, and others. 2011. Probing cellular protein complexes using single-molecule pull-down. *Nature* 473(7348):484–8.
- Kanda H, Ling J, Tomomura S, Noguchi K, Matalon S, Gu JG. 2019. TREK-1 and TRAAK are Principal K⁺ channels at the nodes of Ranvier for rapid action potential conduction on mammalian myelinated afferent nerves. *Neuron* 104(5):960–971.e7.
- Karatas H, Erdener SE, Gursoy-Ozdemir Y, Lule S, Eren-Koçak E, Sen ZD, and others. 2013. Spreading depression triggers headache by activating neuronal Panx1 channels. *Science* 339(6123):1092–5.
- Karsan N, Goadsby PJ. 2018. Biological insights from the premonitory symptoms of migraine. *Nat Rev Neurol* 14(12):699–710.
- Khan S, Amin FM, Christensen CE, Ghanizada H, Younis S, Olinger ACR, and others. 2019. Meningeal contribution to migraine pain: a magnetic resonance angiography study. *Brain* 142(1):93–102.
- Kochetov AV. 2008. Alternative translation start sites and hidden coding potential of eukaryotic mRNAs. *BioEssays* 30(7):683–91.
- Kozak M. 1987. An analysis of 5'-noncoding sequences from 699 vertebrate messenger RNAs. *Nucleic Acids Res* 15(20):8125–48.
- Kozak M. 1999. Initiation of translation in prokaryotes and eukaryotes. *Gene* 234(2):187–208.
- Kunkler PE, Zhang L, Johnson PL, Oxford GS, Hurley JH. 2018. Induction of chronic migraine phenotypes in a rat model after environmental irritant exposure. *Pain* 159(3):540–9.
- Lafrenière RG, Cader MZ, Poulin JF, Andres-Enguix I, Simoneau M, Gupta N, and others. 2010. A dominant-negative mutation in the TRESK potassium channel is linked to familial migraine with aura. *Nat Med* 16(10):1157–60.
- Levitz J, Royal P, Comoglio Y, Wdziekonski B, Schaub S, Clemens DM, and others. 2016. Heterodimerization within the TREK channel subfamily produces a diverse family of highly regulated potassium channels. *Proc Natl Acad Sci U S A* 113(15):4194–9.
- Levy D, Labastida-Ramirez A, MaassenVanDenBrink A. 2019. Current understanding of meningeal and cerebral vascular function underlying migraine headache. *Cephalalgia* 39(13):1606–22.
- Li XY, Toyoda H. 2015. Role of leak potassium channels in pain signaling. *Brain Res Bull* 119(Pt A):73–9.
- Liu P, Xiao Z, Ren F, Guo Z, Chen Z, Zhao H, and others. 2013. Functional analysis of a migraine-associated TRESK K⁺ channel mutation. *J Neurosci* 33(31):12810–24.
- Mi Hwang E, Kim E, Yarishkin O, Ho Woo D, Han K-S, Park N, and others. 2014. A disulphide-linked heterodimer of TWIK-1 and TREK-1 mediates passive conductance in astrocytes. *Nature Commun* 5(1):3227.
- Nahman-Averbuch H, Leon E, Hunter BM, Ding L, Hershey AD, Powers SW, and others. 2019. Increased pain sensitivity but normal pain modulation in adolescents with migraine. *Pain* 160(5):1019–28.
- Nosedá R, Constandil L, Bourgeois L, Chalus M, Villanueva L. 2010. Changes of meningeal excitability mediated by corticotrigeminal networks: a link for the endogenous modulation of migraine pain. *J Neurosci* 30(43):14420–9.
- Noël J, Zimmermann K, Busserolles J, Deval E, Alloui A, Diochot S, and others. 2009. The mechano-activated K⁺ channels TRAAK and TREK-1 control both warm and cold perception. *EMBO J* 28(9):1308–18.
- Nyholt DR, Borsook D, Griffiths LR. 2017. Migrainomics—identifying brain and genetic markers of migraine. *Nat Rev Neurol* 13(12):725–41.
- Nyholt DR, LaForge KS, Kallela M, Alakurtti K, Anttila V, Färkkilä M, and others. 2008. A high-density association

- screen of 155 ion transport genes for involvement with common migraine. *Hum Mol Genet* 17(21):3318–31.
- Olesen J, Ashina M. 2015. Can nitric oxide induce migraine in normal individuals? *Cephalalgia* 35(12):1125–9.
- Olesen J, Burstein R, Ashina M, Tfelt-Hansen P. 2009. Origin of pain in migraine: evidence for peripheral sensitisation. *Lancet Neurol* 8(7):679–90.
- Pereira V, Busserolles J, Christin M, Devilliers M, Poupon L, Legha W, and others. 2014. Role of the TREK2 potassium channel in cold and warm thermosensation and in pain perception. *Pain* 155(12):2534–44.
- Pettingill P, Weir GA, Wei T, Wu Y, Flower G, Lalic T, and others. 2019. A causal role for TRESK loss of function in migraine mechanisms. *Brain* 142(12):3852–67.
- Plant LD. 2012. A role for k2p channels in the operation of somatosensory nociceptors. *Front Mol Neurosci* 5:21.
- Plant LD, Zuniga L, Araki D, Marks JD, Goldstein SAN. 2012. SUMOylation silences heterodimeric TASK potassium channels containing K2P1 subunits in cerebellar granule neurons. *Sci Signal* 5(251):ra84.
- Rainero I, Rubino E, Gallone S, Zavarise P, Carli D, Boschi S, and others. 2014. KCNK18 (TRESK) genetic variants in Italian patients with migraine. *Headache* 54(9):1515–22.
- Royal P, Andres-Bilbe A, Ávalos Prado P, Verkest C, Wdziekonski B, Schaub S, and others. 2019. Migraine-associated TRESK mutations increase neuronal excitability through alternative translation initiation and inhibition of TREK. *Neuron* 101(2):232–245.e6.
- Rua R, McGavern DB. 2018. Advances in meningeal immunity. *Trends Mol Med* 24(6):542–59.
- Schulte LH, May A. 2016. Functional neuroimaging in migraine: chances and challenges. *Headache* 56(9):1474–81.
- Schytz HW, Wienecke T, Olesen J, Ashina M. 2010. Carbachol induces headache, but not migraine-like attacks, in patients with migraine without aura. *Cephalalgia* 30(3):337–45.
- Sheftell F, Rapoport A, Weeks R, Walker B, Gammerman I, Baskin S. 2000. Montelukast in the prophylaxis of migraine: a potential role for leukotriene modifiers. *Headache* 40(2):158–63.
- Spindler BL, Ryan M. 2020. Recent medications approved for preventing migraine headaches. *Am J Med* 133(6):664–7.
- Strassman AM, Raymond SA, Burstein R. 1996. Sensitization of meningeal sensory neurons and the origin of headaches. *Nature* 384(6609):560–4.
- Suzuki Y, Tsutsumi K, Miyamoto T, Yamamura H, Imaizumi Y. 2017. Heterodimerization of two pore domain K⁺ channel TASK1 and TALK2 in living heterologous expression systems. *PLoS One* 12(10):e0186252.
- Thomas D, Plant LD, Wilkens CM, McCrossan ZA, Goldstein SA. 2008. Alternative translation initiation in rat brain yields K2P2.1 potassium channels permeable to sodium. *Neuron* 58(6):859–70.
- Turner DP, Houle TT. 2018. Influences on headache trigger beliefs and perceptions. *Cephalalgia* 38(9):1545–53.
- Uddman R, Edvinsson L, Ekman R, Kingman T, McCulloch J. 1985. Innervation of the feline cerebral vasculature by nerve fibers containing calcitonin gene-related peptide: trigeminal origin and co-existence with substance P. *Neurosci Lett* 62(1):131–6.
- van den Maagdenberg AM, Pietrobon D, Pizzorusso T, Kaja S, Broos LA, Cesetti T, and others. 2004. A Cacna1a knockin migraine mouse model with increased susceptibility to cortical spreading depression. *Neuron* 41(5):701–10.
- van Dongen RM, Zielman R, Noga M, Dekkers OM, Hankemeier T, van den Maagdenberg AM, and others. 2017. Migraine biomarkers in cerebrospinal fluid: a systematic review and meta-analysis. *Cephalalgia* 37(1):49–63.
- Vila-Pueyo M. 2018. Targeted 5-HT. *Neurotherapeutics* 15(2):291–303.
- Vila-Pueyo M, Hoffmann J, Romero-Reyes M, Akerman S. 2019. Brain structure and function related to headache: brainstem structure and function in headache. *Cephalalgia* 39(13):1635–60.
- Wright PD, McCoull D, Walsh Y, Large JM, Hadrys BW, Gaurilcikaite E, and others. 2019. Pranlukast is a novel small molecule activator of the two-pore domain potassium channel TREK2. *Biochem Biophys Res Commun* 520(1):35–40.
- Yamamoto Y, Hatakeyama T, Taniguchi K. 2009. Immunohistochemical colocalization of TREK-1, TREK-2 and TRAAK with TRP channels in the trigeminal ganglion cells. *Neurosci Lett* 454(2):129–33.
- Zerimech S, Chever O, Scalmani P, Pizzamiglio L, Duprat F, Mantegazza M. 2020. Cholinergic modulation inhibits cortical spreading depression in mouse neocortex through activation of muscarinic receptors and decreased excitatory/inhibitory drive. *Neuropharmacology* 166:107951.

THERAPEUTIC USE OF CALCIUM-ACTIVATED CHLORIDE CHANNEL PEPTIDE ACTIVATOR

FILED OF THE INVENTION

- 5 The present disclosure relates to a calcium-activated chloride channel peptide activator and its therapeutic use.

BACKGROUND

Calcium-activated chloride channels (CaCCs) belonging to the Anoctamin protein superfamily play a major role in cell physiology, including signal transduction, regulation of
10 cardiac and neuronal excitability, epithelial secretion and muscle contraction, among others (Hartzell et al., 2005; Pedemonte and Galiotta, 2014). Given this broad range of functions, chloride channel dysfunction leads to a large spectrum of diseases. These diverse pathologies include cystic fibrosis, salivary gland dysfunction, such as in Sjogren's syndrome and caused by radiation injury, dry eye syndrome, dry mouth, gastrointestinal hypomotility disease and
15 cardiac arrhythmia.

TMEM16A was first member of this superfamily to be identified (Caputo et al., 2008; Schroeder et al., 2008; Yang et al., 2008). The structure of TMEM16A was recently elucidated, defining the channel as homodimer consisting of ten transmembrane domains per subunit with an extensive intracellular domain that adopts a ferredoxin-like folding (Dang et
20 al., 2017). Nevertheless, no β -subunit has been identified for this channel up to now.

Several TMEM16A agonists have been identified. For instance, a functional cell-based screen of small-molecule collections allows to identify small molecules reported to activate TMEM16A (Namkung, W. et al. FASEB J. 2011, 25, 4048–4062; WO2013/002793). However, these compounds may be unable to activate endogenous TMEM16A in cells
25 (Centeio R. et al. Int. J. Mol. Sci. 2020, 21, 2557).

Thus, it remains a need to discover new compounds that specifically activate Ca^{2+} -activated chloride channel independently of the presence of calcium and produce sustained activation of Cl^- conductance.

KCNE1 is a 129-residue peptide, with a single short hydrophobic plasma membrane spanning domain and carboxy- and amino-terminal domains facing towards the intracellular and extracellular side, respectively (Takumi, T., et al. 2018, Science, 242, 1042-1045). When injected in *Xenopus* oocytes, KCNE1 produces a slowly activating K^+ current (Takumi, T., et al. 2018, Science, 242, 1042-1045). For this reason, KCNE1 was initially believed to be the minimal sequence that could encode for a K^+ channel (Goldstein, S.A., and Miller, C. 1991, Neuron 7, 403-408; Wang, K.W., and Goldstein, S.A. 1995. Neuron 14, 1303- 9). Experiments in other heterologous cell models questioned this finding since expression of KCNE1 alone is not able to induce currents in mammalian cell lines (Lesage, F., et al. 1993, Receptors Channels, 1, 143-152). This enigma was resolved by the discovery that *Xenopus* oocytes express endogenous KCNQ1 channels, which are modulated by KCNE1 (Barhanin, J. et al. 1996. Nature 384, 78-80; Sanguinetti, M.C. et al. 1996, Nature 384, 80-83). These experiments showed that KCNE1 is not encoding for an α -subunit but for an ancillary (β) subunit of the voltage-dependent potassium KCNQ1 channel that underlies the slow repolarizing component in cardiac action potential (IKs) (Barhanin, J. et al. 1996. Nature 384, 78-80; Sanguinetti, M.C. et al. 1996, Nature 384, 80-83). In addition to the K^+ current described above, a voltage-dependent Cl^- current was observed upon injection of cRNA of KCNE1 in *Xenopus* oocytes (Attali, B. et al. 1993. Nature 365, 850-852), and up to now, the molecular identity of this current remained elusive.

20 SUMMARY OF THE INVENTION

The inventors hypothesized that KCNE1 serves as a β -subunit of the pore forming TMEM16A subunits to induce the KCNE1-induced Cl^- current, described 30 years ago (Attali, B. et al. 1993. Nature 365, 850-852), not anymore gated by Ca^{2+} but exclusively by voltage. Using electrophysiology in heterologous and native systems and single molecule pulldown assays, the inventors demonstrate that KCNE1 interacts physically with TMEM16A, inducing a sustained voltage-dependent chloride current in the absence of increased cytoplasmic Ca^{2+} . Importantly, the inventors found that clinically relevant inherited polymorphisms within the KCNE1-regulating domain, including the common S38G polymorphism, abolish the KCNE1-dependent regulation of TMEM16A, indicating that this current may contribute to inherited pathologies.

The present invention relates to a TMEM16A peptide activator for use as a medicament comprising or consisting of the sequence L-A-R-X1-S-X2-X3-X4-X5 (SEQ ID NO: 3)

wherein said X1 is arginine, lysine or histidine; X2 is proline or glutamine; X3 is arginine or leucine; X4 is serine or arginine and X5 is glycine or aspartic acid.

In particular, the peptide comprises or consists of the sequence L-A-R-X1-S-X2-X3-X4-X5-D-X6-K-L (SEQ ID NO: 4) wherein said X1 is arginine, lysine or histidine, X2 is proline or glutamine, X3 is arginine or leucine, X4 is serine or arginine, X5 is glycine or aspartic acid and X6 is glycine or serine.

In the preferred embodiment, said peptide for use according to the present invention comprises the amino acid sequence L-A-R-R-S-P-R-S-S (SEQ ID NO: 1) or a functional variant thereof, more preferably amino acid sequence L-A-R-R-S-P-R-S-S-D-G-K-L (SEQ ID NO: 2) or a functional variant thereof. In another preferred embodiment, said peptide is of 8 to 100 amino acids residues, preferably 8 to 20 amino acids residues, more preferably 13 to 20 amino acids residues. The peptide for use according to the present invention comprises or consists of an amino sequence which is at least 90 % identical to an amino acids sequence of: SEQ ID NO: 1 or 2, more particularly comprises or consists of an amino acid sequence comprising or consisting of an amino acid sequence having no more than 3 conservative substituted amino acids residues as compared to SEQ ID NO: 1 or 2.

In another aspect, the present invention relates to a nucleic acid or an expression vector comprising said nucleic acid encoding the peptide as described above for use as medicament.

In a preferred embodiment, the peptide, nucleic acid or expression vector is for use in the treatment of diseases caused by chloride channel dysfunction, preferably selected from the group consisting of: cystic fibrosis, dry mouth, dry eye syndrome, cardiac arrhythmia and gastrointestinal hypomobility disease, preferably dry eye syndrome.

In another aspect, the present invention also relates to a pharmaceutical composition comprising the peptide, nucleic acid or expression vector as described above and a pharmaceutically acceptable carrier. The present invention also relates to the peptide of 8 to 100 amino acids residues, preferably 8 to 20 amino acids residues, more preferably 13 to 20 amino acids residues comprising an amino sequence of SEQ ID NO: 1 or 2 or an amino sequence which is at least 90 % identical to an amino acids sequence of: SEQ ID NO: 1 or 2.

Finally, the present invention also relates to the use of the peptide, the nucleic acid or the expression vector as described above as a chloride channel activator.

FIGURE LEGENDS

Figure 1. KCNE1 converts the CaCC TMEM16A into a voltage-dependent chloride channel. (A) Representative current traces showing the effect of expression of either KCNE1 or TMEM16A or both TMEM16A and KCNE1 in HEK293T cells. Traces were generated using pulses between -100 and +100 mV at 20 mV intervals from a holding potential of -80 mV. (B) Summary of current densities obtained at +100 mV. (C-D) Representative traces showing the effect of application of either niflumic acid (NFA, 100 μ M, C), T16A(inh)A01 (10 μ M, C) or Ani9 (300 nM, D). (E-F) Representative traces of TMEM16A alone (E) or co-expressed with KCNE1 (F) in the presence of 1 mM of BAPTA. Currents were elicited by voltage-ramps (from -100 to +100 mV, 1s duration), insets show a summary of current densities obtained at +100 mV. Mann-Whitney test (** $p < 0.01$, *** $p < 0.001$). Mean \pm SEM.

Figure 2. KCNE1 expression does not lead to an increase of intracellular Ca^{2+} . (A) Representative current traces obtained from HEK293T cells transfected with SK4 and either an empty vector or KCNE1 at different Ca^{2+} concentrations. SK4 current is not activated by KCNE1 coexpression showing the absence of intracellular calcium increase. Traces were generated using pulses between -100 and +100 mV from a holding potential at -80 mV. (B) Summary of current densities obtained at +100 mV. Mann-Whitney test (** $p < 0.05$, *** $p < 0.001$). Mean \pm SEM.

Figure 3. KCNE1 and TMEM16A interact in a $2\alpha:2\beta$ complex. (A) Schematic of single molecule pulldown (SiMPull) assay of TMEM16A. Lysates of HEK293T cells co-expressing TMEM16A-GFP and HA-tagged KCNE1 were immobilized on a PEG-passivated coverslip conjugated to a biotinylated anti-HA antibody. (B) Representative TIRF image of single molecules showing the pulldown of TMEM16A-GFP by HA-KCNE1. (C) Representative trace showing two photobleaching steps (red arrows) of TMEM16A-GFP (AU, for Arbitrary Units). (D) Summary of photobleaching step distribution for TMEM16A-GFP. (E-H), same as (A-D) for the SiMPull of KCNE1-GFP by HA-TMEM16A. (I-L) Specificity of the anti-HA antibody. (I-J) SiMPull assay with TMEM16A-GFP in the

absence of HA-KCNE1. (K-L) SiMPull assay with KCNE1-GFP in the absence of HA-TMEM16A.

Figure 4. KCNE1-TMEM16A complex creates a voltage-dependent chloride current in proximal convoluted tubule (PCT) cells. (A) Representative traces obtained from wild type and *kcne1*^{-/-} PCT cells. (B-D) Representative traces from wild type cells after incubation with NFA (100 μM, B), A01 (10 μM, C), Ani9 (5 μM, D). (E) Trace obtained after transfection with siRNA against TMEM16A. (F) Trace obtained from a *kcne1*^{-/-} PCT cell after transfection with KCNE1 cDNA. Currents were generated by voltage-ramps (from -100 to +100 mV, 1s duration). Insets show current densities. Mann-Whitney test (*** p < 0.001). Mean ± SEM.

Figure 5. The pre-transmembrane domain (Nter13) of KCNE1 is sufficient for KCNE1-induced TMEM16A conversion. (A) Cartoon depicting KCNE1 truncated forms used to determine the domains implicated in TMEM16A interaction. (B-C) Representative traces obtained from HEK293T cells co-expressing TMEM16A and KCNE1ΔCt, KCNE1ΔNt (B), KCNE1ΔNt16 or KCNE1ΔNt30 (C). (D) Representative traces showing the effect of the Nter13 and a scrambled peptide on a HEK293T cell expressing TMEM16A alone. Currents were elicited by voltage-ramps (from -100 to +100 mV, 1s duration). Insets show the summary of current densities obtained for the different conditions at +100 mV. Mann-Whitney test (*** p < 0.001). Mean ± SEM.

Figure 6. Nter13 peptide is sufficient to switch the functioning mode of TMEM16A. (A) Representative current traces from a *Xenopus* oocyte, expressing endogenously TMEM16A, obtained after application of the Nter13 peptide (100 μM) and wash-out. (B) Representative traces showing the effect of Nter13 peptide application (100 μM) and its reversion by Ani9 (5 μM) on a HEK293T cell expressing TMEM16A alone. (C) Effect of Nter13 peptide on TMEM16A current over time followed by inhibition through co-application of Ani9 in HEK293T cells. (D) Concentration-response curve representing the current density observed for different peptide concentrations in HEK293T cells expressing TMEM16A. Mean ± SEM.

Figure 7. The KCNE1 S38G and R32H do not impair the KCNQ1 regulation, but abolish TMEM16A regulation. (A) Current traces of whole-cell patch-clamp recordings from cells transfected with wild type KCNQ1 alone and co-transfected with KCNE1 or KCNE1R32H or KCNE1S38G. (B) Summary of current densities obtained for the different

conditions at +40 mV. (C-D) Same as A-B, with cells co-expressing KCNE1 and TMEM16A. Current densities were calculated at +100 mV. Mann-Whitney test (** $p < 0.05$, *** $p < 0.001$). Mean \pm SEM.

DETAILED DESCRIPTION OF THE INVENTION

5 The inventors showed that a KCNE1 subunit interacts with TMEM16-A calcium-activated chloride channel to activate Cl^- conductance, switching TMEM16-A from a calcium dependent to a voltage-dependent channel. In particular, the inventors showed that a N-terminal fragment of the KCNE1 closer to the transmembrane domain of KCNE1 recapitulates the action of KCNE1 on TMEM16-A channel Cl^- conductance.

10 Calcium-dependent chloride channel peptide activator

Thus, the present disclosure relates to a calcium-dependent chloride channel peptide activator also named herein TMEM16A peptide activator comprising or consisting of a functional N-terminal fragment of KCNE1 protein that binds TMEM16A and induces chloride conductance activation.

15 By “calcium-dependent chloride channel activator” it is intended a compound that binds on calcium-dependent chloride channel and increases Cl^- conductance. According to the present disclosure, said calcium-dependent chloride channel activator binds TMEM16A and increase Cl^- conductance.

Herein, the terms "peptide", "oligopeptide", "polypeptide" and "protein" are employed
20 interchangeably and refer to a chain of amino acids linked by peptide bonds, regardless of the number of amino acids forming said chain.

The potassium voltage-gated channel subfamily E regulatory subunit 1 (KCNE1), also known as ISK, JLNS, LQT5, MinK, JLNS2 or LQT2/5 human gene (Gene ID: 3753, updated on 1 Jun-2020) encodes a protein of 129 amino acids (NCBI reference: NP_000210.2).

25 The TMEM16-A activator peptide according to the disclosure comprises or consists of contiguous amino acid residues between positions 30 to 38 (SEQ ID NO: 1), preferably between positions 30 to 42 (SEQ ID NO: 2) (Nter 13Peptide) of the human KCNE1 protein sequence (NCBI reference: NP_000210.2).

Since KCNE1 N-terminal fragment are well conserved, fragment originating from other animal species can be used. *e. g* mouse or rat KCNE1 protein. The positions of KCNE1 amino acids corresponding to those of the human KCNE1 protein can be easily identified by sequence alignments.

- 5 As for example, the TMEM16-A activator peptide comprising or consisting of contiguous amino acid residues between positions 31 to 39, preferably between 31 to 43 of the rat KCNE1 protein sequence (NCBI reference sequence: NP_0371105.1) can also be used. Advantageously, the TMEM16A peptide activator comprises or consists of human N-terminal KCNE1 fragment and bind to human TMEM16A.
- 10 In a particular embodiment, the peptide according to the present disclosure may be a functional variant of the TMEM16A peptide activator as described above.

As used herein, the term "TMEM16A peptide activator functional variant" refers to a polypeptide sequence that is derived from TMEM16A peptide activator as described above and comprises an alteration, *i.e.*, a substitution, insertion, and/or deletion, at one or more
15 (e.g., several) positions, but retains the capacity to activate TMEM16A channel. The variant may be obtained by various techniques well known in the art. Examples of techniques for altering the DNA sequence encoding the native protein, include, but are not limited to, site-directed mutagenesis, random mutagenesis and synthetic oligonucleotide construction.

Preferably, as used herein, the term "variant" or "functional variant" refers to a polypeptide
20 having an amino acid sequence having at least 70, 75, 80, 85, 90, 95 or 99% sequence identity to amino acid sequence of SEQ ID NO: 1 or 2. As used herein, the term "sequence identity" or "identity" refers to the number (%) of matches (identical amino acid residues) in positions from an alignment of two polypeptide sequences. The sequence identity is determined by comparing the sequences when aligned so as to maximize overlap and identity while
25 minimizing sequence gaps. In particular, sequence identity may be determined using any of a number of mathematical global or local alignment algorithms, depending on the length of the two sequences. Sequences of similar lengths are preferably aligned using a global alignment algorithms (*e.g.* Needleman and Wunsch algorithm; Needleman and Wunsch, 1970) which aligns the sequences optimally over the entire length, while sequences of
30 substantially different lengths are preferably aligned using a local alignment algorithm (*e.g.* Smith and Waterman algorithm (Smith and Waterman, 1981) or Altschul algorithm

(Altschul et al, 1997; Altschul et al., 2005). Alignment for purposes of determining percent amino acid sequence identity can be achieved in various ways that are within the skill in the art, for instance, using publicly available computer software available on internet web sites such as <http://blast.ncbi.nlm.nih.gov/> or <http://www.ebi.ac.uk/Tools/emboss/>. Those skilled
5 in the art can determine appropriate parameters for measuring alignment, including any algorithms needed to achieve maximal alignment over the full length of the sequences being compared. For purposes herein, % amino acid sequence identity values refers to values generated using the pair wise sequence alignment program EMBOSS Needle that creates an optimal global alignment of two sequences using the Needleman- Wunsch algorithm,
10 wherein all search parameters are set to default values, i.e. Scoring matrix = BLOSUM62, Gap open = 10, Gap extend = 0.5, End gap penalty = false, End gap open = 10 and End gap extend = 0.5.

Preferably, the term "variant" or "functional variant" refers to a polypeptide having an amino acid sequence that differs from a sequence of SEQ ID NO: 1 by less than 5, 4, 3 or 2
15 substitutions, insertions and/or deletions.

More preferably, the term "variant" or "functional variant" refers to a polypeptide having an amino acid sequence that differs from a sequence of SEQ ID NO: 2 by less than 6, 5, 4, 3 or 2 substitutions, insertions and/or deletions.

In particular, the functional variant is substantially homologous to amino acid sequence SEQ
20 ID NO: 1 or 2. Two amino acid sequences are "homologous", "substantially homologous" or "substantially similar" when one or more amino acid residues are replaced by a biologically similar residue, i.e. conservative substitution.

In a preferred embodiment, the functional variant differs from the amino acid sequence of SEQ ID NO: 1 by one or more conservative substitutions, preferably by less than 5, 4, 3, or
25 2 conservative substitutions

In a more preferred embodiment, the functional variant differs from the amino acid sequence of SEQ ID NO: 2 by one or more conservative substitutions, preferably by less than 6, 5, 4, 3, or 2 conservative substitutions.

By "substituted" or "modified" the present invention includes those amino acids that have been altered or modified from naturally occurring amino acids.

The term "conservative substitution" as used herein denotes the replacement of an amino acid residue by another, without altering the overall conformation and function of the peptide, including, but not limited to, replacement of an amino acid with one having similar properties (such as, for example, polarity, hydrogen bonding potential, acidic, basic, shape, hydrophobic, aromatic, and the like).

Examples of conservative substitutions are within the groups of basic amino acids (arginine, lysine and histidine), acidic amino acids (glutamic acid and aspartic acid), polar amino acids (glutamine and asparagine), hydrophobic amino acids (methionine, leucine, isoleucine and valine), aromatic amino acids (phenylalanine, tryptophan and tyrosine), and small amino acids (glycine, alanine, serine and threonine).

TMEM16 peptide activator capacity of a variant to activate TMEM16A channel may be assessed by any method known by the skilled person as described above. For instance, TMEM16A activity may be assessed by patch-clamp or Two-Electrode-Voltage-Clamp (TEVC) experiments as described in examples in electrophysiology assay. In particular, the capability of a peptide functional variant to induce of voltage-dependent current as described above can be measured by patch-clamp experiments in cells, such HEK293T cells which co-express TMEM16A and said peptide or TEVC experiment on *Xenopus* oocytes which endogenously expressed TMEM16A.

Preferably, amino acid residues important for TMEM16A activation are conserved in the functional variant, said residue corresponds to arginine at the position 32 and/or serine at the position 38 of the human KCNE1 protein sequence (NCBI reference: NP_000210.2 accessed on July 04, 2020).

In a particular embodiment, said TMEM16A peptide activator comprises or consists of a sequence L-A-R-X1-S-X2-X3-X4-X5 (SEQ ID NO: 3) wherein said

- X1 is any one of 20 amino acids, preferably arginine, lysine or histidine,
- X2 is any one of 20 amino acids, preferably proline or glutamine,
- X3 is any one of 20 amino acids, preferably arginine or leucine, and

- X4 is any one of 20 amino acids, preferably serine or arginine and,
- X5 is any one of 20 amino acids, preferably serine or aspartic acid.

In a more preferred embodiment, said TMEM16A peptide activator comprises or consists of the sequence L-A-R-X1-S-X2-X3-X4-X5-D-X6-K-L (SEQ ID NO: 4) wherein said

- 5
- X1 is any one of 20 amino acids, preferably arginine, lysine or histidine,
 - X2 is any one of 20 amino acids, preferably proline or glutamine,
 - X3 is any one of 20 amino acids, preferably arginine or leucine,
 - X4 is any one of 20 amino acids, preferably serine or arginine,
 - X5 is any one of 20 amino acids, preferably serine or aspartic acid and,
- 10
- X6 is any one of 20 amino acids, preferably glycine or serine.

In a more preferred embodiment, said TMEM16A peptide activator comprises or consists of amino acid sequence of SEQ ID NO: 1 or 2.

Preferably, the TMEM16A activator peptide as described above is of 8 to 100 amino acids residues, preferably 8 to 20 amino acids residues, more preferably 13 to 20 amino acids
15 residues.

More preferably, the TMEM16A activator peptide is of 8 to 100 amino acids residues, preferably 8 to 20 amino acids residues, more preferably 13 to 20 amino acids residues and comprises amino acid sequence of SEQ ID NO: 1 or 2 or an amino acid sequence having at least 70, 75, 80, 85, 90, 95 or 99% sequence identity to amino acid sequence of SEQ ID NO:
20 1 or 2 or an amino acid sequence that differs from the amino acid sequence of SEQ ID NO: 1 or 2 by one or more conservative substitutions, preferably by less than 6, 5, 4, 3, or 2 conservative substitutions.

Peptide preparation

Peptides described herein can be synthesized using standard synthetic methods known to
25 those skilled in the art, for example chemical synthesis or genetic recombination.

In a preferred embodiment, peptides are obtained by stepwise condensation of amino acid residues, either by condensation of a preformed fragment already containing an amino acid sequence in appropriate order, or by condensation of several fragments previously prepared, while protecting the amino acid functional groups except those involved in peptide bond

during condensation. In particular, the peptides can be synthesized according to the method originally described by Merrifield.

Examples of chemical synthesis technologies are solid phase synthesis and liquid phase synthesis. As a solid phase synthesis, for example, the amino acid corresponding to the C-terminus of the peptide to be synthesized is bound to a support which is insoluble in organic solvents, and by alternate repetition of reactions, one wherein amino acids with their amino groups and side chain functional groups protected with appropriate protective groups are condensed one by one in order from the C-terminus to the N-terminus, and one where the amino acids bound to the resin or the protective group of the amino groups of the peptides are released, the peptide chain is thus extended in this manner. Solid phase synthesis methods are largely classified by the tBoc method and the Fmoc method, depending on the type of protective group used. Typically used protective groups include tBoc (t-butoxycarbonyl), Cl-Z (2-chlorobenzyloxycarbonyl), Br-Z (2-bromobenzyloxycarbonyl), Bzl (benzyl), Fmoc (9-fluorenylmethoxycarbonyl), Mbh (4, 4'-dimethoxydibenzhydryl), Mtr (4-methoxy-2, 3, 6-trimethylbenzenesulphonyl), Trt (trityl), Tos (tosyl), Z (benzyloxycarbonyl) and Clz-Bzl (2, 6-dichlorobenzyl) for the amino groups; NO₂ (nitro) and Pmc (2,2, 5,7, 8-pentamethylchromane-6-sulphonyl) for the guanidino groups; and tBu (t-butyl) for the hydroxyl groups). After synthesis of the desired peptide, it is subjected to the de-protection reaction and cut out from the solid support. Such peptide cutting reaction may be carried with hydrogen fluoride or tri-fluoromethane sulfonic acid for the Boc method, and with TFA for the Fmoc method.

Alternatively, the peptide may be synthesized using recombinant techniques. In this case, a nucleic acid construct comprising or consisting of a nucleic acid sequence encoding a peptide according to the disclosure, polynucleotides with nucleic acid sequences complementary to one of the above sequences and sequences hybridizing to said polynucleotides under stringent conditions.

The N- and C-termini of the peptides described herein may be optionally protected against proteolysis. For instance, the N-terminus may be in the form of an acetyl group, and/or the C-terminus may be in the form of an amide group. Internal modifications of the peptides to be resistant to proteolysis are also envisioned, e.g. wherein at least a -CONH- peptide bond is modified and replaced by a (CH₂NH) reduced bond, a (NHCO) retro- inverso bond, a (CH₂-O) methylene-oxy bond, a (CH₂-S) thiomethylene bond, a (CH₂CH₂) carba bond, a

(CO-CH₂) cetomethylene bond, a (CHOH-CH₂) hydroxyethylene bond), a (N-N) bound, a E-alcene bond or also a -CH=CH-bond.

For instance the peptide may be modified by acetylation, acylation, amidation, cross-linking, cyclization, disulfide bond formation, formation of covalent cross-links, formation of cysteine, formation of pyroglutamate, formylation, gamma-carboxylation, glycosylation, GPI anchor formation, hydroxylation, iodination, methylation, myristylation, oxidation, phosphorylation, and the like.

The peptides of the invention may be composed of amino acid(s) in D configuration, which render the peptides resistant to proteolysis. They may also be stabilized by intramolecular crosslinking, e.g. by modifying at least two amino acid residues with olefinic side chains, preferably C3-C8 alkenyl chains, preferably penten-2-yl chains) followed by chemical crosslinking of the chains, according to the so-called "staple" technology described in Walensky et al, 2004. For instance, amino acids at position i and i+4 to i+7 can be substituted by non-natural amino acids that show reactive olefinic residues. All these proteolysis-resistant chemically modified peptides are encompassed in the present disclosure.

In another aspect of the invention, peptides are covalently bound to a polyethylene glycol (PEG) molecule by their C-terminal terminus or a lysine residue, notably a PEG of 1500 or 4000 MW, for a decrease in urinary clearance and in therapeutic doses used and for an increase of the half-life in blood plasma. In yet another embodiment, peptide half-life is increased by including the peptide in a biodegradable and biocompatible polymer material for drug delivery system forming microspheres. Polymers and copolymers are, for instance, poly(D,L-lactide-co-glycolide) (PLGA) (as illustrated in US2007/0184015, SoonKap Hahn et al).

Nucleic acid construct and expression vector

The disclosure further relates to a nucleic acid encoding TMEM16A peptide activator according to the present disclosure.

In a preferred embodiment, said nucleic acid encoding TMEM16A peptide is comprised in a nucleic acid construct which further comprises regulatory sequences (such as a suitable promoter(s), enhancer(s), terminator(s), etc.) allowing the expression (e.g. transcription and translation) of a peptide according to the disclosure in a host cell.

The term “nucleic acid construct” as used herein refers to a man-made nucleic acid molecule resulting from the use of recombinant DNA technology. A nucleic acid construct is a nucleic acid molecule, either single- or double-stranded, which has been modified to contain segments of nucleic acids sequences, which are combined and juxtaposed in a manner, which would not otherwise exist in nature. A nucleic acid construct usually is a “vector”, i.e. a nucleic acid molecule which is used to deliver exogenously created DNA into a host cell.

The nucleic acid construct as described above may be contained in an expression vector. The vector may be an autonomously replicating vector, i.e., a vector that exists as an extra-chromosomal entity, the replication of which is independent of chromosomal replication, e.g., a plasmid, an extra-chromosomal element, a mini-chromosome, or an artificial chromosome. The vector may contain any means for assuring self-replication. Alternatively, the vector may be one that, when introduced into the host cell, is integrated into the genome and replicated together with the chromosome(s) into which it has been integrated.

Examples of appropriate vectors include, but are not limited to, recombinant integrating or non-integrating viral vectors and vectors derived from recombinant bacteriophage DNA, plasmid DNA or cosmid DNA. Preferably, the vector is a recombinant integrating or non-integrating viral vector. Examples of recombinant viral vectors include, but not limited to, vectors derived from herpes virus, retroviruses, lentivirus, vaccinia viruses, adenoviruses, adeno-associated viruses or bovine papilloma virus.

In a preferred but non-limiting aspect, a genetic construct of the invention comprises i) at least one nucleic acid of the invention; operably connected to ii) one or more regulatory elements, such as a promoter and optionally a suitable terminator; and optionally also iii) one or more further elements of genetic constructs such as 3'- or 5'-UTR sequences, leader sequences, selection markers, expression markers/reporter genes, and/or elements that may facilitate or increase (the efficiency of) transformation or integration.

The control sequence may include a promoter that is recognized by epithelial cells. The promoter contains transcriptional control sequences that mediate the expression of TMEM16A peptide activator upon introduction into a host cell. The promoter may be any polynucleotide that shows transcriptional activity in cells including mutant, truncated, and hybrid promoters. The promoter may be a constitutive or inducible promoter, preferably a constitutive promoter, and more preferably a strong constitutive promoter.

In another aspect, the invention relates to a host or host cell that expresses (or that under suitable circumstances is capable of expressing) a peptide of the disclosure; and/or that contains a nucleic acid construct of the invention. The method of producing the peptide may optionally comprise the steps of purifying said peptide, chemically modifying said peptide, and/or formulating said peptide into a pharmaceutical composition.

Pharmaceutical composition

In a further aspect, the present disclosure also provides a pharmaceutical composition comprising a TMEM16A peptide activator, a nucleic acid or expression vector encoding said peptide as described above, and a pharmaceutically acceptable excipient.

The pharmaceutically acceptable excipient is selected according to the route of administration and the nature of the active ingredient, e.g. a peptide, a nucleic acid or a vector expression. As used herein, the term "pharmaceutically acceptable" means approved by a regulatory agency or recognized pharmacopeia such as European Pharmacopeia, for use in animals and/or humans. The term "excipient" refers to a diluent, adjuvant, carrier, or vehicle with which the therapeutic agent is administered. As is well known in the art, pharmaceutically acceptable excipients are relatively inert substances that facilitate administration of a pharmacologically effective substance and can be supplied as liquid solutions or suspensions, as emulsions, or as solid forms suitable for dissolution or suspension in liquid prior to use. For example, an excipient can give form or consistency, or act as a diluent. Suitable excipients include but are not limited to stabilizing agents, wetting and emulsifying agents, salts for varying osmolality, encapsulating agents, pH buffering substances, and buffers. Such excipients include any pharmaceutical agent suitable for direct delivery to the eye which may be administered without undue toxicity.

The pharmaceutical composition is formulated for administration by a number of routes, including but not limited to oral, parenteral and local.

The pharmaceutically acceptable carriers are those conventionally used. The pharmaceutical composition comprises a therapeutically effective amount of the peptide/polynucleotide/vector, e.g., sufficient to show benefit to the individual to whom it is administered. The pharmaceutically effective dose depends upon the composition used, the route of administration, the type of mammal (human or animal) being treated, the physical

characteristics of the specific mammal under consideration, concurrent medication, and other factors, that those skilled in the medical arts will recognize.

Possible pharmaceutical compositions include those suitable for oral, rectal, topical, intraocular or parenteral administration. For these formulations, conventional excipient can
5 be used according to techniques well known by those skilled in the art.

Preferably, the pharmaceutical composition is suitable for parenteral or ocular administration. More preferably, the pharmaceutical composition is suitable for ocular administration including topical ocular instillation and intraocular administration or transmucosal administration including nasal sprays.

10 Pharmaceutical compositions according to the invention may be formulated to release the active drug substantially immediately upon administration or at any predetermined time or time period after administration.

Therapeutic use

The present disclosure also relates to the TMEM16A peptide activator, nucleic acid,
15 expression vector according to the present disclosure for use as medicament, preferably for use for the treatment of diseases caused by chloride channel dysfunction.

Diseases caused by chloride channel dysfunction includes as non-limiting examples salivary gland dysfunction such as Sjorgen's syndrome or gland dysfunction caused by radiation injury; cystic fibrosis; gastrointestinal hypomotility disorder; cardiac arrhythmia such as early
20 repolarization syndrome; dry mouth and dry eye syndrome. Diseases caused by chloride channel dysfunction may be treatable by activating chloride channel, in particular TMEM16A channel activators.

Dry mouth due to salivary gland dysfunction is caused by multiple diseases, including Sjogren's syndrome as well as by radiation therapy for head and neck cancers and
25 medications. Dry mouth is often associated with dysphagia, reduced taste sensation and opportunistic infections. TMEM16A channel plays an essential role for fluid secretion in salivary glands (Catalán MA, et al. Proc Natl Acad Sci U S A. 2015;112(7):2263-8).

Dry eye (keratoconjunctivis sicca) is a related disorder that is very common in the elderly, which results from lacrimal or Meibomian gland dysfunction. TMEM16A is the major ion channel regulating saliva secretion by salivary gland acinar epithelial cells (Romanenko et al., 2010. J. Biol. Chem. 285, 12990–13001).

- 5 Gastrointestinal hypomotility disorder refers to inherited or acquired changes that come with decreased contractile forces or slower transit. Gastrointestinal hypomotility disorder includes severe forms, such as pseudo-obstruction or ileus, moderate forms such as functional dyspepsia, gastroparesis, chronic constipation, and irritable bowel syndrome (IBS).
- 10 Cystic fibrosis is a genetic disease that affects the secretory epithelia of a variety of tissues. The ability of epithelial cells in the airways, liver, pancreas, small intestine, reproductive tract and other tissues to transport chloride ions, and accompanying sodium and water, is severely reduced in cystic fibrosis patients, resulting in respiratory, pancreatic and intestinal ailments. In cystic fibrosis, defective chloride transport is generally due to a mutation in a
- 15 chloride channel known as the cystic fibrosis transmembrane conductance regulator (CFTR; see Riordan et al., Science 245:1066-73, 1989).

Cardiac arrhythmia is a group of conditions in which the heartbeat is irregular. According to the present disclosure, cardiac arrhythmia is preferably early repolarization syndrome. Patients of early repolarization syndrome presents current imbalances between epi- and

20 endo-cardial layers resulting in a dispersion of de- and repolarization.

The disclosure provides also a method for treating a disease caused by chloride channel dysfunction according to the present disclosure comprising administering to a patient a therapeutically effective amount of the TMEM16A peptide activator, nucleic acid, expression vector or pharmaceutical composition as described above.

- 25 By “therapeutically effective amount” refers to an amount effective, at dosages and for periods of time necessary to achieve the desired therapeutic result. The therapeutically effective amount of the product of the disclosure, or pharmaceutical composition that comprises it may vary according to factors such as the disease state, age, sex, and weight of the individual, and the ability of the product or pharmaceutical composition to elicit a desired
- 30 response in the individual. Dosage regimens may be adjusted to provide the optimum

therapeutic response. A therapeutically effective amount is also typically one in which any toxic or detrimental effect of the product or pharmaceutical composition is outweighed by the therapeutically beneficial effects.

As used herein, the term "patient" or "individual" denotes a mammal. Preferably, a patient
5 or individual according to the disclosure is a human.

In the context of the disclosure, the term "treating" or "treatment", as used herein, means reversing, alleviating or inhibiting the progress of the disease caused by the chloride channel dysfunction or condition to which such term applies, or reversing, alleviating or inhibiting the progress of one or more symptoms of the disorder or condition to which such term
10 applies.

The product of the present disclosure is generally administered according to known procedures, at dosages and for periods of time effective to induce a therapeutic effect in the patient.

The administration can be systemic or local. Systemic administration is preferably parenteral
15 such as subcutaneous (SC), intramuscular (IM), intravascular such as intravenous (IV) or intraarterial; intraperitoneal (IP); intradermal (ID), interstitial or else. The administration may be for example by injection or perfusion. In some preferred embodiments, the administration is parenteral, preferably intravascular such as intravenous (IV) or intraarterial. The practice of the present disclosure will employ, unless otherwise indicated,
20 conventional techniques, which are within the skill of the art. Such techniques are explained fully in the literature.

In preferred embodiment, said administration is parenteral or ocular administration. More preferably, the ocular administration including topical ocular instillation and intraocular administration is used for the treatment of dry eye syndrome and transmucosal
25 administration including nasal sprays can be used for the treatment of cystic fibrosis.

In a further aspect, the present invention also concerns TMEM16A peptide activator, a nucleic acid, vector as described above for use to activate chloride channel, in particular TMEM16A channel, for example for in vitro diagnostic reagent, drug screening reagent or research tool to activate TMEM16A channel.

The following examples are given for purposes of illustration and not by way of limitation.

EXAMPLES

1. Experimental model and subject details

Molecular biology, gene expression and cell culture

5 mTMEM16A (kindly provided by Dr Lily Yeh Jan) and hKCNE1 cDNA were subcloned in pIRES2eGFP, pXOOM, pcDNA3.1, pCDNA3.1-GFP and pCMV-HA vectors. Truncations and mutations on KCNE1 were generated by PCR. For SiMPull experiments, HA-tags were fused to the N-terminus of sequences, whereas GFP-tags were fused to C-terminal part. HEK293T and PCT cells were transiently co-transfected using Lipofectamine 2000 or the
10 calcium phosphate method with a total amount of 1 and 3.5 μg of DNA, respectively, and seeded on 18 mm diameter coverslips. HEK cells were maintained in DMEM with 5% FBS on poly-L-lysine-coated glass coverslips in 12 well plates. PCT cells from wild type and knock-out mice were microdissected as described previously and maintained in F12 (Gibco) on collagen-coated glass coverslips.

15 Electrophysiology

HEK293T and PCT cell electrophysiology was performed 24 – 48 h after transfection. For whole-cell patch-clamp experiments cells were recorded in a bath solution containing (in mM) 150 NaCl, 5 KCl, 2 CaCl₂ and 10 HEPES, pH 7.4. The glass pipettes (2-5 M Ω of resistance) were filled with (in mM) 5 NaCl, 135 CsCl, 2 MgCl₂, 5 EGTA, 10 HEPES, pH
20 7.3. Total calcium concentration was calculated with Maxchelator (maxchelator.stanford.edu) for a temperature of 20°C. HEK293T and PCT cells were recorded at room temperature in voltage-clamp mode using an Axopatch 200A (Molecular Devices) amplifier. Signals were filtered at 10 kHz and digitalized at 20 kHz. Whole-cell currents were elicited by voltage-ramps (from -100 to +100 mV, 1 s) and I-V stimulation
25 pulses (from -100 to +100 mV in 20 mV increments, 1 s each pulse), holding the cells at -80 mV. Current densities were measured at +100 mV. Cell recordings, data acquisition and analysis of electrophysiology experiments were performed using pClamp software (Molecular Devices).

Single Molecule Pulldown assay

For SiMPull assays, the inventors followed the protocol previously described by Jain et al., 2011. Nature 473, 484-488. Briefly, HEK293T cells co-transfected with an HA-tagged bait protein and a GFP-fused prey protein (applying the widely used eGFP A206K mutant which greatly reduces homodimerization events) were lysed in a buffer containing (in mM): 150 NaCl, 10 Tris pH 7.5, 1 EDTA, protease inhibitor cocktail (Thermo Scientific) and 1.5% IGEPAL (Sigma). Lysates were collected and pulled-down on coverslips passivated with PEG (99%) and biotin-PEG (1%) and treated with neutravidin (1.4 mg/mL, Pierce) and biotinylated anti-HA antibody (15 nM, abcam, #ab26228). Several washes with T50 buffer (in mM: 50 NaCl, 10 Tris, 20 EDTA; 0.1 mg/mL BSA, pH 7.5) were performed to avoid unspecific protein binding. Finally, single molecule complexes were imaged using a 488 nm Argon laser in total internal reflection fluorescence microscopy with a 100x objective (Olympus). 13 x 13 μm^2 movies of 250 frames were acquired at frame rates of 10–30 Hz and analyzed using Fiji software (NIH). Multiple independent experiments were performed for each condition and only the spots which were fully bleached at the end of the illumination were considered. Representative data sets are presented to quantitatively compare the different conditions (minimum 15 movies per condition, at least analyzed traces per movie).

2. Results

KCNE1 shifts TMEM16A from a calcium dependent to a voltage-dependent Cl^- channel

To test the ability of KCNE1 to regulate TMEM16A, the inventors used the HEK293T cell model which does not express neither TMEM16A nor KCNE1 endogenously. Whereas transfection of HEK293T cells with either TMEM16A or KCNE1 alone produced no significant current, co-expression of both proteins induced a voltage-dependent current, whose density was of 18.1 ± 2.8 pA/pF at +100 mV (**Figures 1A and 1B**). The reversal potential was -4.8 ± 1.3 mV, which is similar to the expected reversal Cl^- potential in the experimental conditions used. This chloride current was inhibited by NFA, T16Ainh-A01 (Davis, A.J. et al. 2013. Br J Pharmacol. 168, 773-784) and also by Ani9, the most specific TMEM16A inhibitor (Seo, Y. et al. 2016, PLoS One 11, e0155771) (**Figures 1C-E**). This suggests that KCNE1 switches TMEM16A from a calcium-dependent to a voltage-dependent chloride channel.

To preclude the possibility that KCNE1 activates endogenous calcium channels, the inventors conducted similar experiments in the presence of the fast calcium chelator BAPTA. As shown in **Figure 1F**, BAPTA did not abolish the formation of the voltage-dependent current evoked by co-expression of both proteins (3.70 ± 0.41 pA/pF vs $21.98 \pm$
5 5.32 pA/pF in the absence or presence of BAPTA, $P < 0.001$). To totally rule out a potential modulation of endogenous calcium channels by KCNE1 leading to the TMEM16A activation, the inventors co-expressed KCNE1 with the Ca^{2+} -activated SK4 channel, which has similar calcium sensitivity (Cao, Y.J., and Houamed, K.M. 1999. FEBS Lett 446, 137-141) as TMEM16A. As shown in **Figure 2**, KCNE1 overexpression did
10 not induce any increase of the SK4 current in absence of calcium. Altogether, these results exclude an implication of intracellular Ca^{2+} in a KCNE1-induced activation of TMEM16A.

TMEM16A activation by KCNE1 involves physical interaction

To be considered as auxiliary subunit, a protein has to interact directly and stably with the α -subunits. To test the physical association between TMEM16A and KCNE1, the inventor
15 used the recently developed single molecule pull-down (SiMPull) assay (Jain, A. et al. 2011. Nature. 473, 484-488; Levitz, J. et al. 2016. Proc Natl Acad Sci U S A. 113, 4194-4199; Royal, P. et al. 2019. Neuron. 101, 232-245.e236). This technique enables direct visualization of antibody-immobilized protein complexes (**Figures 3A and 3E**) allowing to determine the composition and stoichiometry within single protein complexes by counting
20 fluorophore bleaching (Jain, A. et al. 2011. Nature. 473, 484-488; Levitz, J. et al. 2016. Proc Natl Acad Sci U S A. 113, 4194-4199; Royal, P. et al. 2019. Neuron. 101, 232-245.e236). After co-transfection with the two putative partners KCNE1 and TMEM16A, one of them fused with an HA affinity tag and the other with a GFP label, and subsequent pull-down, the inventors observed many fluorescent spots for both conditions, TMEM16A-GFP + HA-KCNE1 (**Figure 3B**) and KCNE1-GFP + HA-TMEM16A (**Figure 3F**). This demonstrates a physical interaction between KCNE1 and TMEM16A. Importantly, when HA-KCNE1 or HA-TMEM16A were not co-expressed, no proteins fused to GFP were isolated (**Figure 3J and 3L**), confirming the specificity of the HA-antibody used in SiMPull assays. By analyzing bleaching steps for immobilized HA-KCNE1-TMEM16A- GFP complexes, the
30 inventors were able to determine the number of TMEM16A-GFP subunits within the complex. They found that the majority of fluorescence intensity trajectories showed two-step bleaching ($\sim 70\%$), with the remaining spots bleaching in one step ($\sim 20\%$) or

occasionally three steps (~10%) (**Figures 3C and 2D**). This distribution agrees well with the binomial distribution predicted for a strict dimer based on an estimated GFP maturation probability of ~75% (Ulbrich, M.H., and Isacoff, E.Y. Nat Methods, 4, 319- 2 321; Zacharias, D.A. et al. 2002. Science, 296, 913-916). Analysis of the SiMPull experiment
5 with HA-TMEM16A-KCNE1-GFP showed that most complexes presented two bleaching steps (~65%) and some remaining spots bleached in one (~25%) and three steps (~10 %) (**Figures 3G and 3H**). This distribution corresponds to the presence of two KCNE1-GFP subunits within the protein complex. Therefore, two KCNE1 subunits assemble with a single TMEM16A channel (Dang, S. et al. 2017. Nature. 552, 426-429; Takumi, T. et al. 1988.
10 Science, 242, 1042-1045), following a $2\alpha:2\beta$ stoichiometry.

The complex KCNE1-TMEM16A generates voltage-dependent Cl⁻ currents in proximal convoluted tubule cells

To be considered as a *bona fide* auxiliary subunit, the protein must interact with alpha subunits in a native environment. To confirm that KCNE1 is an auxiliary subunit of
15 TMEM16A in native tissue and to eliminate possible artifacts due to heterologous overexpression, the inventors took advantage of kidney proximal convoluted tubule (PCT) cells obtained from wild type and *kcnel* KO mice (Barrière, H. et al. 2003. J Membr Biol. 193, 153-170). PCT cells are considered as a relevant model as they naturally co-express both TMEM16A and KCNE1 (Faria, D. et al. 2014. Kidney Int. 85, 1369-1381; Vallon, V
20 et al. 2001. J Am Soc Nephrol, 12, 2003-2011) and do not necessitate any genetic manipulation to record TMEM16A channel carried currents. Moreover, while no modification of the K⁺ current was found in PCT cells from *kcnel* KO mice compared to wild type, a DIDS (4,4'-Diisothiocyanostilbene-2,2'-disulfonic acid)-sensitive Cl⁻ conductance was impaired (Barrière al., 2003). The inventors confirmed the loss of current, whose reversal
25 potential was similar to the expected Cl⁻ reversal potential in *kcnel* null PCT cells (18.07 ± 1.21 pA/pF vs 5.37 ± 0.56 pA/pF for PCT wild type and KO mice, respectively, $P < 0.001$) (**Figure 4A**). This current was inhibited by NFA (4.51 ± 0.28 pA/pF), T16A(inh)-A01 (5.52 ± 0.72 pA/pF) and Ani9 (2.88 ± 0.38 pA/pF) (**Figure 4B-D**). Moreover, knock-down of TMEM16A by a previously validated siRNA transfection (Sala-Rabanal, M. et al. 2017. J
30 Biol Chem, 292, 9164-9174) in wild type PCT cells significantly reduced the Cl⁻ current amplitude (4.23 ± 0.48 pA/pF) (**Figure 4E**). This demonstrates the involvement of TMEM16A subunits in the channel complex responsible for the herein studied Cl⁻ current. A

rescue experiment by KCNE1 transfection in *kcne1*^{-/-} cells fully restored the voltage-dependent Cl⁻ current (21.59 ± 1.38 pA/pF) (**Figure 4F**), showing that the absence of chloride current in these cells was only due to the KO of *kcne1* and not due to any modification that might occur during the culture process.

5 **The N-terminal pre-transmembrane domain of KCNE1 is a key for TMEM16A regulation**

KCNE1 is a single transmembrane protein with an extracellular N-terminal part and a C-terminal domain within the cytosol (Takumi, T. et al. 1988. Science, 242, 1042-1045). To determine the interacting site with TMEM16A, the inventors produced a series of truncated KCNE1 forms (**Figure 5A**) and tested them for their ability to regulate TMEM16A. Truncation of the full KCNE1 C-terminal domain did not abolish the KCNE1-mediated TMEM16A regulation (25.04 ± 4.9 pA/pF, $P > 0.15$) (**Figure 5B**). By contrast, deletion of the full N-terminal domain suppressed the ability of KCNE1 to regulate TMEM16A (6.56 ± 0.89 pA/pF, $P < 0.001$) (**Figure 5B**). No effect was observed for the partial N-terminal truncation Δ Nt16 (25.43 ± 4.46 pA/pF) nor Δ Nt30 (25.23 ± 6.62 pA/pF) (**Figure 5C**), demonstrating that the sequence of 13 residues (from L30 to L42) preceding the transmembrane domain is essential for TMEM16A activation. This result is in line with the previous observation, that a partial deletion of KCNE1, including eight of the 13 amino acids (KCNE1 Δ 11-38) abolished the KCNE1-induced chloride current in *Xenopus* oocytes (Attali, B et al. 1993. Nature, 365, 850-852). To check if this small domain is sufficient to recapitulate the properties of the entire KCNE1 on the TMEM16A current, the inventors used a corresponding synthetic peptide (Nter13), bearing the L30-L42 sequence. In HEK293T cells expressing TMEM16A, application of 100 μ M Nter13 elicited an Ani9 sensitive current (15.48 ± 3.25 pA/pF) (**Figure 5D**; **Figures 6A and 6B**). Again, the reversal potential was similar to the current observed when KCNE1 is co-expressed, whereas no effect was observed for an application of scrambled peptide (**Figure 5D**).

KCNE1 polymorphisms inside the TMEM16A-regulating sequence suppress the Cl⁻ current

Within the 13-residues extracellular domain of KCNE1, previous works have shown that the common S38G and R32H polymorphisms, which are not or just poorly affecting the KCNE1-mediated regulation of KCNQ1 (**Figure 7A and 7B**) (Westenskow et al., 2004; Yao et al., 2018), may be related to cardiac arrhythmia (Crump, S.M., and Abbott, G.W.

2014. *Front Genet* 5, 3). The inventors therefore tested the potential of these two KCNE1 variants to regulate TMEM16A. The related disease mutation T7I, which is not in the regulating domain, was used as a control. Whereas mutation T7I did not alter the KCNE1-dependent regulation of TMEM16A (24.69 ± 1.57 pA/pF, $P > 0.4$) (**Figures 7C and 7D**), both mutations R32H and S38G abolished the ability of KCNE1 to modulate the TMEM16A current properties (5.69 ± 1.18 pA/pF and 6.96 ± 0.78 pA/pF for R32H and S38G, respectively) (**Figures 7C and 7D**) suggesting a potential implication of the KCNE1-KCNQ1 in human diseases.

10 DISCUSSION

Most of ion channels are assembled as complexes of a pore forming α -subunit, associated with auxiliary (β) subunits. In this study, the inventors demonstrate that KCNE1, which is classically considered a β -subunit of the cardiac KCNQ1 pore-forming subunit belonging to the voltage- dependent Kv channel superfamily, serves also as an auxiliary subunit of the anoctamin superfamily channel TMEM16A, a Ca^{2+} -activated Cl^- channel (CaCC). By interacting stably with TMEM16A following a $2\alpha:2\beta$ stoichiometry, KCNE1 induces a voltage-dependent current in the absence of intracellular elevation of calcium. KCNE1 polymorphisms within the TMEM16A-interacting domain abolish its ability to regulate TMEM16A, suggesting a possible implication of this voltage-dependent chloride current in human diseases. β -subunits of ion channels provide an important source of diversity of electrical signaling molecular players in cells. Although they cannot induce native currents *per se*, they associate with pore-forming subunits of ion channels and modulate their pharmacological and biophysical characteristics. Their physiological importance is reflected by the large number of diseases linked to their mutations, such as muscular pathologies, epilepsy and cardiac arrhythmias (Adelman, 1995, *Curr Opin Neurobiol.* 5, 286-295; Cannon, 2007, *Neurotherapeutics.* 4, 174-183 ; Crump and Abbott, 2014, *Front Genet.* 5, 3; Vergult et al., 2015, *Eur J Hum Genet.* 23, 628-632). KCNE1 is a famous example of a K_v β -subunit, which associates with KCNQ1 and hERG to control both I_{Ks} and I_{Kr} components of the cardiac action potential and for which more than sixty gene variants have been reported to be associated with human diseases, particularly with cardiac arrhythmias (Barhanin et al., 1996, *Nature.* 384, 78-80; Crump and Abbott, 2014, *Front Genet.* 5, 3; Sanguinetti et al., 1996, *Nature.* 384, 80-83; Sanguinetti et al., 1995, *Cell.* 81, 299-307). Cross-modulation by β -subunits of pore-forming- α -subunits from the same superfamily of

ion channels was shown for Nav and Kv channels (Marionneau et al., 2012. J Neurosci. 32, 5716-5727; Nguyen et al., 2012. Proc Natl Acad Sci U S A. 109, 18577-18582). Nav β_1 was found to coordinate control of Kv and Nav channels which derivate from the same ancestor (Moran et al., 2015, J Exp Biol. 218, 515-525) and belong to the superfamily of voltage-gated ion channels. The results demonstrate cross-modulation of two different superfamilies which are not phylogenetically related: the voltage-gated channels and the anoctamins. The inventors found that, by interacting with TMEM16A, KCNE1 modifies the gating of this member of the anoctamin superfamily, switching it from a calcium-dependent to a voltage-dependent channel. The experiments with different Ca²⁺ chelators and with a Ca²⁺-activated SK channel as a very sensitive reporter demonstrated that activation of this CaCC is independent of any rise of cytosolic Ca²⁺, the natural activator of the channel in the absence of KCNE1 (Caputo et al., 2008. Science 322, 590-594; Schroeder et al., 2008. Cell 134, 1019-1029; Yang et al., 2008. Nature 455, 1210-1215). Clearly, the voltage-dependent chloride channel superfamily is not restricted to the CIC family, but extends to the anoctamin family when combined with KCNE1. This also shows that the difference between Ca²⁺ and voltage-dependent channels is not so strict and that one should rather consider a continuum of biophysical properties.

Whereas the KCNQ1-KCNE1 stoichiometry remains a matter of debate (Morin and Kobertz, 2008. Proc Natl Acad Sci U S A. 105, 1478-1482; Murray et al., 2016. Elife. 5; Nakajo et al., 2010. Proc Natl Acad Sci U S A. 107, 18862-18867; Plant et al., 2014. Proc Natl Acad Sci U S A. 111, E1438-1446), the inventors found by using the SiMPull assay (Jain et al., 2011. Nature. 473, 484-488; Levitz et al., 2016. Proc Natl Acad Sci U S A. 113, 4194-4199; Royal et al., 2019. Neuron. 101, 232-245.e236), that the TMEM16A-KCNE1 complex is composed of 2 α :2 β subunits. The inventors have shown that this complex takes place in HEK cells upon heterologous expression, but also show that it is present in native kidney cells, where it mediates a Cl⁻ conductance, which is sensitive to TMEM16A inhibitors. This Cl⁻ conductance cannot be recorded in KCNE1 knock-out cells or in cell in which KCNE1 has been knock-down, and it is rescued in these cells by KCNE1 re-expression upon transfection. Therefore, the TMEM16A-KCNE1 association is not to only found upon recombinant over-expression, but can be observed in native cells where it participates in the maintenance of the resting membrane potential.

The electrophysiological assays, using truncated forms of KCNE1 and synthetic peptides based on the β -subunit, allowed to determine the crucial role of the N-terminus of KCNE1

in TMEM16A regulation. More specifically, the inventors have observed that the segment closer to the transmembrane domain of KCNE1 is necessary and sufficient to recapitulate the action of the entire KCNE1 on the TMEM16A current. The synthetic peptide generated on the basis of this segment's sequence is the first designed TMEM16A agonist and may be useful for clinical applications. Notably, activation of an apical chloride channel such as TMEM16A triggers the secretion of water, which makes TMEM16A-targeted activators potential drug candidates for treatment of cystic fibrosis or dry eyes syndromes. This 13 amino acid segment bears at least two residues which are subject to polymorphisms (R32H and S38G) related with cardiac arrhythmias (Crump and Abbott, 2014. Front Genet 5, 3).

Whereas several clinically relevant KCNE1 variants were found to modify its ability to regulate KCNQ1, providing a link between these mutations and polymorphisms with cardiac arrhythmias, the KCNE1 S38G poorly impairs KCNQ1 regulation by KCNE1 (Yao et al., 2018. Exp Cell Res 18 363, 315-320). The inventors found that the KCNE1 S38G as well as the R32H mutants, lost their ability to regulate TMEM16A, suggesting a potential role of this chloride current in cardiac arrhythmias.

Along this line, a recent study performed in canine heart suggests a protective role for TMEM16A against risk of arrhythmias by reducing spatial and temporal heterogeneity of cardiac repolarization and early after depolarization (Hegyí et al., 2017. Ca. J Mol Cell Cardiol 109, 27-37).

To sum up, the inventors have found that KCNE1, a well-known auxiliary subunit of voltage-dependent K^+ channels, meets the four needed conditions to be considered as an auxiliary subunit of the anoctamin anion channel superfamily (Adelman, 1995. Curr Opin Neurobiol. 5, 286-295; Arikath and Campbell, 2003. Curr Opin Neurobiol. 13, 298-307. J Biol Chem. 271, 27975-27978; Cannon, 2007. Neurotherapeutics. 4, 174-183; Gurnett and Campbell, 1996. Neuron. 7, 403-408; Trimmer, 1998. Curr Opin Neurobiol. 8, 370-374): first, KCNE1 does not show any ion channel activity by itself, second, KCNE1 and TMEM16A interact directly and stably with a fixed stoichiometry ($2\alpha:2\beta$), third, KCNE1 modifies drastically the TMEM16A function enabling the channel to work in the absence of elevated cytosolic calcium, and fourth, KCNE1 regulates TMEM16A in native tissue. Therefore, KCNE1 fulfills all the criteria of a *bona fide* auxiliary subunit of two distinct classes of ion channel superfamilies which are not phylogenetically related: voltage-gated

cation channels and anoctamin superfamilies. Finally, the TMEM16A-KCNE1 association should be considered when analyzing outcomes of clinically relevant KCNE1 mutations, as emphasized by the finding that two known cardiac arrhythmia related KCNE1 variants, including S38G, lost their ability to regulate TMEM16A.

CLAIMS

1. A TMEM16A peptide activator for use as a medicament comprising or consisting of the amino acid sequence L-A-R-R-S-P-R-S (SEQ ID NO: 1) or a functional variant thereof.
5
2. The peptide for use of claim 1 comprising or consisting of the amino acid sequence L-A-R-R-S-P-R-S-S-D-G-K-L (SEQ ID NO: 2) or a functional variant thereof.
- 10 3. The peptide for use of claim 1 comprising sequence L-A-R-X1-S-X2-X3-X4-X5 (SEQ ID NO: 3) wherein said
 - X1 is arginine, lysine or histidine,
 - X2 is proline or glutamine,
 - X3 is arginine or leucine,
 - 15 - X4 is serine or arginine and
 - X5 is glycine or aspartic acid.
4. The peptide for use of claim 2 comprising or consisting of the sequence L-A-R-X1-S-X2-X3-X4-X5-D-X6-K-L (SEQ ID NO: 4) wherein said
 - 20 - X1 is arginine, lysine or histidine,
 - X2 is proline or glutamine,
 - X3 is arginine or leucine,
 - X4 is serine or arginine,
 - X5 is glycine or aspartic acid and
 - 25 - X6 is glycine or serine.
5. The peptide for use according to any one of claims 1 to 4 wherein said peptide is of 8 to 100 amino acids residues, preferably 8 to 20 amino acids residues, more preferably 13 to 20 amino acids residues.

6. The peptide for use according to any one of claims 1 to 5 comprising or consisting of an amino sequence which is at least 80 % identical to an amino acids sequence of: SEQ ID NO: 1 or 2.
- 5 7. The peptide for use according to any one of claims 1 to 6 comprising or consisting of an amino acid sequence having no more than 3 conservative substituted amino acids residues as compared to SEQ ID NO: 1 or 2.
8. A nucleic acid encoding the peptide as defined in claims 1 to 7 for use as a
10 medicament.
9. An expression vector comprising a nucleic acid for use of claim 8.
10. The peptide according to any one of claims 1 to 7, nucleic acid of claim 8 or
15 expression vector of claim 9 for use in the treatment of diseases caused by chloride channel dysfunction.
11. The peptide, the nucleic acid or the vector for use of claim 10 wherein said diseases
20 caused by chloride channel dysfunction is selected from the group consisting of: cystic fibrosis, dry mouth, dry eye syndrome, cardiac arrhythmia and gastrointestinal hypomobility disease, preferably dry eye syndrome.
12. A pharmaceutical composition comprising the peptide according to any one of claims
25 1 to 7, nucleic acid of claim 8 or expression vector of claim 9 and a pharmaceutically acceptable carrier.
13. A peptide of 8 to 100 amino acids residues, preferably 8 to 20 amino acids residues,
more preferably 13 to 20 amino acids residues comprising an amino sequence of SEQ
ID NO: 1 or 2 or an amino sequence which is at least 90 % identical to an amino acid
30 sequence of: SEQ ID NO: 1 or 2.
14. Use of the peptide as defined in claims 1 to 7, nucleic acid as defined in claim 8 or
expression vector as defined in claim 9 as a chloride channel activator.

ABSTRACT

THERAPEUTIC USE OF CALCIUM-ACTIVATED CHLORIDE CHANNEL PEPTIDE ACTIVATOR

The present disclosure relates to a calcium-activated chloride channel peptide activator and
5 its therapeutic use.

